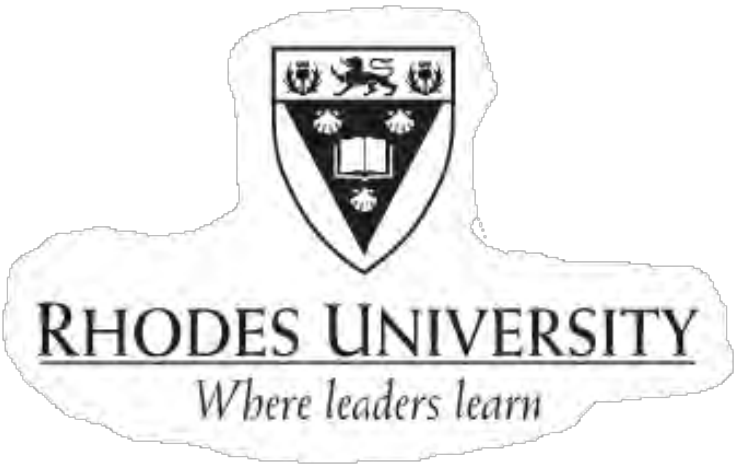

Fluid characteristics in hydrothermal veins of the Twangiza-Namoya Gold Belt, South Kivu and Maniema Provinces, DRC

Thesis submitted to fulfil the
requirements of the degree of
Master of Science
at
Rhodes University

by

Wesson Kyle Reid

Supervisor: Professor Steffen H. Büttner

Submitted in 2019

DECLARATION

I declare that this thesis is my own work, and information from other publications is adequately referenced. It is being submitted in fulfilment for the Master of Sciences degree in the Department of Geology, Faculty of Science, Rhodes University.

Candidate's Name Wesson Kyle Reid

Candidate's Signature 

Signed on this **27th** day of **November 2019.**

ABSTRACT

This study evaluates fluid variations in hydrothermal quartz veins from gold deposits in Kamituga, Lugushwa and Namoya, located in the Twangiza - Namoya Gold Belt (TNGB) of the Kibara Belt in the eastern Democratic Republic of the Congo (DRC). Petrographic, fluid inclusion (FI) microthermometric observations and Raman spectroscopy provided qualitative and quantitative fluid composition data on the hydrothermal and magmatic fluids and their evolution during mineral precipitation.

The formational fluids, based on genetically specific characteristics, were categorized into six distinct FI Types. Type 1 to 4 FIs are common in all TNGB fluids. Type 1 and 2 FIs are high salinity halite bearing FIs that indicate formation fluids that are predominantly metamorphic-sedimentary in source. CO_2 vapour-bearing and the aqueous-saline CO_2 liquid-bearing Type 3 FIs commonly contain CH_4 and/or N_2. Type 4 FIs are saline aqueous and commonly co-genetic with Type 1 and 2 FIs. Type 5 CO_2-rich FIs contain either sulphide crystals, amorphous or crystalline carbon. Type 3 and 5 FIs indicate fluid sources rich in organic materials. Type 6 single aqueous-liquid phase FIs have no vapour bubble, lacked a visible phase change on heating and were not microthermometrically evaluated.

The data indicated a high correlation between fluid composition and gold grades. High Au grade veins correlate with CO_2 bearing Type 3 and 5 FIs - predominantly liquid-bearing CO_2 fluids and quartz veins and fluids that contain increased organic material and sulphides. The polyphase quartz veins show highly variable homogenisation and formational temperatures exceeding 400 °C. Formation conditions indicate high trapping temperatures in relation to the pressures at which fluids were captured. The high depth-temperature gradients are likely associated with mesothermal orogenic gold deposition.

Mineralisation is interpreted to have taken place as a result of mobilisation of fluids during the Pan African orogeny. Based on fluid petrography and microthermometry, gold mineralisation is most likely associated with secondary fluid influx from metamorphic sedimentary sources such as metapelites. The correlation between high gold grades and secondary fluids containing sulphides, high depth-temperature gradients, elevated CO_2, CH_4 and organic materials suggest black shales as a possible primary fluid and gold source.

The development of variable and multiple fluid influx events and interactions with host rocks and imported materials resulted in complex polyphase quartz veins; the product of which created viable gold deposits throughout the TNGB. The six FI Types provides evidence of the diversity in the formation and evolution of gold deposits in the TNGB.

Key Words:
Twangiza - Namoya Gold Belt (TNGB), Democratic Republic of the Congo (DRC), fluid inclusion (FI), primary and secondary fluids, formation conditions, heating and freezing conditions, Raman spectroscopy, Pan African.

ACKNOWLEDGEMENTS

My thanks to Professor Steffen Büttner, my supervisor, for securing funding from Banro Corporation for the DRC field excursion, his guidance in the planning and execution of this study and the many hours spent checking my results.

My gratitude to Banro Corporation, and its employees in the DRC, for their funding, planning and arrangement of logistics and providing geological data and access to their properties and samples in South Kivu and Maniema Provinces.

Special thanks to Gerald Chuwa for the time he spent with us in importing his knowledge and expertise on the area of study and his local geological and his understanding of the DRC as a whole.

My appreciation and respect to John Hepple and his technical staff at Rhodes University Geology Department for the work they did in preparing the thin section and wafers. To the Geology Department at the University of Johannesburg for the use of their Raman Spectrometer.

My thanks to Russell Cranswick for his support in this study and his ongoing friendship.

Rhodes University for the use of all the equipment and facilities used for this research.

Last but not least, my sincerest thanks to my mother and father for their support in financing my studies and for their encouragement when I believed that I would never finish this dissertation. Without your confidence and support in the importance and success of this study, and your confidence in my abilities, this thesis would not have been completed.

LIST OF TERMS AND ABBREVIATIONS

1. **Fluid inclusion (FI):** Microscopic cavity containing entrapped solids, liquids and/or gases derived from a rock forming fluid.
2. **L:** Liquid phase in a fluid inclusion.
3. **V:** Vapour phase in a fluid inclusion.
4. **S:** Solid phase in a fluid inclusion.
5. **H:** Halite
6. **D:** Daughter mineral
7. **Aq**: Aqueous
8. **C:** Carbonic
9. **Clath:** Clathrate
10. **Py:** Pyrite
11. **HH:** Hydrohalite
12. **TNGB:** Twangiza - Namoya Gold Belt
13. **DRC:** Democratic Republic of the Congo
14. **Primary inclusion (P):** A fluid inclusion that was trapped during growth of the host crystal (e.g. via precipitation from a circulating fluid). These inclusions are often found on a crystal growth surface or at the crystal core. The fluids are considered parent fluids from which host mineral precipitate.

15. **Secondary inclusion (S):** A fluid inclusion that forms post crystal growth. These often occur along planar healed fractures within the host mineral. These surfaces cut across multiple grain boundaries. Trails of secondary fluid inclusions were captured during healing of fractures, and represent the fluids present at that time.

16. **Pseudosecondary inclusion (PS):** A fluid inclusion that was trapped during an early stage of host crystal growth. These inclusions also occur along healed fractures, giving the appearance of being secondary FIs. The PS's trails/planes terminate at growth boundaries within the host mineral grain and do not cut across grain boundaries. Similarly, PS like P may be used to determine growth conditions of the host mineral.

17. **Microthermometry:** A non – destructive technique for measuring the temperatures at which thermally induced phase transitions (from solid to liquid and liquid to **vapour** and vice versa) occur in fluid inclusions while being observed under the microscope. The instrument used for this is a heating – freezing stage.

18. **Fluid inclusion assemblage (FIA):** A group of co-genetic fluid inclusions that occur within a defined space (host crystals, growth zones, or healed fractures). For a set of fluid inclusions to constitute a FIA, there needs to be an unambiguous genetic and spatial relationship between evaluated fluid inclusions.

19. **Homogenous entrapment:** Fluid inclusion formed from a single-fluid phase produce a set of fluid inclusions with constant phase proportions.

20. **Heterogeneous entrapment:** Fluid inclusion formed from a multiphase fluid that has undergone unmixing prior to entrapment; producing a set of fluid inclusions with variable phase proportions.

21. **Total homogenization temperature (Th):** The temperature at which a fluid inclusion changes from a multiphase system to a single-phase system. The phase into which homogenization occurs is often stated e.g. Th (L) or Th (V).

22. **Th_{CO2}:** Temperature of CO_2 homogenization.

23. **Temperature of trapping (Tt):** Also referred to as “temperature of formation”.

24. **Temperature of decrepitation (Td):** The temperature at which fluid inclusions irreversibly rupture, resulting in the loss of the FI’s content.

25. **Temperature of melting (Tm):** Temperature of melting/dissolving for example of ice, clathrate or daughter minerals is indicated as Tm ice, Tm clath, Tm halite, Tm KCl, Tm CO_2 etc.

26. **Temperature of final melting (Tmf):** The temperature at which the last solid, (frozen solid during cooling) converts into the liquid phase upon heating.

27. **Temperature of eutectic (Te):** The temperature at which the first recognized formation of liquid occurs on warming in a completely frozen inclusion.

28. **Temperature of nucleation (Tn):** The temperature at which a phase forms during heating or cooling, such as the stage at which a vapor bubble or a solid form from cooling a homogeneous liquid inclusion.

29. **Necking, necking-down:** A post-entrapment process in which large and irregular inclusions tend toward morphological equilibrium by splitting into smaller, more equant inclusions.

30. **Diathermal:** A condition in which fluid inclusions permit instantaneous exchange of heat with their surroundings.

Table of Contents

1. INTRODUCTION, BACKGROUND AND CONTEXT

1.1 INTRODUCTION

In February 2014 a study of the auriferous hydrothermal systems of the Twangiza-Namoya Gold Belt (TNGB) was undertaken in the eastern Democratic Republic of the Congo (DRC) in collaboration with, and with significant logistical support from Banro Corporation Ltd (further referred to as Banro). Banro a Canadian gold exploration and mining company, was able, in April 2002, to retain the rights to four gold properties and 13 exploration permits in the TNGB to target primary gold sources in polyphase hydrothermal systems (O' Donovan et al., 1999 & 2005; Fall, 2008 and Chuwa, 2011). More than 12 million ounces of gold has been identified (reserves, measured, indicated and inferred resource) by Banro as of 2017 (Banro, 2017). Banro reported an inferred resource of 7.26 Mt at Kamituga - graded at 3.9 g/t, corresponding to 0.92 Moz of gold. Lugushwa's inferred resource of 65.01 Mt - graded at 1.54 g/t, corresponds to 3.22 Moz of gold and Namoya's measured and indicated resource of 25.68 Mt - graded at 1.96 g/t signifying 1.62 Moz of gold has an inferred resource of 5.03 Moz - graded at 1.63 g/t, corresponding to 0.26 Moz of gold (Banro, 2017). As of 2019, Banro's four gold deposit sites in the TNGB are in the South Kivu and Maniema Provinces in the eastern DRC (Figures 1.1 & 1.2); Kamituga and Lugushwa are active exploration sites and Namoya and Twangiza are operational mines. Fieldwork for the study was carried out at sites in Kamituga, Lugushwa and Namoya.

The aim of the study is to evaluate the succession and correlation of hydrothermal events associated with gold mineralisation in similar geological environments by analysing the composition and formation of fluid inclusions (FIs) in quartz veins. Due to the complex geological nature of the TNGB a sizeable sample set is required. Poor field exposure required that the bulk of the 42 quartz-dominant vein samples were gathered from drill cores and opencast pits. FI analysis was used as the primary analytical approach as it provided the most suitable and efficient means to examine the evolution of hydrothermal fluid systems and their associated ore deposits (Wilkinson, 2001). Petrographic descriptions, in conjunction with FI heating and freezing results, were used to obtain qualitative and semi-quantitative data. These were then compared and contrasted with Raman spectroscopy that allowed for qualitative evaluations of present molecules.

Figure 1.1: A regional map of the DRC. The encircled region depicts Banro's operational areas in the eastern DRC (adopted from Maps.com).

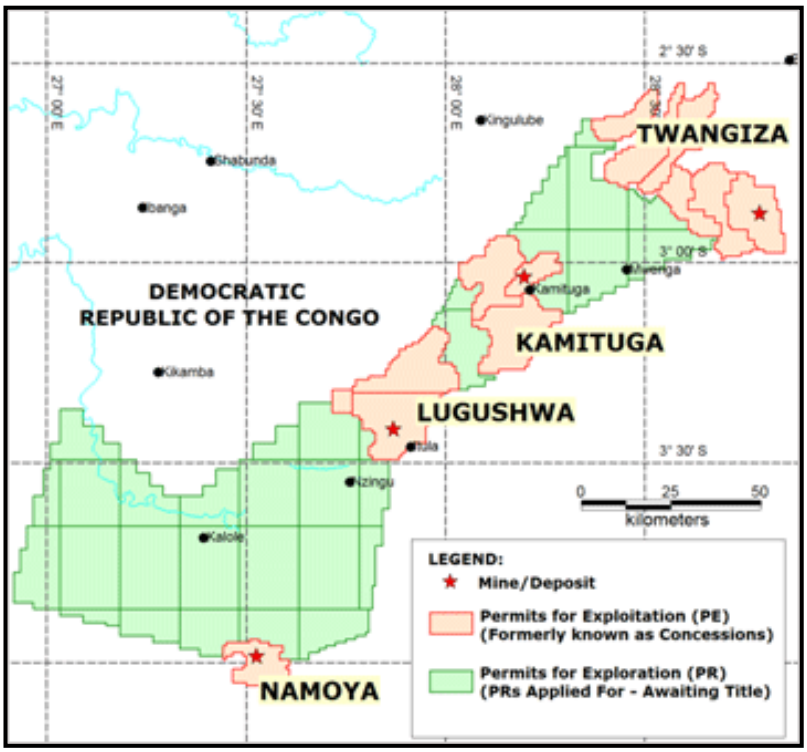

Figure 1.2: Approximate positions of Banro's operational sites in the TNGB (Banro, 2017).

1.2 FLUID INCLUSIONS

Fluid inclusions are microscopic cavities in minerals that trap solids, liquids and/or gases during, or in post-mineral growth (e.g., Roedder, 1984; Goldstein & Reynolds, 1994; Samson et al., 2003). The location, orientation and physical characteristics of FIs indicate the relative age of fluid entrapment events and facilitate the identification of the three categories of FIs - primary, secondary and pseudosecondary (Roedder, 1984; Goldstein & Reynolds, 1994 and Van den Kerkhof & Hein, 2001). FI analysis can be used to identify entrapped fluid formation conditions, as FIs are diathermal, isoplethic and isochoric systems (Samson et al., 2003 and Bodnar, 2003).

1.3 GEOLOGICAL SETTINGS AND GOLD MINERALISATION IN THE TNGB

The Mesoproterozoic Kibara Belt predominates in the TNGB (Chuwa, 2011). Paleoproterozoic rocks of the Ubendian Belt are present in the southern portion of Banro's concessions (Tack et al., 2010) (Figure 1.3). The Neoproterozoic Itombwe Supergroup overlay the Karagwe-Ankole basement in the Twangiza area (Walemba & Masters, 2005). Metamorphic grades, across the length of the TNGB, increases from sub-greenschist facies in Itombwe Supergroup in the north to lower/mid - greenschist facies conditions in the south (Chuwa, 2011). The age and number of metamorphic episodes is unknown. The greenschist facies tectono-metamorphic overprint in rocks of the Itombwe Supergroup indicates Neoproterozoic (or younger) events. These are also likely to have affected the underlying Meso- and Paleoproterozoic units.

Hydrothermal gold deposits in the TNGB are hosted in thick pelitic and psammo-pelitic, and in places, graphite- or carbonaceous-rich meta-sedimentary sequences of Mesoproterozoic and Paleoproterozoic age. Ore formation in the TNGB is poorly understood as the number of fluid influx episodes, their sources, their relative and absolute occurrence and their potential to precipitate gold are largely unknown. Late stage deformational overprinting renders the targeting of specific structural events difficult. According to Chuwa (2011), the presence of tourmaline and/or sulphides correlates with higher Au grades. Gold mineralisation in the TNGB is associated with polyphase quartz vein formation (Fall & Chuwa, 2007 and Chuwa, 2011). The polyphase nature of vein formation is displayed by highly variable vein textures and structures - such as hydrothermal breccias, stockworks, folded veins and veins that show extensive quartz recrystallisation. There appears to be no consistency in the structural features of veins .

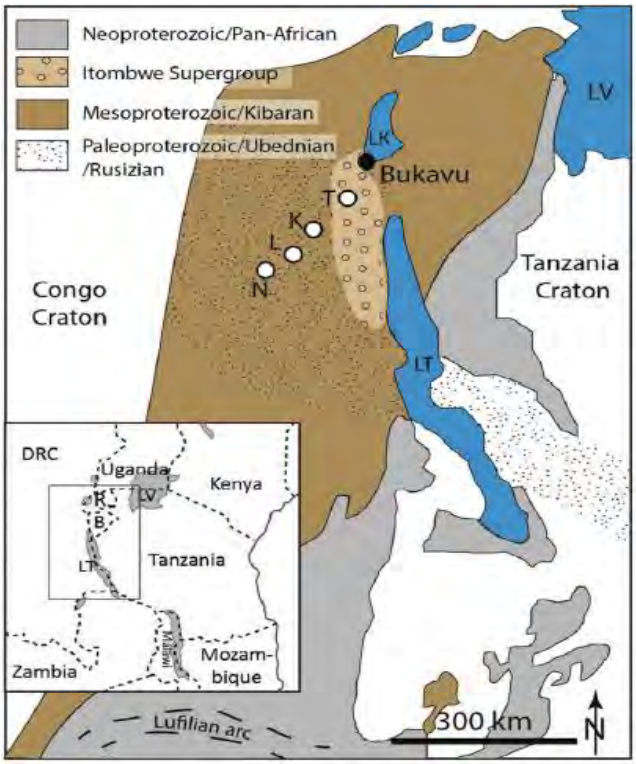

Figure 1.3: A broad age-correlated geological map indicating Banro's concessions within the Kibaran. The Ubende-Rusizian belt divides the Kibaran into NE – Kibara (Karagwe-Ankole belt) and SW – Kibara Belt (Kibara belt, as redefined by Tack et al. (2010)). T =Twangiza; K = Kamituga; L = Lugushwa; N = Namoya. Large water bodies of the Great Lakes region are marked in light blue; LV=Lake Victoria; LT= Lake Tanganyika; LK=Lake Kivu. R = Rwanda; B = Burundi (Büttner et al., 2016) showing geological boundaries taken from Brinckmann et al., 2001, Walemba & Master, 2005 and Tack et al., 2010).

Pohl (1994), Brinckmann et al. (2001) and Pohl, et al. (2013) conducted regional and local studies in Rwanda and Burundi to distinguish the formational processes of gold mineralisation. Regionally, gold mineralisation, particularly in NW Burundi, was ascribed by Brinckmann et al. (1994) to be associated with prominent N-S trending structural features formed during Pan-African deformation processes. Pohl et al. (2013) attributed the late-Kibaran Sn-W granitic episode with gold deposition (~960-1000 Ma). Gold mineralisation in the TNGB is present in areas where Sn-W magmatism is insignificant or absent (Fall, 2008). Based on structural, lithological and hydrothermal alterations observed in the field Fall (2008), described gold mineralisation as mesothermal and reduced intrusion-related. He further proposed that gold mineralisation, based on structural deformation of surrounding lithologies in the TNGB, occurred during the Pan-African. The known granitic magmatism in the TNGB and in other parts of eastern DRC is Kibaran and hence significantly older than the Pan-African orogenic cycle (Melcher et al., 2015). Granites in the TNGB and their absolute age are unknown. Only one pegmatite (late-Kibaran) dated by Büttner et al. (2016) in the Kamituga deposit, established that pegmatite emplacements related to late-Kibaran granitic activity (981±16 Ma; Rb-Sr mineral isochron data). This is associated with the regional late-Meso-to early Neoproterozoic G4 granitic episode (Brinckmann et al., 1994; Pohl et al., 2013 and Melcher et al., 2015). Büttner et al. (2016), proposed that early Pan-African hydrothermal activity occurred at Lugushwa (677 ± 17 Ma; Rb-Sr mineral data), indicating that the region underwent at least two episodes of heat influx that caused hydrothermal vein formation.

1.4 OBJECTIVES OF THE STUDY

The study, in investigating the formational fluids that formed hydrothermal quartz veins in the central and southern TNGB, was achieved by the following:

I. Outlining regional scale geology and gold mineralisation in the Kibara Belt that encompasses the TNGB.

II. Establishing and selecting the appropriate microscopic and mesoscopic methods and analytical procedures required to evaluate fluid types.

III. Comparing local geology, gold mineralisation and fluids from Kamituga, Lugushwa and Namoya.

IV. Conducting field and mesoscopic observations, collecting hand specimens from drill cores and open cast pits that represent lithological/structural and formational and alteration fluid characteristics, secondary mineral formation and host rock alterations to provide insight into vein formation and possible sources of gold within the TNGB.

V. Producing thin sections and wafers to identify fluid inclusion assemblages (FIA.s) using petrography.

VI. Defining the types of fluid inclusions (FIs).

VII. Evaluating the FI types in the wafers using microthermometry, Raman spectroscopy and methods and equations applicable to the identified FI types.

VIII. Determining pressures, temperatures, compositions and density characteristics of FI types at various stages of microthermometry.

IX. Evaluating formation characteristics of fluids from microthermometric and Raman spectroscopy results.

X. Relating fluid characteristics to formational fluids and gold mineralisation on a regional and local scale to determine both fluid sources and possible mineralisation processes of gold that may indicate the most likely sources of gold in the central and southern TNGB.

1.5 STRUCTURE OF THE STUDY

This thesis is structured in ten chapters. **Chapter 1** introduces and outlines the aim of the study. This is followed by a brief description and explanation of the TNGB's location and gold mineralisation.

Chapter 2 describes the scientific and analytical methods and equipment used in the study.

Continuing from chapter 1, **Chapter 3** describes the general characteristics of magmatic and hydrothermal gold mineralisation in the Kibara Belt and reviews the regional and local geology and mineralisation of the TNGB.

In **Chapter 4** the results sections begin with field and mesoscopic observations that describe the origin and characteristics of 42 quartz-dominant vein and host rock samples from Kamituga, Lugushwa and Namoya. Investigated samples are compared in relation to their geological context. Deposit lithologies and alterations are reviewed using field observation and sample descriptions.

In **Chapter 5** six main FI types in the deposits are defined to describe formational fluids in Kamituga, Lugushwa and Namoya. The main physical and compositional characteristic of each FI Type are categorised and illustrated.

Chapter 6 describes and explains the methods and equations used to process microthermometry and Raman spectroscopy data as applied to FI types.

In **Chapter 7**, the six different FI types from across Kamituga, Lugushwa and Namoya are evaluated using petrography, microthermometry and Raman spectroscopy to assess the interdependency between the presence of specific fluids and specific mineral phases.

Chapter 8 evaluates the conditions of fluid entrapment across genetic groups in Kamituga, Lugushwa and Namoya samples using isochore graphs. This allows for the interpretation of fluid sources, formation conditions and the relationship of fluids to gold mineralisation. The graphs were compiled from microthermometric and Raman spectroscopy data as presented in Chapter 7.

In **Chapter 9**, broad trends within and between deposits are evaluated. Inconsistences in findings in relation to literature are outlined and different approaches are proposed to address these.

Chapter 10 presents the conclusion in which core finding and their implications are highlighted.

2. METHODS AND ANALYTICAL PROCEDURES

2.1 INTRODUCTION

Previous interpretations of gold mineralisation in the TNGB were problematic because of small sample sets and because explanations of the crustal evolution in the eastern DRC were extrapolated from studies carried out in the more accessible neighbouring countries of Burundi, Rwanda and Tanzania (Tack et al., 2010). Banro's TNGB drill core samples were assayed across 0.2 - 1m intervals rather than on individual veins and their alteration halos. This strategy, however appropriate for resource estimations, cannot be used for the correlation of fluid influx events to gold grades as it did not produce representative data for individual quartz veins.

Veins from both mineralised and barren core sections were collected for this study to conduct FI analyses and compare their association with geological environments to contextualise vein formation. To avoid too small or too strongly clustered fluid inclusions (FI) for meaningful analysis, preference was given to veins that contained coherent quartz that was transparent rather than milky. One very highly mineralised sample from Namoya came from the oxidation zone. Most samples were taken from drill cores at variable depths within and below the oxidation zone. This optimises the chances of detecting any systematic differences in fluid compositions and structural properties owing to depth transitions in the host rock and quartz veins. Between 10 and 20 samples per deposit site were selected. Figure 2.1 (Van den Kerkhof, 2012) illustrates the sequence of descriptive and experimental steps that was followed in the current study and that allows for the differentiation of fluid types and the interpretation of pressure and temperature (PT) conditions at fluid entrapment.

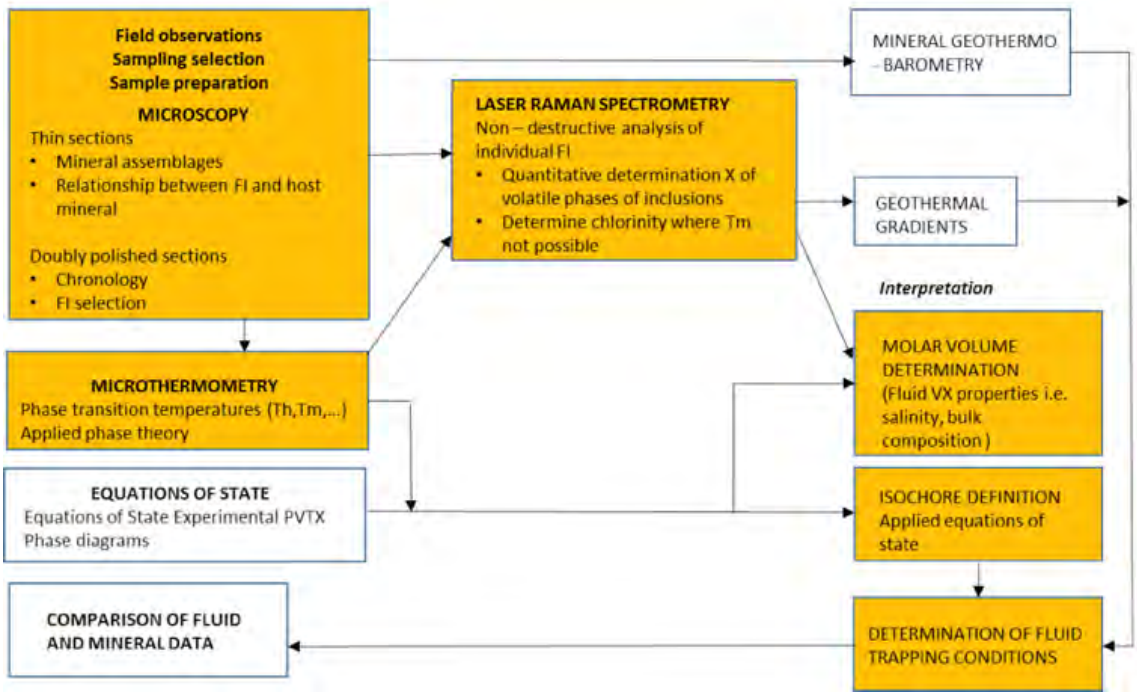

Figure 2. 1: Study procedure for FI and mineral analysis (adopted from Van den Kerkhof, 2012).

2.2 PETROGRAPHIC ANALYSIS

Detailed petrography is crucial for the understanding of formational pressures and temperatures and the compositional data obtained from microthermometry and Raman spectroscopy. The petrographic observations provide an overview of specific fluid influx events that track the temporal evolution and processes of mineralisation of hydrothermal ore deposits. In this context the identification of specific fluid inclusion assemblages (FIAs) is a critical procedure for the analysis and the establishment of relationships between different generations of quartz and FI's categories (Goldstein & Reynolds, 1994).

Optical transmitted and reflected light microscopy of polished thick and thin sections was conducted at Rhodes University using a Leica DM EP microscope, with 5x to 50x objective lenses. Petrographic images were obtained with a Leica digital camera EC3 using LAS E7 imaging software. Heating-freezing stage polished thick sections (200 µm thick FI wafers) and thin wafer sections (50 - 60 µm) were used to analyse large primary and secondary FIs for petrographic descriptions. Thin section samples cut to < 30 µm were made to determine absorption and interference colours, refractive index and relief determination of mineral phases under transmitted and reflected light. The reduction in thickness unfortunately resulted in a loss of large FIs.

FIs and individual fluid phase characteristics were evaluated according to size, shape, orientation, population proportions and relative time of entrapment (Roedder, 1984 and Samson et al., 2003). Based on dominant characteristics, FIs were then categorised into six broad FI types (hereto referred to as Types). Many samples display macroscopic evidence for deformation of veins and/or multiple episodes of mineral precipitation - including recrystallisation, quartz of different grain size, texture, transparency or crosscutting of veins. Sample preparation ensured that the interface between veins and the host rock would be observed. The geological context and characteristics of each sample (vein thickness, mineral assemblage, host rock type, alteration features, Au content and structural features) were recorded during collection. For further reference, primary quartz is either magmatic or hydrothermal quartz that has not undergone any significant recrystallisation. Secondary quartz is a late stage quartz phase or a primary quartz phase that has undergone extensive recrystallisation. Hydrothermal quartz forms from hydrothermal fluids; these fluids can result from basinal fluid interaction, magmatic differentiation, devolatilisation in metamorphic terranes or a combination of these processes.

2.3 MICROTHERMOMETRY

Quantitative and qualitative data of FIs pressures, temperatures, volume and composition (PTVX) can, according to Roedder (1984) and Goldstein & Reynolds (1994), be attained by microthermometry. The wafers were prepared to ~200 µm thickness in order to standardise the microthermometric readings and to prevent fragmentation during heating or cooling. Lakeside 70 C was initially used as an impregnating and mounting medium, however, multiple inconsistencies in melting and remnant residue developed. Great Lakes 3 mm pink plate wax mounting medium was found to be an effective and successful alternative due to its ease of application, low melting point (< 63 °C), adherent qualities to fragmented samples, ease of removal as an effect of its moderate boiling and flash point ~ 230 °C, and its dissolution in solvents.

Microthermometric analysis of FIs was conducted with a Linkam THMSG600 heating - freezing stage in conjunction with a TMS93 regulator and a LNP liquid nitrogen cooling pump system with maximum and minimum temperature between 600 ºC and -180 ºC. The Linkam stage was mounted on a Nikon Eclipse E600 microscope equipped with Nikon long-WD objective lenses of 4x to 100x magnification. A Nikon TV lens C-0.45 X was used with a 2014 Deltapix Invenio camera and software system for on-screen real-time monitoring of FIs during heating and cooling. The heating - freezing stage was calibrated using synthetic FIs standards (FluidInc Denver, Colorado, USA). CO_2 - H_2O (Tm = 6.6 °C Tm cla = +9.9 °C); H_2O - NaCl (Te = -21.2 °C) and H_2O Tm = 0.0 °C, Th = 374.0 °C standards were mounted on a G7 sample holder. To avoid nucleation of metastable phases, samples were cooled to temperatures below -120 °C at 20 °C/minute. Samples were then heated slowly; initially at a rate of 0.5 to 1.0 °C/min at temperatures below 31 °C, and then at 10 °C/min from 31 °C to 450 °C. Following the cracking of glass viewing windows at high temperatures, heating rates were then set at 5 °C/minute above 450 °C to an upper limit of 550 °C. Heating experiments were not conducted to the equipment's maximum limits, as the quartz vein's host rock did not exceed regional greenschist facies metamorphism.

2.4 RAMAN SPECTROSCOPY

The most effective technique for the estimation of qualitative and quantitative volatile components of single FI compositions is, according to Burke (2001) and Frezzotti et al. (2012), the combination of microthermometry data with chemical compositional data obtained from Raman Spectrometry. This is because numerous daughter minerals are not Raman active. Raman spectroscopy was also used to provide an understanding of PTVX properties of fluids at entrapment. Raman gauges energy changes of monochromatic light interacting with Raman-active species (polyatomic molecules or molecular groups). This referred to as the Raman Effect. These molecular entities have several vibrational modes that correspond to specific molecular energy states. The terms for gain or loss in energy for the incident light beam is Stokes and anti-Stokes scattering (Burke, 2001). A Stokes Raman spectrum is a plot of the intensity of scattering vs. the energy gain or loss expressed in wave numbers relative to the source (Δ v cm $^{-1}$, the Raman shift - the changes in wave number compared to the incident light) with the spectral peaks corresponding to the vibrational energy modes (Burke, 2001). Roberts & Beattie (1995) identified different molar volumes if scattering efficiencies are known for different peaks in FIs.

FIs were analysed at the University of Johannesburg's Geology Department using a non-destructive WITec alpha300R confocal laser Raman microscope with a motorised x - y sample stage. Raman spectral measurements were done with a non-polarised 532 nm argon-ion laser. Raman spectra calibration was conducted using a silicon standard. Accumulations were set at 2 to 10 second intervals. Low laser intensities of 5 - 7 watts sets were used with all FIs to prevent band position fluctuations that could adversely affect pressure and composition results. The wavelength constraints of this study were between 100 and 4500.

Compounds relevant for this study using Raman spectroscopy and microthermometry were CO_2, CH_4, H_2S, N_2, H_2O, NaCl, KCl, sulphide inclusions and amorphous carbon or crystalline graphite. Only FIs of ≥2 µm were used for analysis.

3. GEOLOGY AND GOLD MINERALISATION IN THE TNGB

3.1 INTRODUCTION

This chapter deals with the general characteristics of known magmatic and hydrothermal gold mineralisation in the Kibara Belt that potentially could be related to the TNGB's gold mineralisation. Brinckmann et al. (1994) identified two distinct types of gold mineralisation in Burundi and western Rwanda. The first type is associated with post-Kibara granite emplacements that formed gold bearing quartz veins and stockworks. The second type is attributed to the Pan-African event where gold is hosted in hematite breccia zones and associated with mafic wall rocks.

Gold transport appears to be related to reduced sulphur in magmatic and hydrothermal veins in the Kibara Belt (Pohl & Günther, 1990; Brinckmann et al., 2001). Possible structural controls on Au mineralisation are not always evident, but the setting of Au veins is like Sn-W vein systems. Geochemical signatures such as As and Sn enrichment with gold mineralisation is also seen in Sn-W systems. The precipitation of Au is controlled by different factors from the lithophile Sn and W deposits. According to Pohl and Günther (1990) and Brinckmann et al. (2001), the presence of reduced iron and host rock composition is important for the mineralisation of gold. Change in host rock types along a vein may influence the fluid chemistry and subsequent gold mineralisation. The oxidation state is also considered critical in the mineralisation processes. For example, there is a reduction of iron in metadiorites in comparison to metasedimentary rocks. Brinckmann et al. (2001) identified that the initial gold-precipitating fluids in the Kibara Belt contained elevated proportion of liquid CO_2 and were low to moderately saline FIs (7 - 13 wt. % NaCl eq.). The trapping conditions of these fluids was 360 - 450 °C at pressures of 1.7 - 2 kbar. Later fluids presented higher salinities and some fluid inclusions contained halite daughter crystals (Brinckmann et al., 2001).

3.2 REGIONAL GEOLOGY AND GOLD MINERALISATION IN THE TNGB

Banro's TNGB concessions lie on the western edge of the Kibara Belt in South Kivu and Maniema provinces of eastern DRC. They are east of the Tanzania Craton and the Bangweulu Block, and west of the Congo Craton. The Kibara Belt is roughly 1,500 km long, trends NNE-SSW and up to 500 km wide (Pohl, 1994). Fold axes trend north to northeast and folds appear to bend to the west along the Uganda Craton border forming an orocline in the extreme north (Pohl et al., 2013). The Mesoproterozoic Kibara Belt consists of an estimated 10 km thick sequence of the Kibara Supergroup. Primary rocks include siliclastic sedimentary rocks, bimodal volcanic rocks, intraplate mafic sills and rare carbonates (Pohl et al., 2013).

Tack et al. (2010) and Fernandez-Alonso et al. (2012) disputed the interpretation of a single and uniform Kibara Belt. They proposed that two major sub-basins evolved separately with different lithostratigraphic sequences and recommended that the unifying term be abandoned. Tack et al.'s (2010) contestation was that the boundaries between the Meso- and Paleoproterozoic in the South Kivu and Maniema provinces are imprecise as they were not determined by field mapping but by extrapolation from satellite imagery. They further proposed that the south and southwest (DRC and Zambia) be classified as the Kibara Belt, and the northern and northwestern domain (NE DRC, Uganda, Rwanda, Burundi and NW Tanzania) be classified as Karagwe-Ankole Belt. Fernandez-Alonso et al. (2012) reasoned that the formation of the Karagwe-Ankole Belt, to which the Mesoproterozoic basement in the TNGB belongs, is associated with the formation of an aulacogen within the proto-Congo Craton. The rationale was that the Karagwe-Ankole belt underwent an extensive period of sedimentary deposition with extensional or transtensional episodes alternating with possibly two contractional deformation periods that were probably related to global orogenic events (Figure 3.1).

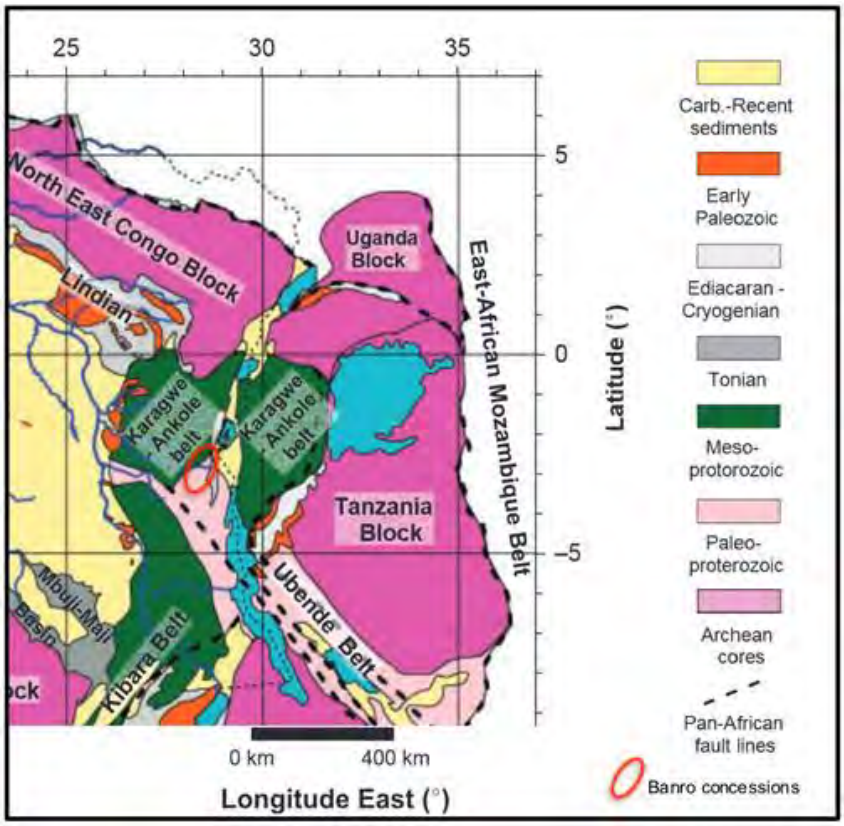

Figure 3.1: Regional geological setting of Banro's concessions (red ellipse; map from Tack et al., 2010).

The association of the basement in the TNGB with the Kibara, Karagwe-Ankole, or the Rusizian periods of deposition and deformation is unresolved. For ease of reference, the term Kibara Belt or NE Kibara Belt will be used for the Mesoproterozoic basement in the TNGB. Cahen et al. (1984) and Pohl (1994) were of the opinion that two regional metamorphic events affected Kibaran sedimentary rocks; with the first event correlating with the formation of batholiths (~1.38 Ma) that formed under intermediate pressures (4 - 5 kbar or ca. 16 - 20 km depth at temperatures of 500 – 600 °C). The second event correlates to the late-/post-Kibara metamorphic

phase associated with G4 granites (~960 - 1000 Ma; Cahen et al., 1984; Pohl, 1994). According to Lehmann et al. (2013), andalusite formed in G4 granite thermal aureoles in metapelitic country rocks. This suggests relatively shallow to mid-crustal emplacement levels and low temperatures of the host rock at the time of emplacement. This is supported by the presence of spodumene in pegmatites - that suggests emplacement at depths of 10 - 16 km. According to Pohl et al. (2013) and Melcher et al. (2015), the regional late-Kibaran G4 granitic magmatism and pegmatite emplacement is widely associated with Sn (Ta-W-Au-Li-Be) mineralisation that took place at the boundary of the Meso- to the Neoproterozoic (~980 Ma). The regional pegmatite and G4 Sn granite emplacement marks the waning stage of the Kibaran orogeny (De Waele et al., 2011 & 2015).

Orogenic structures are dominated by upright to moderately vergent folds (Cahen et al., 1984). The S-type batholithic granites (G1 & G2) that occur in the anticlinoria of these folds are bimodal in composition and distinctly foliated (Cahen et al., 1984). Further work by De Waele et al. (2008) and Tack et al. (2010) concluded that contractional tectonics occurred at 1.38 Ga. They interpreted this as the main structural forming event and the age of the Kibaran orogeny. According to Tack et al. (2010), the major magmatic episode that defined the Kibaran event was followed by a less prominent A-type magmatic activity around 1205 Ma. Further tectonic episodes that postdated the 1.38 Ga main event may be related to the Kibaran orogeny and are largely extensional with a late contractional phase around 1000 Ma (Tack et al., 2010).

The Neoproterozoic tectonic history in the TNGB is poorly understood. Walemba & Masters (2005) attributed the N-S structural trends and the greenschist facies metamorphism in the Neoproterozoic Itombwe Supergroup that overlies the Kibara Supergroup to Pan-African tectonics. The Itombwe Supergroup was deposited over a long period; according to Walemba & Masters (2005), between 1020 ± 50 and 575 ± 83 Ma, and more specifically, according to Fernandez-Alonso et al. (2012) after 710 Ma. The underlying Kibara basement would have been affected by all deformation and metamorphic episodes that are seen in the Itombwe Supergroup. Walemba & Masters (2005) further identified folding and thrusting subsequent to G4 granite emplacement as having occurred during an episode of E-W crustal contraction. According to Cahen et al. (1984) and Walemba & Masters (2005), exposed synclinal structures in the eastern DRC's Itombwe basin developed as late-orogenic Neoproterozoic structures in lower greenschist facies metasedimentary rocks.

It is accepted that the Kibara Belt, formed by Mesoproterozoic rifting of either cratonic or Paleoproterozoic basement, led to the deposition of the Kibara Supergroup, and that the deformation and metamorphism and granitic batholithic intrusions took place at the climax of the Kibaran orogeny at ~1.38 Ga (Tack et al., 2010). A late Kibaran heat pulse at the turn of the Meso-to the Neoproterozoic (960 -1000 Ma), associated with G4 granite emplacement and abundant pegmatites, was the first event associated with ore formation (Sn, Ta, W, Li, Be and Au). During the Neoproterozoic, heat was transferred into the crust episodically, and evidenced by ~720 Ma alkaline and carbonatite intrusions. During the Pan-African orogeny (500 - 600 Ma), Regional metamorphism, as documented in the Itombwe Supergroup, reached greenschist facies conditions (Tack et al., 2010). The crustal evolution in the TNGB is largely unknown (Büttner et al., 2016). At several stages of its

evolution the crust reached thermal conditions conducive to vein formation. Accordingly, any of the Meso- to Neoproterozoic, and in some regions perhaps even Paleoproterozoic events, may have triggered hydrothermal activity and gold precipitation.

3.3 LOCAL GEOLOGY AND GOLD MINERALISATION IN THE TNGB

3.3.1 KAMITUGA

Located in the DRC's South Kivu Province, approximately 100 km southwest of Bukavu and 180 km southwest of Goma, Banro's Kamituga concession comprises three exploration sites covering an area of 649 km² (Banro, 2017) (Figure 3.2).

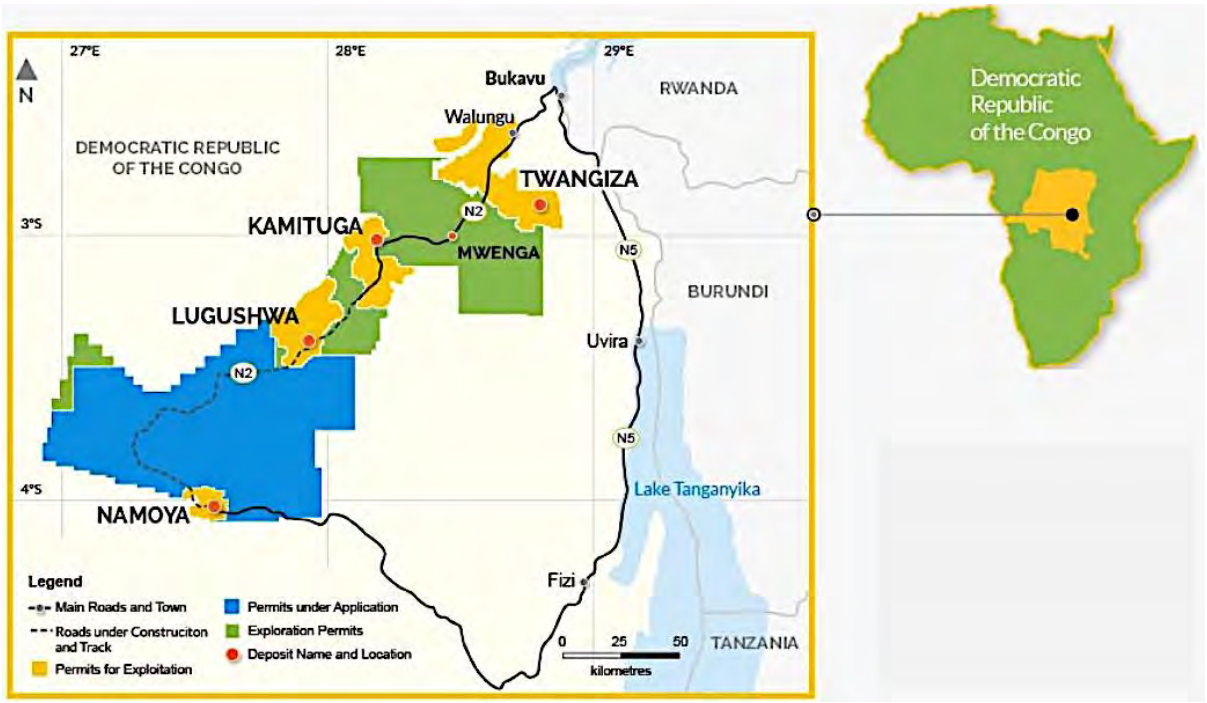

Figure 3.2: TNGB regional map depicting mining exploration and mining (Banro, 2017).

Central regional structural patterns in the TNGB show typical Kibaran NE-SW trends that extend from Kamituga to Lugushwa (Chuwa, 2011). Local, but still km-scale structures in Kamituga include domal structures such as Kibukira in the northwest (Rusill et al., 2009). The Kibukira domal feature (Figure 3.4) was formed on top of a deep-seated granitic intrusion (O'Donovan et al., 2005). Alternately, according to Chuwa (2011), it was due to the rotation of the NNW-SSE trend during an E-W oriented contraction (Figure 3.3). NE-SW regional folds predominate in the southern portion of Kamituga but are cut off by the E-W shear zone in the central portion of the concession (Chuwa, 2011). Gold mineralisation may be related to the formation of the proximal Kibukira dome and/or the intersection of older Kibaran with younger transecting structures (O'Donovan et al., 2005) (Figure 3.3, 3.4 & 3.5). The occurrence of numerous, and in part well-mineralised tourmaline veins at Kibukira and the strong E-W trend of the mineralised veins at Mobale, indicate that the Kibukira-Mobale area was a preferred zone of fluid influx during mineralising events. The number of fluid influx events and their individual association with gold deposition is, however, unclear. The lithology at Kamituga includes a thick pelitic to

psammo-pelitic metasediment sequence. Biotite-muscovite is the peak-metamorphic assemblage. This indicates that greenschist facies was not exceeded during regional metamorphism. Young Neogene basalts cover large parts of the Au-mineralised basements (Figure 3.4).

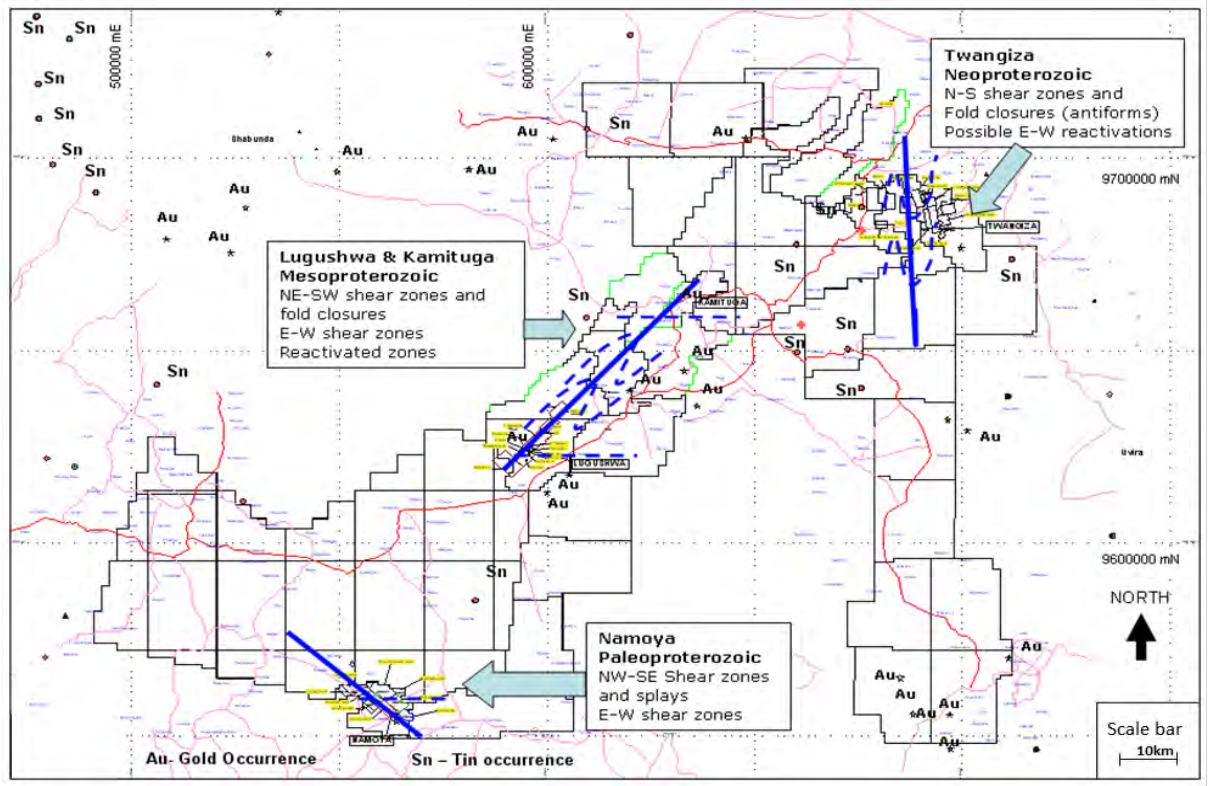

Figure 3.3: The regional structural patterns in the central TNGB show typical Kibaran NE-SW trends that extends from the Kamituga to the Lugushwa deposit (Chuwa, 2011).

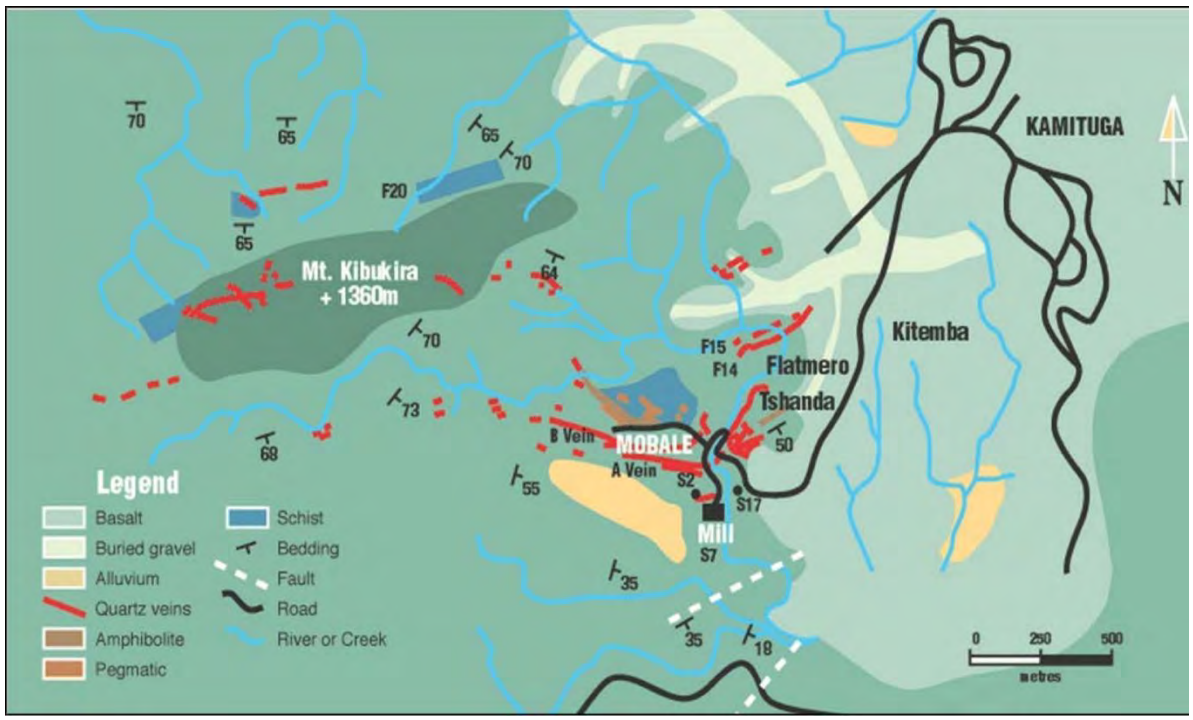

Figure 3.4: Geological map of Kamituga (Mobale) and surrounding prospects. Note the Kibukira domal feature in the northwest (Chuwa, 2011).

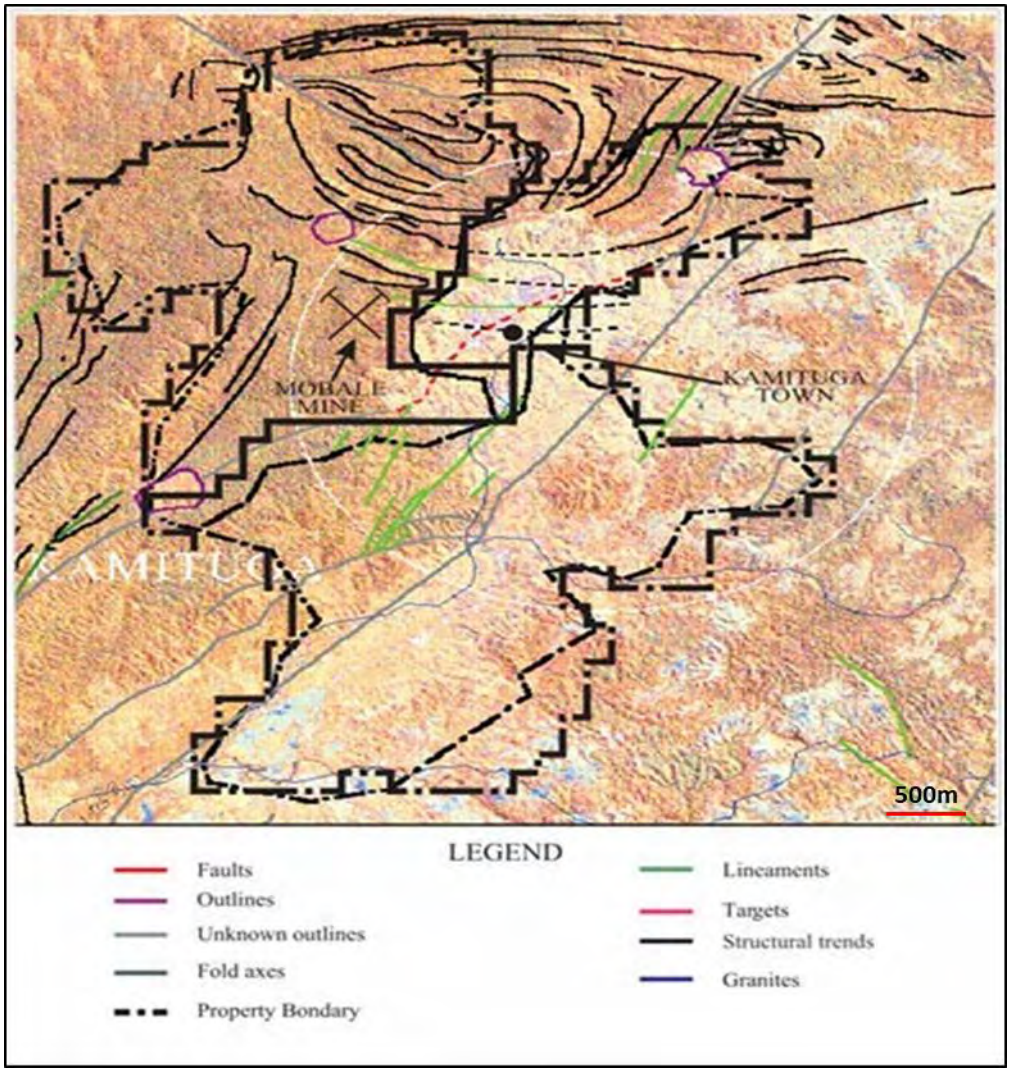

Figure 3.5: Kamituga concession with interpreted structures surrounding the Mobale mine (O'Donovan et al., 2005).

According to O'Donovan et al. (2005) the NE-SW structural trend in the southern and central portion of Kamituga represents regional Mesoproterozoic structural grains. Conjugate veining in the E-W and NW-SE fractures and faults were interpreted as having resulted from the reactivation of the Kibaran structures during the Pan-African orogeny (O'Donovan et al., 2005). They further identified that mineralisation was dominant in robust (non-oxidised) quartz veins that are concordant with the E-W striking 30° to 40° south dipping foliation.

Metapelites typically show well-developed cleavage. The metasediments are intercalated with amphibolite and pegmatitic/granite-greisen intrusive bodies. Metasediments display distinctive contact metamorphic halos when in close proximity to intrusive bodies (both felsic and mafic). Common contact zoning contains actinolite, hornblende, staurolite, garnet (grossular)-biotite–muscovite (O'Donovan et al., 2005). Schists grade into phyllites or quartzites. Quartzites are associated with conglomerates (Chuwa, 2011). Pegmatites range from a few centimeters to meters in thickness with large dikes able to be followed along strikes for several hundred meters. The mineral assemblage of these dikes is predominately quartz, plagioclase, alkali feldspar and muscovite. Accessory minerals such as tourmaline, apatite, spessartine, beryl, spodumene occur together with

sulphides (Chuwa, 2011). Neogene alkaline basalt-containing olivine phenocrysts cover large portions west of the deposit. Access to some high-grade mineralised zones and to placer deposits is made difficult by thick basaltic flows that are up to 25 m thick (Figure 3.3).

Gold deposits in the Kamituga concession, most notably at Mobale, but also other surrounding prospects, occur in proximity to swarms of pegmatitic, tourmalinite and greisen units (Figure 3.4). O'Donovan et al. (2005) proposed that greisens and pegmatitic bodies indicate the involvement of granitoid bodies at shallow depth in the formation of Au, Sn and W mineralisation. The presence of such metals is demonstrated by sphalerite, unspecified antimony mineralisation chalcopyrite together with scheelite and cassiterite in some places (O'Donovan et al., 2005). The relationship between gold precipitation and other metals has, however, not been determined.

Quartz veins ranging from <1 mm to 1.5 m in thickness occur as planar and brittle discordant sheets to discontinuous thin pods and boudins. Some veins show folding with centimeter to meter amplitudes, and, according to Chuwa (2011), belong to earlier fluid influx episodes. Folded veins crosscut by planar veins suggest polyphase hydrothermal fluid influx alternating with regional tectonic events. The Mobale pit is, according to Chuwa (2011), a good example of this (Figure 3.5). O'Donovan et al. (2005) described gold mineralisation as predominately bound to quartz veins and their wall rock lithologies (almost exclusively schists), and high-grade gold depositions to be found only in quartz veins and stockwork systems that contain sulphides (mainly arsenopyrite and pyrite) within schists. Pyrrhotite, galena, stibnite and sphalerite may also be present in addition to pyrite and arsenopyrite in Kamituga's quartz veins. Quartz vein contacts are sharp - indicating minimal incorporation and alteration of the host rock. Mineralised veins have a two-phased gangue component composed of coarse-grained milky-white quartz grains and fine-grained opalescent sucrose quartz that may host visible gold. The latter phase was produced by the brecciation and re-precipitation of the former phase when the vein underwent strain (O'Donovan et al., 2005).

3.3.2 LUGUSHWA

Located in the DRC's South Kivu Province, approximately 150 km southwest of Bukavu and 240 km southwest of Goma, Banro's Lugushwa concession covers 641 km². As in Kamituga, Lugushwa contains three exploration sites (Banro, 2017) (Figure 3.2). The regional NE-SW Kibaran trend is the most prominent structure but is crosscut by a subsequent regional shearing (ENE-WSW) (Figure 3.6). The degree of metamorphism is similar to that of Kamituga (lower greenschist facies). Shear zones in Lugushwa display intense foliation in the dominantly meta-sedimentary schists (O'Donovan et al., 2005; Skead, 2007). Auriferous quartz veins outcrop at Mapale, Simali, Lugushwa and Kakangara's summits (Figure 3.7).

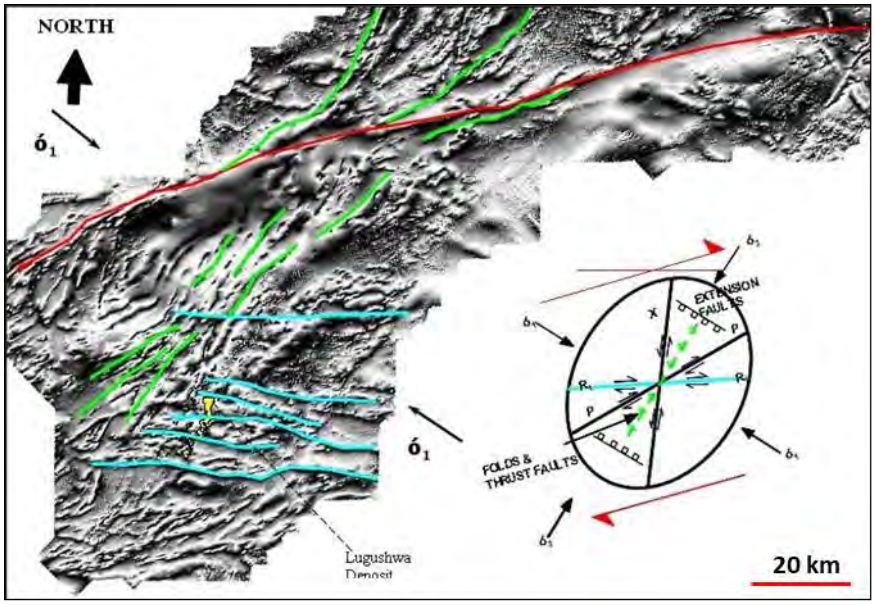

Figure 3.6: Magnetic intensity data highlights Lugushwa's regional NE-SW structural grains and interpreted regional shear zones and folds (Chuwa, 2011).

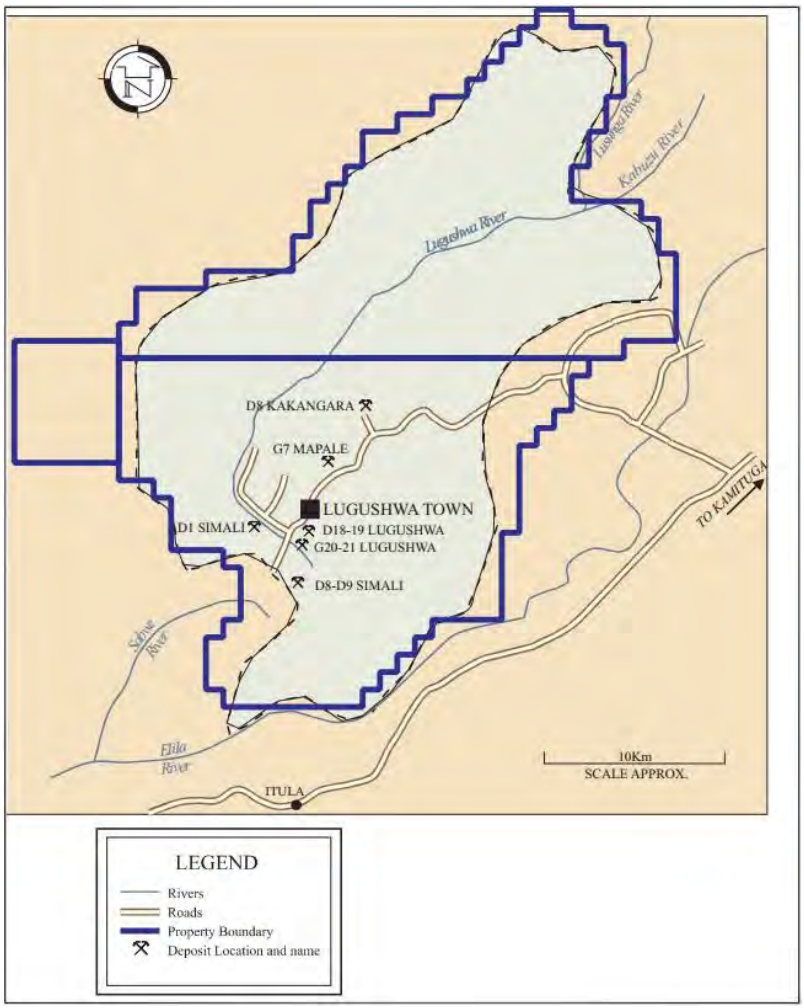

Figure 3.7: Lugushwa concessions depicting ore deposits (O'Donovan et al., 2005).

Lithologies (from the lower beds up) include: (i) Quartzites and sandstones - mainly massive and often interbedded with schists. (ii) Chloritic schists and micaschists - red to grey in colour, frequently with disseminated sulphide agglomerates - mainly arsenopyrite. These schists constitute the bulk of the lithologies present in Lugushwa and are described as highly altered and fine-grained (O'Donovan et al., 2005). Blue-violet schists contain tourmaline and garnet. Feldspar was found only occasionally (D1 Simali 'Filon de Luxe' deposit). (iii) Amphibolites presented in three thin bands, predominantly in the Mapale deposit. They are fine-grained massive or schistose. (iv) Granites and pegmatites - located at peripheries of the concession are associated with Sn mineralisation. (v) Quartz veins - stringers and stockwork are present in all Lugushwa's lithologies.

The main Lugushwa deposit is located in a km-scale, northeast plunging, broad, open anticline with parasitic folds and shear zones (Figure 3.8). Lugushwa's E-W Riedel shears are prominent in the southern portion of the concession (Fall, 2007a; Fall & Chuwa, 2007). As in Kamituga, the E-W trending faults were repetitively reactivated. The mineralisation is located within a 1 km long segment bound by two NE-SW shear zones (Figure 3.6). Mineralised quartz veins range from 3 to 50 cm and are predominantly non-fibrous and coarse-grained. Thicker shear zones contain veinlets and stringers (associated with sulphides and calcite) that extend into the country rock. Crosscutting veinlets are typical in the more intensively veined areas (Fall & Chuwa, 2007).

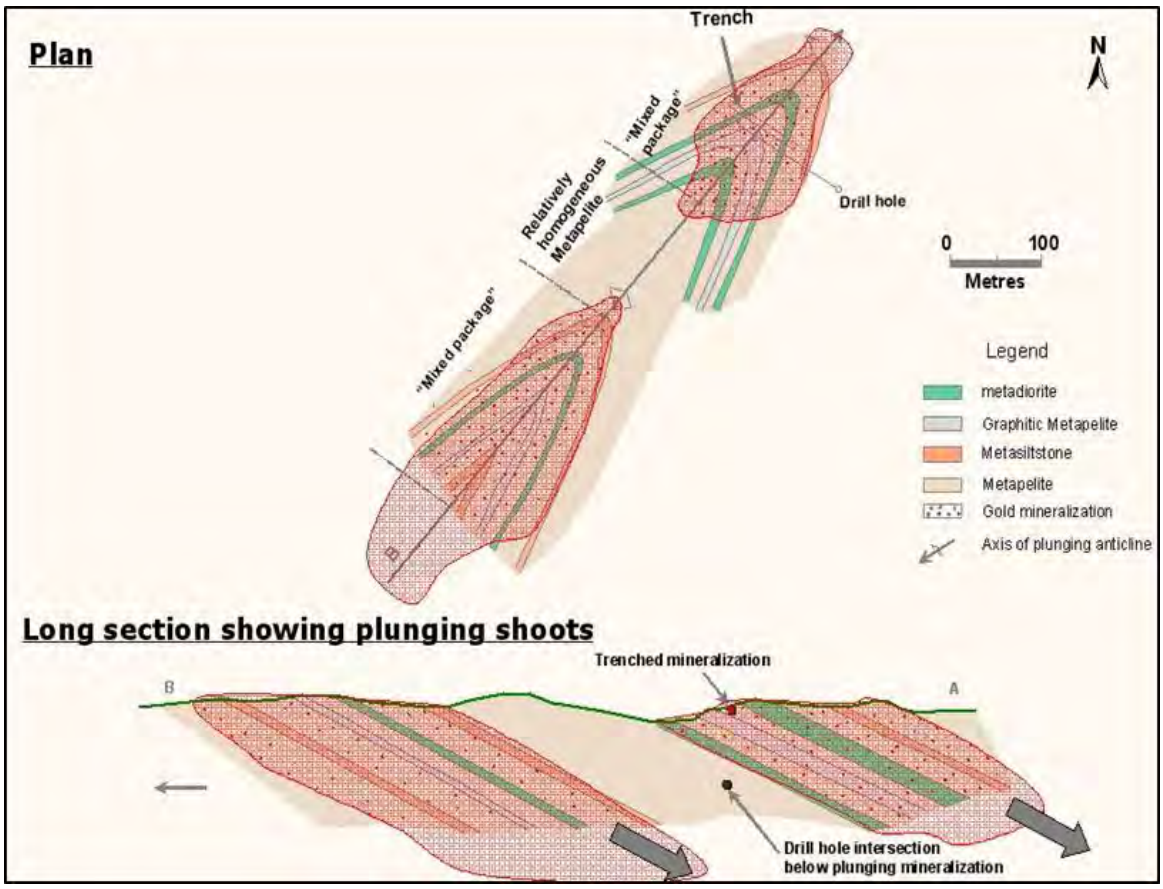

Figure 3.8: Geology and structural control of mineralisation in Lugushwa (Fall & Chuwa, 2007).

Mineralisation in veins and stockworks is associated with dissemination of arsenopyrite, tourmaline, biotite and chlorite alterations (Fall & Chuwa, 2007). Hydrothermal alteration zones are more apparent within hinges of NE-plunging folds at boundary regions of interbedded metasiltstone and metapelites.

Mineralised zones in fold hinges are hosted within interbedded metapelites, intercalated with metasiltstones and quartzite and intruded by undulating metadiorites sills (5 - 80 m thick). Gold mineralisation in Lugushwa predominately occurs in intercalated metabasites, quartzitic-sandstone and sulphide-bearing (mainly arsenopyrite) schists. Schistose metapelites with quartzitic interlayers correlate with high gold grades, whereas homogeneous metapelites are less mineralised or contain no mineralisation (Figure 3.8). Disseminated gold mineralisation in host rock schists is seen but is not always associated with arsenopyrite. The style and extent of mineralisation in the host rock is not known as prior research only investigated high-grade quartz veins and stockworks (Fall & Chuwa, 2007). The mineralised quartz veins contain small amounts of sulphides, carbonate, tourmaline, and micas and, in rare cases, barite and cassiterite. Surface mapping and drill core structures depicted a near-parallel relationship between orientation of bedding, foliation and quartz veins (Figure 3.9). This suggests hydrothermal injections along planar structures, and thereby a certain degree of structural control over mineralisation.

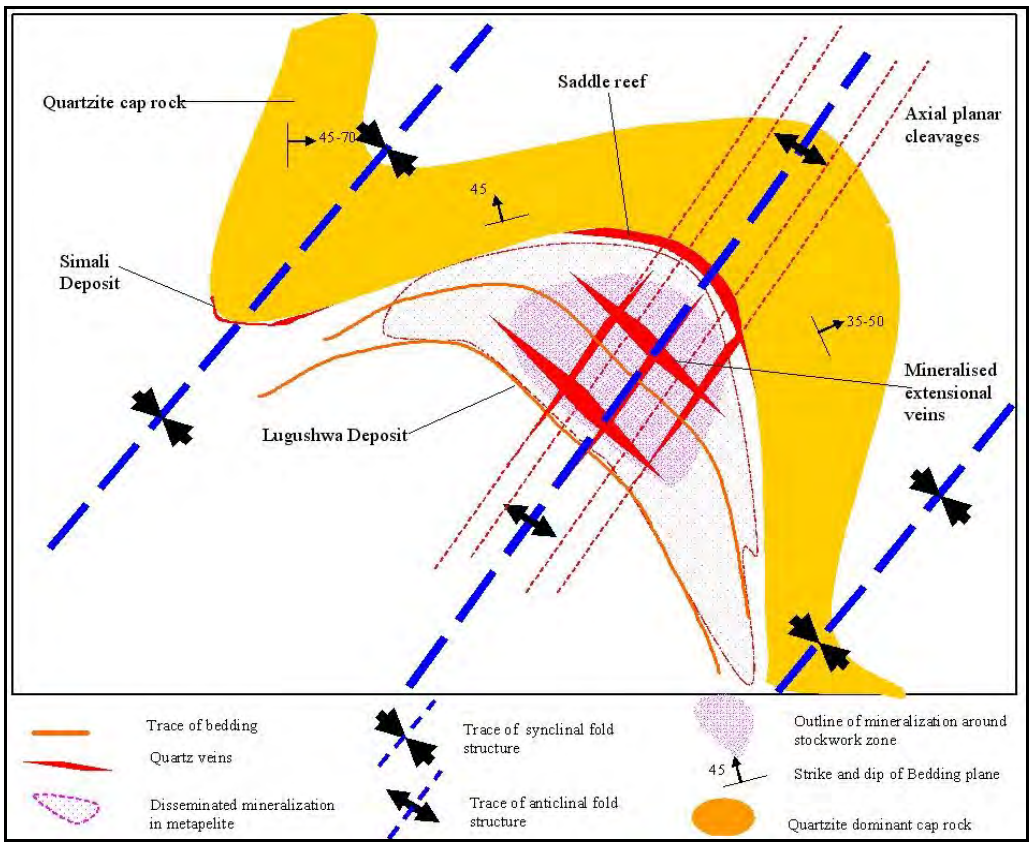

Figure 3.9: Structural controls and mineralisation features in Lugushwa (Chuwa, 2011).

3.3.3 NAMOYA

Located in the DRC's Maniema Province approximately 225 km southwest of Bukavu, Banro's Namoya deposit extends across the boundaries between the NW-SE trending Paleoproterozoic (Rusizian) basement in the northeast and Karoo-age (Mesozoic) sediments in the southwest (Banro, 2017). This variable geology corresponds to a change in topography from the mountainous northeast to open plains in the southwest. The two main lithologies in the area are metasedimentary and hypabyssal intrusive rock that had undergone lower to mid-greenschist facies metamorphism and deformation (Chuwa, 2011). The Paleoproterozoic structural trends in Namoya differ from the Kibaran trends in Kamituga and Lugushwa. Landsat imagery taken south of Namoya depicts folds with fold axes plunging at a shallow to moderate angle towards WNW and ESE. The folds are bounded by large scale WNW and ESE trending dextral thrust faults (Chuwa, 2011). The NW-SE structural grain in the northeastern part of the deposit extends to the central portion of the deposit (Mbuya et al., 2008). The intersection between NW-SE and conjugate subordinate E-W structures resulted in circular to oval shaped structural features. Other overprinting NE-SW planar features abruptly end at a NW-SE shear zone (Fall, 2007b). The highest gold grades in Namoya are located within this zone (Figure 3.10).

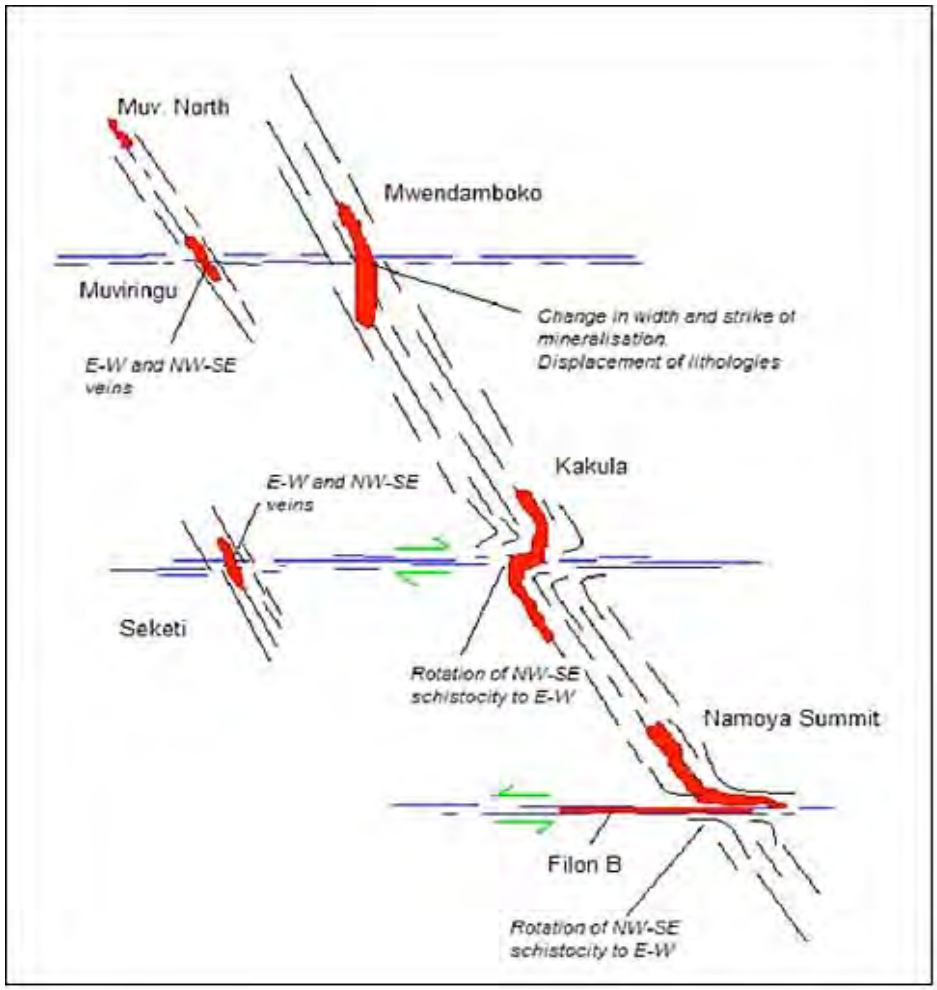

Figure 3.10: Conjugate shear zone intersections and relationship of orebodies (red) in Namoya (Mbuya et al., 2008).

The metamorphic grades in Namoya vary from low- to mid-greenschist facies, somewhat higher than in Lugushwa and Kamituga. This higher grade is also expressed in the presence of a distinctively stronger foliation compared to Kamituga and Lugushwa. Abundant sericite and chlorite in schistose fabric of metasediments are present throughout the deposit. Quartz veins and stockworks are hosted by schistose metasediments that had been intruded by sills and dykes. Quartz veins show pinch-and-swell structures, boudins and small-scale folding. Characteristics of Namoya's metasedimentary rocks are, according to Chuwa (2011), (i) Sericite schist - fine-grained, varied in colour, depending on chlorite content, from green to beige. Contains quartz, sericite, carbonate, chlorite and opaque minerals in variable proportions and grain sizes. (ii) Graphitic schist - dark grey in colour, rich in graphite with sericite, minor quartz and carbonate, and potentially has a carbonaceous mudstone or shale as protolith. (iii) Silicified schist - has characteristics of hydrothermal alterations and consists of feldspar, micas and quartz with shale/siltstone protolith features.

Dolerite and quartz porphyry are the main intrusive igneous rocks found in Namoya. The characteristic hydrothermal alteration assemblage is described by Chuwa (2011) as "intense quartz veining with associated silicification and sulphidation of host rock". Alterations grade into chlorite-sericite carbonate schist with decreasing silicification (Chuwa, 2011).

The strong NW-SE structural control at Namoya is perpendicular to the Kibaran trend and therefore not a typical Pan-African event. The oblique angle, according to O'Donovan et al. (2005) indicates a reactivation of earlier structures. Multiple injections resulted in numerous quartz vein phases. There appears to be a correlation between thick veins, small spacing and high gold grades. Tourmaline is associated with quartz veins, particularly in the upper levels of Mwendamboko.

Mineralisation in the Namoya deposit appears to be structurally controlled along a 2.5 km NW-SE trending corridor dominated by sericite schist that hosts irregular quartz vein and stockwork zones. Mineralisation is prominent along ridgelines and the summits of Mt. Mwendamboko, Mt. Namoya, Mt. Kakula and Mt. Muviringu. The mineralised quartz veins and stockworks are sub-vertical, have pinch-and-swell features and are characteristic of shear zone vein swarms. The term 'stockworks' is applied loosely as they are not orthogonal in the true sense of the term. Irregular sheets, nested vein sets, ladder veins and veinlets are at low angles to each other (O'Donovan et al., 2005).

The high-grade ore body, Filon B, located SW of Mt. Namoya's summit, is hosted in E-W quartz veins along a shear zone (Figures 3.10 & 3.11). The mineralisation is considered to have occurred in structures formed during brittle-ductile shearing (O'Donovan et al., 2005). These structures plunge either moderately or steeply to the SE (Banro, 2017). Mineralisation along Mwendamboko-Namoya ridge occurs along a NW-SE dextral shear zone, with the highest-grade areas associated with E-W and NNW-SSE crosscutting shear zones (Figure 3.10).

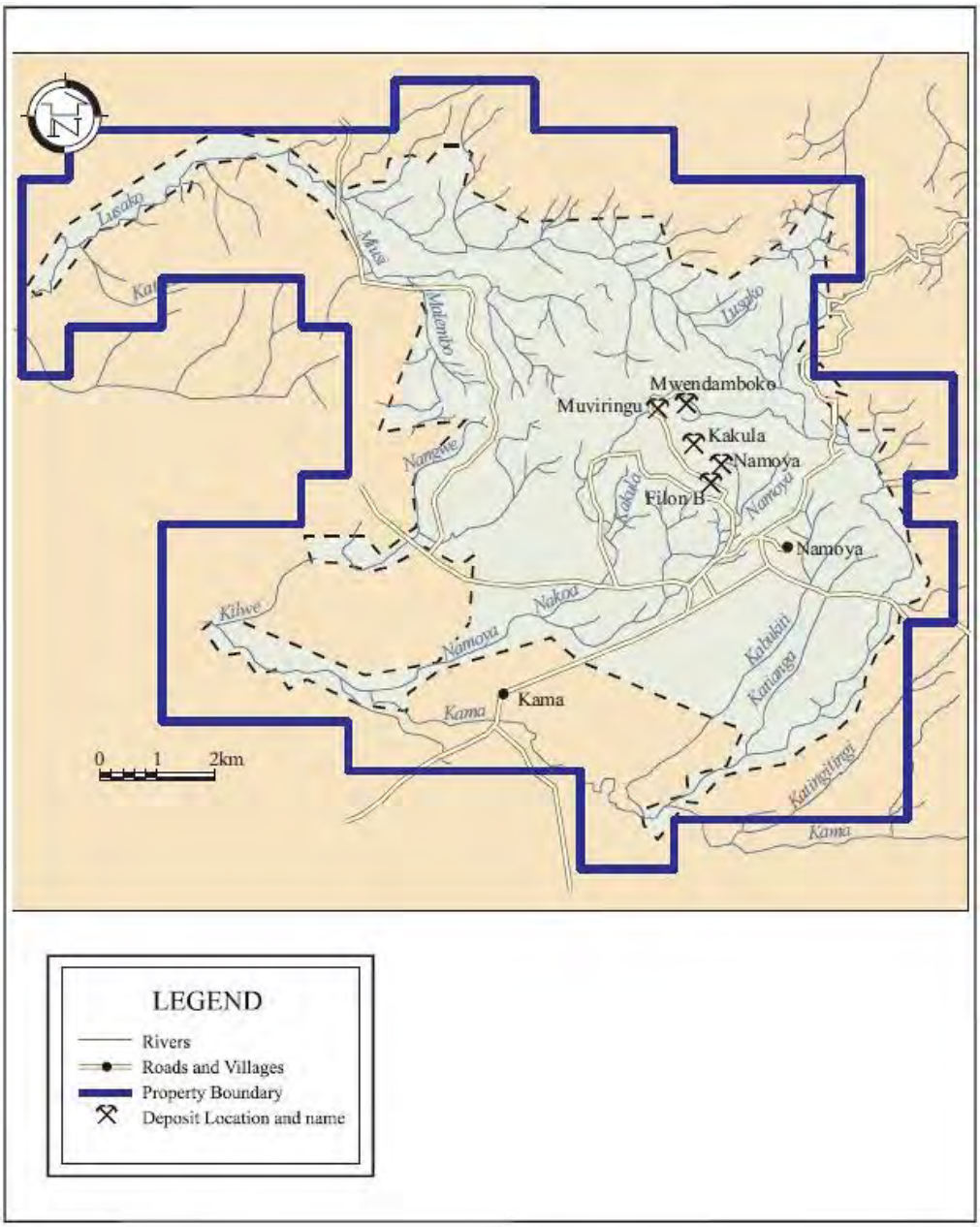

Figure 3.11: Namoya concessions depicting ore deposits (O'Donovan et al., 2005).

Geochemical analysis of mineralised veins indicates increased levels of gold with arsenic, tin, barium, lead and copper (Fall, 2007b). Mineralisation is also associated with sulphides (primarily pyrite and arsenopyrite), tourmaline and calcite in close proximity to quartz veins (O'Donovan et al., 2005). The highest grades of gold are in sulphide-rich quartz veins and stockwork zones hosted in schist - specifically at quartz and sulphide grain boundaries (O'Donovan et al., 2005). O'Donovan et al. (2005) proposed that the NW-SE shear zone is a long-lived, multiple reactivated shear zone - possibly with a Kibara and a Neoproterozoic Pan-African kinematic history.

4. FIELD AND MESOSCOPIC OBSERVATIONS

Field and mesoscopic observations outlined in the following chapter describe the origin and characteristics of the 42 quartz-dominant vein and host rock samples from Kamituga, Lugushwa and Namoya. This chapter does not contain evidence from thin section observations. The relevant microstructures will be described in the context of the fluid inclusion petrography in Chapter 7.

4.1 KAMITUGA

The Kamituga concession is dominated by metasediments that predominantly consisting of schists, quartz phyllites and metapelites. Both amphibolite and metadiorites are typical and are associated with pegmatites and greisen units that suggest granitoid bodies at shallow depths. Both metadiorites and amphibolites are intercalated with metapelites. Hydrothermal alteration is restricted to zones of quartz veining and stockworks. The nature of the alteration varies depending on host rock lithology.

4.1.1 PEGMATITE AND TOURMALINE

The pegmatite from which Ktm-3 from drill core KDD033 was sampled, is approximately 3 cm thick. It is light grey/green to dark grey in colour and ranges from fine- to coarse-grained. It is dominated by large equant quartz, feldspars (albite and alkali feldspar), muscovite (> 1mm) and tourmaline (Figure 4.1). The pegmatite sample contains minor sulphide (pyrite and arsenopyrite) but no visible gold within or near the pegmatite.

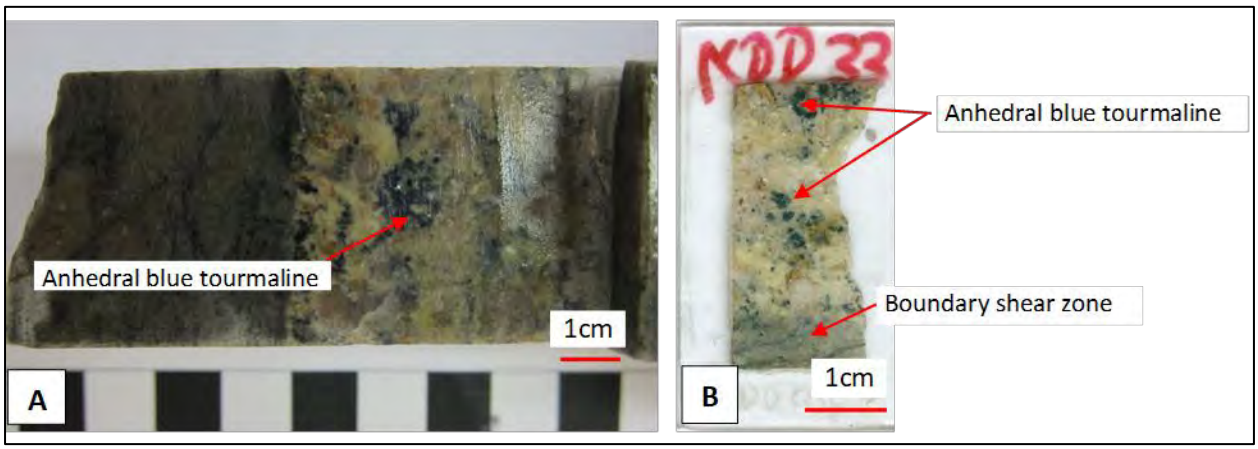

Figure 4.1: (A) KDD033 pegmatite drill core. Ktm-3 sample. (B) Thin section cut from Ktm-3. A muscovite rich pegmatitic vein with abundant blue anhedral tourmaline. Not mineralised.

A blue and a fine-grained brown tourmaline is present in pegmatite sample Ktm-3. The blue tourmaline is located in the centre of the earlier formed (primary) quartz gains. The brown fine-grained tourmaline forms segregated phenocrysts within the alteration halo of the quartz vein and is interpreted as a metasomatic phase, whereas the blue tourmaline is considered pegmatitic (cf. Büttner et al., 2016). Blue tourmaline is present only in the pegmatite vein. Brown fine-grained tourmaline, however, is also observed outside of the pegmatite vein where it may form zones of massive coarse-grained quartz with clusters or stringers of acicular brown to greenish tourmaline (15% to 20% of rock volumes; Figure 4.2). The accessory minerals associated with this tourmaline are biotite, muscovite, orthoclase and sulphides (arsenopyrite with minor pyrite).

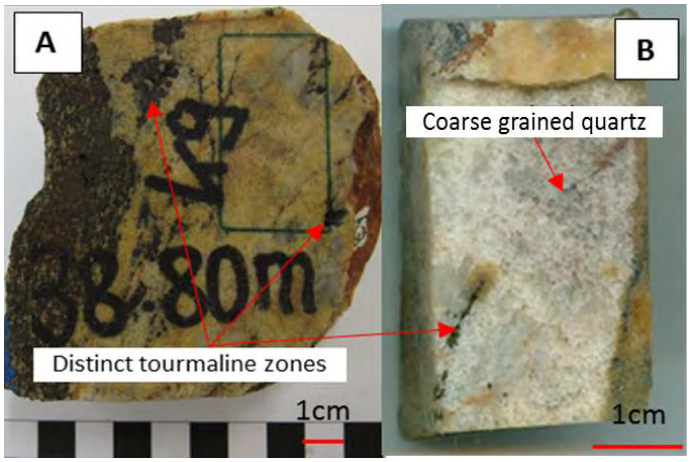

Figure 4.2: (A) K9 core sample. (B) Block displaying distinct coarse-grained quartz within a tourmaline-rich foliated quartz diorite. Au mineralised 0.36 g/t.

4.1.2 METABASITE AND DIORITE (ORTHO-AMPHIBOLITE)

Kamituga's metabasites occur as both massive bodies and as schistose rocks along shear zones. The mineral composition is consistent across all selected samples, with a predominance of hornblende, actinolite, quartz, biotite and muscovite with accessary plagioclase and sulphides (pyrite, pyrrhotite, chalcopyrite and arsenopyrite). Metabasites, logged as amphibolite by Banro (2017), display a distinct foliation formed by biotite. Primary magmatic phases, such as hornblende and plagioclase are largely replaced by the assemblage that was stable during the greenschist facies conditions of the metamorphic overprint - most frequently chlorite and biotite.

The metabasites grade into less sheared and metamorphosed dioritic rocks, in which more of the primary igneous texture and assemblage is preserved and show intense alterations. Such altered diorites contain ~20 vol % hornblende, ~25 vol % quartz and feldspar (orthoclase and albite) and ~30 vol % secondary white mica, chlorite and minor biotite. Tourmaline and sulphides are present in variable amounts 5 - 15 vol % (Figures 4.2, 4.3 & 4.4). Both tourmaline and sulphides occur along fracture zones - although tourmaline is also found as intragranular grains in quartz.

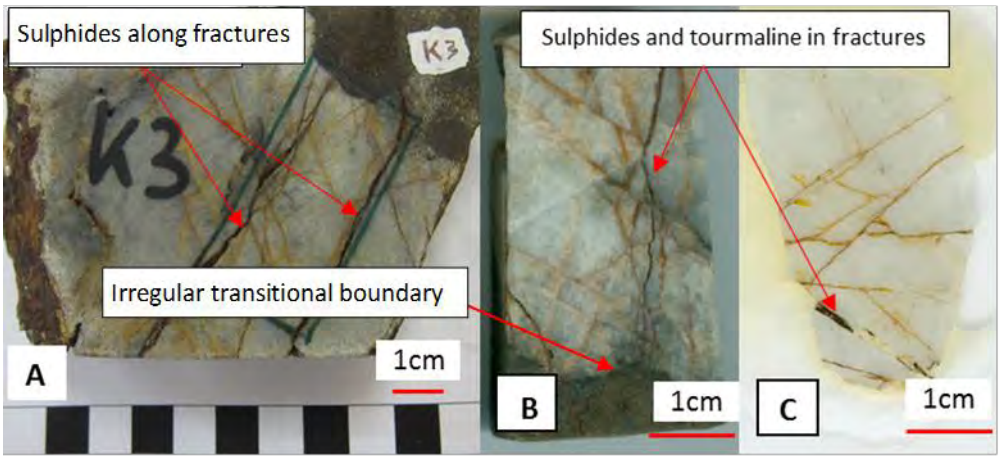

Figure 4.3: (A) K3 core sample. (B & C) Block and thin section. Quartz vein has an irregular and transitional boundary with tourmaline alteration in weathered diorite. Note the abundance of sulphides and tourmaline along fractures. Au mineralised 1.69 g/t.

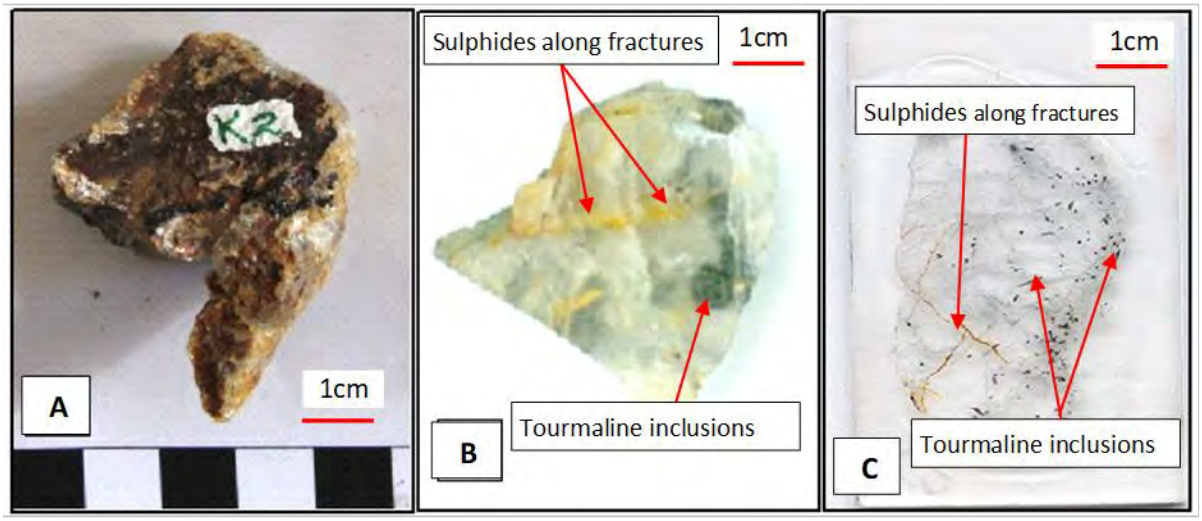

Figure 4.4: (A) K2 outcrop sample. (B & C) Block and thin section. Quartz sample was hosted in slightly weathered diorite. Tourmaline is interspersed as inclusions in quartz. (C) Sulphide occurs along secondary fractures. (B) Au mineralised 0.6 g/t.

4.1.3 SCHIST

Siliceous and mica schists were found in Kamituga. Light green siliceous schist is associated with extensive quartz veining and stockworks. The mineral composition is chlorite, sericite and epidote - with variable amounts of muscovite, biotite and minor sulphides (< 5 %, pyrite and arsenopyrite). Sucrose quartz occurs together with granoblastic quartz in quartz veins and disseminated within hosted rock siliceous schists. The light grey to dark grey mica schist, most likely derived from a pelitic protolith, consists primarily of biotite with less abundant quartz, muscovite and sulphides (primarily pyrite, some arsenopyrite). Amorphous and crystalline graphite occurs in small but variable amounts in both quartz and mica rich schists. In quartz veins associated with these schists, the amount of disseminated sulphides and graphite correlates with the apparent degree of hydrothermal alteration in the alteration halo. Sulphides seldom exceed 5 vol % in alteration zones or quartz veins.

4.1.4 METAPELITE

Weakly foliated, very dark grey to black graphitic metapelites predominate in the Kamituga area (Figures 4.5, 4.6 & 4.7). Slightly laminated metapelites contain carbonaceous material together with muscovite, biotite, chlorite, albite and quartz and are associated with hydrothermal alterations and minor schistose zones near quartz veins. Chlorite, carbonate and sulphide reaction halos line the margins of quartz veins within sulphide bearing metapelites (Figure 4.7).

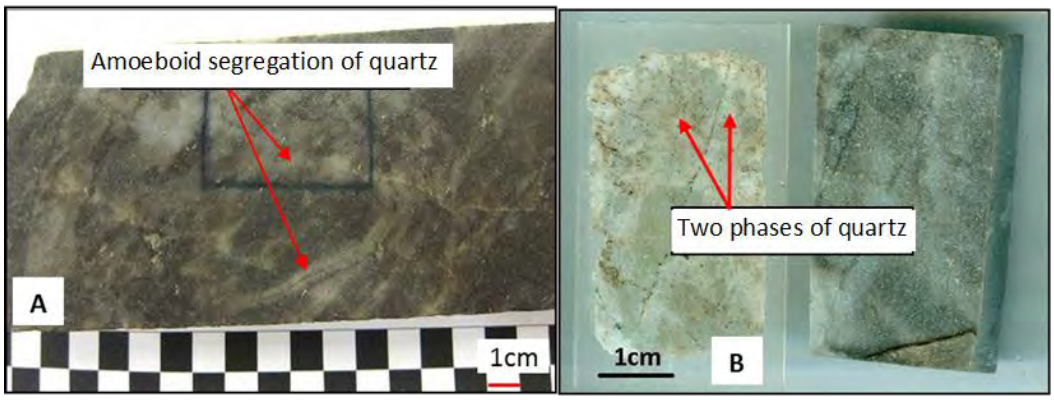

Figure 4.5: (A). K16 core sample. Amoeboid segregation of vein quartz out of dark quartz-rich metapelite. (B). Thin section (left) and cut-off block (right) showing two quartz phases. Large transparent crystals are surrounded by a finer-grained light-coloured quartz variety. Not mineralised.

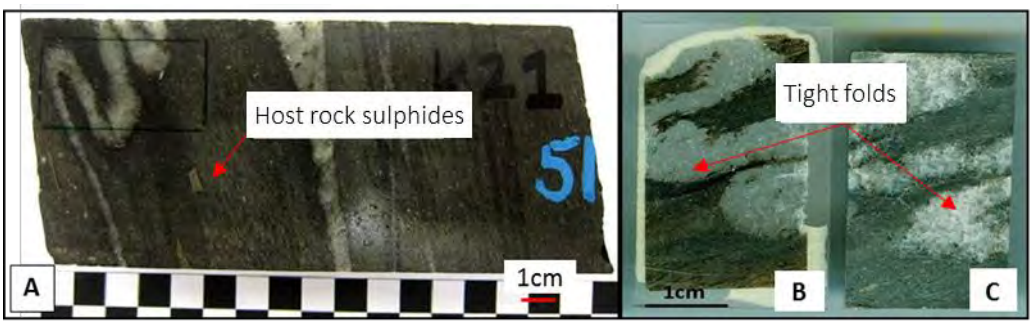

Figure 4.6: (A) K21 core sample. (B) Thin section and (C) Block. Tight small-scale folds in the quartz vein and prominent pyrrhotite grains in the host rock metapelite. Au mineralised 1.07 g/t.

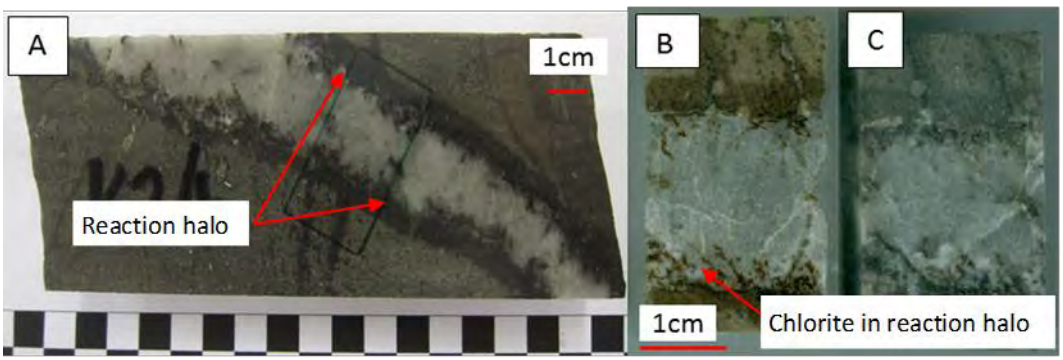

Figure 4.7: (A) K24 core sample. (B) Block and (C) Thin section. Chlorite and sulphide reaction halo lining margin of quartz vein within sulphide bearing metapelite. B shows chlorite along hydrothermal quartz grain boundaries. Not mineralised.

4.1.5 QUARTZ PHYLLITE

Finely laminated (≤ 2 mm) phyllite consists primarily of fine-grained quartz and mica that is typically stained red by iron oxides. Minor amorphous and crystalline graphite is present together with fine-grained chlorite and sericite. This gives a golden waxy sheen to laminated surfaces. Phyllites do not usually show quartz veining or stockworks.

4.1.6 QUARTZ VEINS

Quartz veins range in thickness from < 1 mm to over 1.5 m. The full lateral extent of the veins is, however, unknown due to poor exposure. Vein characteristics are highly variable from pinch-and-swell, boudins to discordant planar veins and stockworks. Folding in thin veins of less than 2 cm thickness suggests fluid influx preceded a major regional deformation episode (Figure 4.6). Two distinct quartz phases were identified in veins; a coarse prismatic, milky-white fluid inclusion-rich quartz, and a fine-grained opalescent sucrose quartz. Textural characteristics indicate that the fine-grained opalescent sucrose quartz was formed by recrystallisation of the earlier coarse prismatic phase (Figure 4.8; see Chapter 7 Figure 7.10 for further details). Opalescent sucrose quartz in Kamituga appears to correlate with elevated gold grades (Chuwa, pers. commun. February 2014). The two quartz phases are both associated with variable amounts of sulphides, such as pyrite, arsenopyrite, pyrrhotite, galena and sphalerite.

Amoeboid segregations of quartz in metapelites with diffuse and irregularly shaped boundaries to the hosting metapelite (Figure 4.5) suggest that the fluids from which this vein's quartz was precipitated were mobilised in the pelitic host rocks nearby via more-or-less in-situ segregation and precipitation. Hence, material from the metasedimentary sequence may have contributed to the formation of the hydrothermal system in Kamituga. Similar patterns that suggest fluid activity proximal to its source are seen in places in Lugushwa and Namoya. However, most commonly the contacts between hydrothermal veins with their host rocks are sharp or show gradual boundaries along overall planar or folded contacts. These veins appear to have formed by hydraulic fracturing, fluid influx and precipitation of materials distally sourced.

Disseminated vein material in the host rock adjacent to veins is typically pyrite. Conversely, entrainment of small host rock fragments is a common feature within hydrothermal veins. Small vein offshoots in metapelitic or dioritic host rocks contain biotite, muscovite/ sericite, tourmaline and sulphides. The sulphides are primarily located within the sacchoroidal (sucrose) quartz component of veinlets.

Mineralised veins and stockworks are rich in tourmaline and sulphides (Figures 4.2, 4.3, 4.4, 4.8 & 4.9). Light green siliceous schist and graphitic metapelites and altered metadiorites contain the bulk of mineralised veins. Arsenopyrite is the dominant sulphide in veins and disseminates into the host rock (Figure 4.3 and 4.9).

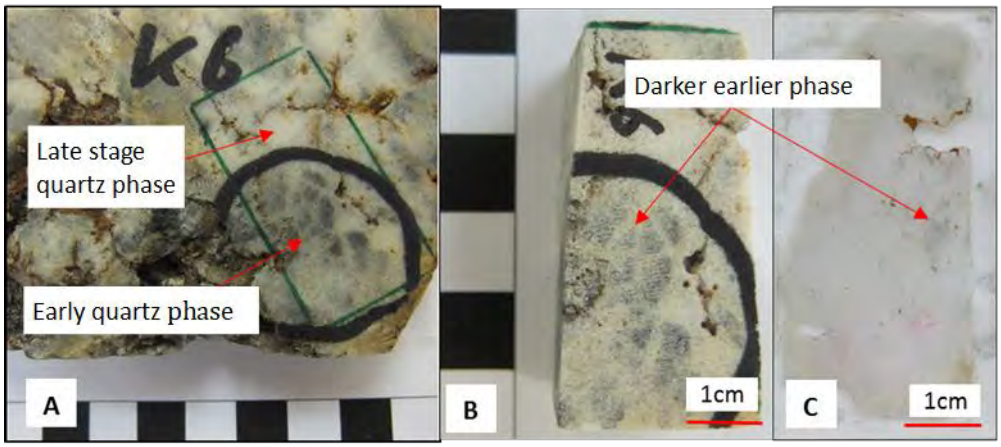

Figure 4.8: (A) K6 core sample. (B) Block and (C) Thin section. Note the variance in quartz type - the earlier dark quartz within the lighter quartz. Pitting due to sulphide resorption is visible throughout the sample. Au mineralised 1.69 g/t.

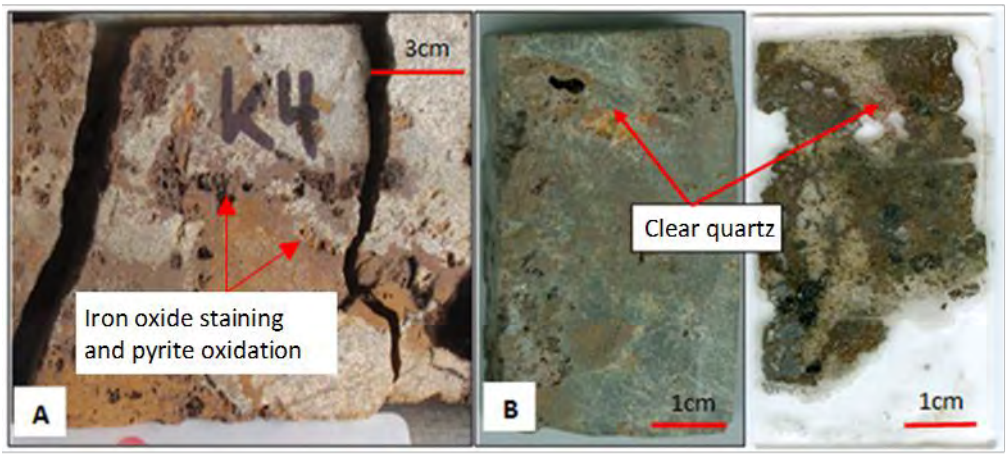

Figure 4.9: (A) K4 core sample. (B) Block and (C) Thin section. Altered sulphide-rich and weathered diorite, with minor disrupted quartz veins. Au mineralised 12.5 g/t.

4.2 LUGUSHWA

Rock in the Lugushwa area are dominantly weakly to moderately foliated and fine-grained. The foliation is less prominent than in Kamituga's metasediments. Intense cleavage is rare and confined to local shear zones. Most metasediments are metasiltstones and metapelites that are biotite-, muscovite- and chlorite-rich and contain secondary carbonates and sulphides. Calcitic carbonate veins form at high angles to host rock layering and carbonates spread out along the interface of metasediment and concordant quartz veins. Thin carbonate veinlets crosscut quartz veins, suggesting that the influx of carbonaceous fluids post-dated the formation of quartz veins (Figure 4.10).

Carbon and crystalline graphite appear to be hydrothermal precipitates and are restricted to thin interbedded transitions of metapelite to metasiltstones or metadiorites. The pegmatites and associated quartz veining in Lugushwa are similar to those in Kamituga, although pegmatites and granitic bodies are less frequently intersected in drill holes. Pegmatites and granites are not gold mineralised.

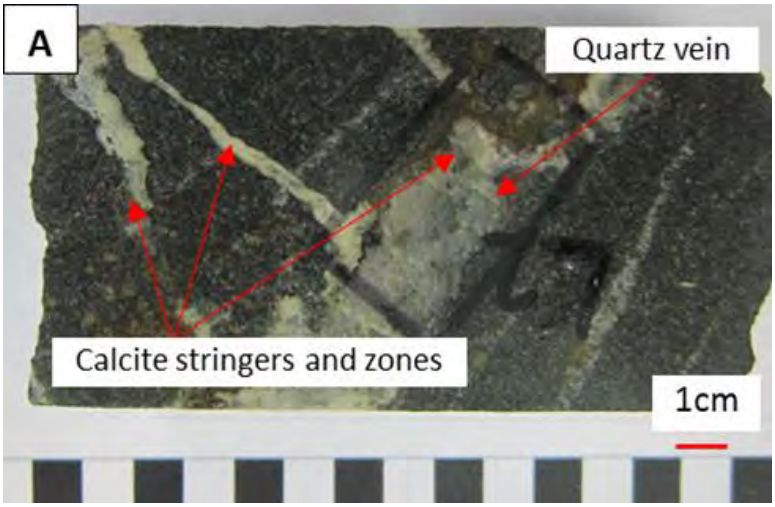

Figure 4.10: (A) L2 core sample. Sulphide bearing diorite with composite quartz and secondary calcite veining. Calcite veinlets crosscut the quartz vein (arrow). Not mineralised.

4.2.1 METAPELITES

Metapelites are generally non-foliated, beige to dark grey in colour and dominated by biotite, chlorite and sericite. Intensely foliated zones show intense reddish-brown weathering, turning the primary rock into reddish-brown saprolite. Hand specimen and petrographic work on selected samples indicate, at minimum, three varieties of metapelites: (i) porphyritic; (ii) calcareous; and (iii) graphitic metapelites. Porphyritic metapelites is a term used by mine geologists for sedimentary rocks that have porphyroblasts of biotite, muscovite, chlorite and or goethite/limonite that exceed 2 mm. Samples classified as calcareous metapelites contain carbonate and carbonaceous material (calcite, minor amorphous and crystalline graphite material) and sulphides. Intensely foliated chlorite and mica are present in larger proportions in metapelites that are associated with isolated amorphous and crystalline carbon/graphite. Slightly foliated, dark grey graphitic metapelites grade into beige colour due to carbonate increase and graphite decrease. Muscovite, biotite, chlorite, albite and quartz are the main mineral components. Oxidation and weathering, most prominent along the boundary of metapelites and intercalated diorites, turns metapelites into light brown and grey saprolitic rock (Figure 4.11). As in Kamituga, Lugushwa's graphitic metapelites show increased hydrothermal alternation and sulphide enrichment near quartz veins.

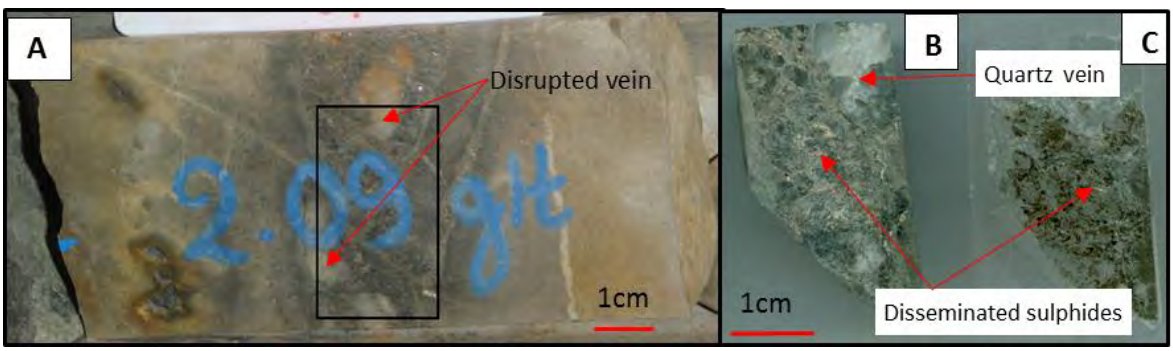

Figure 4.11: (A) L7 core sample; (B) block and (C) thin section. Disrupted vein and sulphides and irregular boundaries in weathered metapelite. Au mineralised at 2.09 g/t.

4.2.2 METASILTSTONE

Lugushwa's metasiltstones grade into metapelites with a low quartz content ~25 - 30 %, rendering them indistinguishable in fresh material. Metasiltstones are typically harder, more siliceous, and do not show visible foliation. Weathered metasiltstones partly disintegrate and form a silty, slightly rough porous surface. Weathered metapelites, by contrast, have a coarser texture and contain coarser-grained quartz or quartz aggregates. Metasiltstones in thin section off-cut blocks, have near equal proportions of quartz and sericite/muscovite.

4.2.3 METADIORITES

Metadiorites were the only igneous rock sampled within the Lugushwa concession. Fine-grained and melanocratic, the metadiorites appear similar to dark metapelites in hand specimens (Figure 4.10, 4.12 & 4.13). Thin sections indicate ~20 vol % hornblende, ~40 vol % biotite and chlorite, ~25 - 30 vol % quartz, feldspar and minor carbonates, tourmaline and sulphides.

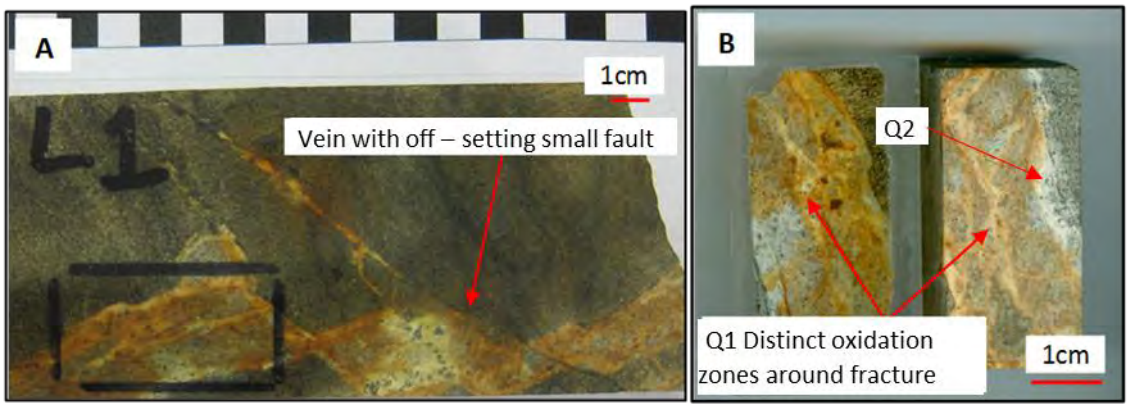

Figure 4.12: (A) L1 core sample. Oxidised quartz vein hosted in diorite, displaced by small-scale faults. (B) Thin section and block. The second quartz generation Q2 shows less oxide staining than the earlier quartz Q1. Not mineralised.

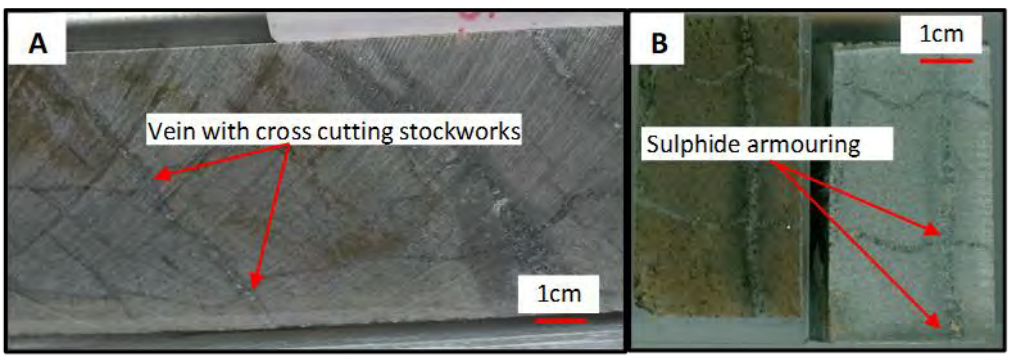

Figure 4.13: (A) L4 core sample. (B) Thin section and block. Several ~2 mm thick quartz-sulphide veins, parallel and connected by non-planar 1 mm veins at high intersection angles, forming small stockworks in sulphide bearing altered diorites. Not mineralised.

Narrow metadiorite sills exhibit hydrothermal alterations – particularly where there is increased Au mineralisation (pers. commun. Chuwa, 26 February 2014). As in Kamituga, hydrothermal alterations within metadiorites show a pronounced increase in arsenopyrite, calcite and quartz veining. Sulphide contents vary from <1 to 10 vol % with arsenopyrite, pyrrhotite, chalcopyrite, pyrite and minor amounts of sphalerite. Minor brownish green and blue tourmaline occur with sericite and biotite in the alteration zone.

4.2.4 QUARTZ VEINS

Quartz veins at the Lugushwa site are predominantly polyphase sheeted parallel vein swarms, ladder veins and stockworks (Figure 4.12 & 4.13). Vein characteristics are generally similar to those in Kamituga. Ductile vein deformation, such as small-scale folding, is not common. Sharp vein displacement along minor faults suggests a brittle deformation environment subsequent to vein formation (Figure 4.12). Vein stockworks appear to be two independent sets of veins that crosscut each other, and hence are not stockworks in the narrow sense. An earlier (primary), oxidised, coarse-grained vein generation is crosscut by a later (secondary), fine-grained vein generation (Figure 4.12).

Hydrothermal alteration of the host rock by quartz veins and stockworks is more extensive in Lugushwa than in both Kamituga and Namoya, as is late stage secondary precipitation of calcite within and across quartz veins (Figure 4.10). The late stage nature of calcite precipitation is evident in crosscutting relationships. Increased hydrothermal alterations result in quartz vein halos with increased proportions of biotite, tourmaline and calcite.

Gold mineralisation predominately, as explained by Chuwa in a personal conversation on 26 February 2014, occurs along brittle-ductile zones, or along brittle fractures at the interface between metapelite, metasiltstones and metadiorites where quartz veining and stockworks formed (pers. comm.). According to Chuwa (pers. comm. 2014), an association exists between veins and ore formation with zones of rheological contrasts. Gold is visible within quartz veins and stockworks along vein fringes. Mineralisation, both within metasediments and metadiorites, proximal to veins, is predominantly related to arsenopyrite, tourmaline, and biotite and chlorite alteration (pers. comm). The precipitation of disseminated alteration phases decreases with distance from the vein (Fall & Chuwa, 2007). Fall (2007a) identified that relative sulphide concentrations correlate with mineralisation across all host rock types in Lugushwa's mineralised zones - with arsenopyrite as the most common sulphide, followed by pyrrhotite and pyrite. Fall (2007a) further identified that arsenopyrite hosts the gold mineralisation in diorite and its quartz veins - with free gold associated with arsenopyrite.

4.3 NAMOYA

Common rock types in Namoya are sericite, silicified and graphitic schists, metadiorites and dolerites. Metasedimentary and intrusive rocks are usually intercalated and indicate evidence of low- to mid-greenschist metamorphism. A field observation was that ductile shearing, late stage brittle deformation and an increase in visible gold is more prevalent in Namoya compared to both Kamituga and Lugushwa.

4.3.1 SCHISTS

Three types of schist occur in the Namoya deposit: (i) graphitic; (ii) mica; (iii) silicified. Graphitic schist is dark grey and contains less sericite, carbonate and quartz than mica schist and silicified schist. Carbonate veins are atypical and assumed to have developed from protolith carbonate mudstone. It is texturally unclear whether carbonate is a late hydrothermal impregnation or a primary phase, or both. The greenish-brown mica schist consists of a fine-grained matrix with quartz lenses, sericite, carbonate, chlorite and sulphides in variable concentrations and grain sizes (Figure 4.14). The beige, light to dark grey mica schist consists primarily of biotite with less sericitic muscovite and sulphides (primarily pyrite and arsenopyrite) (Figures 4.14, 4.15 & 4.16). Silicified schist shows evidence of hydrothermal alterations overprinting a graphitic schist protolith.

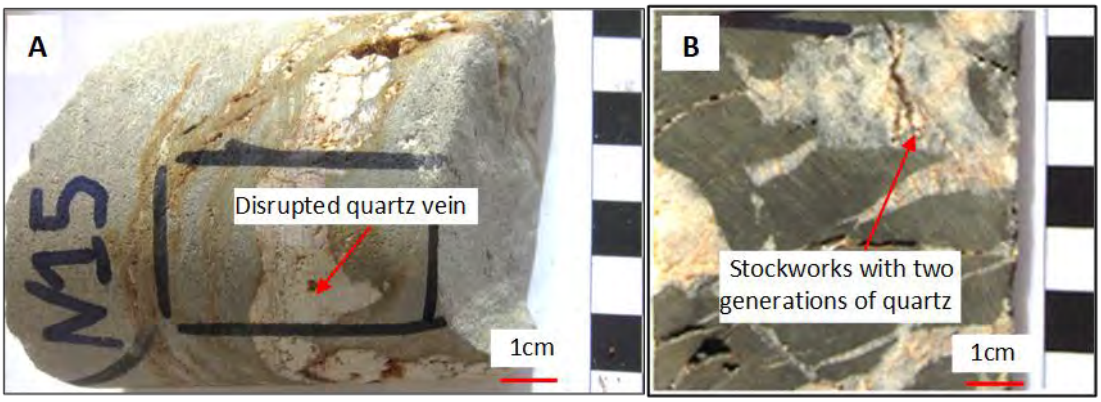

Figure 4.14: (A) N15 core sample. White muscovite schist with open to tight folds. Au mineralised 2.72 g/t. (B) N16 core sample with stockworks in altered chlorite-rich diorite. Au mineralised at 1.6 g/t.

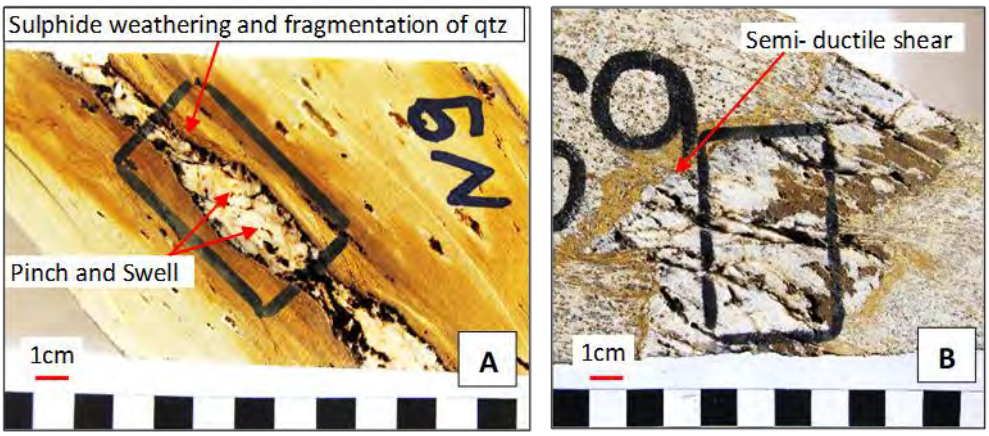

Figure 4.15: (A) N9 core sample. Sulphide weathered quartz vein with peripheral alteration halo parallel to foliation of white muscovite schist. Not Mineralised. (B) N6 core sample. Sulphide bearing sericite schist with intense deformation along semi-ductile shear zone, with brittle offset grading into folding of the vein. Not mineralised.

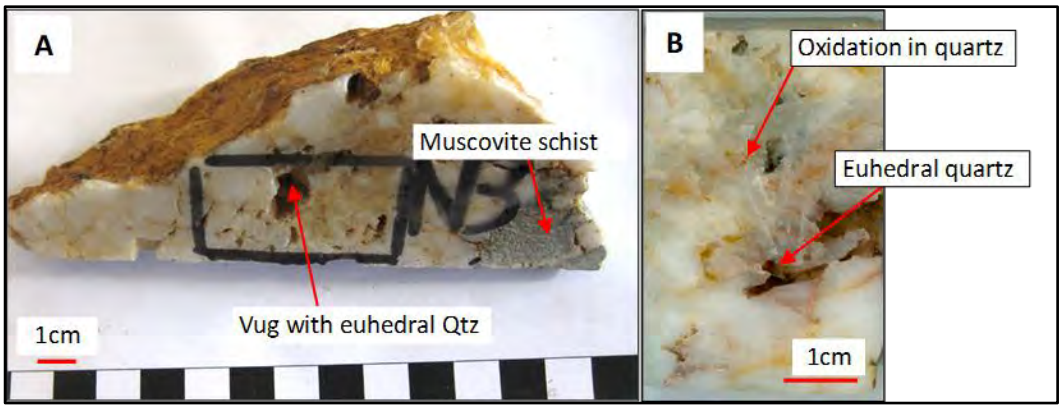

Figure 4.16: (A) N3 core sample. Quartz vein hosted in muscovite schists. (B) N3 cut block. Euhedral quartz in vugs indicate open space filling. Au mineralised at 0.26 - 15.75 g/t.

4.3.2 METADIORITES

Metadiorites in Namoya are similar to those in Kamituga and Lugushwa except they are more foliated and weathered. Metadiorites contain equigranular leucocratic and mafic minerals - plagioclase, chlorite, calcite minor quartz, graphite and hornblende. They have massive (1 mm) equigranular euhedral lath-shaped plagioclase and clinopyroxene crystals (Figure 4.17). Primary magmatic textures are obliterated, and the mineral assemblage is retrogressed in highly foliated zones. Leucocratic and mafic minerals are well aligned to the macroscopically visible foliation. Mineral modes vary with the intensity of retrogression that increases the sheet silicate and calcite content. Mineral proportions vary - plagioclase (20 - 40 vol %), clinopyroxene (10 - 20 vol %), biotite and chlorite (10 - 30 vol %), calcite ~10 %, quartz 5 %, white mica 5 %, hornblende 5 %, graphite 5 %.

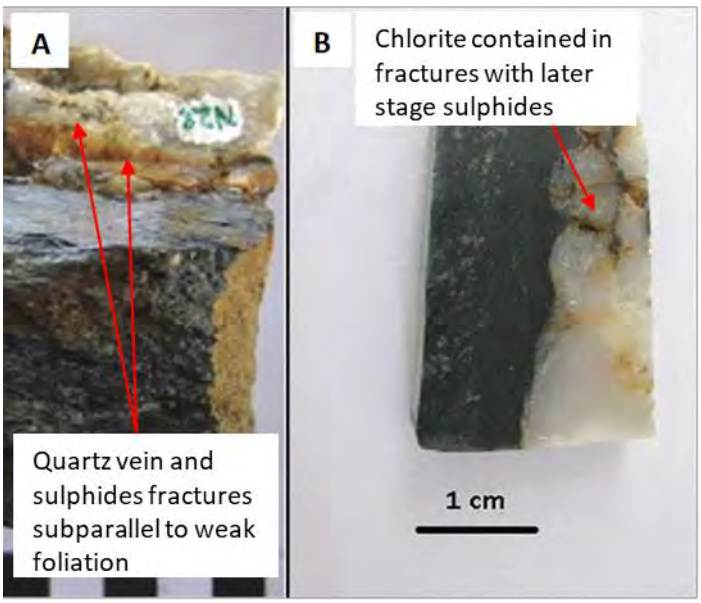

Figure 4.17: (A) N2 core sample. (B) Cut block. Quartz with chlorite-rich alteration near sulphides at the boundary with host rock diorite. Not mineralised.

4.3.3 QUARTZ VEINS

Two distinct quartz phases were assessed from across Namoya's samples; a relatively older, coarse-grained, milky white or Fe oxide or hydroxide particles, and a recrystallized, fine-grained, opalescent sucrose quartz. In vugs, clear euhedral quartz typically indicates open space filling (Figure 4.16). Quartz vein alteration zones contain sulphides (arsenopyrite, pyrrhotite and pyrite), carbonate (calcite), sericite, chlorite and tourmaline. Iron oxides and hydroxides that resulted from the oxidation of sulphides make it difficult to identify original alteration phases. The alteration intensity usually increases with proximity to hydrothermal veins. Calcite is more abundant at the margins of veins, disseminating into host rocks.

Metadiorite quartz veins at Namoya are similar to those in Kamituga in that they show features indicative of brittle to ductile deformation, such as pinch-and-swell, boudinage and disruption of veins (Figure 4.15). Stockworks are also present. Veins vary in thickness from a few millimetres to several metres, with small-scale folding and shearing seen in veins that are thinner than 4 cm.

Mineralisation in quartz veins in Namoya is associated with dominant structural trends in which the greatest number of stockworks and irregular and crosscutting veins occur. Vein sheets along the trend of foliated schists and shear zones deliver high gold grades (Figure 4.15). Mineralised zones are extensively oxidised - possibly due to their proximity to shear zones and their exposure to ground water (Figure 4.17 & 4.18).

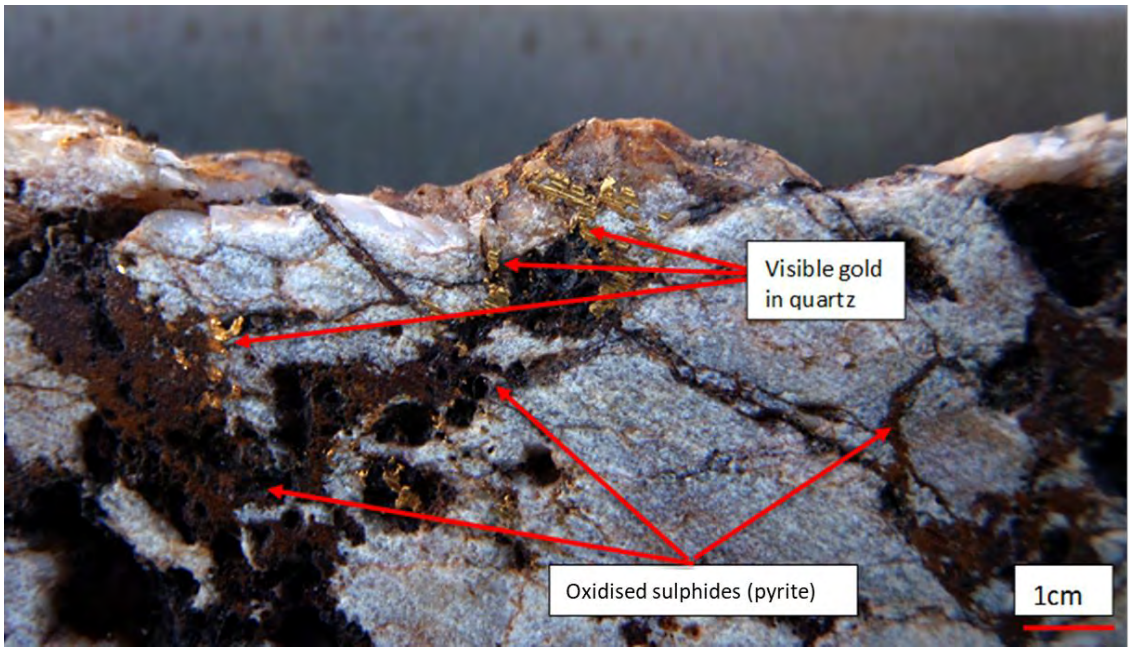

Figure 4.18: Highly mineralised sample N5 from Namoya (1460g/t). Note the abundant and large gold particles and oxidised sulphides (presumably pyrite).

5. CHARACTERISTIC OF SIX FLUID TYPES IN THE TNGB

This chapter presents the characteristics of the six main FI types (henceforth referred to as Types) present in the analysed samples from Kamituga, Lugushwa and Namoya. The main physical and compositional characteristics of each Type, including size, phase compositions, their distribution and relative timing of entrapment (primary, pseudosecondary and secondary), and their occurrence in either mineralised or unmineralised veins is described in the text. Table 5.1, at the end of this chapter, summarises the physical and chemical properties of the six fluid types and their occurrence in FIAs. This table also presents representative illustrations of the physical appearance of the FI Types.

5.1 TYPE 1 FIs

Type 1 FIs are predominately found in unrecrystallised quartz. Type 1 fluids are typically contained in quartz that formed early in the growth sequence. Type 1 and 2 FIAs are predominantly, but not exclusively, found in veins hosting tourmaline, especially those from Lugushwa and Kamituga. Type 1 FIs are found in both mineralised and unmineralised veins.

Type 1 FIs are elongate to equidimensional and consist of three phases - liquid aqueous, aqueous vapour bubble, and halite phases (often distinctly cubic in shape). They are variable - both in size (2 - 22 µm for pseudosecondary and primary FIs, 2 - 8 µm for secondary FIs) and salinity (26.3 - 50 wt.% NaCl eq.). Type 1 FIs are predominantly primary and pseudosecondary. Type 1 FI are predominately found in primary hydrothermal grains versus recrystallised quartz in which these FI Types are absent. Type 1 FIs in hydrothermal grains are highly saline primary Type 1 FIs and occasional secondary Type 1 FIs. Type 1 FIs homogenise by dissolution of the vapour and solid phases into the aqueous liquid phase. This dissolution sequence of the vapour and solid phases is interchangeable.

Phase proportions are highly variable with either halite or liquid as the dominant phase. Vapour bubbles are never the dominant phase although, in a few instances, they are larger than halite - especially in FIs with low Th and low to moderate salinity (< 30 wt.% NaCl eq.). The presence of cations other than Na^+ was identified using the equilibrium temperature Te (see Chapter 6, Section 6.8).

5.2 TYPE 2 FIs

Type 2 FIs, like Type 1 FIs, are predominately found in unrecrystallised quartz. Type 2 primary FIs are associated with Type 1 primary FIs near tourmaline in early hydrothermal unrecrystallised quartz. Type 2 primary FIs are only present in Lugushwa and Kamituga samples. They have the same relation to mineralised and unmineralised veins as Type 1 primary FIs. Type 2 primary FIs homogenise to the liquid phase.

Type 2 FIs are elongate to equidimensional and consist of three or more phases - liquid aqueous, aqueous vapour, and solid halite daughter phases (distinctly cubic in shape) like Type 1 FIs. In addition, a second or even third daughter phase is present. As with Type 1, Type 2 FIs are highly variable both in size (4 - 24 µm for primary and pseudosecondary, and 2 - 7 µm for secondary FIs), and in salinity (26.3 - 50 wt.% NaCl eq.).

Petrographic properties and microthermometry (see Chapter 7) indicate that daughter minerals other than halite are predominately KCl, $FeCl_2$ or $CaCl_2$. Sylvite (KCl) is isotropic and prismatic in habit and has a similar refractive index to halite (1.47 vs. 1.54). Sylvite's microthermometric properties distinguish it from halite (Van den Kerkhof & Hein, 2001; see Chapter 6).

Fe-chlorides are easier to identify as they are light green, have moderate to high birefringence, a variable refractive index and are tabular, rhombic or hexagonal (Van den Kerkhof & Hein, 2001). Cations, other than Na^+ were identified using the equilibrium temperature Te. Phase proportions can be highly variable, with either halite or liquid as the dominant phase. Vapour is never the dominant phase, although the bubble can be larger than the halite in lower -Th/salinity FIs (< 30 wt.% NaCl eq.). Daughter crystals other than halite are always volumetrically smaller than all other phases.

5.3 TYPE 3 FIs

Type 3 FIs are equidimensional or irregular in shape and consist of two or three phase - a minor liquid aqueous phase with trace amounts of CO_2, and either an aqueous/CO_2 vapour phase and /or a liquid CO_2 phase. Across all deposits, Type 3 FIs are highly variable in size (3 - 20 µm for primary and pseudosecondary and 2 - 6 µm for secondary) and predominately have low salinities (<12 wt. % NaCl eq.). They never contain daughter crystals. Detectable levels of both CH_4 and N_2 are found in some Type 3 FI. The presence of CO_2 and the absence of daughter crystals distinguishes Type 3 from Type 1 and 2 FIs.

Primary Type 3 FIs have distinct 'negative' crystal shapes that developed dissolution and precipitation, reducing the surface energy of the FI (as Van den Kerkhof and Hein,2001). The vivid high-density aqueous component has a refractive index of 1.32 - 1.33. The less dense CO_2 liquid has a much lower refractive index of 1.195 and has a yellow absorptive colour. CO_2 vapour has the lowest density of the phases with an even lower refractive index and appears dark grey to black (Van den Kerkhof & Hein, 2001). Either the liquid CO_2 or the vapour aqueous/CO_2 phase dominates within the FI. Small variations in the ambient temperature can affect this phase proportion and change it from one to the other. All Type 3 FIs (primary, pseudosecondary and secondary) homogenise by either vapour bubble expansion or by expansion of CO_2 liquid.

Type 3 FIs are found in unmineralised and mineralised veins in primary hydrothermal and in recrystallised quartz that formed from hydrothermal vein quartz by plastic deformation. Large, single (>10 µm) primary Type 3 FIs are observed in mineralised hydrothermal grains. Small (2 - 6 µm) Type 3 FIAs (primary and secondary) are more prolific in mineralised than in unmineralised veins. The highest Au mineralised veins correlate with Type 3 FI that contain the highest CO_2 and lowest saline levels. CH_4 was always identified in mineralised veins using Raman spectroscopy and inferred from variances in Tm of CO_2.

5.4 TYPE 4 FIs

Type 4 FIs are elongate, equidimensional and irregular in shape and consist of two phases - a dominant aqueous liquid phase and an aqueous vapour phase. Together with the vapour phase the aqueous liquid phase may contain trace amounts of dissolved CO_2, as evident from Raman analysis. Type 4 FIs are variable in both size (3 - 25 µm for primary and pseudosecondary and 1 - 6 µm for secondary) and salinity (0 - 35 wt. % NaCl eq.). Type 4 FIs can

have salinities higher than 26.3 wt. % NaCl eq., but do not nucleate halite. Te variations suggest that the highest salinities for Type 4 FIs tend to contain the highest concentration of cations other than Na^+, which explains the absence of halite. Homogenisation occurs by either vapour expansion or vapour contraction. Type 4 FIs are found both within mineralised and unmineralised veins as primary, pseudosecondary and secondary. Type 4 FI with traces of CO_2 are frequently found together with Type 3 FIs that have lower salinities and higher CO_2 levels, and these commonly occur in samples with significant Au grades.

5.5 TYPE 5 FIs

Type 5 FIs are equidimensional, irregular and elongated and contain three phases - an aqueous liquid, a black solid (graphite, amorphous carbon and sulphides) and either a CO_2 liquid or an aqueous/CO_2 vapour phase. Type 5 FIs are highly variable in size (3 -18 µm for primary and pseudosecondary and 3 - 5 µm for secondary). Type 5 FIs are predominately primary and pseudosecondary. However, secondary FIs are seen in recrystallised quartz - particularly together with Type 3 FIs. Where no halite is present, Type 5 FIs have low salinities (<10 wt.% NaCl eq.). In rare instances Type 5 FIs have high salinities similar to Type 1 and 2 FIs. In these instances, small halite daughter crystals form a fourth phase with salinity levels between 26 - 30 wt. % NaCl eq. This rare Type 5 FI is found in early (primary) hydrothermal quartz together with highly saline Type 1 and 2 FIs. The liquid CO_2 phase in Type 5 FIs contains trace amounts of amorphous graphite, particularly when the vein is hosted in metapelites. Phase proportions are highly variable, and any of the three different phases may occupy the highest volume proportion.

Type 5 FIs are found both within mineralised and unmineralised veins but are distinctly associated with sulphide phases (pyrite and arsenopyrite) in mineralised veins. All phases in Type 5 FIs homogenise during heating, except the solid phases of carbon and sulphide. This suggests that the carbon and sulphides were trapped as solids (heterogeneous entrapment).

5.6 TYPE 6 FIs

Type 6 FIs are equidimensional or irregular with a single aqueous liquid phase without a visible vapour bubble. There is no visible phase change up to 550 °C. Raman and cooling data indicate low salinities of less than 18 wt. % NaCl eq. Type 6 FIs are predominately small secondary (2 - 5 µm), but larger primary and pseudosecondary FIs (5 - 22 µm) occur in hydrothermal quartz with Type 3 and 4 FIs. Type 4 and 6 FIs are ubiquitous across the three Au deposits.

Table 5.1 Main characteristics of FI Types 1 to 6 in Kamituga, Lugushwa and Namoya.

Designation	Type 1	Type 2	Type 3	Type 4	Type 5	Type 6
Annotated illustration of FI Types (not to scale)	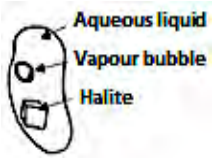	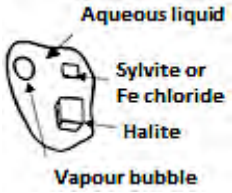	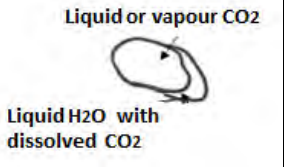		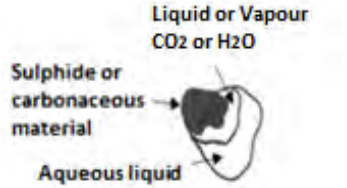	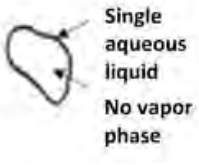
Description	3-phase FI with small vapour bubble, cubic halite daughter solid (NaCl) and high salinity aqueous solution > 26.3 wt. % NaCl eq.	4- or more phase FI with small vapour. bubble, large cubic halite daughter solid and a 2nd smaller daughter solid (predominately KCl or $FeCl_2$); high salinity aqueous solution > 26.3 wt. % NaCl eq.	2 to 3 phase, vapour/liquid CO_2 dominant FI with small proportion of aqueous liquid. The large vapour bubble is CO_2 rich. It may contain other volatile components CH_4 or N_2. May contain 3 phases: V CO_2, L CO_2 and L H_2O.	2-phase liquid dominant FI with often small vapour bubble. Variable salinity levels i.e. 0 – 35 wt. % NaCl eq. NB: possible that FI does not nucleate halite at 26.3 wt. % NaCl eq.	3-phase vapour or liquid dominant FI containing amorphous black material (carbonite, graphite or sulphides i.e. pyrite or arsenopyrite) Liquid is aqueous low salinity, vapour or second liquid is predominately CO2. In rare instances these FI are 4 - phase with a small halite cube.	Single liquid phase FI Often very low salinity FI
Size proportions	2 - 22 µm	2 - 24 µm	2 - 20 µm	1 - 25 µm	3 - 18 µm	1 - 22 µm
Phase types at ambient temperature (23 °C). Sequence indicates relative phase proportion in FI	Halite saturated L + V + H H + L + V	Halite saturated and secondary daughter mineral L + V + H +D H + L + V +D L + H +V +D	Halite undersaturated with CO_2 enrichment V + L V + L_1 + L_2	Halite undersaturated and in places with trace amounts of CO_2 L + V	Mostly halite under-saturated S + L + V S + V + L V+ L + S L + V + S + H	Halite undersaturated Only visible phase H_2O L
Occurrence: mineralised or unmineralised quartz veins	Both mineralised and unmineralised	Both mineralised and unmineralised	Both mineralised and unmineralised. But dominantly mineralised	Both mineralised and unmineralised	Both mineralised and unmineralised But dominantly mineralised	Both mineralised and unmineralised
Predominantly primary, secondary or pseudosecondary	Dominantly primary and pseudosecondary. Very rarely secondary	Primary and pseudosecondary	Dominantly primary	Primary, secondary and pseudosecondary	Dominantly primary and pseudosecondary	Mainly secondary, but also primary or pseudosecondary when in association with Type 3 and 4 FI

Table 5.1 Cont. Main characteristics of FI Types 1 to 6 in Kamituga, Lugushwa and Namoya.

Designation	**Type 1**	**Type 2**	**Type 3**	**Type 4**	**Type 5**	**Type 6**
Occurrence: samples	K2, K3, K4, K6, K7, K9, K10, K12, K14, K19, K22, Ktm-1, Ktm-2, Ktm-3, Ltm-1,Ltm-2,L2, L3, L4, L6, L7, L15, L17, L19, L20, L21, N23, N28, N6, N9, N3, N5, N11,	K2, K3, K6, K7, K9, K12, K14, K19, Ktm-1, Ktm-2, Ktm-3, L2, L3, L4, L6, L7, L17	Occurs in all samples	Occurs in all samples; the most common FI Type	K2, K3, K4, K6, K7, K9, K10, K12, K14, K16, K19, K21, K22, K24, Ktm-1, Ktm-2, Ktm-3, Ltm-1, Ltm-2, L2, L3, L4, L6, L7, L15, L17, L19, L20, L21, N23, N28, N6, N9,N3, N5, N10	Occurs in all samples
Description of quartz variety FI is trapped in or other minerals it is associated with	The percentage proportions of the FI's often increases in a large unaltered quartz grain These FI often achieve highest salinity in pegmatites especially in close proximity to tourmaline	The percentage proportions of the FI's often increases in a large unaltered quartz grain These FI achieve highest salinity in pegmatites especially in close proximity to tourmaline	Occurs in both inclusion rich ('dirty') altered primary quartz and clear secondary (recrystallised.) quartz varieties Often associated with high gold grades, particularly if these FI are larger than other surrounding FI, and CO_2 forms liquid and vapour components below 22°C	Occurred in primary Qtz and secondary (recrystallised.) clear quartz varieties	Occurs in large, clear quartz variety Often associated with late stage fluid phase and sulphides or carbonates in fractures	Occurs in all quartz varieties

6. METHODS OF INTERPRETATION

This chapter describes the methods and equations used to process the data obtained from microthermometry and Raman spectroscopy as applied to the interpretation of FI Types.

6.1 H_2O-NaCl UNDERSATURATED AQUEOUS FLUIDS (≤26.3 wt. % NaCl eq.)

Hall et al. (1988) determined the freezing-point depression of H_2O-NaCl solutions for compositions ranging from 0 - 23.2 wt. % NaCl eq. (Figure 6.1). Fluid Inclusions with salinities below eutectic composition (23.2 wt. % NaCl eq.) will freeze to form a mixture of ice and hydrohalite (NaCl $2H_2O$) in proportions consistent with the average salinity levels. On heating, at the eutectic, both ice and hydrohalite melt together until hydrohalite is completely dissolved and only ice melting continues (NaCl <23.2 wt. %) during subsequent heating. With further heating, the ice melts, diluting the salinity of the liquid phase, and therefore, final ice melting temperatures (freezing point depression) correlate with salinity levels (Figure 6.1). Bodnar (1993) formulated Equation EQ1 that correlates the freezing point depression to salinities for temperatures between 0 and -21.2 °C.

EQ1

Salinity (wt. % NaCl eq.) = $1.78\,\Theta - 0.0442\,\Theta^2 + 0.000557\,\Theta^3$

Θ is the depression of the freezing point (°C)

Ice and hydrohalite ($NaCl{\cdot}2H_2O$) are present in FIs with salinities between the eutectic composition (23.3 wt. % NaCl eq.) and the peritectic composition (26.3 wt.% NaCl eq.) when cooled (Bodnar & Vityk, 1994) (Figure 6.1). In FIs with these salinities, at the eutectic, both ice and hydrohalite melt together until, in this case, ice is completely dissolved and only hydrohalite melting continues (26.3 wt.% NaCl >23.3 wt.%) during subsequent heating. With further heating, the hydrohalite dissociates between the eutectic (-21.2 °C) and the peritectic (0.1 °C) temperatures. The salinity for these FIs can then be determined based on ice and hydrohalite dissociation temperatures as determined by Sterner et al. (1988) and Bodnar et al. (1989). An important consideration in these hydrohalite bearing FIs Types is the slow response in the rate of melting of the hydrohalite. Metastability for several minutes to hours at temperatures above 0.1 °C is an indicator of hydrohalite rather than ice (Bodnar & Vityk, 1994). According to Bodnar & Vityk (1994), FIs between the eutectic and peritectic compositions are underreported in literature due to the misidentification of hydrohalite dissociation with ice melting.

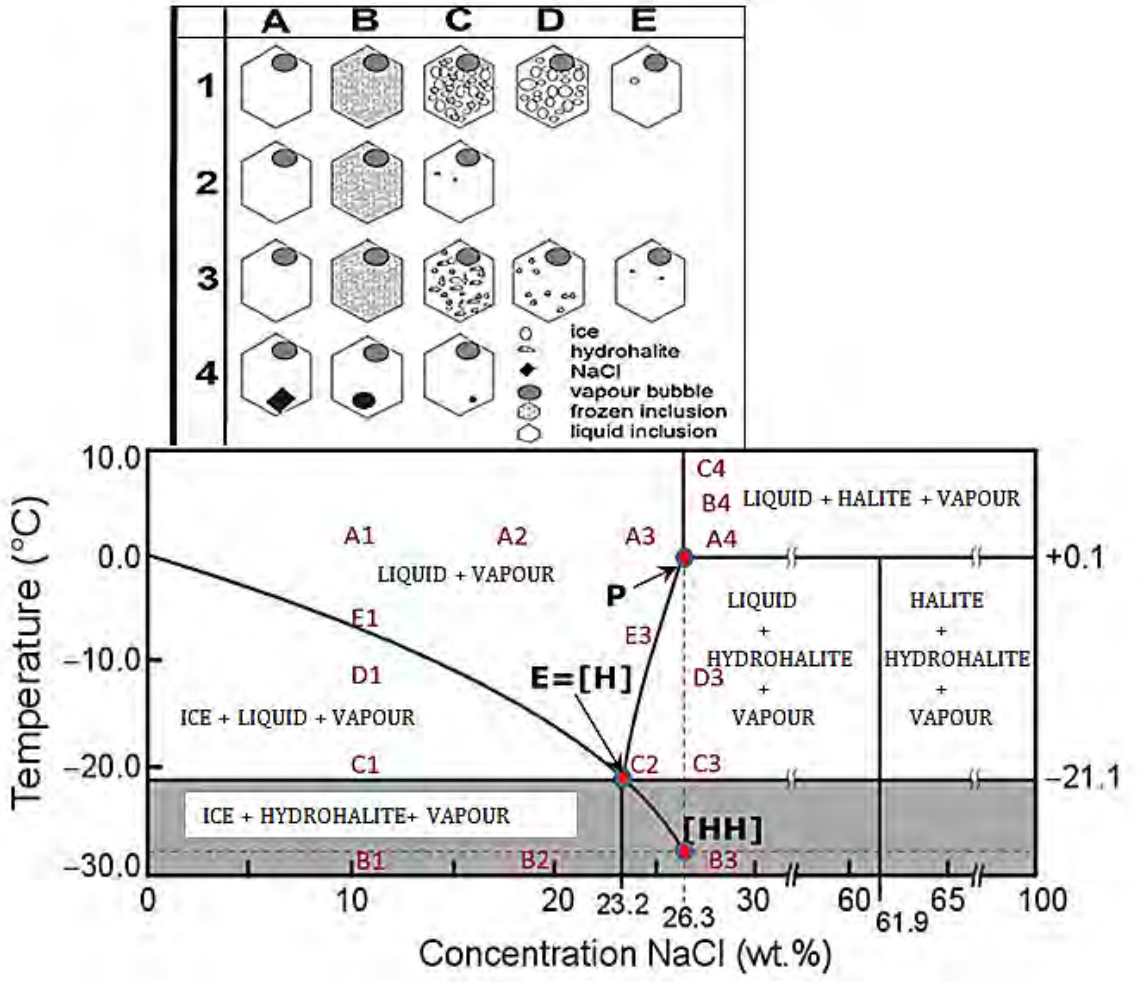

Figure 6.1: Phase transitions during microthermometry of the H_2O-NaCl (Type 1, 2 and 4 FI) (0 to ≤ 100 wt. % NaCl eq.) system. The top portion illustrates the visible features of phase transitions in alphanumeric coding. Numerals depict increasing salinities. Alphanumeric symbols signify the phase characteristics of FIs at different salinity concentrations and temperature levels. The phase diagram shows the position of individual phase stabilities in T - X space with corresponding alphanumeric codes referring to the upper diagram. All phases coexist with vapour. Point E = H = C2 = eutectic (HH + Ice + L) = no halite present; eutectic point: - 21.2 °C, 23.2 wt. % NaCl eq. (HH)= metastable eutectic (Ice +L ± halite) = no hydrohalite present. In halite-bearing inclusions Point P = peritectic 0.1 °C, 26.3 wt. % NaCl eq. (reaction point halite ↔ hydrohalite) (Huizenga & Touret, 1999; Schmidt-Mumm, 2008).

6.2 H_2O-NaCl SATURATED AQUEOUS FUIDS (>26.3 wt. % NaCl eq.)

Type 1 & 2 FIs contain >26.3 wt. % NaCl eq., halite solids at room temperature, and variable intermediate and final phase changes leading up to total homogenisation (Figure 6.1). Final phase changes include the dissolution of halite before dissolution of the vapour bubble, and vice versa, during total homogenisation. Solid halite forms in FIs containing >26.3 wt. % NaCl eq. This, however, does not mean that all fluids with salinities >26.3 wt. % NaCl eq. nucleate halite crystals. According to Bodnar & Vityk (1994), FIs with less than 30 wt. % NaCl eq. rarely nucleate halite and are therefore rarely reported in literature. Sterner et al. (1988) developed an equation that determines salinity for >26.3 wt. % NaCl eq. FIs as a function of halite dissolution temperatures under vapour-saturated conditions - Equation 2 (EQ2).

EQ2

Salinity (wt. % NaCl eq.) = $26.242 + 0.4928\,\Psi + 1.42\,\Psi^{2} - 0.223\,\Psi^{3} + 0.04129\,\Psi^{4} + 6.295 \times 10^{-3}\,\Psi^{5} - 1.967 \times 10^{-3}\,\Psi^{6} + 1.1112 \times 10^{-4}\,\Psi^{7}$

$\Psi = T\,(°C)/100.$

EQ2 relates solubility of NaCl in water from the peritectic temperature (0.1 °C) to the NaCl triple point (801 °C or the critical point temperature, whichever is lower). EQ2 is limited to FIs in which halite and vapour bubbles disappear at the same temperature (homogenisation occurs along the three-phase liquid + vapour + halite fluid curve) (Bodnar & Vityk, 1994).

6.3 TOTAL HOMOGENISATION BY HALITE DISSOLUTION

As described, most salinity determining methods require the presence of a vapour phase at final homogenisation. Lecumberri-Sanchez et al. (2012) developed equations to model PVTX conditions for halite dissolution at Th. The equations were derived for bulk salinity, densities, pressures and dP/dT slope of the isochores in the liquid field. In this model, Tm represents total homogenisation temperatures at halite dissolution. This model can be applied to Type 1 and 2 FIs with Tm from 100 to 600 °C, and for pressures along the liquid-vapor-halite curve to 300 MPa. FI salinities, densities and pressures are obtained by Equation 3 (EQ3), Equation 4 (EQ4) and Equation 5 (EQ5).

EQ3

$X_m = {}^{X1}{}_{i=0}\,(b_i T_m^{\,i})$

X_m is salinity in wt. % NaCl eq. and b_i and X_1 are fitting coefficients defined in Lecumberri-Sanchez et al. (2012). The bulk density or liquid density at T_m is obtained by Equation 4 (EQ4).

EQ4

$q_m = {}^{X2}{}_{i=0}(c_i T_m^{\,i})$

q_m is density in g/cm³ and c_i and X_2 are fitting coefficients defined in Lecumberri-Sanchez et al. (2012). Pressure at T_m is obtained by equation 5 (EQ5).

EQ5

$P_m = 0.1^{x^3}{}_{i=0}\,(a_i\,T_m^{\,i})$

P_m is the pressure at T_m in MPa and a_i X_3 are fitting coefficients defined in Lecumberri-Sanchez et al. (2012).

6.4 ISOCHORE DETERMINATION FOR AQUEOUS FIs

FI's pressures can be determined using isochores when homogenisation temperature and composition of FIA's are known. This is valid for H_2O-NaCl undersaturated hydrous fluids in which total homogenisation takes place by vapour disappearance, or when FIs homogenise by simultaneous disappearance of vapour bubble and halite crystals. Applicable FIs are Type 1, 2 & 4. An equation of Bodnar & Vityk (1994) established the correlation between trapping temperature and pressure, salinity, and homogenisation temperatures for NaCl undersaturated hydrous FIs - Equation 6 (EQ6).

EQ 6

$dP/dT\ (bar/°C) = as + bs*Th + cs* Th + cs*Th^2$

dP/dT is the slope of the iso-Th line (≈ isochore), Th is the homogenisation temperature (°C), and 'as', 'bs' and 'cs' are salinity-dependent fitting parameters defined in Bodnar & Vityk (1994). Pressure controls the density of the fluids and hence the magnitude of the pressure corrections that must be added to Th to get Tt. The equation is valid for pressures up to 6 kbars, 0 - 40 wt. % NaCl eq. and temperatures below the critical temperature or Th from 50 to 700 °C (Bodnar & Vityk, 1994).

6.5 ISOCHORE DETERMINATION FOR AQUEOUS FIs

This section pertains to Type 1 and 2 FIs. Lecumberri-Sanchez et al. (2012) developed an isochore equation to evaluate fluids that homogenise by halite dissolution after liquid-vapour homogenisation. In this model, Tm represents total homogenisation temperatures at halite dissolution temperatures. The observed vapour and liquid homogenisation ($Th_{L \rightarrow V}$), in conjunction with Tm, can be used to determine the slopes of the isochores in the liquid field using Equation 7 (EQ7).

EQ7

$dP/dT = 0{:}1^{X3}{}_{i=0}(U_i T_m^i)$

dP/dT is the slope in the liquid field in MPa/°C and U_i are fitting coefficients defined in Lecumberri-Sanchez et al. (2012).

6.6 PROGRAM HOKIEFLINCS H_2O-NaCl

HOKIEFLINCS-H_2O-NACl program incorporates all EQ1 - 7 equations (Steel-MacInnis et al., 2012). The advantage of this program over other FI programs is that it includes multiple equations and allows for multiple FI's input data. The program outputs fluid salinity, density and isochore slopes. Pressure corrections are determined using isochore slope and a slope-intercept method and an input of either a P or T estimates.

6.7 EVALUATION OF IMMISCIBLE FLUID IN H_2O-NaCl SYSTEMS

According to Bodnar et al. (1985), two-phase (immiscible) FIs are seen in epithermal precious metal deposits and are indicative of gold magmatic-hydrothermal ore deposits, and therefore are relevant to this study in relation to Type 4 FIs. Knight & Bodnar (1989) determined the relationship between salinity and critical temperature (Tc) in the H_2O-NaCl systems using Equation 8 (EQ8).

EQ8

$Tc\ (°C) = 374.1 + 8.8\ \phi + 0.1771\ \phi^2 - 0.0211\ \phi^3 + 7.334 \times 10^{-4}\ \phi^4$

ϕ is salinity in wt. % NaCl eq. The equation is valid for formation temperatures up to 800 °C, 1.5 kbars and 30 wt. % NaCl eq. solutions, which covers most magmatic-hydrothermal systems (Figure 6.2).

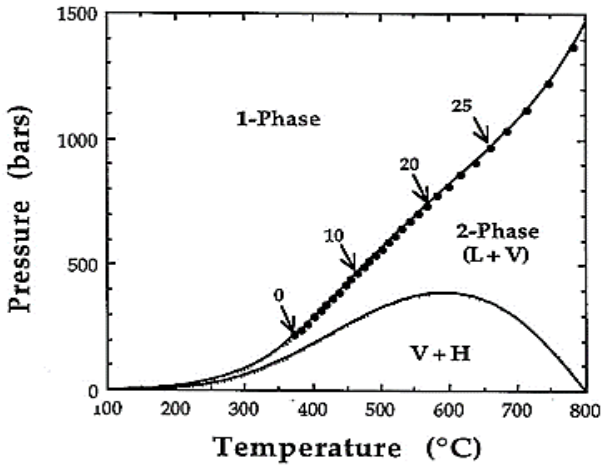

Figure 6.2: NaCl-H_2O PT system illustrating the projection of critical points to high temperatures and pressures with increasing NaCl concentrations (0 - 25 wt. % NaCl eq. highlighted with arrows). These critical points represent the minimum conditions for immiscible fluids at a given salinity (Bodnar & Vityk, 1994).

6.8 Te - EUTECTIC TEMPERATURES

Cations in hydrothermal fluids (Na^+, K^+, Ca^{2+}, Mg^{2+}, Fe^{2+} and Fe^{3+}) are usually charge-balanced by Cl^- anions and can form optically identifiable salt crystals if oversaturation is exceeded (Roedder, 1984; Boiron and Dubessy, 1994). Microthermometric determination of eutectic melting temperatures facilitates the identification of dissolved salts. Due to different solubilities of complex mixtures of salts or ions, aqueous dominated FIs have different Te. Eutectic temperature, or the temperature of first melting, can be identified as the first liquid phase to appear in an aqueous dominated FI when heated from -180 °C (Roedder, 1984). First melting is identifiable when vapour bubbles become rounded on heating after having been compressed by ice. Such bubbles are more easily identified in the interstices between several ice crystals rather than around a single ice crystal (Roedder, 1984).

Te will deviate from the typical -21.2 °C if dissolved salts, other than NaCl, are present in FIs. The NaCl-H_2O system has very low Te (between -35 and -28 °C) if high concentrations of NaCl are present (> 26 wt. % NaCl) (Roedder, 1984 and Boiron and Dubessy, 1994). Roedder (1984), Hall et al. (1988), Davis et al. (1994), Goldstein and Reynolds (1994) and Schmidt-Mumm (2008) provided ranges for eutectic melting temperatures for dissolved salts in the liquid phase of FIs. KCl-H_2O systems can have Te up to -9 °C. NaCl-KCl-H_2O Te (-23.4 to -22.9 °C) is similar to the NaCl-H_2O system (Table 6.1). Depending on the concentrations of Na vs. Fe, Ca or Mg in the system, Te will range from -33 °C to -85 °C. In the $CaCl_2$-H_2O system that does not contain Na, Te is consistently below -50 °C. This makes it easily distinguishable from the NaCl-KCl-H_2O system range of -23.4 to -22.9 °C. The NaCl-KCl-$CaCl_2$-H_2O system is associated with Type 2 FIs that freeze to form a mixture of ice, hydrohalite, sylvite and antarcticite ($CaCl_2 \cdot 6H_2O$). Antarcticite dissolves first at the eutectic (-52 °C), leaving a fine-grained mixture of ice, hydrohalite and sylvite in the liquid phase.

Table 6.1. Te ranges in aqueous FIs correlate to dissolved salts in hydrothermal and magmatic systems (Roedder, 1984; Hall et al., 1988; Davis et al., 1994; Goldstein and Reynolds, 1994 and Schmidt-Mumm, 2008).

Te (°C)	Possible composition
- 21.1	NaCl - H_2O for (< 26 wt. % NaCl eq.)
-85 to -47	NaCl - $CaCl_2$ - H_2O
-80 to -33	NaCl - $MgCl_2$ - H_2O
-23.4 to -22.9	NaCl - KCl - H_2O
-10.6 to -9	KCl - H_2O
-38 to -33	$MgCl_2$ - $FeCl_{2(3)}$ - H_2O
-55 to -49.8	$CaCl_2$ - H_2O

6.9 TERNARY HYDROUS SALINE SYSTEMS

The dominant ternary salt system is NaCl-KCl-H_2O and is applicable for Type 2 FIs that contain halite and sylvite daughter minerals. Daughter crystals of sylvite and halite are distinguished by phase changes between the ternary eutectic (-22.9 °C) and +-150 °C. Halite shows retrograde solubility whereas KCl dissolves rapidly in this temperature range. The path of most Type 2 FIs that contain sylvite and halite is similar to the path taken by the fluid phase on heating a FI containing KCl and NaCl daughter crystals (dashed line in Figure 6.3).

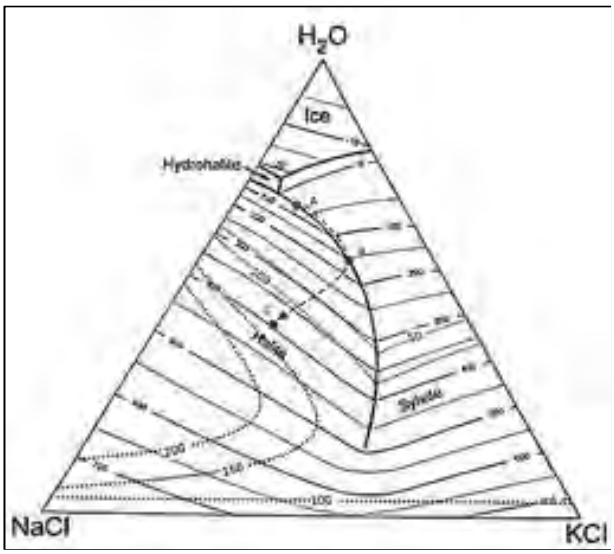

Figure 6.3: The vapour-saturated solubility in the NaCl-KCl-H_2O system is indicated by isotherms (°C - thin solid lines) and isobars (kg/cm2 - dotted lines). Dashed line - path taken by the fluid phase on heating a FI containing daughter crystals of KCl and NaCl (Samson et al., 2003).

Determining $FeCl_2$, $CaCl_2$ and $MgCl_2$ in TNGB FIs is problematic, because very few Type 2 FIs nucleate solid phases. Accordingly, dissolution temperatures cannot be determined. Furthermore, graphical representation of phase changes is not possible because phase transitions are difficult to observe due to their small size relative to other daughter minerals (NaCl and KCl). Inferred estimations can, however, be made on the basis of observations of few small daughter minerals of $FeCl_2$, $CaCl_2$ and $MgCl_2$ in some Type 2 FIs.

6.10 AQUEOUS-CARBONIC FIs

FIs with H_2O-CO_2 and other volatiles and minor secondary components (NaCl) are significant in TNGB hydrothermal mineralisation. Types 3, 4 and 5 FIs have measurable concentrations of CO_2, CH_4, N_2 and H_2S. Higher concentrations of CO_2 can have significant effects on raising the pressure along the liquid-vapour curve into a divariant field in PT space (Shepherd et al., 1985). This means that phase separation can occur at higher pressures and therefore greater depths than in saline solutions. Wilkinson (2001), using Henley's (1984) equations, developed illustrations to indicate this point (Figure 6.4).

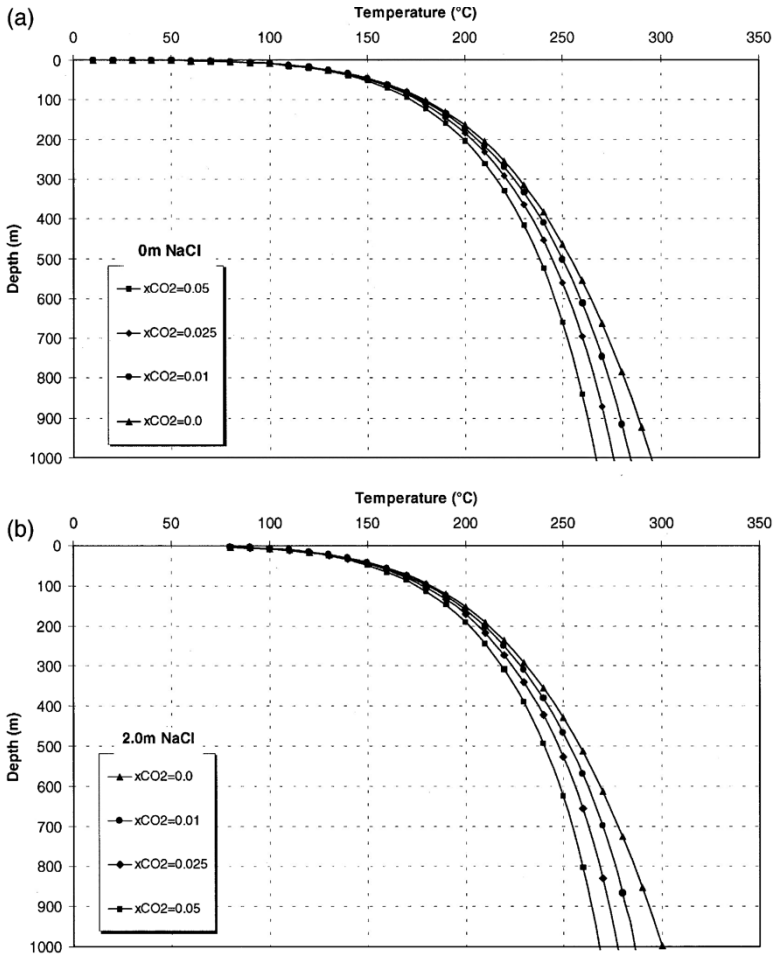

Figure 6.4: Effervescence-depth curves for NaCl-H2O solutions containing 0 - 5 mol % CO_2. (a) 0-molar NaCl and (b) 2-molar NaCl. An increase in CO_2 content intensifies effervescence. An increase in salinity has the opposite effect. The effect of dissolved CO_2 is more significant than elevated salinity (Wilkinson, 2001).

The quantitative evaluation of the TNGB carbonic FIs requires an understanding of the dominant binary H_2O-CO_2system followed by the H_2O-CO_2-NaCl system, as published by Roedder (1984), Barton & Chou (1993), Erokhin (1993), Bakker et al. (1996), Diamond (1992, 1994, 2000 & 2001) and Bakker (1997). The effects of CH_4, N_2, H_2S on the H_2O-CO_2 and H_2O-CO_2-NaCl systems were determined qualitatively using published material by Dubessy et al. (1992), Diamond (1994), Thiéry et al. (1994), Bakker (1997) and Van den Kerkhof and Thiéry (2001). Microthermometric phase change measurements for the H_2O-CO_2 and H_2O-CO_2-NaCl systems were measured from -120 °C to 32 °C. Melting occurs at -56.6 °C (Tm CO_2 - triple point of CO_2) if the CO_2 is pure and no other

volatile vapour is present. Melting occurs at even lower temperatures if CH_4 and N_2 are present, (Roedder (1984). The salinity of the H_2O-CO_2-NaCl system is determine by clathrate (Tmcl) melting that occurs between -15 and +10 °C. Clathrate melting is, however, difficult to identify as its refractive index is close to that of water.

6.11 H_2O-CO_2 PRESSURE AND COMPOSITIONAL DETERMINATION

Homogenisation of the CO_2 phase takes place in two ways. Either the internal bubble contracts - resulting in vapour to liquid (V - l) homogenisation, or alternatively, the internal bubble expands resulting in liquid to vapour (l - V) homogenisation. The homogenisation type is critical in determining formation pressures (Figure 6.5). Homogenisation of CO_2 occurs between -56.6 and +31.5 °C depending on pressure, H_2O versus CO_2 fraction in the fluid (Roedder, 1984).

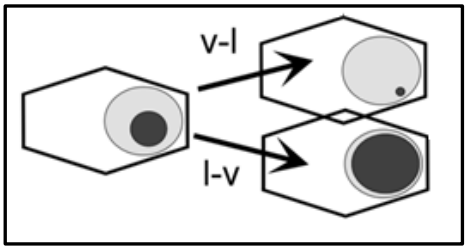

Figure 6.5: Modes of homogenisation of the CO_2 phase. Either vapour to liquid (V-l), or liquid to vapour (l-V) (Schmidt-Mumm, 2008).

The H_2O-CO_2 system investigated in the TNGB consist predominately of high X_{H2O} and low X_{CO2}. Bulk molar volume of FIs can be determined by identifying the pressures and temperatures at homogenisation. FIs with high X_{H2O}, and low X_{CO2}, cool from a supercritical homogeneous liquid along an isochore (Figure 6.6). This means the intersection of the miscibility boundary of the H_2O rich limb (bubble surface) results in two phases; a bubble of CO_2 liquid encased by aqueous liquid, and a CO_2 bubble that nucleates within the carbonic liquid with progressive cooling. Clathrate forms between +10 and -30 °C. Ice will form on further cooling. X_{H2O} compositions vary from 0.852 to 0.985 in the TNGB carbonic FIs. The carbonic phases vary in volume from <2 to 95 vol. % as outlined by Diamond (2001). Generally, there is a larger volume proportion of liquid CO_2 present at the triple point in the higher X_{CO2} TNGB FIs.

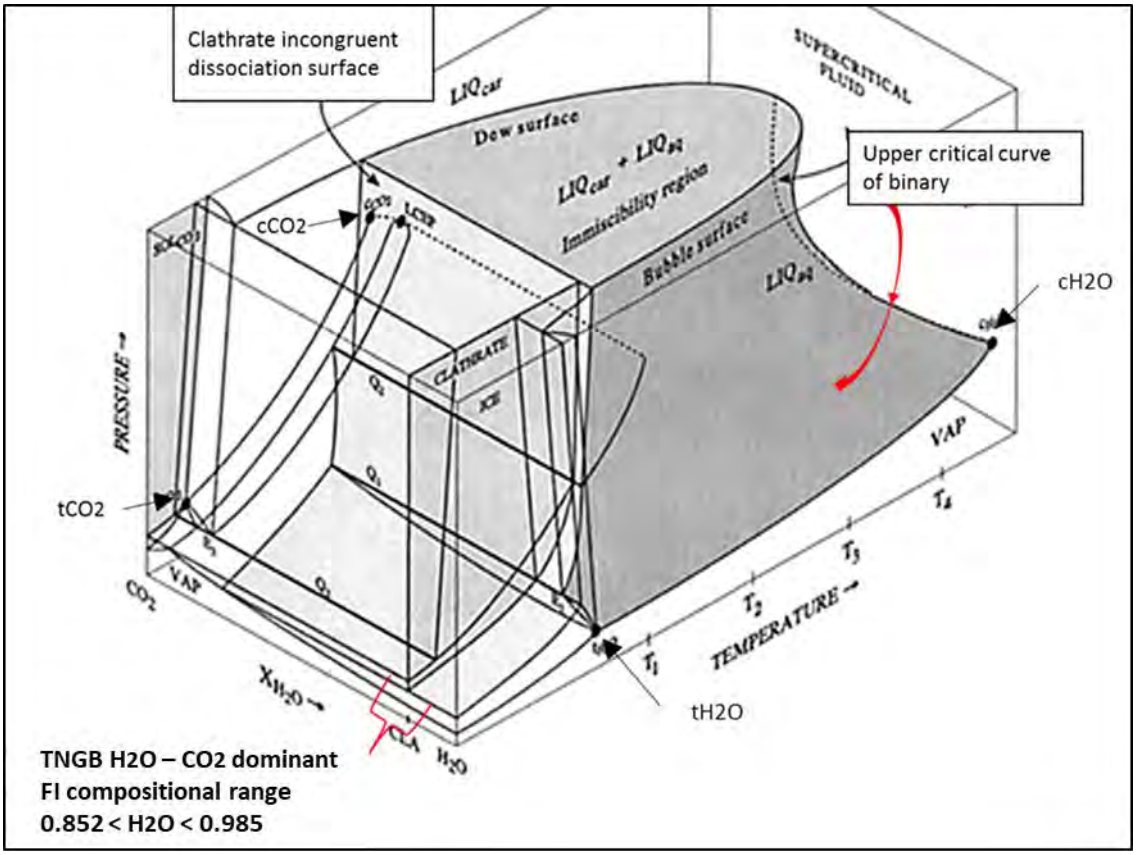

Figure 6.6: The PTX equilibrium model for the H_2O-CO_2 system (not to scale). The region of liquid-liquid immiscibility, the clathrate dissociation surface, and the compositional planes of solid CO_2 and clathrate are shaded. Note: tCO_2 = triple point of CO_2 at -56.6 °C and 5 bar. tH_2O = triple point of H2O at 0.01 °C and 0.006bar. cCO_2 = critical point of CO_2 at 31.1 °C and 74 bar. cH_20 = critical point of H_2O at 374 °C and 221 bar. The bracketed area on the X_{H2O} axis and the red arrow point in the direction of phase changes with temperature with relevant isochores of the 'bubble surface' change for carbonic FIs in the TNGB (Diamond, 2001).

Diamond (2001) outlined a quantitative method for bulk molar V - X in high X_{H2O} and low X_{CO2} FIs using low and high temperature measurements. This method correlates the Th tot measurements with the low temperature phase transition of Th CO_2 (Figure 6.7).

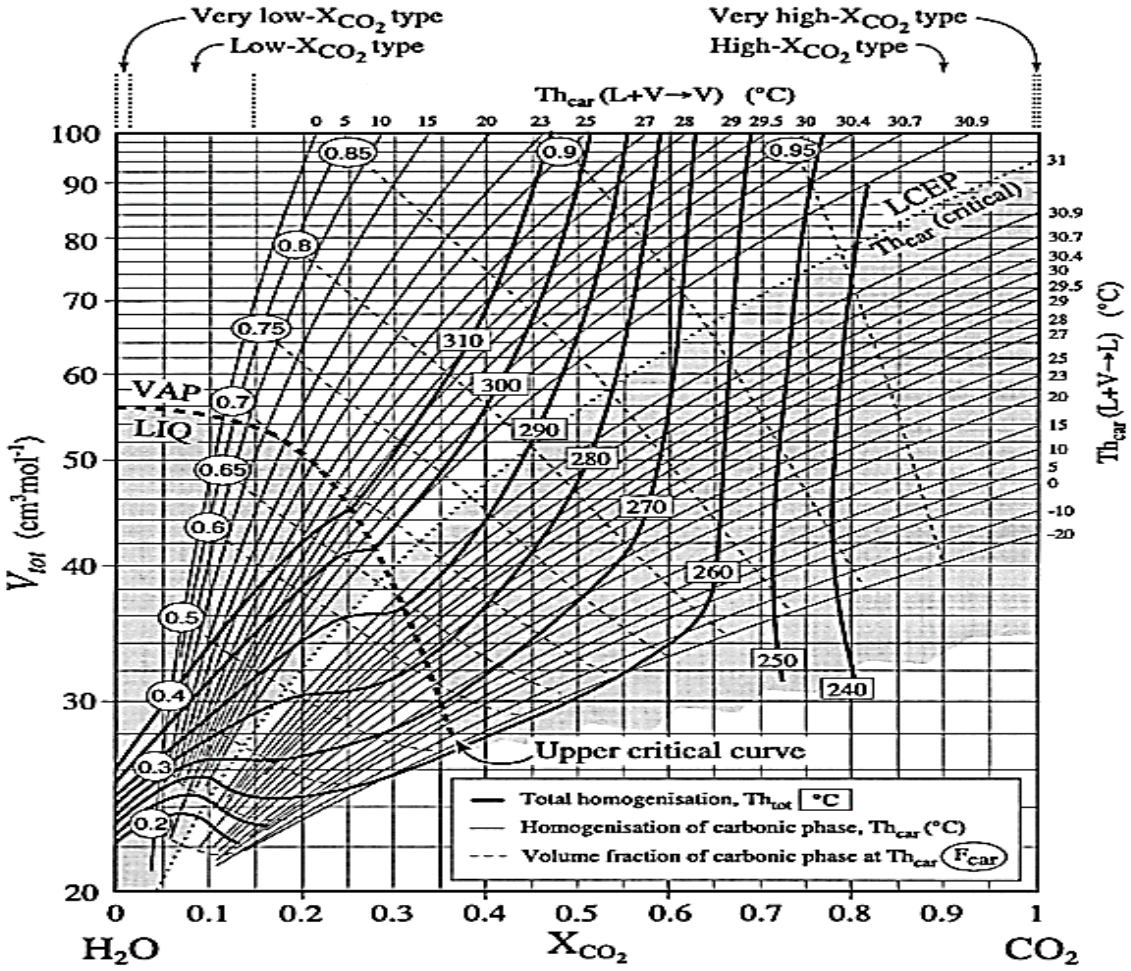

Figure 6.7: Total molar volume (Vtot) vs. total mole fraction CO_2 (X_{CO2}) for the CO_2-H_2O system. The compositional types delimited on the top axis refer to those in the text and 6.6. Shaded quadrants illustrate the four principal modes of FI behaviour during microthermometry. FIs that undergo total homogenisation to a liquid phase - plot to the left of the upper critical curve (LIQ field). FIs that homogenise to the vapour - plot to the right (VAP field). Inclusions with carbonic phases that homogenise to the vapour phase - plot above the dotted LCEP curve. FIs that homogenise to the liquid phase - plot below the LCEP curve. $Thco_2$ is denoted as Th car. Light dashed contours - volume fractions of the carbonic phase visible at Th car. Vtot and X_{CO2} is determined by intersecting the measured Thtot and Thcar values, while taking homogenisation into account (Bakker and Diamond, 2000).

6.12 H_2O-CO_2-NaCl FI SALINITY DETERMINATION

The methods of calculating salinities from final ice melting temperatures cannot be applied to Type 3, 4 and 5 aqueous-carbonic FIs because of the overestimation of salinities based on Tm ice values occurs due to aqueous phases bound in clathrate and the obscurement of visible ice melting. Chen (1972) developed an equation to determining salinities for the H_2O-CO_2-NaCl system from clathrate melting - Equation 9 EQ9. Fall et al. (2011) determined FI PTXV characteristics that combine microthermometric and Raman Spectroscopic techniques on clathrate melting.

EQ9

$W = 0.00098241 (10 – T) (T^2 + 45.385T + 1588.75)$

W is the wt. % NaCl eq. and T is the final clathrate melting temperature (°C).

The values of W calculated by EQ9 deviate from experimentally determined values by an average of 1.33 %. This equation is valid for all salinities between 0 and the eutectic salinity 24.2 wt. % NaCl eq., provided that the clathrate phase melts in the presence of both liquid and vapour CO_2. FI isochore generation for this study relied on CO_2 – NaCl – H_2O isochores generated from Brown and Lamb (1989), using equations by Kerrick and Jacobs (1981) and Bowers and Helgeson (1983). These values were then compared against Bower and Helgeson's (1985) calculations in the Fortran program - 'DENFIND'; that allows for corrections in FIs that in the H_2O - CO_2 - NaCl system homogenise above 350 °C.

6.13 H_2O-CO_2 TOGETHER WITH CH_4 AND N_2

Other volatiles, such as CH_4 and N_2 further expand the immiscibility ranges of H_2O-CO_2 (Zhang & Frantz, 1992). CH_4 and N_2 together with NaCl increase the physiochemical differences between CO_2 and H_2O molecules. The addition of CH_4 and N_2 tends to drive the dissociation curve of clathrate to higher temperatures opposite to the effect of salts (Dubessy et al., 1992; Diamond, 1994 and Bakker, 1997). Thiéry et al. (1994) and Van den Kerkhof and Thiéry (2001) identified that elevated concentrations of CH_4 and N_2 present within CO_2 have discreet phase transitions. According to Diamond (2001), Raman spectroscopy becomes the only accurate means to determine PTVX formation conditions when multiple components are added to a system. Liquid-vapour equilibria and calculation of the molar volume in the CO_2-CH_4-N_2 were never determined in TNGB FIs. Their presence was, however, identified through Raman spectroscopy.

6.14 RAMAN SPECTROSCOPY

According to Roedder (1984), FIs are most successfully analysed by coupling microthermometry with Raman spectroscopy. He also considered Raman spectroscopy to be the most effective qualitative and quantitative method to evaluate single FIs, as microthermometry requires CO_2 homogenisation to be observed. Rosso and Bodnar (1995) developed a method to determine the CO_2 vapor pressure (where $P_{CO2} \approx$ P internal) in FIs with low bulk density and no visible CO_2 homogenisation. Rosso and Bodnar's (1995) method is used to interpret band splitting of v_1-$2v_2$ Fermi diad; with increasing densities, the CO_2 Fermi diad bands shift to lower frequencies (or wavenumbers) (Figure 6.8).

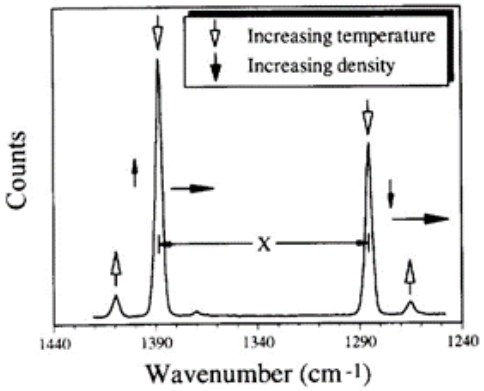

Figure 6.8: CO_2 bands shift as a result of temperature and density effects. The arrow size is proportional to the change experienced by each band. Fermi diad bands shift to lower wave number with increasing density. The lower band shifts more rapidly than the upper band (Rosso and Bodnar, 1995).

Garrabos et al. (1980) identified that the frequency shift of the lower band has higher density dependence than the upper band. Conversely the intensity ratio of the upper band to the lower band increases with increasing densities (Figure 6.9). This allows for the detection of low concentrations of CO_2 and interpretation of densities to approximately ±0.2 g/m^3. Fall et al's. (2011) equation relates CO_2 density to the splitting of the Fermi diad for CO_2 in H_2O-CO_2-NaCl FIs using Equation 10 (EQ10).

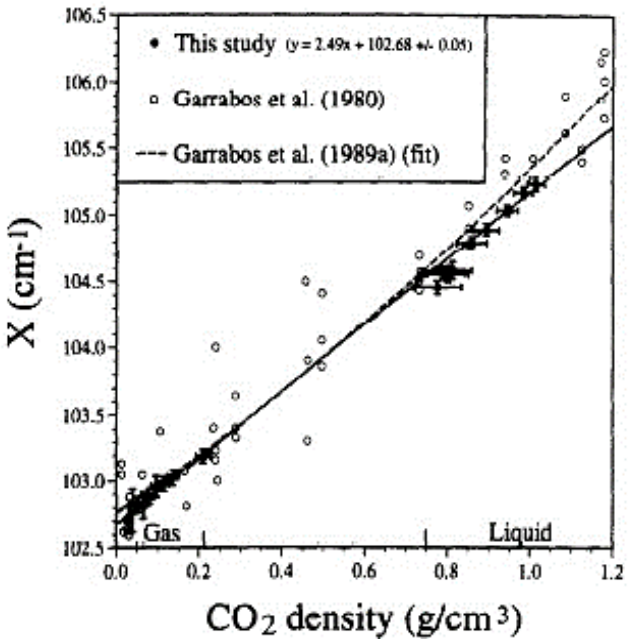

Figure 6.9: The Fermi diad bands splitting (X) is a linear function of density (Garrabos et al., 1980 & 1989 and Rosso and Bodnar, 1995).

EQ10

$pCO_2 = -0.030314551 \times \Delta^3 + 9.432834797 \times \Delta^2 - 997.9384933 \times \Delta + 33780.38242$ (10)

Where pCO_2 is the density of carbon dioxide in g/cm^3, and Δ is the distance between the two peaks of the Fermi diad in cm^{-1}.

The O - H stretching region (2800 - 3800 cm^{-1}) in Raman spectra of aqueous solutions is sensitive to variations in salinity. Mernagh & Wilde (1989) calculated the skewing parameters from Raman microprobe spectra to determine the salinity aqueous phase of FIs at room temperature. This method can be applied to most chloride solutions that occur in FIs. The water band shifts from 3407 cm^{-1} for pure water to approximately 3450 cm^{-1} for a saturated NaCl solution (26.5 wt. % NaCl eq. at room temperature) (Figure 6.10). This effect is mainly a result of an increased chloride concentration. This method complements microthermometric data and allows for the determination of salinity when clathrate formation precludes accurate determination of salinity. This method is also suited to salinity calculations in which phase changes are difficult to discern due to the small size and irregular shape of FIs (Mernagh and Wilde, 1989). Studies of synthetic FIs of the NaCl-H_2O system shows that salinities up to halite saturation can be determined to within ± 2 wt. % NaCl eq. The Raman microprobe is also able to readily analyse the small volume of liquid in vapor-rich inclusions. The total salinity of the fluid at the time of trapping cannot be derived from Raman spectra in FIs that contain halite crystals. In these cases, only the salinity of the saturated aqueous phase is obtainable.

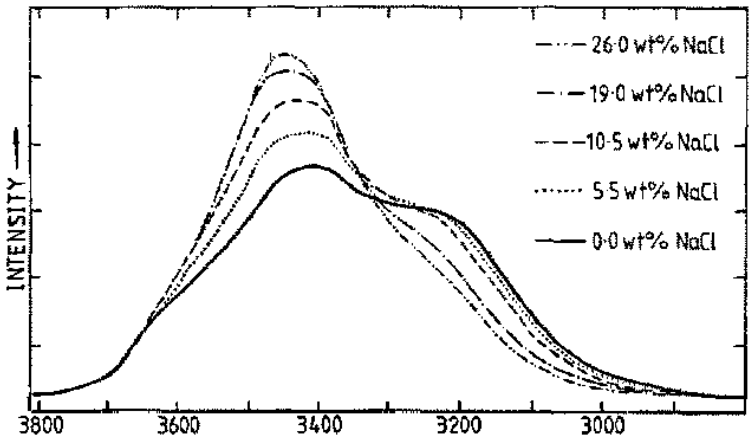

Figure 6.10: The Raman O-H stretching bands vary with fluctuations in NaCl concentration in aqueous saline FIs (Mernagh & Wilde, 1989).

7. DEFINING GENETIC GROUPS USING MICROTHERMOMETRY AND RAMAN SPECTROSCOPY

7.1 INTRODUCTION

Chapter 7 combines the information from Chapters 4 and 5 in which six different fluid Types were distinguished in terms of their composition and petrographic variations and the general macroscopic features of their hosting hydrothermal veins. An interdependency between the presence of specific fluids and specific mineral phases allows for the distinction between different groups of veins defined by combinations of mineral assemblage and associations of fluid types. These will be referred to as "Groups" or 'genetic Groups" (Figure 1). In this regard it will be demonstrated that the presence or absence of tourmaline correlates with the presence or absence of specific fluid Types. It will also be noted that the only analysed pegmatite sample is from Kamituga (Ktm-3); and assigned to the fluid-mineralogical association - Group 1. Further to this it will be shown that the presence or absence of tourmaline correlates with the presence or absence of specific fluid Types. Group 2 are hydrothermal veins that contain tourmaline. Group 3 are hydrothermal veins that are tourmaline-free. Groups 2 and 3 are present in all Kamituga, Lugushwa and Namoya's deposits.

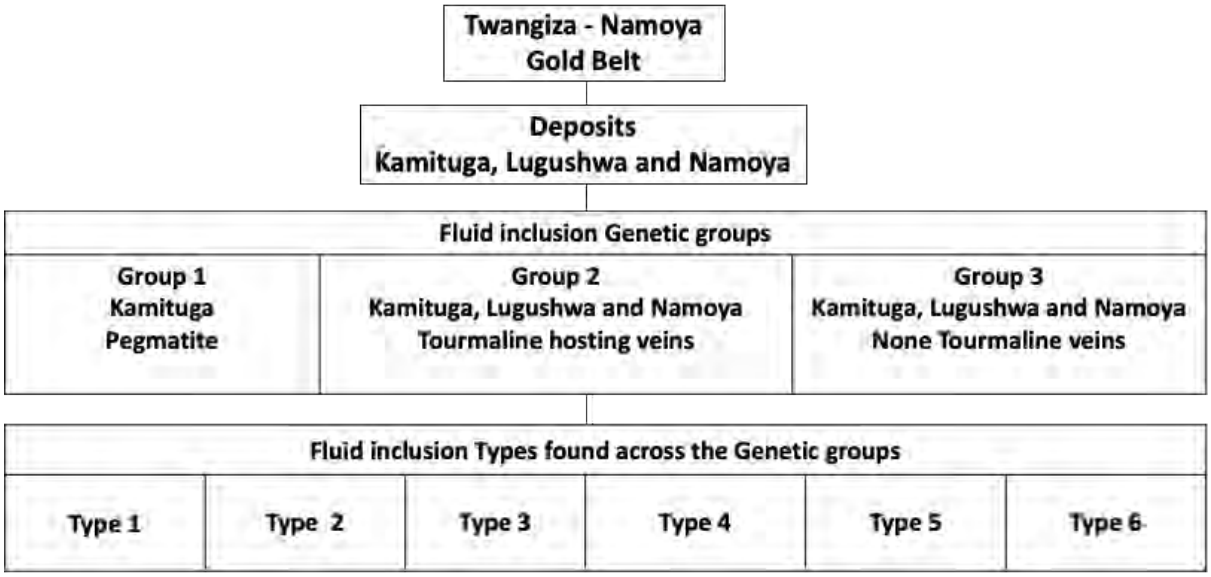

Figure 7.1 Diagrammatical representation of the relationship between areas, Genetic groups and fluid inclusion Types in the TNGB.

In the context of the Groups, this chapter also considers the gold grade as a relevant feature. It will become evident that the Groups, irrespective of their fluids' compositional similarities, formed at different pressures and temperatures (PT) in different parts of the TNGB. This requires that the microthermometric data be described in the context of the Groups. A separate description of the Groups and the related thermometric data was considered, but such a text structure would either cause loss of context or to the presentation of redundant material.

In order to streamline the text in the following sections the reader can assume that all FIs homogenise to the aqueous liquid phase unless stated otherwise. Only Type 1, 2, 3 and 4 FIs were thermometrically evaluated, because Type 5 and 6 FIs have unfavourable phases and/or phase proportions for thermometric evaluation. Furthermore, Type 5 FIs decrepitate before Th is reached, rendering them unsuitable for accurate PT evaluation. Type 1, 2, 3 and 4 FIs, present in the majority of samples, provided enough data to compare fluid capturing conditions at Kamituga, Lugushwa and Namoya. Salinity and total homogenisation histograms are normalised to ten readings for each FI type found in the different quartz phases across the samples in that Group (Figure 7.8, 7.9, 7.21, 7.22, 7.32, 7.33, 7.38, 7.39, 7.46, 7.47, 7.55, 7.56, 7.62 and 7.63).

7.2 KAMITUGA - GENETIC GROUPS

7.2.1 KAMIUGA GROUP 1: PEGMATITE (Ktm-3)

Group 1 is defined by the pegmatitic assemblage and fluids in sample Ktm-3 from drill core KDD033 (Table 7.1). It was the only pegmatite sourced from the three deposits. Boron isotopic variations and geochronological data and preliminary FI results were obtained from the sample in conjunction with Büttner et al. (2016). Ktm-3's pegmatitic conditions of formation set it apart from other samples that were taken from lower temperature hydrothermal veins. This thin, approximately 3 cm thick vein, contains the mineral assemblage quartz, plagioclase, alkali feldspar, tourmaline, white mica and minor sideritic carbonate (cf. Büttner et al., 2016). Apatite and sulphide minerals (pyrite and arsenopyrite) are present as accessory phases. Sample Ktm-3 contains 1 - 5 mm quartz grains, with most showing partial recrystallisation. Primary FIs are present in pegmatitic primary quartz. Secondary FIs are present along healed micro-fractures in pegmatitic and recrystallised quartz. Quartz recrystallisation is prominent along quartz-tourmaline grain boundaries.

Table 7.1: Macro- and microscopic descriptions of Kamituga Group 1, 2 and 3 samples and primary, pseudosecondary and secondary FI Types.

Group	Drill core or Sample site	Sample No.	Depth metres & vein thickness (cm) respectively	Deformation features of veins	Au grade g/t	Macroscopically visible sulphides	Macroscopically visible number of quartz species & Types	Tourmaline /carbonate present	Host rock and general notes	FI Types present *Listed in decreasing abundance. Blue represents primary or pseudosecondary FIs and red secondary FIs.
1	KDD033	Ktm-3	118.80/3	Sheared	0	Pyrite & arsenopyrite	1	Y/Y	Muscovite -rich pegmatitic vein in metapelite.	T1, T2, T4, T6, T3, T5 T4, T6, T3
2	KDD037	Ktm-1	60.50/3	Sheared	3.04 -5.62	Arsenopyrite & pyrite	1	Y/Y	Tourmaline crystals up to 2 cm long grow semi-perpendicular to vein boundary with diorite.	T1, T2, T3, T4, T5, T6 T3, T4, T6, T5
2	KDD004	Ktm-2	121.5/1-2	Foliated	15	Arsenopyrite, pyrite, pyrrhotite, chalcopyrite	1 Individual fractured grain between sulphides & crosscut by sulphides	Y/Y	Foliated metadiorites, highly altered with high percentage sulphides.	T1, T2, T3, T4, T6, T5 T3, T4, T6, T5
2	KDD003	K2	53.6/1800	Microfractures with iron oxides, hydroxides.	0,6	Yes, microscopic arsenopyrite & pyrite	1	Y /N	Slightly weathered diorite.	T1, T2, T3, T4, T5, T6 T3, T4, T6, T5
		K3	60/15	Microfractures with iron oxides, hydroxides.	1.69	Yes, microscopic arsenopyrite & pyrite	1	Y/N	Slightly weathered diorite, irregular transition boundary with diorite.	T3, T4, T5, T1, T2, T6 T3, T5, T4, T6,
		K4	67.7/1-9	Alteration by late stage sulphide rich fluid	12.5	Altered sulphide-rich zone. Arsenopyrite & pyrite.	1	Y/N	Slightly weathered diorite.	T3, T4, T6, T5, T1 T3, T4, T6, T5
		K6	84/10-15	Brecciated	1.69	Sulphide resorption holes. Arsenopyrite & pyrite	2 Brecciated dark quartz in milky quartz matrix.	Y/N	Altered quartz diorite.	T1, T2, T3, T4, T5, T6 T3, T4, T6, T5 (p and s FI (None recrystallised quartz contains more T1 and T2 primary FIs).
2	KDD003	K7	117.3/7	None	0	Yes, microscopic arsenopyrite & pyrite.	2 Dark & light grey	Y /N	Altered quartz diorite.	T4, T6, T3, T5, T1, T2 T4, T6, T3, T5, (primary and secondary FIs occurrence dependent on quartz Type. i.e. none recrystallised darker quartz more saline with more T1 and T2 and high salinity T4 FIs).

Table 7.1 cont.: Macro- and microscopic descriptions of Kamituga Group 1, 2 and 3 samples and primary, pseudosecondary and secondary FI Types.

Group	Drill core or Sample site	Sample No.	Depth metres and vein thickness (cm) respectively	Deformation features of veins	Au grade g/t	Macroscopically visible sulphides	Macroscopically visible number of quartz species & Types	Tourmaline /carbonate present	Host rock and general notes	FI Types present *Listed in decreasing occurrence. Blue represents primary or pseudosecondary FIs and red secondary FIs.
2	KDD031	K9	38.8/30	Intense foliation Microfractures with iron oxides, hydroxides.	0.36	Arsenopyrite and pyrite.	1	Y/N	Foliated quartz diorite. Tourmaline rich halo at interface to host rock.	T1, T2, T3, T4, T5, T6 T3, T4, T6, T5
2		K10	56.5/several metres	Alteration by late stage sulphide rich fluid with hydroxide and oxides	4.69	Arsenopyrite and pyrite.	2 (dark grey Qtz brecciated in milky quartz matrix.	Y/N	Quartz diorite.	T3, T4, T5, T6, T1 T3, T4, T6, T5
3	Mount Kibukira field samples	K12	NA	None	Not assayed from mineralised zone	Pyrite	1	N/N	Weathered saprolite Part of N - S fractures.	T3, T4, T5, T6, T1, T2 T3, T4, T6, T5
2		K14	NA	None	Not assayed from mineralised zone	Pyrite	2	Y/N	Weathered saprolite Part of E – W fractures.	T3, T5, T4, T6, T1, T2 T3, T4, T5, T6
3	KDD015	K16	51.5/1-5	Amoeboid Segregation	<0.5	Only visible under microscope. Pyrite and arsenopyrite	2	N/N	Amoeboid segregation of quartz out of dark metapelite. Abundant biotite in quartz vein.	T4, T5, T6, T3, T4, T6, T5
3		K19	77.4/2	Segregation	4.28	Only visible under microscope. Pyrite and arsenopyrite	2	N/N	Quartz vein at interface of metasiltstone & metapelite. Abundant biotite in quartz vein.	T3, T4, T6, T5, T1, T2 T3, T4, T6, T5
3		K21	85.2/3-10	Folded, pinched—and-swell (plastic folding)	1.07	Abundant disseminated sulphides (Pyrite and Arsenopyrite) and pyrrhotite stringers	2 Large clear regular shaped quartz vs. irregular fractured dirty host quartz	N/N	Dark metapelite folded.	T3, T4, T6, T5 T3, T4, T6, T5
3		K22	96.5/3-10	Undeformed	4.03	Vein margin and small specs throughout the vein. Pyrite and arsenopyrite	2 Transparent milky quartz (30%) vs. opaque. Some fibrous quartz.	N/N	Dark carbonaceous metapelitic.	T3, T4, T6, T5, T1 T3, T4, T6, T5
3		K24	99.3/1-3	Undeformed	<0.5	Pyrite and Arsenopyrite	1	N/N	Sulphide bearing metapelite. Reaction halo lining margin of quartz vein within sulphide bearing metapelite.	T4, T5, T6, T3, T4, T6, T5

Quartz near tourmaline contains highly saline Type 1 and 2 primary and pseudosecondary FIs and low salinity Type 3, 4 and 6 primary FIAs. Tourmaline grains (0.5 - 2.5 mm) do not show optical zonation and show colourless to strong blue pleochroism (Figure 7.2). Tourmaline appears dark blue to black in hand specimens. A second concentrically zoned, yellow to brown finer-grained tourmaline is present in alteration halos. Pyrite is present within quartz grains as 30 - 100 µm anhedral - to lath-shaped inclusions. Pyrite occurs in the matrix with white mica (0.1 - 2.5 mm) and with secondary chlorite grains. Small white mica (10 - 150 µm) grains appear to have formed by recrystallisation along white mica margins. Other minerals such as alkali feldspar, sideritic carbonate and accessory apatite are spatially associated with white mica.

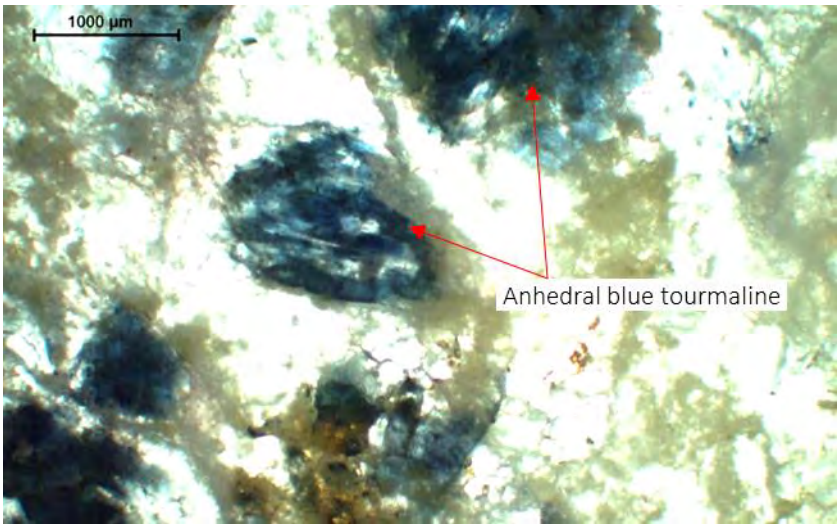

Figure 7.2 Ktm-3 Group 1 pegmatite. Blue tourmaline grains viewed under plane polarised light.

7.2.1.1 PRIMARY FIs in Ktm-3

In large unrecrystallised pegmatitic quartz grains, numerous irregular-to-spherically shaped primary FIs range in size from 1 - 8 µm. Type 1 and 2 primary FI are prolific and most numerous in unrecrystallised quartz near tourmaline. These have been interpreted to be co-genetic with tourmaline. Type 1 and 2 primary FIs contain large halite cubes - suggesting that the initial fluid influx was highly saline. This is typical of pegmatitic fluids (Roedder, 1984). In addition to halite, Type 2 primary FIs contain solid phases; these are sylvite (KCl) and Fe-chlorides ($FeCl_n$) as determined through microthermometry and petrography (Figure 7.3A). Sylvite is common in all Type 2 primary FIs. Fe-chloride daughter crystals associated with quartz containing blue tourmaline were observed in ~20% of Type 2 primary FIs. This suggests that there was a higher concentration of K than Fe ions in primary fluids.

The interpretation that pegmatite fluids are Fe-rich (Büttner et al., 2016) is supported by the presence of Fe-chloride solids in Type 2 primary FIs found in quartz associated with Fe-rich blue tourmaline. According to Roedder (1984) and Wilkinson (2001), high salinity brines - denoted by large halite crystals, sylvite and/or Fe chlorides are typically associated with granitoid bodies. In contrast to primary pegmatitic quartz the recrystallised quartz contains few primary FIs, suggesting that during recrystallisation most FIs were eliminated.

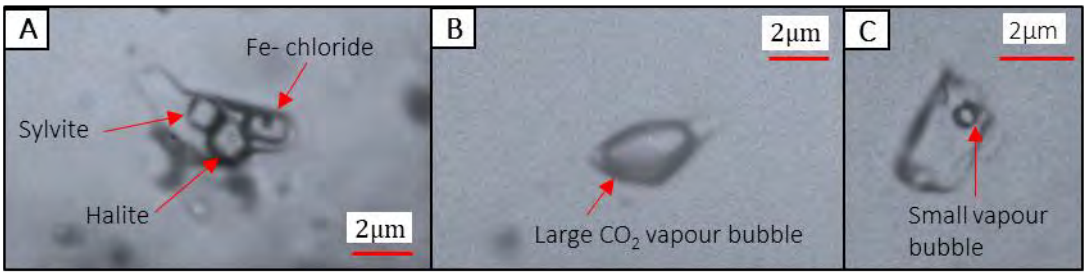

Figure 7.3: Ktm-3 primary and secondary FIs. (A) Type 2 primary FI with large halite, sylvite and iron chloride (tabular or rhombic daughter mineralinterpreted as lawrencite). (B) Small Type 3 primary FI near blue tourmaline. (C) Type 4 secondary FIs with small vapour phase.

Other primary FIs in Type 1 and 2 primary FIAs are vapour -rich Type 3 (Figure 7.3 B) and highly saline but halite-free Type 4, and vapour-poor Type 6 primary FIs (Table 7.1). CO_2 vapour -rich Type 5 primary FIs are present with FIAs in sulphide-containing quartz grains. Type 5 primary FIs are located close to both host rock boundaries and to sulphide grains. No FIs containing CH_4 and N_2 were identified in sample Ktm-3. Most CO_2 vapour-rich Type 3 primary FIs are found proximal to concentrically zoned yellow to brown tourmaline and Type 1, 2, 4 and 6 primary FIs. CO_2 vapour-rich Type 3 FI are observed as pseudo-secondary inclusion trails in quartz; suggesting a co-genetic relationship. The predominance of CO_2 vapour-rich Type 3 primary FIs is a characteristic of effervescence in pegmatites - similarly seen in granitoid samples (Wilkinson, 2001). Type 4 and 6 FIs, with small vapour phases and a few CO_2 vapour-rich Type 3 FIs, were the only secondary FIs found along healed fractures (Figure 7.3 C).

Type 1 and 2 primary FIs, associated with blue tourmaline, are more numerous and have higher Th than those associated with the concentrically zoned yellow to brown tourmaline. They also display total homogenisation by the dissolution of halite. According to Ramboz, et al. (1982), if one of several solids are present in a FI these fluid inclusions can only represent fluid-fluid immiscibility if melting temperatures of solids Tm is not higher than the fluid's homogenisation temperature. Melting temperature that equal Th is characteristic of unmixing of a fluid saturated with solids. Immiscibility of fluids generally yields fluids of contrasting density and composition, for example a high-density liquid enriched in dissolved salts and poor in (but not free of volatiles) and a low density vapour rich in volatiles and dissolved salts (Ramboz, et al.,1982). Type 1 primary FIs have Tm (halite) between 360 - 442 °C (avg. 393 °C) and Th (L - V) of 346 - 430 °C (avg. 378 °C) as calculated from Lecumberri-Sanchez's (2012) equations. Salinities of Type 1 primary FIs range between 43.8 and 52.8 wt. % NaCl eq. (avg. 47.2 wt. % NaCl eq.) High salinity causes the formation of vitric ice that recrystallises at very low temperatures - changing the ice to a dark brown, almost black colour. Total homogenisation pressures and densities were determined using the spreadsheet from Steel-MacInnis et al. (2012). Type 1 primary FIs in sample Ktm-3 (KDD033) have Th pressures of 24.8 - 33.5 MPa (avg. 29 MPa). This does not reflect the conditions of fluid entrapment that occurred at considerably higher PT conditions. The fluid densities are 1.10 - 1.13 g/cm^3, (avg. 1.11 g/cm^3) (Table 7.2). Sylvite-only Type 2 primary FIs have Te that occurs at -23 °C to -25 °C as calculated from equations in Roedder (1984). This suggests the presence of sylvite (KCl) (Roedder, 1984) that was possibly influenced by $FeCl_2$ and NaCl in solution. Type 2 primary FIs, with solid Fe-chloride, have Te of -28 °C to -32 °C. This Te range is influenced by

the presence of large KCl daughter phases (Roedder, 1984). Type 1 and 2 primary FIAs, present near blue tourmaline, contain Type 3 and 4 primary FIs with homogenisation temperatures below 330 °C (Table 7.2). Type 4 primary FIs have Th (L - V), 294 - 324 °C (avg. 303 °C) with 7.9 - 26.6 wt. % NaCl eq. (avg. 18.6 wt. % NaCl eq.) and total homogenisation pressures and densities of 7.5 - 9.4 MPa (avg. 7.8 MPa) and 0.81-0.96 g/cm^3, (avg. 0.90 g/cm^3) as per Sterner et al. (1988), Bodnar (1993) and Steel-MacInnis et al's. (2012) calculations. These low pressures and densities are not indicative of fluid capture as they represent conditions at total homogenisation.

Table 7.2: Microthermometric and Barometric Data of Type 1, 3, and 4 primary FIs for Kamituga Group 1.

Phase relationship	FI Type	Tm	Final phase melting	$Th_{(L-V)}$	wt. % NaCl	T @ homog. (°C)	P @ homog. (bar)	r_{BULK} (g/cm_3)	Reference
None recrystallised primary quartz, with blue tourmaline associated primary FIs	Upper Th final by halite Tm for Type 1 FIs	442	Halite	430	52.8	442	335	1.13	Lecumberri-Sanchez et al. (2012) and Steel-MacInnis et al. (2012)
None recrystallised primary quartz, with blue tourmaline associated primary FIs	Lower Th final by halite Tm for Type 1 FIs	360	Halite	346	43.8	360	248	1.11	Lecumberri-Sanchez et al. (2012) and Steel-MacInnis et al. (2012)
None recrystallised primary quartz, with blue tourmaline associated primary FIs	Avg. Th final by halite Tm for Type 1 FI	393	Halite	378	47.2	393	290	1.11	Lecumberri-Sanchez et al. (2012) and Steel-MacInnis et al. (2012)
None recrystallised primary quartz, with blue tourmaline associated primary FIs	Upper Th final by Th (L - V) for Type 4 FIs	2	Hydrohalite	324	26.6	324	94	0.96	Sterner et al. (1988) and Steel-MacInnis et al. (2012)
None recrystallised primary quartz, with blue tourmaline associated primary FIs	Lower Th final by Th (L - V) for Type 4 FIs	-5	Ice	294	7.9	294	75	0.81	Bodnar (1993) and Steel-MacInnis et al. (2012)
None recrystallised primary quartz, with blue tourmaline associated primary FIs	Avg. Th final by Th (L - V) for Type 4 FIs	-15	Ice	303	18.6	303	78	0.90	Bodnar (1993) and Steel-MacInnis et al. (2012)
None recrystallised primary quartz, with blue tourmaline associated primary FIs	Upper Th Type 3 FIs	8	Clathrate	310	0	310	248	0.96	Chen (1972) and Fall et al. (2010)
None recrystallised primary quartz, with blue tourmaline associated primary FIs	Lower Th Type 3 FIs	10	Clathrate	287	4.0	287	57	0.57	Chen (1972) and Fall et al. (2010)
None recrystallised primary quartz, with blue tourmaline associated primary FIs	Avg. Th Type 3 FIs	9	Clathrate	303	2.0	303	62	0.75	Chen (1972) and Fall et al. (2010)
None recrystallised secondary quartz, with yellow-brown tourmaline associated primary FIs	Upper Th final by halite Tm for Type 1 FIs	389	Halite	371	46.8	389	314	1.11	Lecumberri-Sanchez et al. (2012) and Steel-MacInnis et al. (2012)
None recrystallised secondary quartz, with yellow-brown tourmaline associated primary FIs	Lower Th final by halite Tm for Type 1 FIs	328	Halite	318	40.7	328	185	1.10	Lecumberri-Sanchez et al. (2012) and Steel-MacInnis et al. (2012)
None recrystallised secondary quartz, with yellow-brown tourmaline associated primary FIs	Avg. Th final by halite Tm for Type 1 FIs	340	Halite	323	41.9	340	273	1.11	Lecumberri-Sanchez et al. (2012) and Steel-MacInnis et al. (2012)
None recrystallised secondary quartz, with yellow-brown tourmaline associated primary FIs	Upper Th final by Th (L - V) for Type 1 FIs	325	Halite	362	40.1	362	127	1.05	Lecumberri-Sanchez et al. (2012) and Steel-MacInnis et al. (2012)
None recrystallised secondary quartz, with yellow-brown tourmaline associated primary FIs	Lower Th final by Th (L - V) for Type 1 FIs	292	Halite	330	37.5	330	89	1.05	Lecumberri-Sanchez et al. (2012) and Steel-MacInnis et al. (2012)
None recrystallised secondary quartz, with yellow-brown tourmaline associated primary FIs	Avg. Th final by Th (L - V) for Type 1 FIs	303	Halite	340	38.4	340	100	1.05	Lecumberri-Sanchez et al. (2012) and Steel-MacInnis et al. (2012)
None recrystallised secondary quartz, with yellow-brown tourmaline associated primary FIs	Upper Th final by Th (L - V) for Type 4 FIs	-23	Ice	360	24.3	360	156	0.86	Bodnar (1993) and Steel-MacInnis et al. (2012)
None recrystallised secondary quartz, with yellow-brown tourmaline associated primary FIs	Lower Th final by Th (L - V) for Type 4 FIs	-18	Ice	301	21.0	301	71	0.96	Bodnar (1993) and Steel-MacInnis et al. (2012)
None recrystallised secondary quartz, with yellow-brown tourmaline associated primary FIs	Avg. Th final by Th (L - V) for Type 4 FIs	-21	Ice	348	23.0	348	133	0.90	Bodnar (1993)
None recrystallised secondary quartz, with yellow-brown tourmaline associated primary FIs	Upper Th final by Th (L - V) for Type 3 FIs	6	Clathrate	346	4.0	346	248	0.96	Chen (1972) and Fall et al. (2010)
None recrystallised secondary quartz, with yellow-brown tourmaline associated primary FIs	Lower Th final by Th (L - V) for Type 3 FIs	8	Clathrate	290	7.5	290	49	0.13	Chen (1972) and Fall et al. (2010)

Table 7.2 cont.; Microthermometric and barometric data of Type 1, 3, and 4 primary FIs for Kamituga Group 1.

Phase relationship	FI Type	Tm	Final phase melting	$Th_{(L-V)}$	wt. % NaCl	T @ homog (°C)	P @ homog. (bar)	r_{BULK} (g/cm_3)	Formulae/ References
None recrystallised secondary quartz, with yellow-brown tourmaline associated primary FIs	Avg. Th final by Th (L - V) for Type 3 primary FIs	7	Clathrate	320	5.8	320	57	0.57	Chen (1972) and Fall et al. (2010)
None recrystallised secondary quartz, yellow-brown tourmaline associated Type 3, 4 and 6 not associated to Type 1 and 2 primary FIs in close proximity	Upper Th final by Th (L - V) for Type 4 primary FIs	-8	Ice	341	11.7	341	137	0.80	Bodnar (1993)
None recrystallised secondary quartz, yellow-brown tourmaline associated Type 3, 4 and 6 not associated to Type 1 and 2 primary FIs in close proximity	Lower Th final by Th (L - V) for Type primary 4 FIs	-4	Ice	280	6.5	280	61	0.81	Bodnar (1993)
None recrystallised secondary quartz, yellow-brown tourmaline associated Type 3, 4 and 6 not associated to Type 1 and 2 primary FIs in close proximity	Avg. Th final by Th (L - V) for Type 4 primary FIs	-5	Ice	293	7.9	293	74	0.81	Bodnar (1993)
None recrystallised secondary quartz, yellow-brown tourmaline associated Type 3, 4 and 6 not associated to Type 1 and 2 primary FIs in close proximity	Upper Th final by Th (L - V) for Type 3 primary FIs in Type 4 and 6 FIAs	7	Clathrate	333	5.8	333	248	0.96	Chen (1972) and Fall et al. (2010)
None recrystallised secondary quartz, yellow-brown tourmaline associated Type 3, 4 and 6 not associated to Type 1 and 2 primary FIs in close proximity	Lower Th final by Th (L - V) for Type 3 primary FIs in Type 4 and 6 FIAs	10	Clathrate	274	0.0	274	49	0.13	Chen (1972) and Fall et al. (2010)
None recrystallised secondary quartz, yellow-brown tourmaline associated Type 3, 4 and 6 not associated to Type 1 and 2 primary FIs in close proximity	Avg. Th final by Th (L - V) for Type 3 primary FIs in Type 4 and 6 FIAs	8	Clathrate	310	4.0	310	57	0.57	Chen (1972) and Fall et al. (2010)
Type 4 secondary FIs	Upper Th final by Th (L - V) for Type 4 primary FIs	-3	Ice	260	5.0	260	45	0.83	Bodnar (1993)
Type 4 secondary FIs	Lower Th final by Th (L - V) for Type 4 primary FIs	0	Ice	170	0	170	8	0.90	Bodnar (1993)
Type 4 secondary FIs	Avg. Th final by Th (L - V) for Type 4 primary FIs	-2	Ice	243	3.4	243	34	0.84	Bodnar (1993)

Type 3 FIs have Th (L - V) of 287 - 310 °C (avg. 303 °C). Clathrate melting temperatures and Fermi diad spacing of 104 - 105 cm^{-1} indicate salinities of ≤ 4 wt. % NaCl eq., fluid densities of 0.57 - 0.96 g/cm^3 and pressures of 5.7 - 24.8 MPa at clathrate melting as calculated from equations from Chen (1972) and Fall et al. (2011) (Table 7.2). According to Bodnar and Vityk (1994), FIs that display total homogenisation by dissolution of halite (such as Type 1 and 2 primary FIs in this sample) are not related to effervescence. Type 3 and 4 primary FIs, related to effervescence, can consequently not be genetically related to Type 1 and 2 primary FIs - irrespective of their close proximity to each other. It is therefore likely that the pegmatite melt contained two different fluids.

Type 1 and 2 primary FIAs that are near concentrically zoned yellow to brown tourmaline in alteration halos display homogenisation by dissolution of halite, or alternately by liquid-vapour homogenisation. Type 1 primary FIs are homogenised by halite dissolution at Th of 328 - 389 °C (avg. 340 °C) with salinities of 40.7 - 46.8 wt. % NaCl eq. (avg. 41.9 wt. % NaCl eq.) as calculated from Lecumberri-Sanchez's (2012) equations. These values are comparatively lower than Type 1 primary FIs positioned close to blue pegmatitic tourmaline. Fluids with total homogenisation by halite dissolution have Th pressures of 18.5 - 31.4 MPa (avg. 27.3 MPa) and densities of 1.10 - 1.11 g/cm^3 (avg. 1.11 g/cm^3) as calculated from Steel-MacInnis et al's. (2012) equations (Table 7.2). Type 1 primary FIs, with Th (L - V) at 330 - 362 °C (avg. 340 °C), have similar Th and slightly lower salinities 37.5 - 40.2 wt. % NaCl eq. (avg. 38.4 wt. % NaCl eq.) than Type 1 primary FIs with Th by halite loss (Sterner et al., 1988). FIs homogenised by (L - V) dissolution have Th pressures of 8.9 - 12.7 MPa (avg. 10 MPa) and average densities of 1.05g/cm^3 (Table 7.2) as calculated using Sterner et al's. (1988) equations.

Type 1 primary FIs are closely related to cogenetic Type 2 sylvite-bearing primary FIs that have the same range of phase change temperatures. Due to their KCl content, Type 2 FIs can be evaluated using Sterner et al's. (1987) ternary diagrams for the H_2O - NaCl - KCl system. Fluid densities, at Th, range between 5 - 10 MPa and have an average composition of 28 wt. % NaCl eq., 18 wt. % KCl and 54 wt. % H_2O. The H_2O - NaCl - KCl ternary diagram does not, however, account for the presence of Fe-chlorides in solution in Type 2 primary FIs. This is not regarded as a factor of significant error as the density is similar to Type 1 primary FIs in FIAs with a Te that ranges between -21 to -27 °C. Type 1 primary FIs are nearly identical to the Te-range of Type 2 primary FIs near blue tourmaline that are Fe-chloride free. Type 2 primary FIs associated with tourmaline, particularly the blue variety, contain small secondary solids that are too small to be identified microthermometrically or with Raman spectroscopy. These small secondary solids do not dissolve before decrepitation. This suggests that some FIs entrained solid particles from the host or the fluid source, or less likely, FIs were altered after formation. This lack of total homogenisation was seen frequently in Type 2 primary FIs containing Fe-chlorides. Roedder (1984) identified FIs that contain Fe-chlorides and sylvite in addition to halite to generally indicate a high-temperature geological environment.

Type 3, 4 and 6 primary FIs that are contained in quartz near concentrically zoned yellow to brown tourmaline in alteration halos have homogenisation temperatures similar to Type 1 and 2 primary FIAs that homogenised by Th (L - V). Homogenisation temperatures of Type 1 and 2 primary FIs never have more than a 30 °C deviation

in homogenisation by Th (L - V). This suggests that Type 1 and 2 primary FIs were captured simultaneously with Type 3, 4 and 6 primary FIs. Type 4 FIs associated with Type 1 and 2 primary FIs have Th of between 301 - 360 °C (avg. 348 °C). Type 4 primary FIs have high salinities of 21.0 - 24.3 wt. % NaCl eq. (avg. 23.1 wt. % NaCl eq.) and display Th pressures of 7.1 - 1 5.6 MPa, (avg. 13.3 MPa) and densities of 0.86 - 0.96 g/cm^3 (avg. 0.90 g/cm^3) as calculated from Bodnar (1993) and Sterner et al's. (1988) equations. Irrespective of high salinity levels, and despite having conducted numerous heating-freezing experiments, no evidence of hydrohalite formation was found in Type 4 primary FIs. Considering the high salinities and the proximity to halite-containing Type 1 and 2 primary FIs, the lack of hydrohalite in Type 4 primary FIs was unexpected. At time of writing there was no explanation for this.

Type 3 primary FIs, associated with Type 1, 2 and 4 primary FIAs homogenise between 290 - 346 °C (avg. 328 °C) and display lower salinities of 4.0 - 7.5 wt. % NaCl eq. (avg. 5.8 wt.% NaCl eq.) in both liquid and vapour CO_2-rich FIs as calculated from Chen's (1972) equations. Some CO_2 vapour-rich Type 3 FIs expand rapidly near total homogenisation but do not homogenise into an aqueous phase. This corresponds to low pressure conditions of entrapment and low fluid densities (Roedder, 1984) (Figure 7.4).

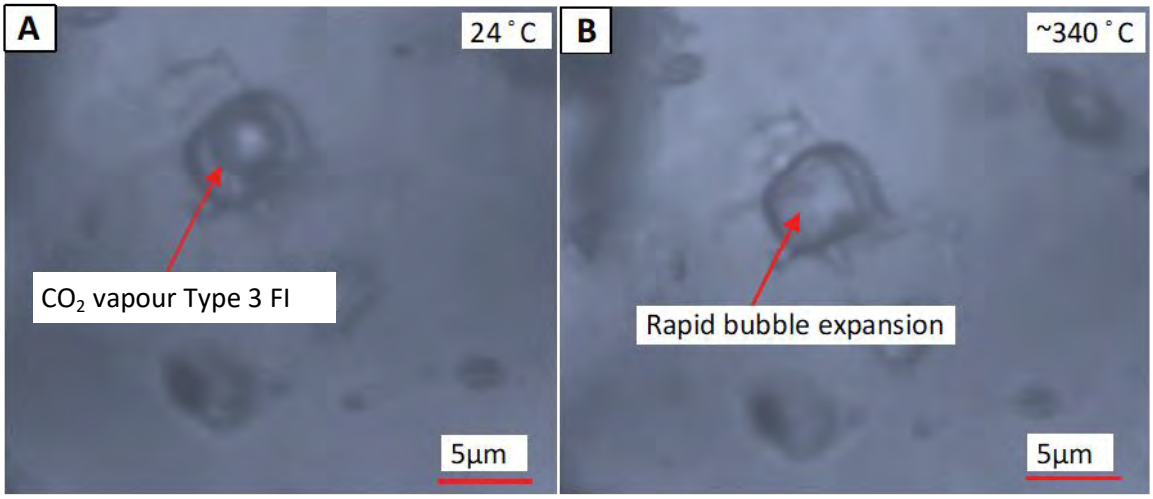

Figure 7.4: Ktm-3 vapour Type 3 primary FI. (A) At ambient temperature (24 °C) with large CO_2 vapour-rich bubble. (B) Vapour bubble rapidly expanding at a rate between 339 - 341 °C homogenise to a vapour phase.

Fermi diad spacing of 103 to 105 cm^{-1} indicates a wide range of densities (0.13 - 0.96 g/cm^3), corresponding to pressures of 4.9 - 24.8 MPa at clathrate melting as calculated using Fall et al's. (2011) equations (Figure 7.5). As Type 3's are primary FIs, as are Type 1, 2 and 4, the capturing pressure should be identical. Textural evidence, such as minor pinching and discolouration around Type 3 primary FIs suggests a secondary alteration processes that may have affected the phase change temperatures of some Type 3 primary FIs. The close spatial and textural (cluster) relationship between Type 1, 2, 3, 4 and 6 primary FIs, and their similar homogenisation temperature ranges, indicate effervescence [boiling and fluid – fluid (H_2O-CO_2)] prior to capturing of the fluids (Table 7.2).

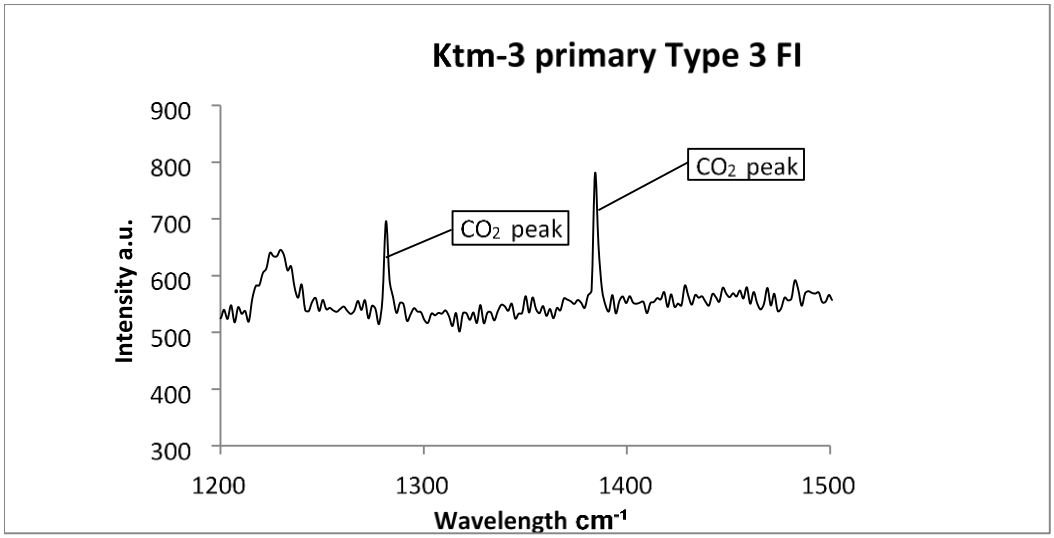

Figure 7.5: Ktm-3 vapour-rich Type 3 primary FI as seen in Figure 7.4. FI at ambient temperature depict CO_2 peaks at 1283 cm^{-1} and 1387 cm^{-1}. No evidence of CH_4 or N_2.

Some FIAs, present near yellow to brown tourmaline, contain no Type 1 and 2 primary FIAs, but do contain Type 3, 4, 5 and 6 primary FIAs. Type 3, 4, 5 and 6 primary FIAs have lower Th and salinities compared to Type 1, 2, 3, 4 and 6 primary FIAs. Type 4 primary FIs in these FIAs have Th between 280 - 341 °C, (avg. 293 °C) and < 12.0 wt. % NaCl eq as calculated from Sterner et al. (1988) and Bodnar's (1993) equations. Pressures at Th are 7.1 - 13.7 MPa (avg. 7.4 MPa) with densities of 0.78 - 0.81 g/cm^3 (avg. 0.81 g/cm^3) as calculated using Steel-MacInnis et al's. (2012) equations. Type 3 primary FIs, associated with Type 3, 4, 5 and 6 FIAs, homogenise at 274 - 333 °C (avg. 318 °C) and contain lower salinities 0 - 5.8 wt. % NaCl eq. (avg. 2.0 wt. % NaCl eq.) in both liquid and CO_2 vapour-rich FIs as calculated using Chen's (1972) equations. Clathrate melting temperatures and Fermi diad spacing of 103 to 105 cm^{-1} indicate densities of 0.13 - 0.96 g/cm^3 and pressures of 4.9 - 24.8 MPa as calculated using Fall et al's. (2011) equations (Table 7.2).

FIAs with and without Type 1 and 2 primary FIs could have formed from a single primary pegmatitic fluid. This is possible due to either phase separation of an aqueous fluid, or by direct separation from a crystallising melt (Bodnar et al., 1993). The differences in Th indicates that Type 3, 4, 5, 6 primary FIAs would be related to late-pegmatitic influx rather than fractionation of a primary pegmatitic fluid. An alternate explanation is that there is a metasomatic interaction between pegmatitic and host rock fluids within the alteration halo.

Pegmatite sample Ktm-3 is not mineralised and contains no CH_4 and N_2. A notable feature of Groups 2 and Group 3 fluids is the presence of CH_4 and N_2 in gold mineralised samples. Pegmatite Type 3 FI's CO_2 melting temperature of approximately -56 to -57 °C indicate, according to Roedder's (1984) own findings, an improbability of other volatile components associated with CO_2 and H_2O. Type 5 FIs do not homogenise prior to decrepitation. The opaque phase, present at decrepitation, shows little or no reduction in size. This indicates heterogeneous entrapment. This opaque phase was identified as HS^{-1} using Raman spectra - suggests a sulphide component (Figure 7.6). Melts or fluids are more likely to entrain and contain solid particles than vapour phases

(Bodnar et al., 1993). Type 5 FIs are therefore likely to represent undissociated primary pegmatitic fluids. This is an important notion as these FIAs are frequently observed in Au-mineralised samples in other genetic Groups.

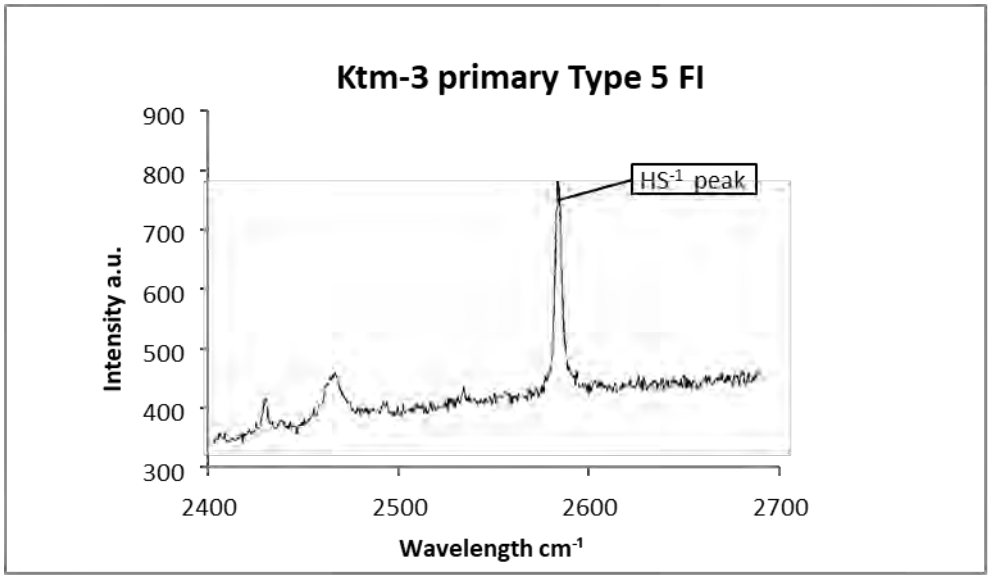

Figure 7.6: Ktm-3 Type 5 primary FI. Darker phase is interpreted to be HS-1 at 2574 cm^{-1}.

7.2.1.2 SECONDARY FIs

All Type 3, 4 and 6 secondary FIAs (<3 µm) in healed fractures in KTM-3 have homogenisation temperatures Th 170 - 260 °C (avg. 243 °C), 100 °C lower than primary and pseudosecondary FIs. The presence of Type 3 CO_2 vapour-rich secondary FIs in close proximity to Type 4 and 6 aqueous-rich secondary FIs indicates effervescence. Raman spectra of the liquid component in Type 4 secondary FIs indicate low salinity values (Figure 7.7). These low salinities correlate to higher ice melting temperatures and salinities values of 0 - 5.0 wt. % NaCl eq. (avg. 3.4 wt. % NaCl eq.) as calculated using Bodnar's (1993) equations. It also correlates to fluid densities at Th of 0.83 - 0.90 g/cm^3 (avg. 0.84 g/cm^3) at pressures of 0.8 - 4.5 MPa (avg. 3.4 MPa) as calculated using Steel-MacInnis et al's. (2012) equations. The phase changes in Type 3 secondary FIs are not clearly visible, and Raman spectra were not reproducible. Microthermometric and barometric information could therefore not be obtained.

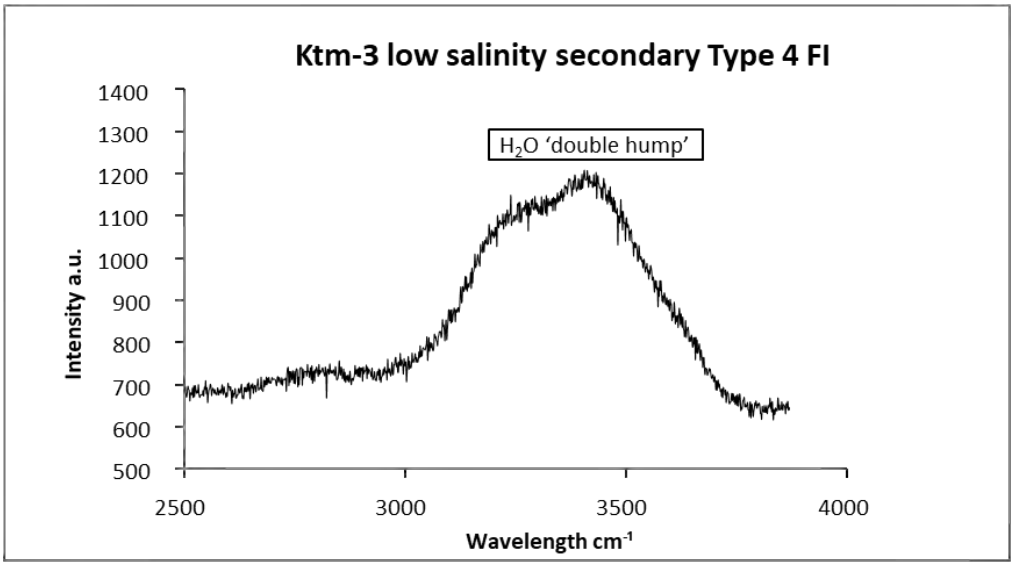

Figure 7.7: Ktm-3 low salinity Type 4 secondary FIs. Low salinities of the aqueous phase in Type 4 are indicated by the shallow 'double hump' in the Raman spectra.

In summary, the characteristics of Group 1 Ktm-3 pegmatitic fluids suggest an early formation of pegmatitic quartz-tourmaline assemblage through magmatic crystallisation. The early formed (primary) mineral phases and the pegmatitic quartz and tourmaline are associated with highly saline primary fluids. Lower-salinity primary FIs occur within quartz along the margin of the pegmatite vein - away from tourmaline. Jackson et al. (1989) and Kelly and Turneaure (1970) related similar observations to late (secondary) pegmatitic influx together with meteoric water, rather than fractionation of a primary pegmatitic fluid. The distinct temperature, salinity variances and phase transitions - especially in Type 1 FIs, indicate a minimum of two distinct stages of fluid evaluated during fractionation. These stages are associated with either primary pegmatitic quartz - texturally related to blue magmatic tourmaline, or to secondary quartz - associated with yellow to brown tourmaline in alteration halos. The two stages overlap in Th. Magmatic Type 1 primary FIs do, however, occupy higher temperature domains of between 420 - 460 °C and have higher salinities than fluids in alteration halos (Figures 7.8 and 7.9).

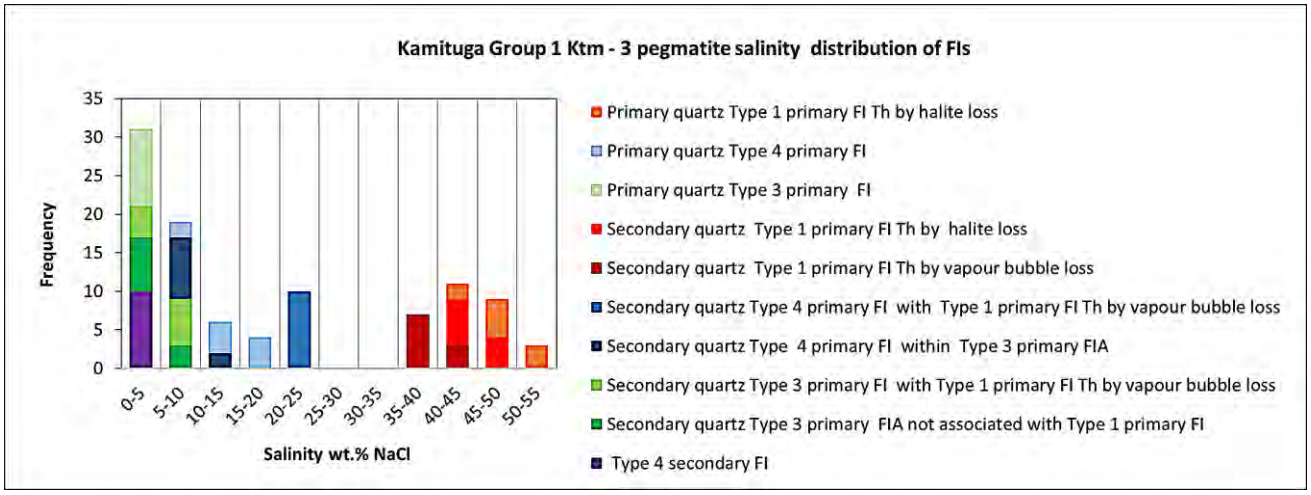

Figure 7.8: Ktm-3 pegmatite salinity distribution for Types 1, 3 and 4 primary FIs. Primary quartz is associated with blue tourmaline. Secondary quartz is associated with yellow to brown tourmaline.

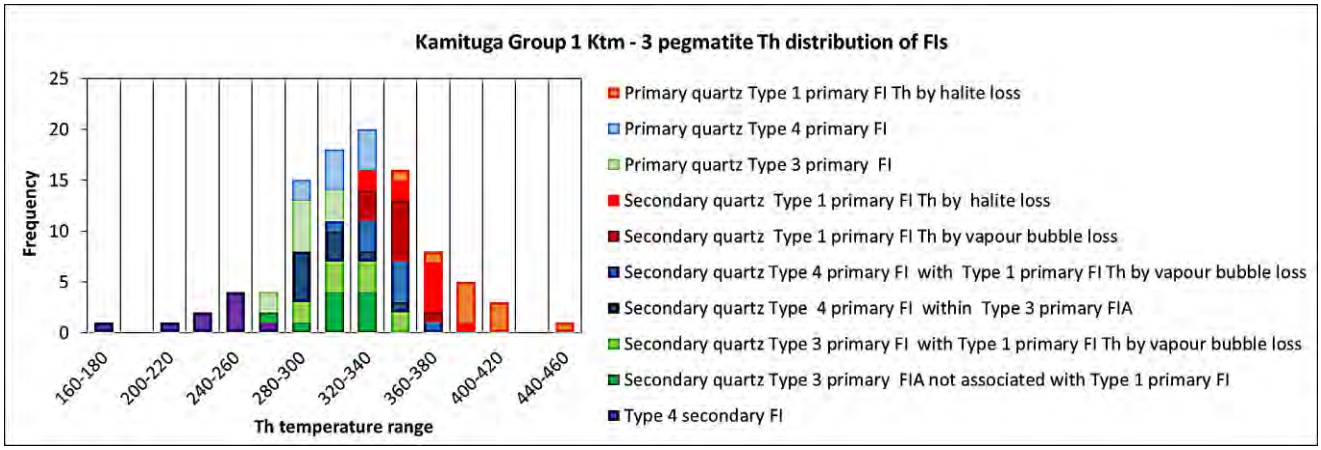

Figure 7.9: Ktm-3 pegmatite Th distribution for Types 1, 3 and 4 primary FIs. Primary quartz is associated with blue tourmaline. Secondary quartz is associated with yellow to brown tourmaline.

There is little evidence of intake of organic materials (C and CH_4) from the surrounding metasediments in the alteration halos and the pegmatite. There is, however, a distinct transition from Fe-rich tourmaline associated Type 1 and 2 primary FIs with higher Th and higher salinities, to Fe-poor tourmaline associated Type 3 and 4 primary FIs with lower Th, salinities, and highly variable formation pressures. This is interpreted as an alteration period that is not directly related to pegmatite emplacement. Whether emplacement and alteration are related to the same geological period or are entirely unrelated events cannot be evaluated on the basis of the available data.

7.2.2 KAMITUGA GROUP 2: TOURMALINE-BEARING HYDROTHERMAL VEINS

All of Kamituga's Group 2 samples are tourmaline-bearing hydrothermal veins (Table 7.1). Most sampled veins were hosted in diorites and show some plastic deformation, expressed in subgrain formation and recrystallisation of quartz. Tourmaline is prismatic and similar to the secondary yellow - brown finer-grained variety of tourmaline present in the alteration halos of Group 1 pegmatite Ktm-3 sample. Kamituga Group 2 tourmaline exhibits concentric optical zonations (Figure 7.10A). Most Group 2 samples display a distinct late-stage sulphide growth along margins of fragmented tourmaline and hydrothermal quartz. The Au grade is typically higher where such sulphides are more abundant (Figure 7.10B) (Table 7.1). Arsenopyrite is the predominant sulphide in diorite hosted veins. Group 2 typically contains quartz, tourmaline, muscovite, sulphides (arsenopyrite > pyrite) and minor amounts of calcite. Roedder (1984) interpreted a similar combination of constituents to be typical of a pneumatolytic and metamorphic hydrothermal system.

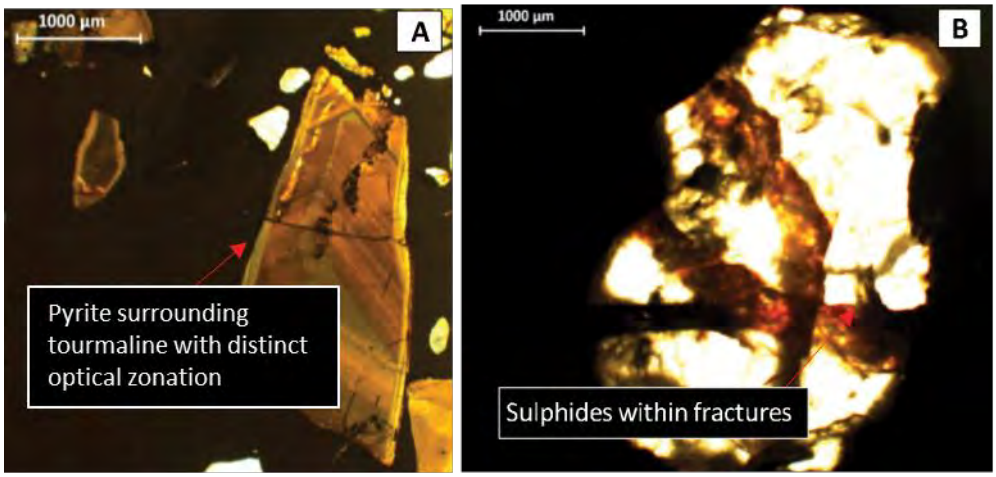

Figure 7.10: Ktm-2 Group 2 sulphide and tourmaline-bearing sample. (A) Fragmented tourmaline within pyrite. Tourmaline has multiple clear concentric optical zonations with shades of browns through to dark green. (B) Fractured quartz containing interstitial pyrite and arsenopyrite. Mineralised sample Au grade: 15g/t.

Group 2 Type 3 primary FIs contain liquid CO_2. This differs from Group 1 Type 3 primary FIs that contain vapour CO_2. According to Roedder (1984), liquid CO_2 FIs are typical of hydrothermal fluids formed by metamorphic devolatilisation reactions. Compared to Group 1 pegmatite, the overall salinity of Group 2 is lower. There are fewer Type 1 and 2 primary FIs in Group 2 than in Group 1. Only 5 - 10% of Group 2 Type 2 primary FIs contain Fe-chloride daughter crystals. Wilkinson (2001), previously postulated that lower salinities and fewer Fe-chloride daughter crystals in FIs suggest a vein system that is not related to granitoid fluid sources.

Group 2 Type 1, 5 and 6 primary FIs were affected by greenschist facies plastic deformation - as indicated by quartz recrystallisation. Alteration halos, seen in many of the samples, likely formed during the greenschist facies deformation. This interpretation is based on the smaller number of secondary FIs that extend into recrystallised quartz. Recrystallised quartz, in these samples, contains sulphide and organic material inclusions along grain boundaries; and the unrecrystallised quartz contains finely dispersed sulphide inclusions (Figure 7.11). Type 3 primary FIs, located along altered grain boundaries of secondary stage quartz, also contain H_2S,

CH_4 and N_2. This suggests that late-stage fluids either interacted with, or was sourced from, rocks rich in sulphides and organic materials.

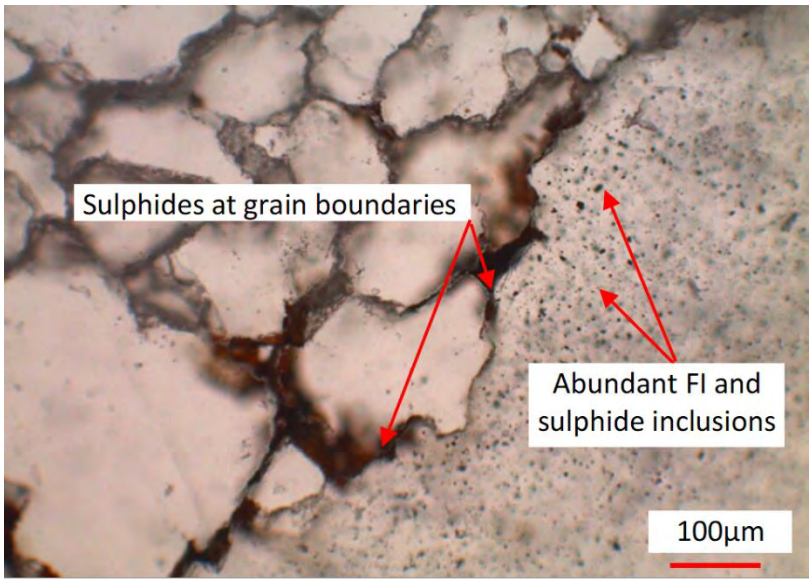

Figure 7.11: K6. (Right) Primary quartz with numerous FIs and solid sulphide inclusions. (Left) Secondary recrystallised quartz - most solids and FIs have been removed. Sulphides, and in places graphite or amorphous carbon, are present along grain boundaries.

The tourmaline-rich quartz veins of the highly mineralised samples Ktm-1, Ktm-2, K4 and K10, contain numerous interstitial sulphides. These sulphides show textural relationships to the hosting diorite - from which they appear to be extracted. Sulphur isotopes studies support this relationship (Moloto, 2018). These four samples have up to 50 vol % sulphide - with arsenopyrite more abundant than pyrite (Table 7.1). Tourmaline with green - brown core-rim zonation, with small oscillatory zonation in the brown rim zone, is either fragmented and/or forms intact prisms from 40 µm to 2 cm in length. Oscillatory zonation is prominent in smaller tourmaline fragments (Figure 7.10A). Quartz grains hosting the tourmaline are typically fractured. Quartz fragments and aggregates show distinct undulose extinction, but no subgrain formation or recrystallisation. Pyrite and arsenopyrite filled fractures and surrounded quartz-tourmaline fragments (Figure 7.10B). Tourmaline shows visible globular or amoeboid resorption. Resorption embayments are filled with pyrite and arsenopyrite. High-angle grain boundaries of hydrothermal quartz bulge in places in the highly mineralised samples; of Ktm-1, Ktm-2, K4 and K10. These features suggest minor grain boundary migration, but the absence of new grains in these textures indicates that recrystallisation did not take place. Ktm-1, Ktm-2, K4 and K10 samples contain tourmaline within quartz veins that subsequently underwent minor plastic deformation. The injection of sulphur and iron-rich fluids caused brittle failure and fragmented of the quartz-tourmaline vein. Parts of the original material was resorbed and replaced by sulphur minerals (cf. Figures 2 f and g in Büttner et al., 2016). Commonly, the late stage iron-sulphides are texturally and spatially associated with calcite - as observed along fractures between quartz grains and sulphides. This suggests that the secondary sulphur-rich fluid also contained CO_2 and calcium. This carbonaceous and sulphur-rich fluid influx occurred after the solidification and subsequent plastic

deformation of the primary quartz-tourmaline vein, and hence is likely a fluid influx episode that is not related to the formation of the original quartz-tourmaline vein.

Sulphide influx is less prominent in mineralised samples K2, K3 and K9 in which fractured quartz grains are filled with late stage iron oxides and hydroxides (Table 7.1). These oxides/hydroxides become progressively less concentrated proximal to the centre of the vein. This results in a gradational compositional change from the centre of the vein towards its boundary (Table 7.1).

In the non-mineralised samples: K6, K7 and K14, fluid compositions were macroscopically distinguishable in two different quartz phases; a light and a dark quartz (Table 7.1). The dark quartz consists of coarse (0.5 - 1 mm) hydrothermal grains that are brecciated and contain numerous FIs and small sulphides, graphite, amorphous carbon and tourmaline. It also exhibits prism-parallel subgrain boundaries and deformation bands - indicating plastic deformation and recrystallisation. The second lighter shade of finely recrystallised quartz grains form 100 - 700 µm grains that contain few, if any, fluid or solid inclusions and are optically strain-free (Figure 7.11). In places, the grain boundaries are straight and intersect at 120° angles - forming foam textures. Recrystallisation is typically seen along quartz-tourmaline interfaces. Graphite and a fine-grained amorphous carbon form along grain boundaries in zones with recrystallised quartz. This suggests that quartz recrystallisation was associated with an influx of a late reducing carbon/CO_2-rich fluid. The recrystallised finer-grained quartz contains solids and FIs along grain boundaries that are similar to those in the earlier (primary) hydrothermal quartz. Small sulphides and FIs along the grain boundaries of recrystallised quartz might be redistributed material from former inclusions in the primary/ dark quartz phase. The recrystallised quartz grains are free of sulphide inclusions (Figure 7.11).

Gold grades appear to be higher in zones that show 'sugary' recrystallised quartz, (pers. communication Chuwa, 2014) suggesting that at least some of the Au mineralisation may be related to the overprint of primary veins under conditions of plastic deformation. The recrystallisation of quartz suggests minimum temperatures of 290 °C at deformation (Voll, 1976). Well-developed foam textures indicating effective static recrystallisation - further suggest that temperatures may have been higher than this minimum temperature; well within the greenschist facies.

7.2.2.1 PRIMARY FIs

Group 2 FIA's Type 1 and 2 primary FIs are similar to Group 1 pegmatite. Type 1 and 2 primary FIs are, however, more numerous around tourmaline at the centre of large quartz grains. Type 1 and 2 primary FIs are larger (4 - 10 µm) and contain larger halite daughter crystals than Group 1 pegmatite's FIAs (Figures 7.12A and 7.13A and 7.13B). The halite daughter crystals occupy a smaller proportion of FIs compared to pegmatite - inferring similar proportions. The secondary daughter phases in Type 2 primary FIs are sylvite and Fe-chloride and are generally smaller than those in the pegmatite. Type 2 primary FIs containing Fe-chlorides are 10 % less numerous than those in Group 1 pegmatite.

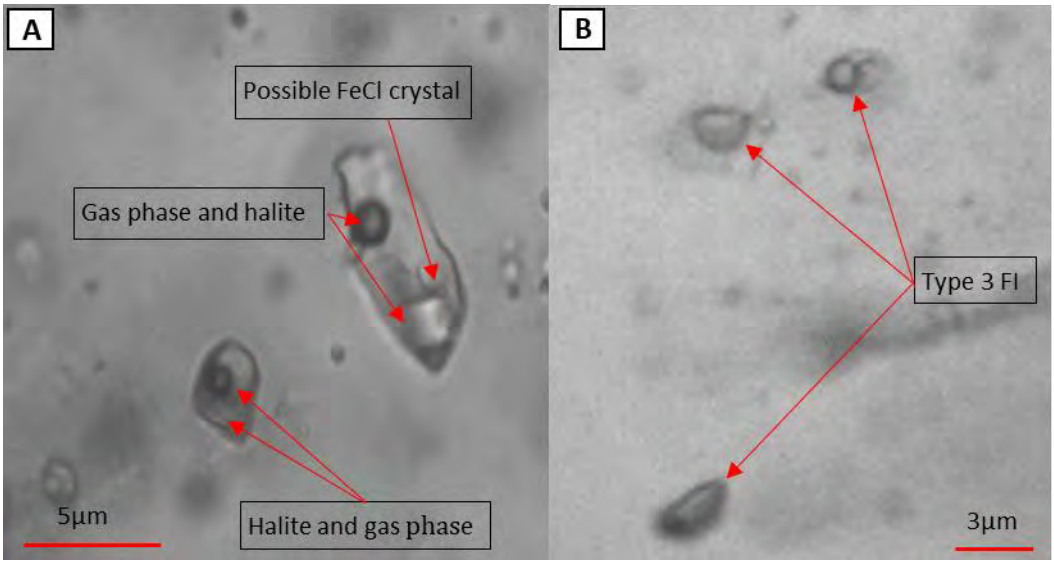

Figure 7.12: K4 primary FIs. (A) Characteristic Type 1 and 2 FIs. (B) Type 3 FIA assemblage with varying proportions of vapour.

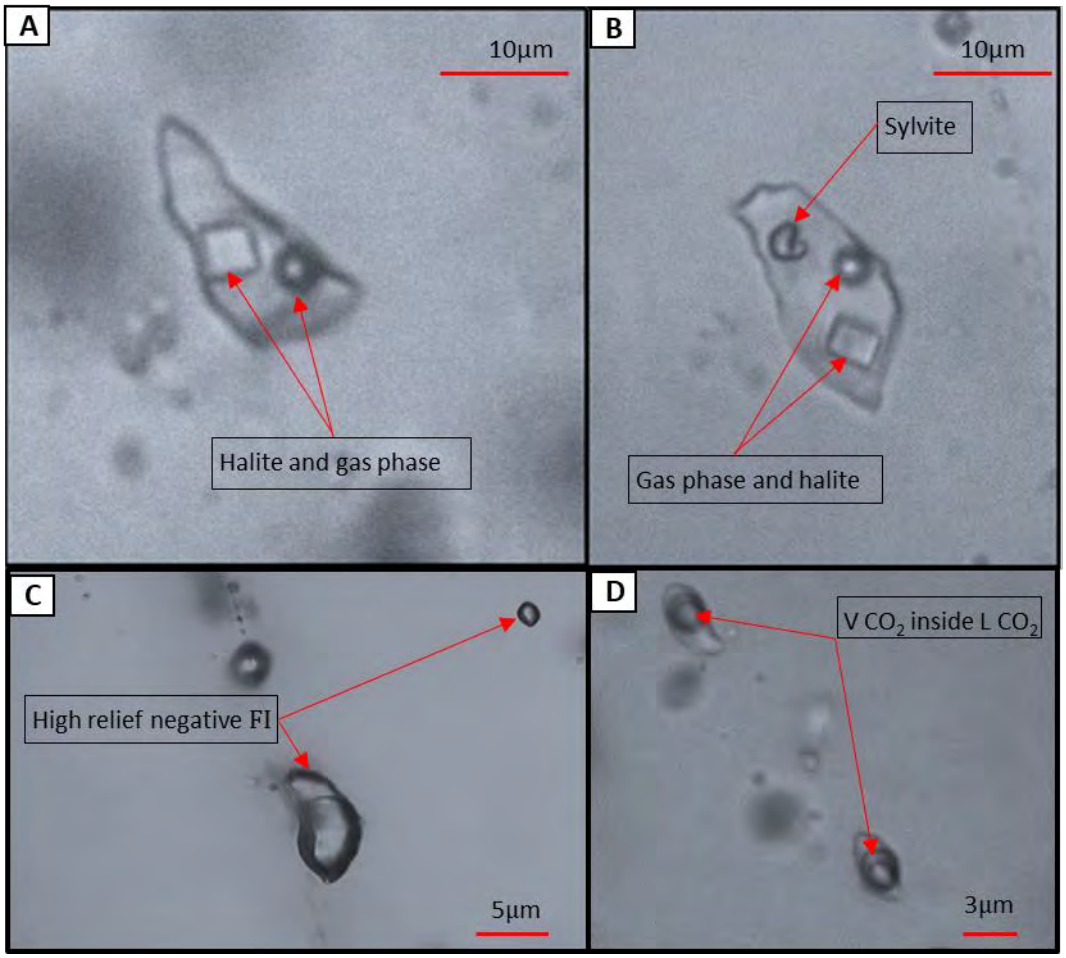

Figure 7.13: K2 primary FIs. (A) Type 1 primary FI with halite (cuboid) aqueous liquid and vapour. (B) Type 2 primary FI with halite and sylvite daughter mineral (denoted by rounded edges and rapid solubility at higher temperatures), and aqueous phase with small vapour bubble. (C) Type 3 primary FI with negative high relief liquid phase. (D) Type 3 primary FI within recrystallised grains with distinct V_{CO2} within L_{CO2}.

There is a correlation between Type 1 and 2 primary FIs and small elongated and equidimensional Type 3, 4, 5 and 6 primary FIs (2 - 5 µm). CO_2 vapour-rich Type 3 and 4 primary FIs in FIAs do not occur as frequently as in similar Group 1 FIAs. The abundance of Type 3 primary FIs has been interpreted as indicative of the intensity of effervescence (see Chapter 6, Section 6.10). Hence, the smaller quantity of Type 3 primary FIs may suggest that effervescence was less intense in Group 2 compared to Group 1 veins at Kamituga (Figures 7.4 and 7.12B). There are more Type 5 primary FIs (sulphide or carbonate bearing) in Group 2 compared to Group 1 samples. A few Type 5 primary FIs have a liquid CO_2 phase (Figure 7.14A). Particularly larger Type 5 primary FIs contain halite cubes, indicating highly saline fluids (Figure 7.14B).

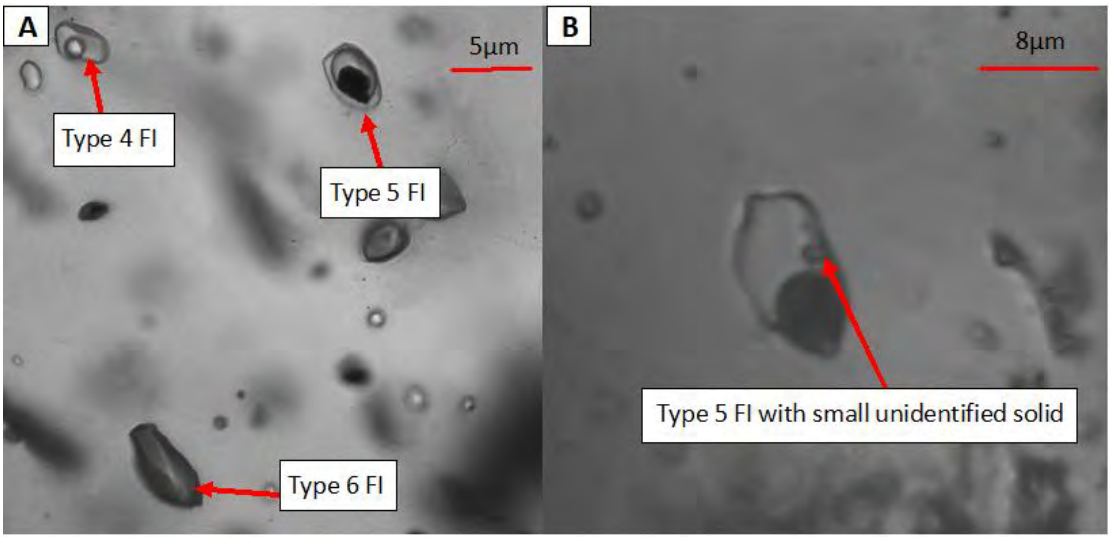

Figure 7.14: K14 primary FIs. (A) Association of Type 4, 5 and 6 primary FIs. Type 5 FI with a high concentration of liquid CO_2. (B) Larger Type 5 FI near tourmaline contains small unidentified solids believed to be halite.

Group 2 Type 1 and 2 primary FIAs associated with tourmaline have highly variable Th. The larger Type 1 and 2 primary FIs display the highest homogenisation temperatures and predominantly homogenised by vapour bubble disappearance or simultaneous bubble and halite dissolution (Figures 7.15 and 7.16; Table 7.3). Some Type 2 primary FIs have unknown daughter minerals that remain undissolved at decrepitation. Final homogenisation for Type 1 primary FIs by vapour bubble disappearance or simultaneous bubble and halite dissolution range from 300 - 411 °C (avg. 348 °C) (Table 7.3). Type 1 primary FI salinities range from 40.0 to 48.7 wt. % NaCl eq. (avg. 42.2 wt. % NaCl eq.) and pressures range from 8.8 - 18.6 MPa (avg. 11.9 MPa) at homogenisation - with densities of 1.06 -1.09 g/cm^3 (avg. 1.07 g/cm^3) calculated using Sterner et al. (1988) and Steel-MacInnis et al's. (2012) equations (Table 7.3).

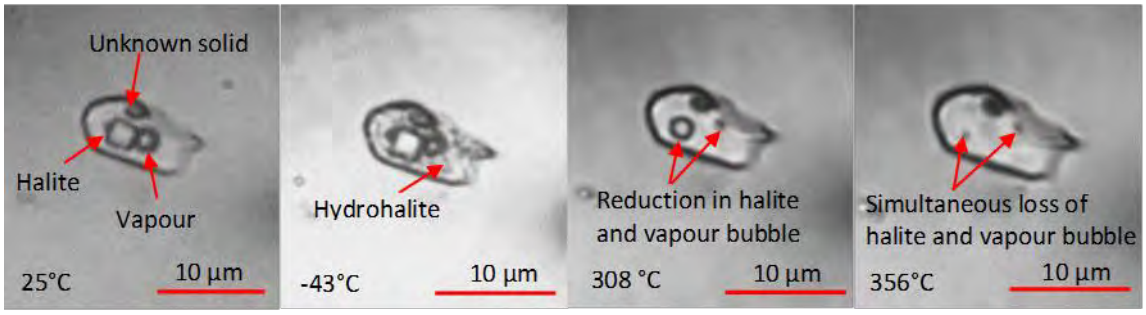

Figure 7.15: K7 Type 2 primary FIs. At ambient temperature; freezing point of -43 °C; 308 °C and 356 °C. Hydrohalite forms at -43 °C. Slow reduction in both halite and vapour bubbles, and eventual homogenisation with a remaining unidentified solid particle at 356 °C. Halite and vapour phase dissolution take place almost concurrently at 356 °C. The unidentified solid remains stable up to decrepitation at 456 °C.

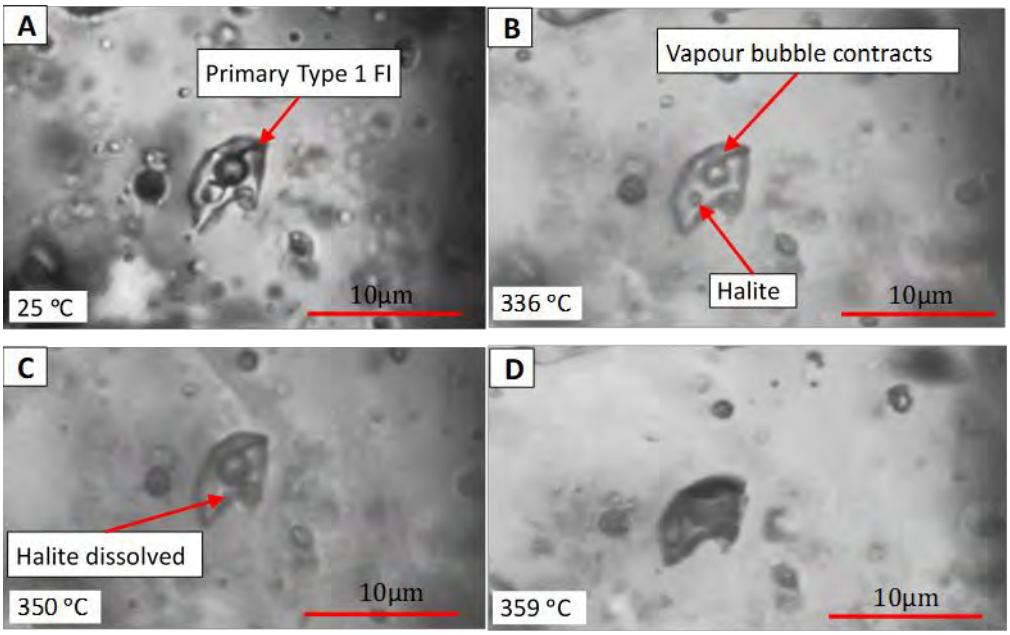

Figure 7.16: K3 Type 1 primary FI at various temperatures. (A) At ambient temperature. (B) Vapour bubble contraction and rapid dissolution of halite at 336 °C. (C) Heating to 350 °C - halite dissolves and vapour bubble begins to expand again before contracting. (D) Total homogenisation at 359 °C (L - V).

As in Group 1, Group 2 Type 2 primary FI's Te (-23 °C to -25 °C) and daughter crystal homogenisation temperatures indicate sylvite and Fe-chloride as the dominant daughter minerals. The average composition of Type 2 fluids containing only sylvite as a daughter crystal is 35.0 wt. % NaCl eq., 22.0 wt. % KCl and 43.0 wt. % H_2O. Ternary diagrams for Group 2 Type 2 primary H_2O-NaCl-KCl system (Sterner et al. 1987) indicate a slightly higher pressure (12.5 - 15 MPa) than the pressure determined for Group 1. This density range correlates closely with Type 1 primary FIs. The Fe-chloride content therefore appears not to impact the validity of pressures determined using the H_2O-NaCl-KCl diagram (Sterner et al. 1987) - although this diagram does not take Fe-chloride into consideration. Sylvite (~95% vol. of none halite solids in Type 2 primary FIs) is significantly more abundant as a daughter crystal than Fe-chloride (5% vol. of none halite solids in Type 2 primary FIs). Typically, Type 2, as in Group 1, FI do not completely homogenise. Type 1 and 2 primary FI's homogenisation temperatures

are similar to co-formational Type 3 and 4 primary FIs. Type 3 and 4 FI's Th ranges from 279 to 361 °C (avg. 325 °C). Type 4 primary FIs salinity's range from 17.8 to 26.1 wt. % NaCl eq. (avg. 24.2 wt. % NaCl eq.) as calculated using Bodnar's (1993) equations.

Table 7.3: Microthermometric and barometric data of Type 1, 3 and 4 primary and secondary FIs for Kamituga Group 2.

Phase relationship	FI Type	Tm	Final phase melting	$Th_{(L-V)}$	wt. % NaCl. Eq	T @ homog. (°C)	P @ homog. (bar)	r_{BULK} (g/cm_3)	Reference
Secondary quartz tourmaline associated Type 1 primary FIs	Upper Th final by Th (L - V) for Type 1 FI	411	Halite and vapour bubble	411	48.7	411	186	1.09	Sterner et al. (1988), Steel-MacInnis et al. (2012)
Secondary quartz tourmaline associated Type 1 primary FIs	Lower Th final by Th (L - V) for Type 1 FI	300	Halite and vapour bubble	300	40.00	300	88	1.06	Sterner et al. (1988), Steel-MacInnis et al. (2012)
Secondary quartz tourmaline associated Type 1 primary FIs	Avg. Th final by Th (L - V) for Type 1 FI	342	Halite and vapour bubble	348	42.2	348	119	1.07	Sterner et al. (1988), Steel-MacInnis et al. (2012)
Secondary quartz tourmaline associated Type 4 and 6 primary FIAs	Upper Th final by Th (L - V) for Type 4 FI	-1	Hydrohalite	361	26.1	361	148	0.91	Sterner et al. (1988), Steel-MacInnis et al. (2012)
Secondary quartz tourmaline associated Type 4 and 6 primary FIAs	Lower Th final by Th (L - V) for Type 4 FI	-14	Ice	279	17.8	279	55	0.92	Bodnar (1993), Steel-MacInnis et al. (2012)
Secondary quartz tourmaline associated Type 4 and 6 primary FIAs	Avg. Th final by Th (L - V) for Type 4 FI	-14	Hydrohalite	325	24.2	325	98	0.93	Sterner et al. (1988), Steel-MacInnis et al. (2012)
Secondary quartz tourmaline associated Type 3 primary FIs	Upper Th Type 3 FIs	3	Clathrate	301	11.9	301	248	0.96	Chen (1972) and Fall et al. (2011)
Secondary quartz tourmaline associated Type 3 primary FIs	Lower Th Type 3 FIs	7	Clathrate	280	5.8	280	57	0.57	Chen (1972) and Fall et al. (2011)
Secondary quartz tourmaline associated Type 3 primary FIs	Avg. Th Type 3 FIs	5	Clathrate	290	9.0	290	62	0.75	Chen (1972) and Fall et al. (2011)
Primary quartz tourmaline associated Type 1 primary FIs	Upper Th final by halite Tm for Type 1 FI	419	Halite	356	50.0	419	784	1.16	Lecumberri-Sanchez et al. (2012) and Steel-MacInnis et al. (2012)
Primary quartz tourmaline associated Type 1 primary FIs	Lower Th final by halite Tm for Type 1 FI	352	Halite	309	43.2	352	601	1.13	Lecumberri-Sanchez et al. (2012) and Steel-MacInnis et al. (2012)
Primary quartz tourmaline associated Type 1 primary FIs	Avg. Th final by halite Tm for Type 1 FI	366	Halite	310	44.6	366	762	1.15	Lecumberri-Sanchez et al. (2012) and Steel-MacInnis et al. (2012)
Secondary quartz, Type 4 and 6 primary FIs associated with Type 3 primary FIAs	Upper Th final by Th (L - V) for Type 4 FI	-8	Ice	346	11.7	346	145	0.77	Bodnar (1993) and Steel-MacInnis et al. (2012)
Secondary quartz, Type 4 and 6 primary FIs associated with Type 3 primary FIAs	Lower Th final by Th (L - V) for Type 4 FI	-6	Ice	261	9.2	261	45	0.86	Bodnar (1993) and Steel-MacInnis et al. (2012)
Secondary quartz, Type 4 and 6 primary FIs associated with Type 3 primary FIAs	Avg. Th final by Th (L - V) for Type 4 FI	-7	Ice	310	10.5	310	92	0.81	Bodnar (1993) and Steel-MacInnis et al. (2012)
Secondary quartz, Type 3 associated with Type 4 and 6 primary FIAs	Upper Th Type 3	7	Clathrate	325	5.8	325	640	1.08	Chen (1972) and Fall et al. (2011)
Secondary quartz, Type 3 associated with Type 4 and 6 primary FIAs	Lower Th Type 3	9	Clathrate	283	2.0	283	57	0.57	Chen (1972) and Fall et al. (2011)

Table 7.3 cont.: Microthermometric and barometric data of Type 1, 3 and 4 primary and secondary FIs for Kamituga Group 2.

Phase relationship	**FI Type**	**Tm**	**Final phase melting**	**$Th_{(L-V)}$**	**wt. % NaCl**	**T @ homog. (°C)**	**P @ homog. (bar)**	**r_{BULK} (g/cm_3)**	**Reference**
Secondary quartz, Type 3 associated with Type 4 and 6 primary FIAs	Avg. Th Type 3	8	Clathrate	309	4.0	309	248	0.96	Chen (1972) and Fall et al. (2011)
All Type 4 and 6 secondary FIs throughout samples	Upper Th final by Th (L - V) for Type 4	-10	Ice	239	14.0	239	30	0.93	Bodnar (1993) and Steel-MacInnis et al. (2012)
All Type 4 and 6 secondary FIs throughout samples	Lower Th final by Th (L - V) for Type 4	-5	Ice	172	7.9	172	8	0.95	Bodnar (1993) and Steel-MacInnis et al. (2012)
All Type 4 and 6 secondary FIs throughout samples	Avg. Th final by Th (L - V) for Type 4	-6	Ice	201	9.2	201	15	0.94	Bodnar (1993) and Steel-MacInnis et al. (2012)
Non-mineralised Type 3 secondary FIs throughout samples	Upper Th Type 3	3	Clathrate	210	5.0	210	57	0.57	Chen (1972) and Fall et al. (2011)
Non-mineralised Type 3 secondary FIs throughout samples	Lower Th Type 3	8	Clathrate	186	4.0	186	49	0.13	Chen (1972) and Fall et al. (2011)
Non-mineralised Type 3 secondary FIs throughout samples	Avg. Th Type 3	5	Clathrate	202	9.0	202	53	0.30	Chen (1972) and Fall et al. (2011)
All mineralised samples Type 3 secondary FIs throughout samples	Upper Th Type 3	3	Clathrate	239	11.9	239	57	0.57	Chen (1972) and Fall et al. (2011)
All mineralised samples Type 3 secondary FIs throughout samples	Lower Th Type 3	7	Clathrate	200	5.8	200	49	0.13	Chen (1972) and Fall et al. (2011)
All mineralised samples Type 3 secondary FIs throughout samples	Avg. Th Type 3	4	Clathrate	215	10.5	215	53	0.30	Chen (1972) and Fall et al. (2011)

Type 3 liquid CO_2-rich primary FIs and combinations of liquid and vapour rich CO_2 Type 3 primary FIs are less saline with 5.8 - 11.9 wt. % NaCl eq. (avg. 7.5 wt. % NaCl eq.) (Table 7.3) as calculated using Chen's (1972) equations. Density and pressure correlations in these Type 3 & 4 primary FIAs are detailed in Table 7.3. Type 3 and 4 primary FIs that are in close proximity to Type 1 FIs, homogenise within a temperature interval of ±20 °C of each other. These Type 1 primary FIs homogenise by vapour dissolution and not by halite dissolution. This may suggest that Type 3, 4, 6 and some Type 1 primary FIs were captured simultaneously.

Some other, larger Type 1 and 2 primary FIs, homogenise by halite dissolution after vapour has been taken up by the liquid, rather than by simultaneous vapour bubble/halite loss (Figure 7.17). These Type 1 primary FI exists exclusively in Kamituga's Group 1 and 2. In larger Type 1 primary FIs, Tm (equal to Th) is significantly higher (Th, 352 - 419 °C; avg. 366 °C) than in other Type 1 primary FIs. The preceding homogenisation of vapour and liquid (L - V), leaving halite in liquid, occurs at 309 - 356 °C (avg. 310 °C). Salinities are 43.2 - 50.0 wt. % NaCl eq. (avg. 44.6 wt. % NaCl eq.; Lecumberri-Sanchez et al., 2012). This has implications for the determination of fluid pressure at capturing. The fluid densities at total homogenisation are 1.13 - 1.16 g/cm^3 (avg. 1.15 g/cm^3; Table 7.3), yielding total homogenisation pressures of 60.1 - 78.4 MPa (avg. 76.2 MPa). These are, however, not identical to formation conditions that will be determined by isochore intersections (see Chapter 8, Section 8.2). High Th/Tm Type 1 and 2 primary FIs are therefore not only different in their physical properties from other Type 1 and 2 primary FIs, but also different from Type 3 and 4 primary FIs in the same FIA. This suggests that FIs underwent secondary alteration (Roedder, 1984).

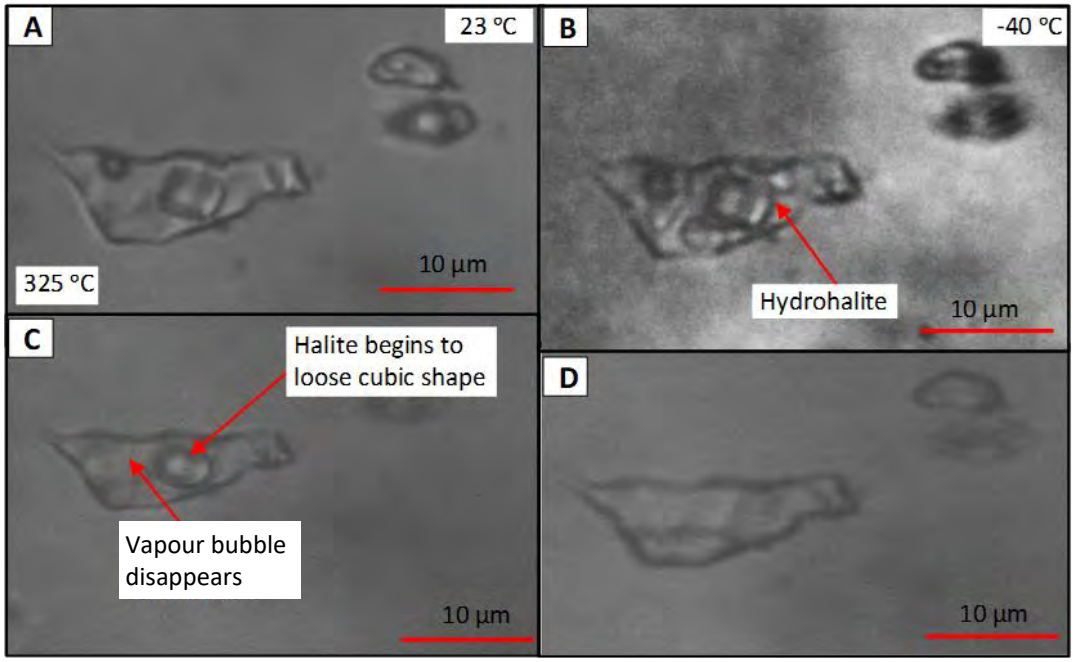

Figure 7.17: K2 Type 1 primary FI. (A) With high Th/Tm and large halite cube and small aqueous vapour phase. (B) Forms hydrohalite at -40 °C. (C) Vapour phase disappears before halite. (D) Total homogenisation occurs at 370 °C.

Type 3 primary FIA clusters have large vapour CO_2 phases and smaller liquid CO_2 phases. These Type 3 primary FIs are typically larger than >5 µm, and hence larger than Group 1 FIs (Figure 7.14 C and 7.14D). Type 3 primary FIs occur in two textural locations. (i) in large secondary quartz grains that do not host tourmaline and (ii) in recrystallised hydrothermal quartz that contain numerous sulphide inclusions. Both suggest a late-stage capture in the evolution of Group 2 veins.

In secondary quartz grains, (i) FIs are typically in the center of recrystallised quartz and (ii) FIs lie along grain boundaries. Type 3 primary FIs, as clusters, contain CO_2-rich Type 4 primary FIs (only identifiable by Raman spectroscopy). In recrystallised quartz, salinities of Type 3 and Type 4 are further reduced compared to Type 3 primary FIs genetically associated with Type 1 primary FIs. Temperatures of homogenisation and fluid densities remain within similar ranges as Type 3 primary FIs in FIAs in unrecrystallised quartz. Type 3 and 4 primary FIs have Th within 261 - 346 °C (avg. 310 °C). Salinities are variable at 9.2 - 11.7 wt. % NaCl eq. (avg. 10.5 wt. % NaCl eq.) for Type 4 FIs, and 2.0 - 5.8 wt. % NaCl eq. (avg. 4.0 wt. % NaCl eq.) for Type 3 primary FIs as per Chen (1972) and Bodnar's (1993) calculations (Table 7.3). Type 4 primary FIs homogenise at pressures of 4.5 - 14.5 MPa (avg. 9.2 MPa) and densities of 0.77 - 0.86 g/cm^3 (avg. 0.81 g/cm^3) calculated using Steel-MacInnis et al's. (2012) equations. Type 3 liquid CO_2-rich primary FIs homogenise to liquid CO_2 at 10 - 14 °C - indicating an increase in densities compared to more CO_2 vapour-rich Type 3 primary FIs in Group 1 (Roedder, 1984). Clathrate melting temperatures and Fermi diad spacing of 104 to 105.5 cm^{-1} indicate pressures of 5.7 - 64.0 MPa and densities of 0.57-1.08 g/cm^3 as calculated using Fall et al's. (2011) equations (Table 7.3). There are few FIs in recrystallised quartz, although, in mineralised samples, profuse numbers of Type 5 primary FIs are found with Type 3 primary FIs near grain boundaries - especially in samples that contain >10 vol % sulphides. The solid black phase within Type 5 FIs is either pyrite or graphite. The CO_2 melting temperatures and Raman spectra in Type 3 and 5 primary FIs in mineralised samples indicate that volatile components are either CO_2-N_2 or CO_2-CH_4 .In mineralised samples, liquid CO_2-rich Type 3 primary FIs show increased densities, determined by CO_2 homogenisation temperatures (Th CO_2) below 12 °C. Clathrate melting temperatures and Fermi diad spacing of 105 - 105.5 cm^{-1} indicate pressures of 24.8 - 64.0 MPa and densities of 0.96 - 1.08 g/cm^3 as calculated using Fall et al's. (2011) equation.

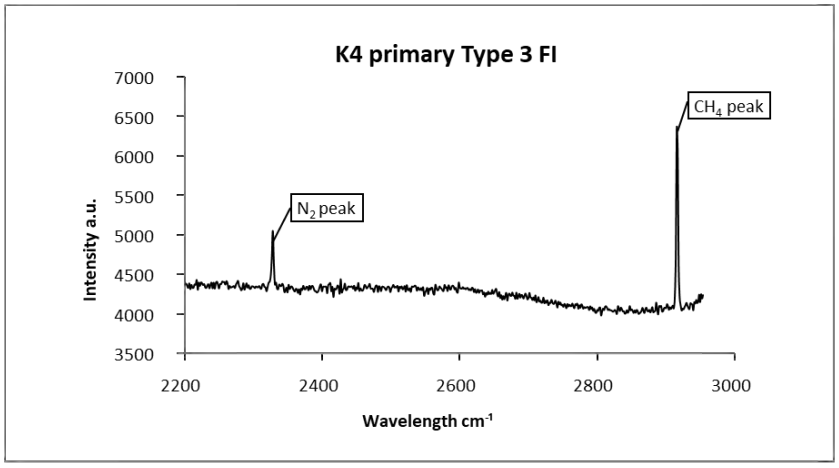

Figure 7.18: K4 liquid CO_2-rich Type 3 primary FI. At ambient temperature Type 3 FIs have a large CO_2 vapour-rich bubble within a liquid CO_2 bubble. Raman spectra indicating disproportional quantities of CH_4 to N_2. Type 3 FIs peak amplitudes vary dramatically from one spectra to the next.

In several very high-density Type 3 primary FIs, a second bubble develops at approximately 150 °C (Figure 7.19). This occurrence indicates high density CO_2 FIs with a possibly additional volatile component - typically CH_4 or N_2 (Roedder, 1984).

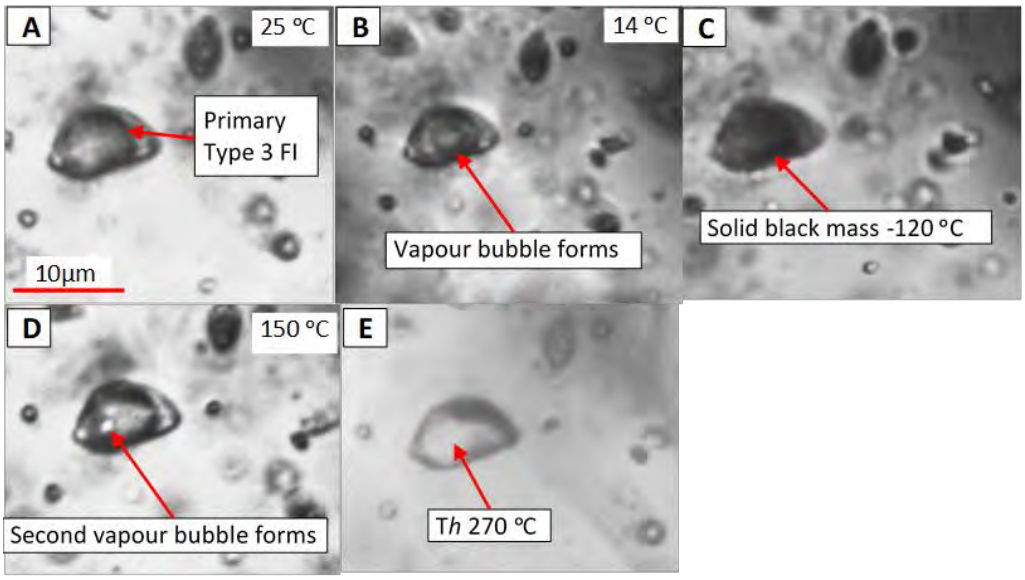

Figure 7.19: K3 liquid CO_2-rich Type 3 primary FIs. (A) liquid CO_2-rich Type 3 primary FIs at ambient temperature. (B) Vapour CO_2 bubble formation in CO_2 liquid phase. (C) Solid mass of crystals form within FIs at -120 °C. (D) vapour bubble forms again within secondary liquid phase after 150 °C and disappears thereafter. (E) Total homogenisation at 270 °C by loss of liquid CO_2 bubble.

7.2.2.2 SECONDARY FIs

There are secondary FIs throughout Kamituga Group 2 samples with more Type 3, 4 and 6 secondary FIs in mineralised samples that have more intense quartz recrystallisation than unmineralised samples. These secondary FIs are predominantly aqueous liquid Type 4 FIs. The proportion of the vapour phase increases with the size of secondary FIs. Many of the larger Type 4 FIs (> 3 µm) contain a vapour phase of >50 vol %. FIs <3 µm with a 5 - 30 vol % vapour. Group 2 Type 4 secondary FIs formed at much lower temperatures 172 - 239 °C (avg. 201 °C) than Group 2 Type 4 primary FIs. Most Type 4 secondary FIs are low to moderately saline 7.9 - 13.9 wt. % NaCl eq. (avg. 9.2 wt. % NaCl eq.) with homogenisation pressures of 0.8 - 3.0 MPa (avg. 1.5 MPa) and densities of 0.93 - 0.95 g/cm^3 (avg. 0.94 g/cm^3) as per Bodnar (1993) and Steel-MacInnis et al's. (2012) calculations.

Irregularly shaped CO_2 vapour-rich Type 3 FIs (avg. 3 µm) occur in FIAs with low salinities 4.0 - 11.9 wt. % NaCl eq. (avg. 7.5 wt. % NaCl eq.) (Figure 7.20). Fermi diad spacing of 103 - 104 cm^{-1} indicate densities of 0.13 - 0.57 g/cm^3 and pressures of 4.9 - 5.7 MPa at clathrate melting as calculated using Fall et al's. (2011) equations (Table 7.3). Type 3 secondary FIs in mineralised samples have higher Th compared to unmineralised samples. Mineralised samples contain Type 3 secondary FIs in 3, 4 and 6 FIAs that formed at temperatures between 215 - 239 °C (avg. 215 °C). Salinities remain similar to unmineralised samples (Table 7.3). In mineralised samples the number of irregularly shaped Type 3 secondary FIs increases in sulphide-rich zones (Figure 7.20). Type 3 secondary FI trails extend across multiple quartz grains - frequently to the boundaries of quartz veins and host rocks.

In mineralised samples, recrystallised quartz has detectable levels of either CH_4 or N_2 within all Type 3 secondary FIs, suggesting the influx of organic-rich fluids during or after the episode of plastic deformation. N_2 is, however, not present together with CH_4 in individual FIs. CH_4 and N_2 enrichment correlates with the presence of carbonaceous/graphitic material that also may have been introduced during recrystallisation. The influx of organic material is particularly prominent in Au-mineralised samples.

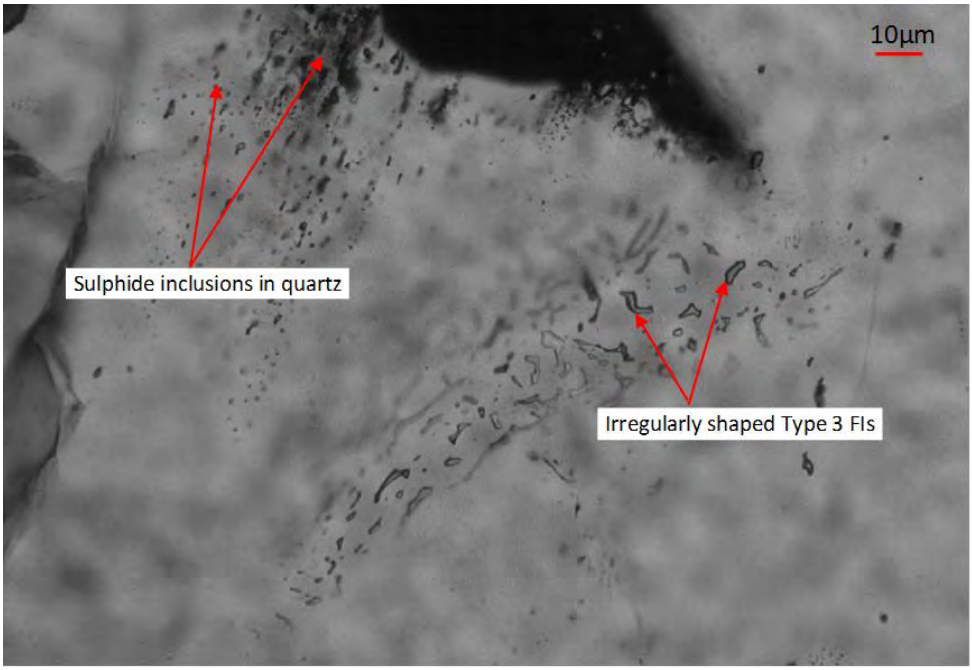

Figure 7.20: Ktm-2. Elongate, irregularly shaped CO_2 vapour-rich Type 3 FIs located near sulphides.

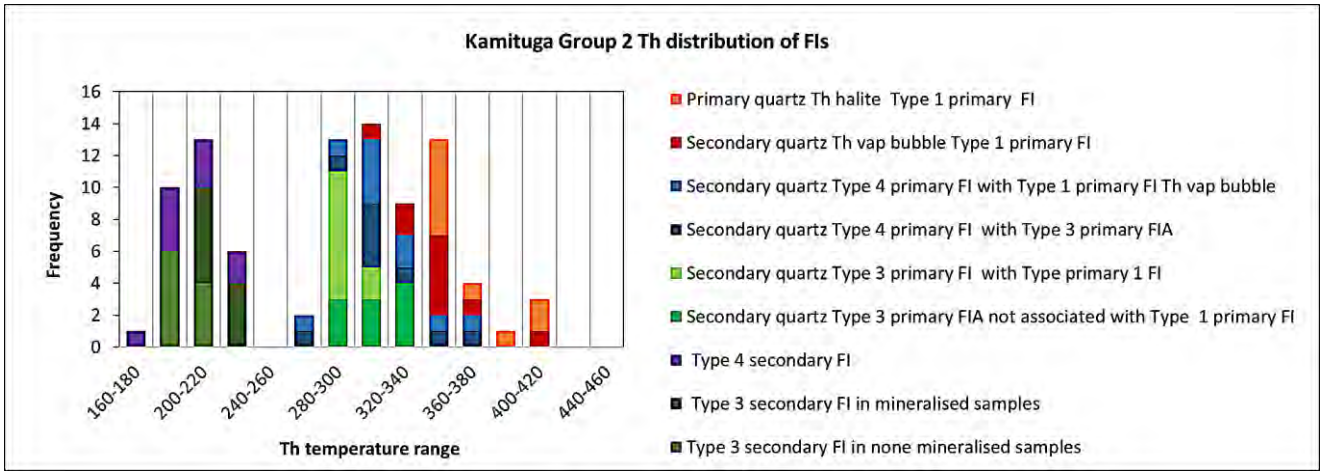

Figure 7.21: Group 2 Th distribution for Types 1, 3 and 4 primary and secondary FIs in primary and secondary quartz. Note the close correlation of primary and secondary quartz Type 1 FIs to that of Group 1 Ktm-3 quartz.

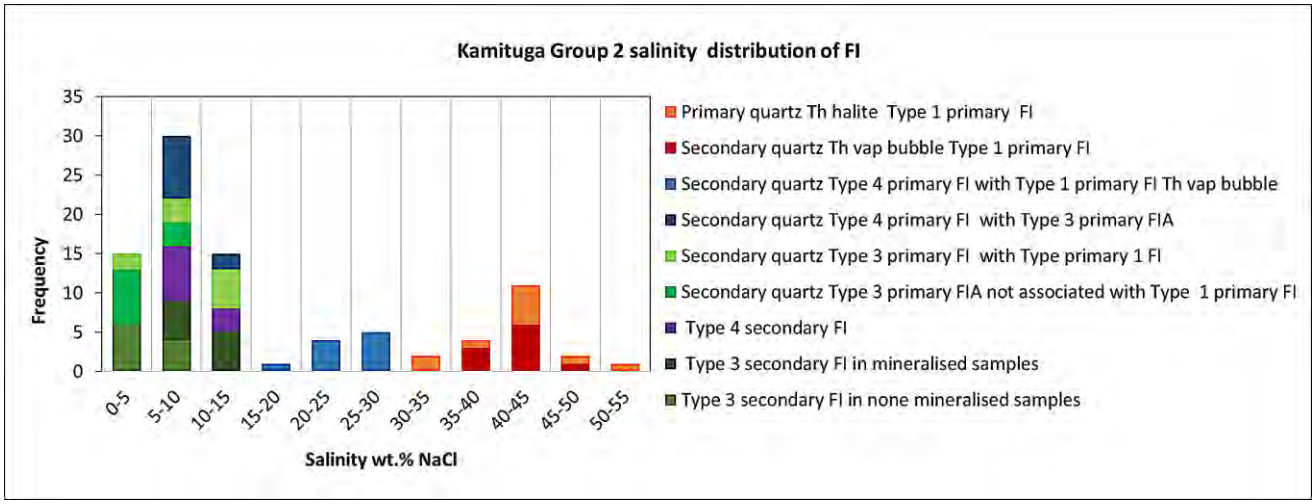

Figure 7.22: Group 2 salinity distribution for Types 1, 3 and 4 primary and secondary FIs in primary and secondary quartz. Note the close correlation of primary and secondary quartz Type 1 FIs to that of Group 1 Ktm-3 quartz.

In summary, data collected and analysed from Kamituga Group 2 indicates an early hydrothermal crystallisation of the primary quartz-tourmaline assemblage, together with some sulphides present in primary quartz. Overall Th and salinity of FIs suggest at least two different hydrothermal events (Figures 7.21 and 7.22). Subsequent plastic deformation led to quartz recrystallisation. During this episode sulphide was mobilised and precipitated in textural association with the deformed parts of the veins. Since sections where quartz recrystallisation is observed "sugary quartz", in the terminology of Banro's staff, typically contain higher gold grades, also gold may have been mobilised and precipitated in these veins during this stage. These episodes are associated with the capturing of secondary fluids, which are rich in CO_2 and organic materials (C, N_2 and CH_4). Higher gold grade samples contain particularly more recrystallised quartz, sulphides and CO_2-rich Type 3 FIs - especially the liquid CO_2-rich Type 3 FIs. Th of Type 3 secondary FIs in mineralised samples is higher than in unmineralised ones, suggesting that mineralising fluids were introduced at somewhat higher temperatures than unmineralised fluids of the same type.

7.2.3 KAMITUGA GROUP 3: TOURMALINE-FREE HYDROTHERMAL VEINS

Kamituga Group 3's defining characteristic is the hydrothermal (non-magmatic/-pegmatitic) origin of veins and the absence of tourmaline (Table 7.1). In contrast to Kamituga Group 2 veins, primarily hosted in dioritic rocks, Group 3 veins are hosted in metapelites. As in Kamituga Group 2 veins, late stage sulphide-rich fluids are a dominant feature in most samples, with pyrite being more abundant than arsenopyrite in Group 2 (with a py-aspy ratio of 60:40) (Table 7.1). Au grades tend to be higher in both Kamituga's Group 2 and 3 samples that contain more sulphides and recrystallised quartz. Kamituga Group 3 has fewer Type 1 and 2 primary FIs in comparison to Kamituga Group 1 and 2. The reduced number of FIs correlates with lower salinity levels in comparison to Groups 1 and 2 FIs. In Type 2 primary FIs no Fe-chlorides is present, but sylvite and Ca/Mg chloride occur as secondary daughter phases. As in Kamituga Group 2, Type 3 primary FIs in Group 3 samples are rich in CO_2 liquid. Type 3 primary FIs contain detectable levels of CH_4 and N_2 in mineralised samples.

A prominent feature of Kamituga Group 3 is the high abundance of carbon material such as graphite and amorphous carbon - both of which are present nearby and along quartz grain boundaries. Close to the vein margins, host rock material may be seen as entrained crystals or crystal aggregates. At vein margins these entrained minerals and rock fragments are oriented parallel to vein boundaries. The Group's dominant mineral assemblage is quartz, muscovite, chlorite, biotite and sulphides. These mineral assemblages are typical of a hydrothermal rather than a pneumatolytic system (Nockolds et al., 1978 and Roedder, 1984). Nockolds et al. (1978) and Roedder (1984) considered such assemblages to be commonly associated with greenschist facies metamorphic fluids.

Sulphides, either as small interstitial grains (a few µm), or as larger grains (up to 2 mm), both between quartz and similar in size to quartz, are common in most Kamituga Group 3 samples. However, sulphides predominantly occur along quartz fractures near vein-host rock boundaries, suggesting a secondary sulphur influx. Sulphides are frequently found with biotite in alteration halos (Figures 7.23 and 7.24). Reddish-brown Fe-hydroxide and oxide stains formed along networks of fractures and near vein boundaries (Table 7.1). These fractures crosscut multiple secondary FI trails. Mineralised Kamituga Group 3 samples frequently contain distinct Fe-hydroxide and oxide alterations near host rock boundaries. Precipitation of Fe-hydroxides and oxides is, however, likely to be related to exhumation and weathering - postdating the hydrothermal history of the veins' formation (Table 7.1).

Hydrothermal quartz along vein-host rock boundaries is typically extensively fractured. These fractured grains show numerous subgrains and undulose extinction, but very little recrystallisation. The vein margins may be gradational (Figure 7.23). Macroscopically such veins contain amoeboid quartz segregation that together with microscopically gradational contact of host material in boundary quartz phases indicate that vein material was proximally sourced (Figure 4.5) (Table 7.1).

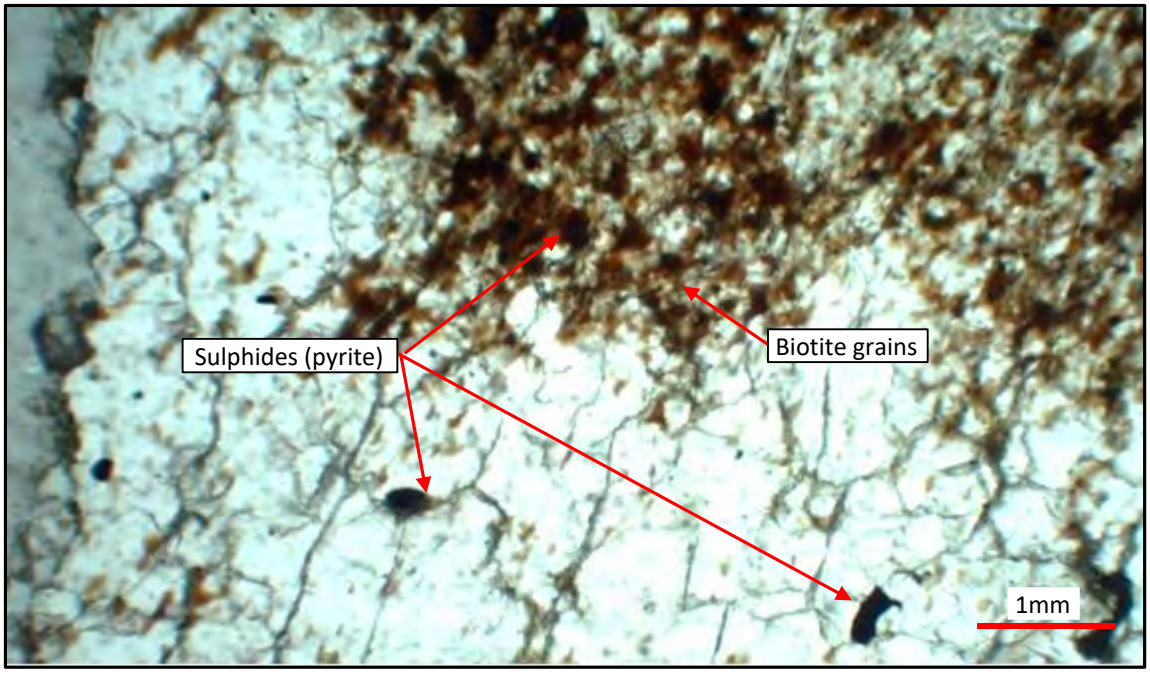

Figure 7.23: Sample K19. Gradational boundary between host rock and quartz veins. The host rock contains biotite and sulphides that protrude into the quartz vein. Macroscopically this texture appears as amoeboid segregation with transitional character between host rock and vein. Sulphides (pyrite) in the vein appears similar in texture and size to those in the host rock.

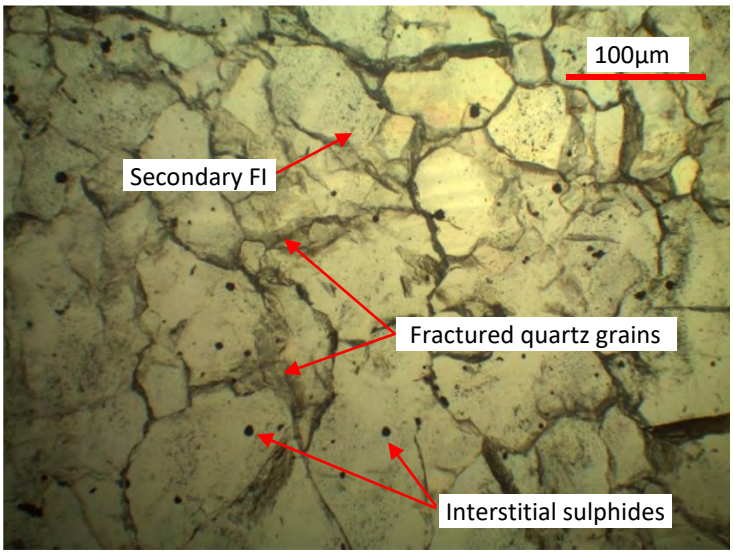

Figure 7.24: Sample K21. Intergranular sulphides in fractured but unrecrystallised quartz grains.

7.2.3.1 PRIMARY FIs

Liquid CO_2-rich Type 3 primary FIs are the dominant FI Type, and on average are larger than those in Kamituga Group 1 and 2 (>5µm). According to Roedder (1984), large liquid CO_2-rich FIs are indicative of high-density hydrothermal systems. Where present, Type 1 and 2 primary FI, such as in samples K12, K19 and K22, are typically very small (Table 7.1). Typically Type 1 & 2 primary FIs in Group 3 samples have smaller halite daughter crystals than those in Group 1 and Group 2 (Figure 7.25).

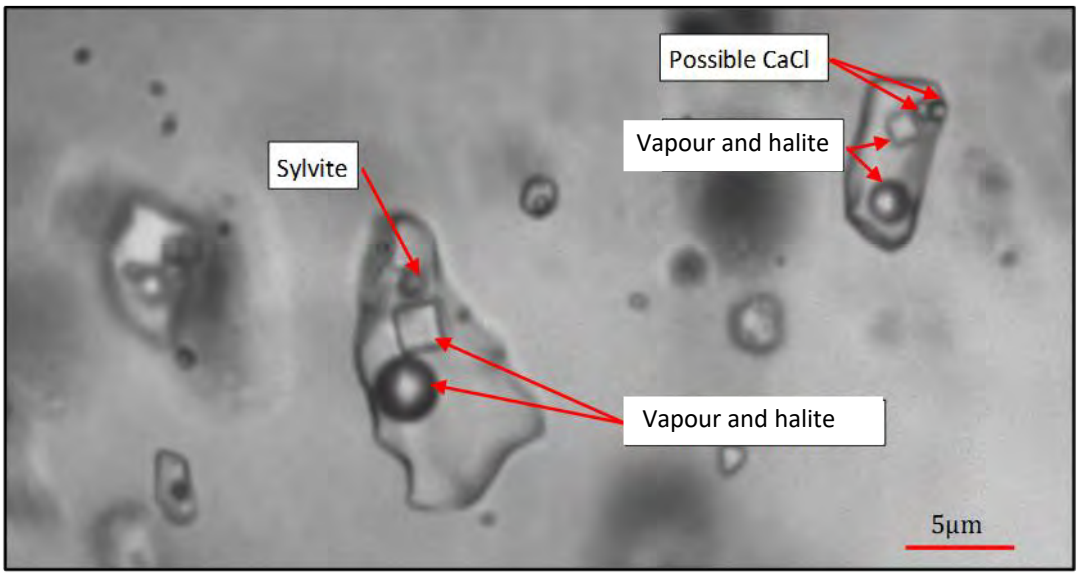

Figure 7.25: K19 primary hydrothermal quartz with Type 2 primary FIs. Daughter crystals are halite, sylvite and possibly $CaCl_2$. The liquid and vapour phase are aqueous.

The overall salinity in Group 3 is lower than Groups 1 and 2 because there are fewer highly saline Type 1 and 2 primary FIs. There are few secondary daughter minerals other than halite and sylvite in Group 3 Type 2 primary FIs. Based on dissolution temperature and petrographic features, this daughter phase is believed to be Ca/Mg chloride and not Fe-chloride as in Kamituga Group 1 and 2 (Figure 7.26). According to Wilkinson (2001) the absence of Fe-chlorides, together with the lack of carbonates, suggest that the source of fluids is not related to granitic intrusions.

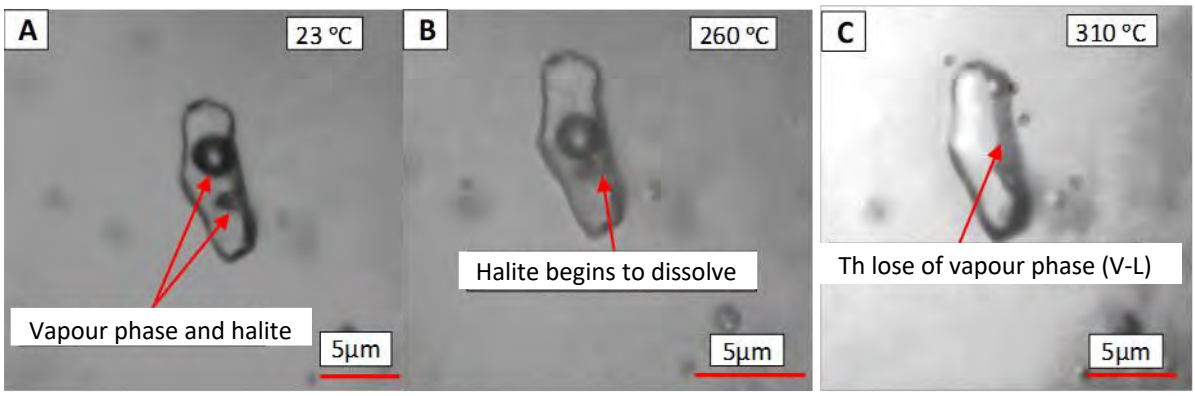

Figure 7.26: K19 aqueous Type 1 primary FI. (A) At ambient temperature. (B) Loss of small halite grain on heating. (C) Complete homogenisation occurs at 310 °C (V-L).

As in Group 2's large Type 1 and 2 primary FIs, Group 3's similarly large Type 1 and 2 primary FIs have the highest homogenisation temperatures. In Group 3 Type 1 and 2 primary FI's homogenisation occurs by simultaneous loss of halite and vapour bubbles, or the loss of vapour bubbles after halite dissolution (Figures 7.26 and 7.27). Unlike Groups 1 and 2, no Group 3's Type 1 and 2 primary FIs reach total homogenisation by halite dissolution.

Type 1 and 2 primary FIs have Th (L - V) of 280 - 403 °C (avg. 311 °C) with a salinity range of 31.9 - 42.9 wt. % NaCl eq. (avg. 35.0 wt. % NaCl eq.) calculated using Sterner et al's. (1988) equations.

Total homogenisation pressures are 4.7 - 18.7 MPa (avg. 7.1 MPa) with densities of 1.03 - 1.05 g/cm^3 (avg. 1.04) g/cm^3), calculated using Steel-MacInnis et al's. (2012) equations (Table 7.4). Type 2 primary FI's average composition is 33 wt. % NaCl eq., 20% KCl and 47% H_2O with pressures of 12.5 - 14 MPa (Sterner et al., 1987). Relative size proportion of sylvite to Ca/Mg chlorides indicates <5 % Ca/Mg chloride occurrence in Type 2 primary FIs. Overall Te of -24 °C to - 25 °C indicates quantitatively less Fe-chlorides in solution (Roedder, 1984).

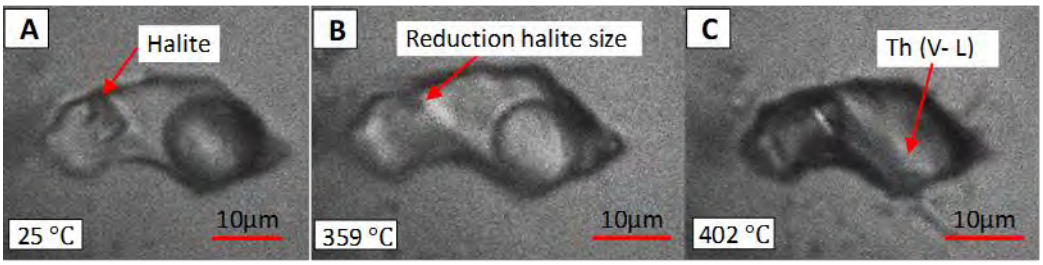

Figure 7.27: K22 Type 1 primary FI. (A) At ambient temperature. (B) Halite is almost completely dissolved at 359 °C. (C) Loss of vapour bubble and total homogenisation at 402 °C.

In Group 3 samples, Type 1 and 2 primary FIs are related to surrounding Type 3 and 4 primary FIs, with which they form FIAs. Unlike in Groups 1 and 2, Type 3 and 4 primary FIs in Group 3 homogenise within ±10 °C of Type 1 and 2 in FIAs (Table 7.4). This suggests a coeval entrapment. Group 3 Type 3 and 4 primary FIs homogenise between 245 - 342 °C. Type 4 primary FIs have distinctly higher salinities than Type 3 primary FIs, with salinities of 25.6 - 26.3 wt. % NaCl eq. (avg. 25.9 wt. % NaCl eq.) vs. 5.8 - 14.5 wt. % NaCl eq. (avg. 11.9 wt. % NaCl eq.) as per Chen (1972) and Bodnar's (1993) calculations (Figure 7.28). Hydrohalite remains stable up to 0° C on heating in Type 4 FIs as is indicative of the highly saline environment (Bodnar and Vityk, 1994). Type 4 primary FIs display total homogenisation pressures of 2.9 - 11.9 MPa (avg. 5.5 MPa) and densities of 0.93 - 1.03 g/cm^3 (avg. 0.99 g/cm^3) calculated using Steel-MacInnis et al's. (2012) equations. There is an increase in salinity of Type 1, 2 and 4 primary FIs toward the center of quartz veins. This feature was not observed in Type 3 primary FIs. The CO_2-rich Type 3 primary FIs are either liquid or vapour-dominant. The CO_2 liquid-dominant inclusions are distinctly optically negative in comparison to the quartz and FIs around them (Figure 7.29).

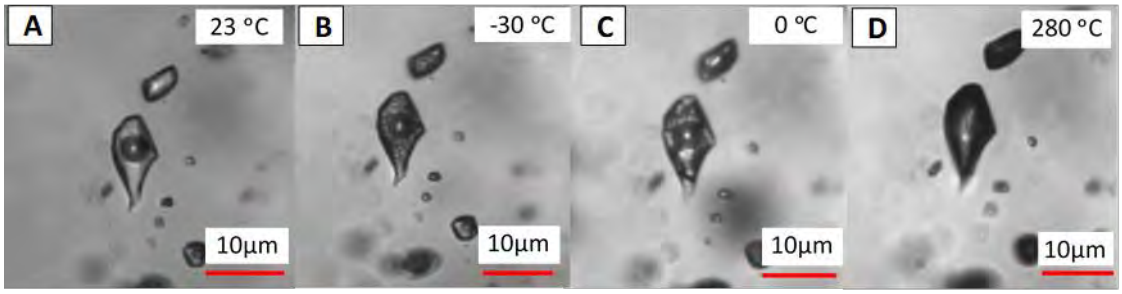

Figure 7.28: K6 Type 4 primary FI. (A) At ambient temperature. (B) Hydrohalite is evident with a small reduction in vapour bubble size at -30 °C. (C) Hydrohalite is stable to 0 °C. (D) Th at 280 °C.

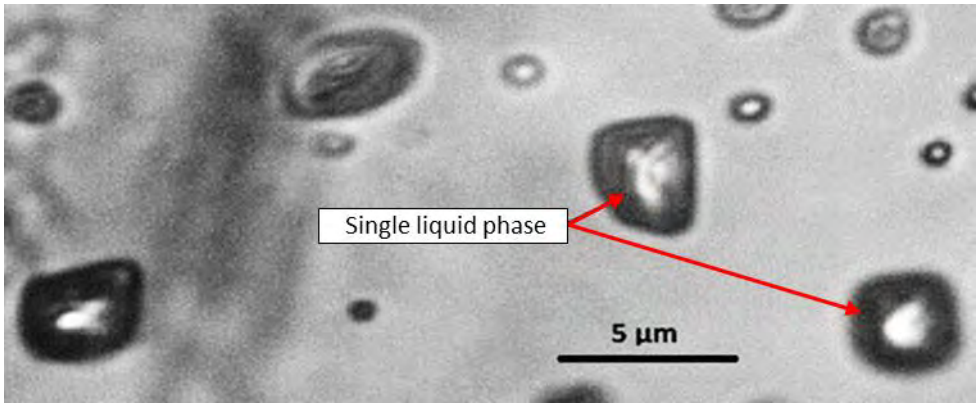

Figure 7.29: K19 Type 3 primary FIs. Distinctly negative relief with almost a single liquid CO_2 phase.

Table 7.4: Microthermometric and barometric data of Type 1, 3 and 4 primary and secondary FIs for Kamituga Group 3.

Phase relationship	FI Type	Tm	Final phase melting	$Th_{(L-V)}$	wt. % NaCl eq	T @ homog. (°C)	P @ homog. (bar)	r_{BULK} (g/cm$_3$)	Reference
Primary (Hydrothermal) quartz Type 1 primary FI	Upper Th final by Th (L - V) for Type 1 FI	356	Halite	403	42.9	403.0	187	1.03	Sterner et al. (1988) and Steel-MacInnis et al. (2012)
Primary (Hydrothermal) quartz Type 1 primary FIs	Lower Th final by Th (L - V) for Type 1 FI	200	Halite	280	31.9	280.0	47	1.05	Sterner et al. (1988) and Steel-MacInnis et al. (2012)
Primary (Hydrothermal) quartz Type 1 primary FIs	Avg. Th final by Th (L - V) for Type 1 FI	260	Halite	311	35.3	311.0	71	1.03	Sterner et al. (1988) and Steel-MacInnis et al. (2012)
Primary (Hydrothermal) quartz Type 4 primary FIs	Upper Th final by Th (L - V) for Type 4 FI	0	Hydrohalite	342	26.3	342.0	119	0.93	Sterner et al. (1988) and Steel-MacInnis et al. (2012)
Primary (Hydrothermal) quartz Type 4 primary FIs	Lower Th final by Th (L - V) for Type 4 FI	-3	Hydrohalite	245	25.6	245.0	29	1.03	Sterner et al. (1988) and Steel-MacInnis et al. (2012)
Primary (Hydrothermal) quartz Type 4 primary FIs	Avg. Th final by Th (L - V) for Type 4 FI	-5	Hydrohalite	285	25.9	285.0	55	1.0	Sterner et al. (1988) and Steel-MacInnis et al. (2012)
Primary (Hydrothermal) quartz Type 3 primary FIs	Upper Th final by Th (L - V) for Type 3 associated with Type 4 and 6 FI	1	Clathrate	338	14.5	338.0	248	0.96	Chen (1972) and Fall et al. (2011)
Primary (Hydrothermal) quartz Type 3 primary FIs	Lower Th final by Th (L - V) for Type 3 FIs associated with Type 4 and 6 FI	7	Clathrate	278	5.8	278.0	57	0.57	Chen (1972) and Fall et al. (2011)
Primary (Hydrothermal) quartz Type 3 primary FIs	Avg. Th final by Th (L - V) for Type 3 FIs associated with Type 4 and 6 FI	4	Clathrate	311	10.5	311.0	62	0.75	Chen (1972) and Fall et al. (2011)
Secondary (Recrystallised) quartz Type 3 primary FIs	Upper Th final by Th (L - V) for Type 3 FI associated with Type 5 and 6 FI	6	Clathrate	306	7.5	306.0	248	0.96	Chen (1972) and Fall et al. (2011)
Secondary (Recrystallised) quartz Type 3 primary FIs	Lower Th final by Th (L - V) for Type 3 FIs associated with Type 5 and 6 FI	9	Clathrate	270	2.0	270.0	57	0.57	Chen (1972) and Fall et al. (2011)
Secondary (Recrystallised) quartz Type 3 primary FIs	Avg. Th final by Th (L - V) for Type 3 FIs associated with Type 5 and 6 FI	8	Clathrate	289	4.0	289.0	120	0.86	Chen (1972) and Fall et al. (2011)
None mineralised Type 4 secondary FIs throughout samples	Upper Th final by Th (L - V) for Type 4 FI	-9	Ice	275	12.9	275.0	54	0.88	Bodnar (1993) and Steel-MacInnis et al. (2012)
None mineralised Type 4 secondary FIs throughout samples	Lower Th final by Th (L - V) for Type 4 FI	-3	Ice	156	5.0	156.0	5	0.95	Bodnar (1993) and Steel-MacInnis et al. (2012)
None mineralised Type 4 secondary FIs throughout samples	Avg. Th final by Th (L - V) for Type 4 FI	-2	Ice	201	3.4	201.0	15	0.89	Bodnar (1993) and Steel-MacInnis et al. (2012)
Mineralised Type 4 secondary FIs throughout samples	Upper Th final by Th (L - V) for Type 4 FI	-9	Ice	350	12.9	350.0	151	0.78	Bodnar (1993) and Steel-MacInnis et al. (2012)
Mineralised Type 4 secondary FIs throughout samples	Lower Th final by Th (L - V) for Type 4 FI	-5	Ice	280	7.9	280.0	61	0.83	Bodnar (1993) and Steel-MacInnis et al. (2012)
Mineralised Type 4 secondary FIs throughout samples	Avg. Th final by Th (L - V) for Type 4 FI	-6	Ice	300	9.2	300.0	70	0.80	Bodnar (1993) and Steel-MacInnis et al. (2012)

Group 3 has a variety of deformation and alteration features. These include small-scale folds, veins with pinch-and-swell features and reaction halos at vein boundaries. As a general observation these features frequently occur in quartz veins hosted in metapelites (Table 7.4). Group 3, in particular, has structural deformation features associated with reaction halos containing pyrite, biotite and muscovite. The halos probably formed during greenschist facies plastic deformation. This supposition is based on localised recrystallisation and xenocrystic or xenolithic host rock components that originated proximal to recrystallised quartz. Recrystallised quartz predominately occurs in reaction halos that show few FIs.

Group 3's recrystallised grains, although less numerous when compared to Group 2, show texturally uniform characteristics. Similar to Group 2, the recrystallised quartz contains numerous Type 3 and 5 primary FIAs, especially in samples that contain high quantities of sulphides. Along recrystallised quartz grain boundaries in Group 3 samples Type 3 and 5 primary FIs are even more prominent than in Group 2. The solid black phase within Group 3 Type 5 primary FIs has a proportionally larger component of pyrite and/or graphite/ amorphous carbon, and a higher proportion of liquid CO_2 compared to Group 2. Unlike Kamituga Group 2 Type 5 primary FIs, Kamituga Group 3 Type 5 primary FIs do not contain arsenopyrite, pointing to a substantial organic-rich fluid source. Group 3 Type 3 and 5 primary FI's CO_2 melting temperature of between -57 °C to -58 °C infers the presence of a volatile phases such as CH_4 (Roedder, 1984). Type 3 primary FIs are more dominant and have higher concentrations of CH_4 in Type 3 and 5 primary FIAs. Type 3 primary FIs have Th of 270 - 306 °C (avg. 289 °C) and low salinities, < 8.0 wt. % NaCl eq., (avg. 4.0 wt. % NaCl eq.) as calculated using Chen's (1972) equations (Figure 7.30). Larger liquid-dominated CO_2-rich Type 3 (3- 5 µm) FIs are found in close proximity to sulphide grains. In mineralised samples, liquid CO_2-rich Type 3 primary FIs have the highest densities of Type 3 primary FI, as determined by Fermi diad spacing. The CO_2 homogenisation is below 14 °C. By contrast, Type 3 primary FIs in Groups 1 and 2 associated with tourmaline, homogenise above 17 °C. This suggests that there is a progressive increase in CO_2 fluid density from Groups 1 and 2 to Group 3 veins.

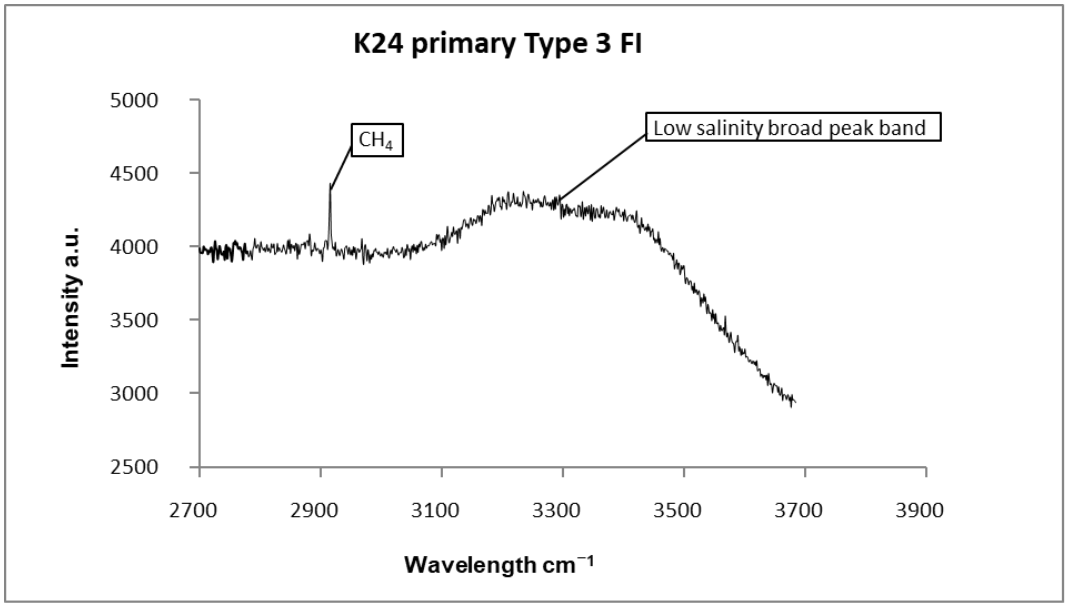

Figure 7.30: K24 liquid CO_2 rich Type 3 primary FIs spectra depicting low salinity with CH_4. There is no evidence of N_2.

In a number of very high-density Type 3 primary FIs, a second vapour bubble develops around 135 °C. According to Roedder (1984), the occurrence of a second vapour bubble indicates high density CO_2 FIs, as seen in mineralised Group 2 samples. Type 3 and 5 primary FIs in Group 3 are, in these FIAs, genetically related to each other due to a phase separation of aqueous fluids prior to capturing, or due to direct separation from a crystallising melt and a subsequent contamination of solids (pyrite and graphite) (Bodnar et al., 1993).

Two macroscopically distinct quartz varieties are present in Group 3 veins. Darker quartz with a cloudy appearance is present particularly along vein margins where graphitic material is present along microfractures (Figure 7.31A). The cloudy appearance may be further intensified by fine-grained biotite-chlorite intergrowths. There is less fracturing and contamination towards the centre of the veins where the quartz shows a lighter colour (Figure 7.31B). Despite their different appearances, both quartz phases are interpreted to have formed during the same hydrothermal precipitation process.

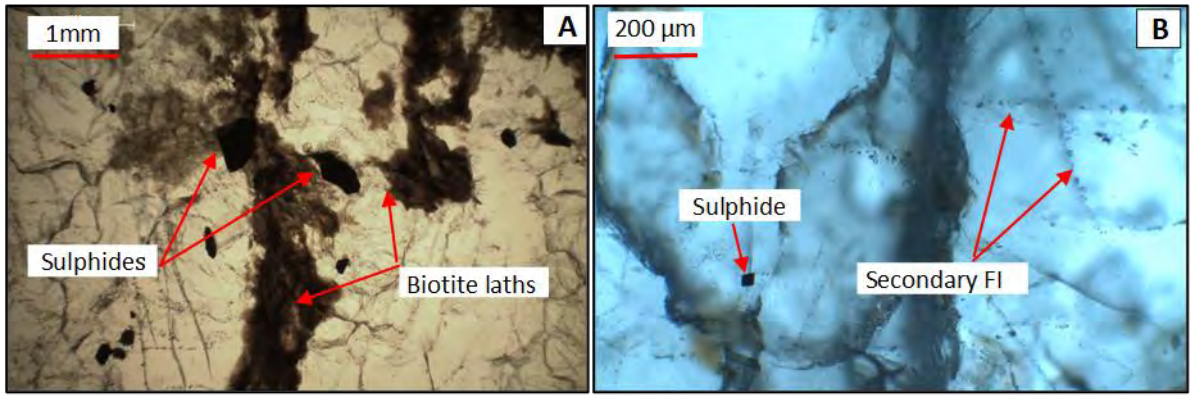

Figure 7.31: K24 Group 3 vein. (A) Biotite and sulphides with quartz containing numerous secondary FIs close to vein margins. (B) Clearer quartz with fewer fractures and very minor sulphide/biotite contamination and fewer secondary FI trails in centre of vein.

7.2.3.2 SECONDARY FIs

A common feature of Group 3 quartz is the profusion of Type 4 and 6 secondary FIs along healed fractures. The profusion of fractures with secondary FIs commonly obstructs the identification of primary FIs. The few Type 3 secondary FIs present in Group 3, are seen in Au mineralised samples, and predominantly occur along host rock boundaries in both recrystallised and unrecrystallised grains, frequently with Type 5 secondary FIs. This volume proportion difference in the FIs can be due to the same fluid at different P-T conditions of trapping and/or heterogeneous trapping. Type 3 and 4 secondary FIAs homogenise between Th of 156 - 350 °C (avg. 245 °C) and consistently show low salinities 3.4 - 12.9 wt. % NaCl eq. (avg. 5.0 wt. % NaCl eq.) as per Chen (1972) and Bodnar's (1993) calculations. Total homogenisation pressures are 0.5 - 15.1 MPa (avg. 1.5 MPa) and densities are 0.78 - 0.95 g/cm^3 (avg. 0.89 g/cm^3) (calculated using Fall et al. (2011) and Steel-MacInnis et al's. (2012) equations (Table 7.4). Unmineralised samples contain secondary FIs that have Th below 275 °C and few Type 3 secondary FIs. Mineralised samples, by contrast, have FIs with higher salinities >7 wt. % NaCl eq. and Th over 280 °C and Th within ±20 °C of the primary FIs in recrystallised quartz as per Chen (1972) and Bodnar's (1993) calculations. The total homogenisation pressures are 6.1 - 15.1 MPa (avg. 7.0 MPa and densities range between 0.78 - 0.83 g/cm^3

(avg. 0.80 g/cm^3) calculated using Fall et al. (2011) and Steel-MacInnis et al's. (2012) equations (Table 7.4). Accurate analysis and visible clathrate changes are inconclusive for salinity and density determinations for Group 3 Type 3 secondary FIs due to their small size. Lower temperature secondary FIs probably reflect the involvement of meteoric water or epithermal fluids (Rossetti and Colombo, 1999). This, however, does not reflect the large areas over which epithermal fluids would have affected and evolved. Meteoric fluids, or an overprinted epithermal system, are invoked for these lower Th and salinity FIs.

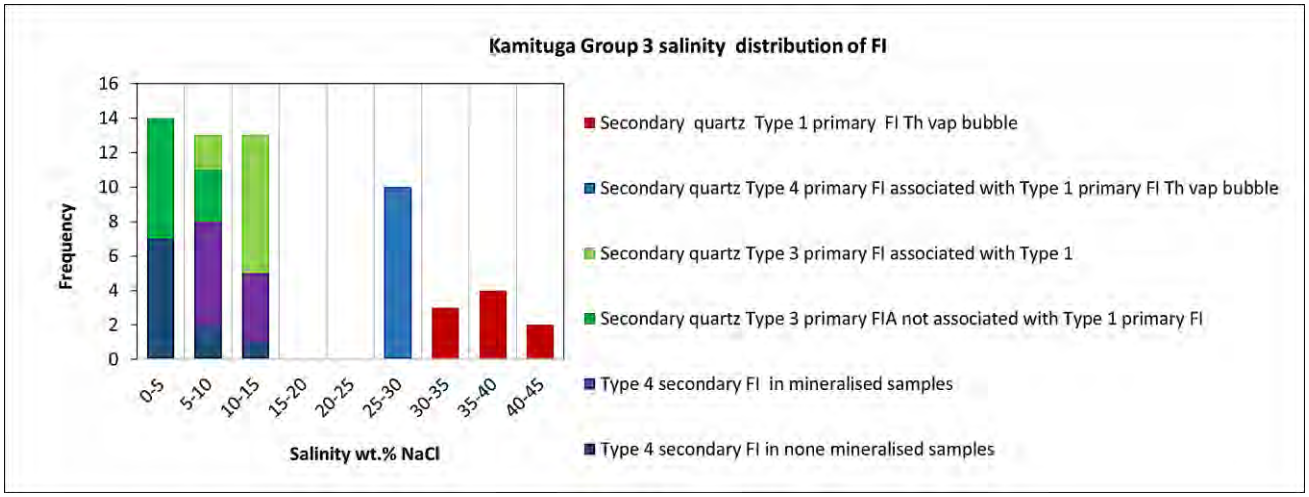

Figure 7.32 Group 3 saline FI distribution for Types 1, 3 and 4 primary and secondary FIs. Type 1 FI are less prevalent as there are fewer samples that contain them (Table 7.4).

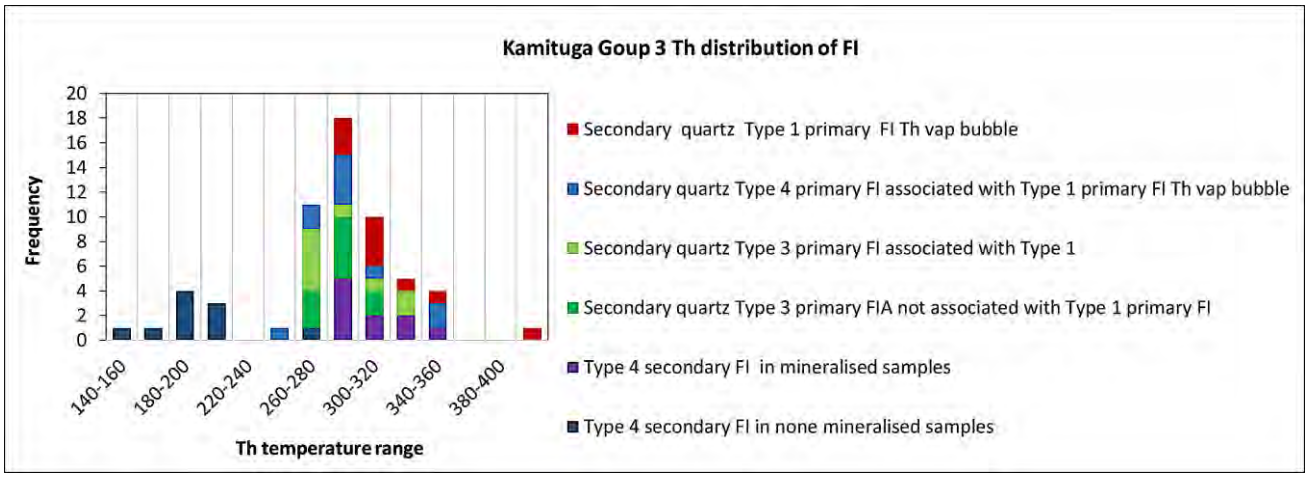

Figure 7.33: Group 3 Th FI distribution for Type 1, 3 and 4 primary and secondary FIs. Type 1 FI are less prevalent as there are fewer samples that contain them (Table 7.4).

In summary, Kamituga Group 3 veins formed as a result of the early formation of primary quartz and sulphides by hydrothermal precipitation. Subsequent plastic deformation recrystallised quartz, mobilised sulphides and was related to an influx of fluids rich in CO_2 and organic materials (C and CH_4) into the quartz veins. Th and salinity of FIs indicate the probability of two different fluids, although the different fluids could not always be identified (Figures 7.32 and 7.33). Samples with higher gold grade contain more liquid CO_2-rich Type 3 FIs (Table 7.1). Group 3's mineralised samples have distinctly higher Th in secondary FIs than those in Group 1 and 2, and in unmineralised Group 3 samples, suggesting that Au mineralisation was related to an episode of higher

temperature fluid influx. Furthermore, higher gold grades in recrystallised quartz suggest that gold was added or mobilised and concentrated during deformation and during a fluid influx event that post-dated the fluid influx that formed the primary veins. Kamituga Group 3 secondary FIs have similar homogenisation temperatures and salinities as primary FIs in extensively recrystallised quartz; particularly in mineralised samples. This suggests a common fluid source and sequential formation of these primary and secondary fluids. The same relationship was identified in Kamituga Group 2 metapelite-hosted fluids but was not as prevalent as in Group 3.

7.3 LUGUSHWA - GENETIC GROUPS

7.3.1 LUGUSHWA GROUP 1: PEGMATITE

No pegmatite was sampled in Lugushwa.

7.3.2 LUGUSHWA GROUP 2: TOURMALINE-BEARING HYDROTHERMAL VEINS

Lugushwa Group 2 samples, Ltm-1 and Ltm-2, are tourmaline-bearing hydrothermal quartz veins that define this Group. Samples Ltm-1 and Ltm-2 contain lath-shaped tourmaline with light to medium brown pleochroism. Concentrically zoned pale green, yellow to brown finer-grained variety of tourmaline is dispersed throughout Ltm-1 and Ltm-2. In colour and zonation this tourmaline is similar to the alteration halos of Kamituga (Ktm-3) Group 1 pegmatite and Kamituga's Group 2 tourmaline-bearing samples (Table 7.5 and Figure 7.34). Lugushwa Group 2 samples contain tourmaline, muscovite, biotite, calcite and accessory apatite. Late stage sulphides (arsenopyrite pyrite and chalcopyrite in sample Ltm-2 hosted in diorite), Fe-oxides and hydroxides are present in both samples (Table 7.5).

Primary quartz-tourmaline assemblages have interstitial and intergranular sulphides. Secondary quartz precipitation in Group 2 was observed along fractures in quartz and tourmaline. There is a close spatial association of secondary stage quartz with a younger interstitial sulphide generation, suggesting a genetic link between them. These secondary quartz-sulphide associations are, in turn, crosscut by calcite that precipitated along new fractures, indicating a third stage fluid influx event (Figure 7.34A). Late stage (third fluid influx) sulphides and amorphous carbon/graphite are similarly present along fractures and grain boundaries of recrystallised quartz. This suggests that the third, organic and sulphur-bearing fluid was injected during or after quartz recrystallisation (Figure 7.34A). This late stage injection is more prominent than in Kamituga Group 2 samples. The late stage fluids along recrystallised grain boundaries, especially in the metapelite-hosted sample Ltm-1, contain more sedimentary sourced components (amorphous carbon and graphite) than Kamituga Group 2.

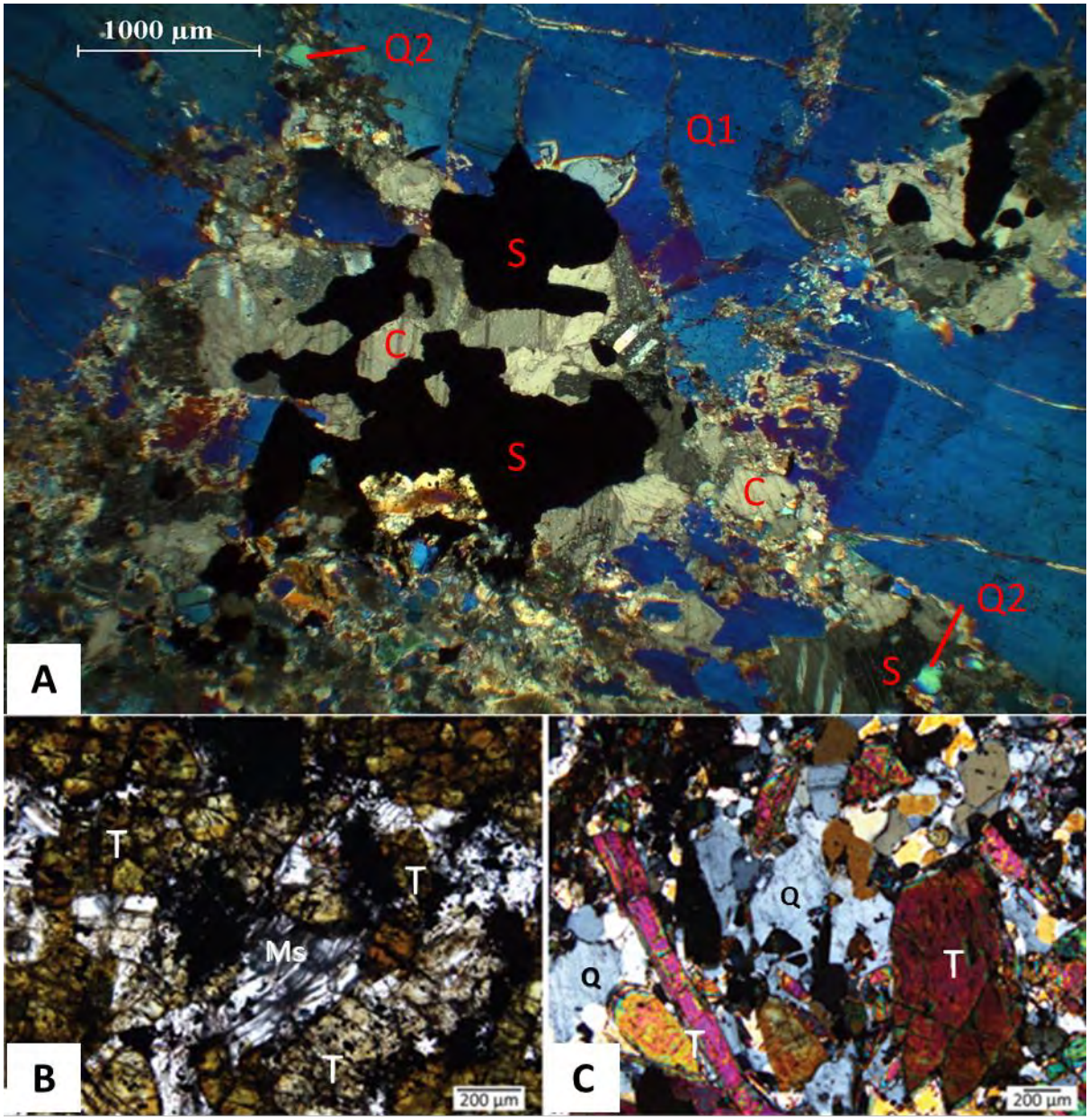

Figure 7.34(A) Ltm-1 indicating the presence of late stage sulphides (S) and calcite (C) within fracture zones of primary quartz (Q1). The secondary recrystallised quartz (Q2) is associated with the influx of sulphides and calcite. (B) Tourmaline-rich zone of Ltm-2 with pleochroic but optically unzoned tourmaline (T) and white mica (MS). Patches of opaque Fe-oxide precipitated in clusters and along fractures in tourmaline. (C) Inclusion-rich hydrothermal quartz (Q) and clear recrystallised quartz with few or no inclusions in tourmaline-rich zone(T) of Ltm-1; CPL (modified from Büttner et al., 2016).

The late stage greenschist facies plastic deformation that preceded or is coeval with the third fluid influx formed centimetre thick muscovite, biotite, sulphide and iron oxide/ hydroxide in alteration halos of Ltm-1 (Table 7.5). The generation and mobilisation of the third fluid is possibly related to the greenschist facies plastic deformation and lead to the precipitation of sulphide and calcite (Tables 7.2).

In both Lugushwa Group 2 samples, Ltm-1 and Ltm-2, undulose extinction in muscovite and quartz are common and resemble similar features in Kamituga Group 2. Extensive quartz recrystallisation occurs in close proximity to tourmaline grains. Quartz recrystallisation is most evident between tourmaline fragments, and where there is evidence of late stage sulphide and calcite injections. Recrystallised quartz is a prominent feature in the

alteration halo of sample Ltm-1, and similar to features seen in Kamituga's tourmaline-bearing hydrothermal quartz veins (Tables 7.1 and 7.2) (Figure 7.34B). Recrystallised grains lack interstitial solid inclusions and form strain-free grains with straight grain boundaries and foam textures (Figure 7.34C). The widespread recrystallisation of quartz is the most prominent feature of the regional greenschist facies plastic deformation.

Fe-oxide and hydroxides, as in Kamituga Group 2 and 3, are present in granular patches and fractures in quartz and tourmaline. Fe-oxide and hydroxides crosscut multiple secondary FI trails. In Lugushwa Group 2, Fe-oxides and hydroxides are considered to be surface-near alterations or weathering - postdating all hydrothermal and regional deformation processes.

Table 7.5: Macro- and microscopic description of Lugushwa Groups 1, 2 and 3 samples and primary, pseudosecondary secondary FI Types.

Group	Drill core or Sample site	Sample No.	Depth metres and vein thickness (cm) respectively	Deformation features of vein	Au grade g/t	Macroscopically visible sulphides	Macroscopically visible number of quartz species and type	Tourmaline/ carbonate present	Host rock (HR) and general notes	FI Types present *Listed in decreasing occurrence. Blue represents primary or pseudosecondary FIs and red secondary FIs.
2	LDD 013	Ltm-1	104.5/1	Disrupted	0.33 - 0.76	Y Pyrite > arsenopyrite	1	Y/Y	Brecciated metapelite with alteration halo	T3, T1, T4, T6, T5 T4, T6, T3
2	LDD109	Ltm-2	10.7/0.1	None	0.26 -1.06	Y Pyrite <arsenopyrite	1	Y/Y	Diorite	T3, T1, T4, T6, T5 T4, T6, T3
3	LDD162	L1	36.3/1	Fractured	0	Y	1	N/N	Diorite just below metasiltstone	T4, T6, T3 T4, T6
3		L2	46.8/ 0.3	Fractured	0	Y and in HR	1	N /Y calcite	Stockwork in sulphide bearing diorite	T4, T6, T1, T2, T3, T5 T4, T6
3		L3	72.5/3	Fragmented	1.76	Y and HR resorption hole	1	N/N	Sulphide bearing diorite. Darker phase of quartz visible at vein boundary.	T4, T6, T3, T1, T2, T5 T4, T6, T3
3		L4	84.5/0.4	Slight fragmentation of stockworks	0	Y and in HR	1	N/N	Stock work sulphide bearing diorite. Darker phase of quartz visible at vein boundary.	T4, T6, T1, T2, T3, T5 T4, T6, T3
3	LDD129	L6	64.5/0.4	Disrupted	0	N	1	N/N	Transition of dark graphitic, fine grained metapelite to metapelite with Qtz segregation.	T4, T6, T3, T1, T2, T5 T4, T6, T3
3		L7	31.8/2	Disrupted	2.09	Y	1	N/N	Metapelite with Qtz segregation	T4, T6, T3, T1, T2, T5 T4, T6, T3
3	LDD052	L15	50.5/1	Disrupted	7.32	Y abundant	1	N/N	Diorite just below upper boundary	T3, T4, T6, T5, T1 T4, T6, T3
3		L17	158.5/4	Brecciated	0	N	1	N/Y calcite	Diorite	T4, T6, T1, T2, T3, T5 T4, T6
3	Field samples at G20 -21	L19	NA/12	None	Mineralised zone but not assayed	Y	1	N/N	Vein occurs with 2 m wide subvertical swarm of quartz. Graphitic metapelite	T4, T6, T3, T5, T1 T4, T6, T3
3	Near drill hole LDD 013 Field samples at G20 -21	L20	NA/3	None	Mineralised zone but not assayed	Y	1	N/N	Graphitic metapelite	T4, T6, T3, T5, T1 T4, T6, T3

Table 7.5 cont.: Macro- and microscopic description of Lugushwa Groups 1, 2 and 3 samples and primary, pseudosecondary secondary FI Types.

Group	Drill core or Sample site	Sample No.	Depth metres and vein thickness (cm) respectively	Deformation features of vein	Au grade g/t	Macroscopically visible sulphides	Macroscopically visible number of quartz species and type	Tourmaline/ carbonate present	Host rock (HR) and general notes	FI Types present *Listed in decreasing occurrence. Blue represents primary or pseudosecondary FIs and red secondary FIs.
3	Near drill hole LDD 013 Field samples at G20 -21	L21	NA/4	None	Mineralised zone but not assayed	Y	1	N/N	Graphitic metapelite	T4, T3, T6, T1, T5 T4, T6, T3

7.3.2.1 PRIMARY FIs

The overall salinity of Lugushwa Group 2 tourmaline-bearing samples is similar to Kamituga Group 3's tourmaline-free samples. Unlike Kamituga Group 2 and 3, Lugushwa's samples have no Type 2 primary FIs - only Type 1 primary FIs, and high salinity Type 4 primary FIAs. The absence of FIs with secondary daughter minerals such as sylvite and Fe-chlorides is not typically of a granitic fluid source (Wilkinson, 2001). Primary unrecrystallised, but plastically deformed quartz, in close proximity to recrystallised quartz surrounding tourmaline, contain Type 1 primary FIs. These Type 1 FIs vary greatly in size (2 - 8 µm) and have different halite volume proportions (10 - 40 vol %). Lugushwa Group 2 Type 1 primary FIs homogenise by vapour bubble disappearance into liquid (V - L), or by simultaneous bubble and halite loss. As in Kamituga Group 3, Lugushwa Group 2 samples do not homogenise by halite dissolution (Table 7.6). Final homogenisation for Type 1 by vapour bubble disappearance, or by simultaneous bubble and halite loss, occurs at temperatures ranging between 304 - 389 °C (avg. 336 °C) (Table 7.6). Type 1 primary FIs have salinity ranges of 37.2 - 41.6 wt. % NaCl eq. (avg. 39.6 wt. % NaCl eq.), total homogenisation pressures of 6.2 - 16.6 MPa (avg. 9.2 MPa) and densities of 1.03 - 1.08 g/cm^3 (avg. 1.07 g/cm^3) calculated using Steel-MacInnis et al's. (2012) equations (Table 7.6).

Overall, Lugushwa Group 2 has primary quartz Type 1 FIAs that consist of Type 1, 3, 4 and 6 primary FIs (Figure 7.35). These FIAs are similar to those in Kamituga Group 2 in that they are randomly oriented and concentrated around tourmaline. Unlike Kamituga Group 2, Lugushwa Group 2 has no clusters of Type 1 primary FIAs in secondary stage recrystallised or secondary injected quartz. Like Kamituga Group 2, and more so Kamituga Group 3, Type 3 primary and pseudosecondary FIs contain a prominent liquid CO_2-rich component (Figure 7.35B). As with Kamituga Group 2 there is a distinct abundance of small equidimensional Type 3, 4 and 6 primary FIs (avg. 2 - 5 µm). CO_2 vapour-rich Type 3 and 4 FIs are, however, not as numerous in Lugushwa Group 2 FIAs as in all Kamituga samples. This is an indication that effervescence was not as prevalent in Lugushwa deposits.

Type 3, 4, 5 and 6 primary FIs in FIAs have a Th range of 263 - 342 °C (avg. 309 °C) (Table 7.6). Type 4 primary FIs have salinities of 18.6 - 24.5 wt. % NaCl (avg. 21.7 wt. % NaCl eq.) and 7.5 - 10.5 wt. % NaCl (avg. 9 wt. % NaCl eq.) for liquid CO_2, or a combination of liquid and vapour CO_2 Type 3 primary FIs as per Chen (1972) and Bodnar's (1993) calculations (Table 7.6). Clathrate melting temperatures and Fermi diad spacing of 104 to 105 cm^{-1} (Figure 7.36) indicate pressures of 5.7 - 24.8 MPa and densities of 0.57 - 0.96 g/cm^3 at clathrate melting for Type 3 primary FIs as calculated using Fall et al's. (2011) equations. Many Type 5 primary FIs (CO_2-rich with a solid phase) containing xenocrystic pyrite, graphite and carbon in FIAs with other fluid Types, do not homogenise before decrepitation. According to Roedder (1984) decrepitation before homogenisation is indicative of a metamorphic rather than a granitic fluid source. This particularly applies to sample Ltm-1 that is hosted in a brecciated metapelite.

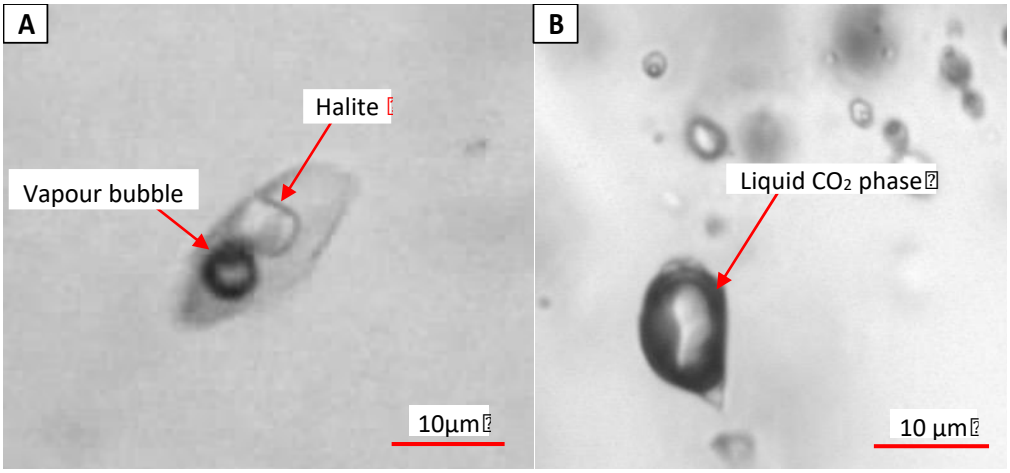

Figure 7.35: (A) Primary quartz of Ltm-1 indicating large Type 1 primary FI. (B) Large Type 3 primary FI with distinct liquid CO_2 phase.

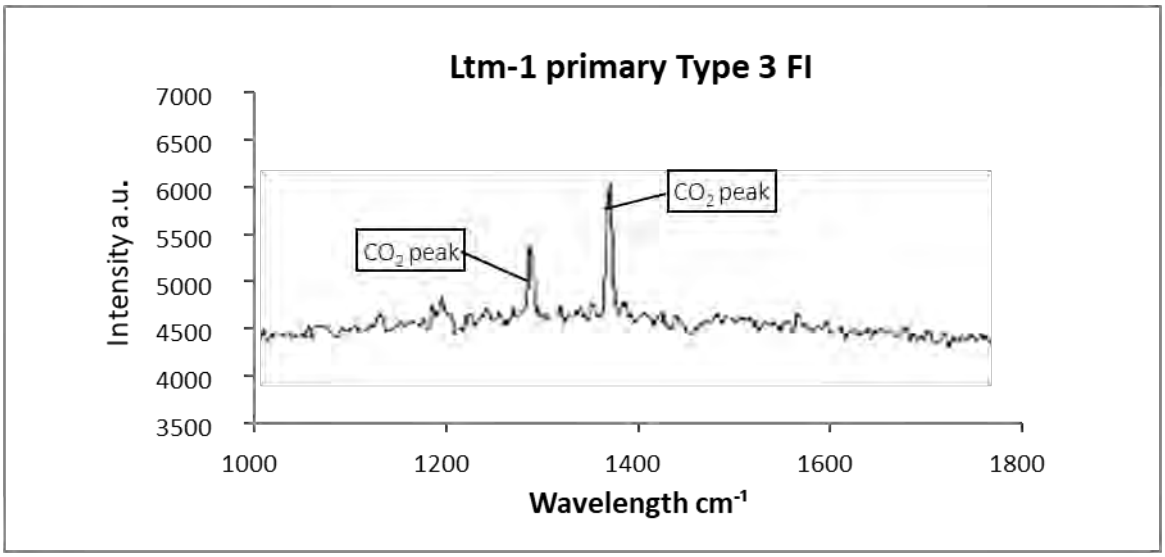

Figure 7.36: Raman spectra indicating spectra for Type 3 primary FI liquid phase (Figure 7.35B) indicating peaks at 1281 cm^{-1} and 1385 cm^{-1}, indicating a Fermi diad spacing of 104 cm^{-1}.

Table 7.6: Microthermometric and barometric data for Type 1, 3 and 4 primary and secondary FIs for Lugushwa genetic Group 2.

Phase relationship	**FI Type**	**Tm**	**Final phase melting**	**Th $_{(L-V)}$**	**wt. % NaCl eq.**	**T @ homog. (°C)**	**P @ homog. (bar)**	**r_{BULK} (g/cm_3)**	**Reference**
Primary (Hydrothermal) quartz Type 1 primary FIs	Upper Th final by Th (L - V) for Type 1	342	Halite	389	41.6	389.0	166	1.03	Sterner et al. (1988) and Steel-MacInnis et al. (2012)
Primary (Hydrothermal) quartz Type primary FIs	Lower Th final by Th (L - V) for Type 1	289	Halite	304	37.2	304.0	62	1.08	Sterner et al. (1988) and Steel-MacInnis et al. (2012)
Primary (Hydrothermal) quartz Type 1 primary FIs	Avg. Th final by Th (L - V) for Type 1	320	Halite	336	39.8	336.0	92	1.07	Sterner et al. (1988) and Steel-MacInnis et al. (2012)
Primary (Hydrothermal) quartz Type 4 primary FIs	Upper Th final by Th (L - V) for Type 4	-12	Hydrohalite	342	24.5	342.0	121	0.92	Sterner et al. (1988) and Steel-MacInnis et al. (2012)
Primary (Hydrothermal) quartz Type 4 primary FIs	Lower Th final by Th (L - V) for Type 4	-15	Ice	263	18.6	263.0	42	0.95	Bodnar (1993) and Steel-MacInnis et al. (2012)
Primary (Hydrothermal) quartz Type 4 primary FIs	Avg. Th final by Th (L - V) for Type 4	-19	Ice	309	21.7	309.0	82	0.93	Bodnar (1993) and Steel-MacInnis et al. (2012)
Primary (Hydrothermal) quartz Type 3 primary FIs	Upper Th Type 3	4	Clathrate	301	10.5	301.0	248	0.96	Chen (1972) and Fall et al. (2011)
Primary (Hydrothermal) quartz Type 3 primary FIs	Lower Th Type 3	6	Clathrate	280	7.5	280.0	57	0.57	Chen (1972) and Fall et al. (2011)
Primary (Hydrothermal) quartz Type 3 primary FIs	Avg. Th Type 3	5	Clathrate	292	9.0	292.0	72	0.79	Chen (1972) and Fall et al. (2011)
Secondary (Hydrothermal) quartz Type 4 primary FIs	Upper Th final by Th (L - V) for Type 4	-7	Ice	315	10.4	315.0	99	0.80	Bodnar (1993) and Steel-MacInnis et al. (2012)
Secondary (Hydrothermal) quartz Type 4 primary FIs	Lower Th final by Th (L - V) for Type 4	-5	Ice	232	7.9	232.0	27	0.89	Bodnar (1993) and Steel-MacInnis et al. (2012)
Secondary (Hydrothermal) quartz Type 3 primary FIs	Avg. Th final by Th (L - V) for Type 4	-6	Ice	281	9.2	281.0	61	0.84	Bodnar (1993) and Steel-MacInnis et al. (2012)
Secondary (Hydrothermal) quartz. Type 3 FIs associated with Type 4 and 6 primary FIAs	Upper Th Type 3	6	Clathrate	308	7.5	308.0	640	1.08	Chen (1972) and Fall et al. (2011)
Secondary (Hydrothermal) quartz. Type 3 FIs associated with Type 4 and 6 primary FIAs	Lower Th Type 3	8	Clathrate	283	4.0	283.0	248	0.96	Chen (1972) and Fall et al. (2010)
Secondary (Hydrothermal) quartz. Type 3 FIs associated with Type 4 and 6 primary FIAs	Avg. Th Type 3	7	Clathrate	296	5.8	296.0	378	0.98	Chen (1972) and Fall et al. (2011)
All Type 4 and 6 secondary FIs throughout samples	Upper Th final by Th (L - V) for Type 4	-8	Ice	243	11.7	243.0	32	0.91	Bodnar (1993) and Steel-MacInnis et al. (2012)
All Type 4 and 6 secondary FIs throughout samples	Lower Th final by Th (L - V) for Type 4	-5	Ice	222	7.9	222.0	23	0.90	Bodnar (1993) and Steel-MacInnis et al. (2012)
All Type 4 and 6 secondary FIs throughout samples	Avg. Th final by Th (L - V) for Type 4	-7	Ice	235	10.5	235.0	28	0.91	Bodnar (1993 and Steel-MacInnis et al. (2012)
All Type 3 secondary FIs throughout samples	Upper Th Type 3	5	Clathrate	272	9.0	272.0	248	0.96	Chen (1972) and Fall et al. (2011)
All Type 3 secondary FIs throughout samples	Lower Th Type 3	7	Clathrate	238	5.8	238.0	57	0.57	Chen (1972) and Fall et al. (2011)
All Type 3 secondary FIs throughout samples	Avg. Th Type 3	6	Clathrate	249	7.5	249.0	62	0.75	Chen (1972) and Fall et al. (2011)

There is a significant increase in the number of Type 3 FIs in secondary stage hydrothermal quartz that is not recrystallised and is not associated with tourmaline (Figure 7.37A). Secondary quartz, co-formational with sulphides, contain numerous liquid CO_2 rich Type 3 FIs. Lugushwa Group 2 Type 3 primary and pseudosecondary FIAs have a greater volume liquid phase compared to similar mineralised secondary quartz in Kamituga Group 2 Type 3 FIAs. A small number of FIAs, with low salinity Type 4 and 6 FIs (1 - 3 µm), were present in both Ltm-1 and Ltm-2 samples. No Type 5 FIs were observed. Type 3 FIAs cluster at the centre of grains, especially in intergranular sulphide-rich quartz grains, with the majority having a greater number of disproportionately large equidimensional or elongated FIs (>5 µm).

CO_2 melting temperatures in Lugushwa Group 2 Type 3 FIAs vary from -57 °C to -58 °C, rather than -55.6 °C that would be indicative of pure CO_2 (Roedder, 1984). This suggests, that in addition to pure CO_2 and H_2O, there are other volatile components present. Raman analysis identified CH_4 and N_2. CH_4 suggests input from organic-rich sources such as metapelitic host rocks. Micro-thermometric analyses suggest that CH_4, and possibly N_2 are highly concentrated in irregularly shaped Type 3 FIs.

Type 3 and 4 FIAs have Th of 232 - 315 °C (avg. 281 °C). Type 4 FIs salinities are 7.9 - 10.4 wt. % NaCl eq. (avg. 9.2 wt. % NaCl eq.) and Type 3 FIs are 4.0 - 7.5 wt. % NaCl eq. (avg. 5.8 wt. % NaCl eq.) (Table 7.6) as per Chen (1972) and Bodnar's (1993) calculations. Type 4 FIs homogenise at pressures of 2.7 - 9.9 MPa (avg. 6.1 MPa) and densities of 0.80 - 0.89 g/cm^3 (avg. 0.84 g/cm^3) calculated using Steel-MacInnis et al's. (2012) equations. Liquid CO_2-rich Type 3 FIs homogenise to the liquid phase at 11 - 13 °C. This indicates an increase in density compared to Type 3 FIs in Kamituga Group 2. Clathrate melting temperatures and Fermi diad spacing of 104 - 105.5 cm^{-1} indicate pressures of 3.5 - 3.8 MPa and densities of 0.57 - 1.08 g/cm^3 as calculated using Fall et al's. (2011) equations.

7.3.1.2 SECONDARY FIs

Type 4 and liquid CO_2-rich Type 3 secondary FIs (1-5 µm) have characteristically low salinities (Figure 7.37B). Recrystallised quartz predominantly contains secondary FIs found along healed cracks, indicating post-recrystallisation capturing. The only difference between secondary and recrystallised quartz is that recrystallised quartz contains fewer large liquid CO_2-rich Type 3 secondary FIs. Type 3 FIs within recrystallised hydrothermal quartz show higher concentrations of CH_4 and, to a lesser extent, N_2. This is consistent with carbon/graphitic material that was deposited during quartz recrystallisation.

Secondary FI vapour phase proportions vary with FI size across all quartz phases. Large Type 4 FIs (> 2 µm) contain a vapour phase that is >50 vol % of the FI. Small Type 4 FIs (< 2 µm) have 5 - 20 vol % vapour. Type 4 FIs display Th of 222 - 243 °C (avg. 235 °C) and salinities of 7.9 - 11.8 wt. % NaCl eq. (avg. 10.5 wt. % NaCl eq.) with total homogenisation pressures of 2.3 - 3.2 MPa (avg. 2.8 MPa) and densities of 0.90 - 0.91 g/cm^3 (avg. 0.91 g/cm^3) as per Bodnar (1993) and Steel-MacInnis et al's. (2012) calculations. Type 3 secondary FIs had distinctly higher Th than Type 4 secondary FIs. Th ranges from 238 - 272 °C (avg. 249 °C) and salinities range between 5.8 - 9.0 wt. % NaCl eq. (avg. 7.5 wt. % NaCl eq.) as calculated from Chen (1972) and Fall et al's. (2011) equations.

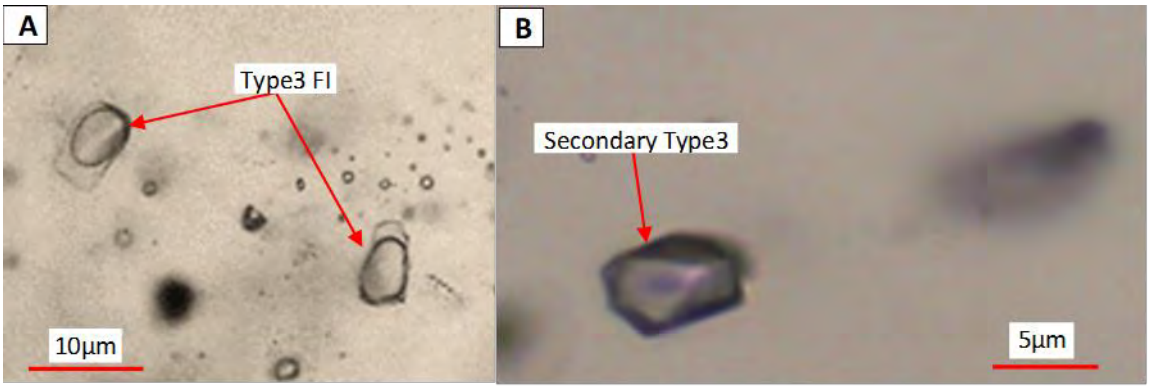

Figure 7.37: (A) Secondary none recrystallised quartz of Ltm-1 indicating large Type 3 pseudosecondary FIs. (B) Recrystallised quartz of Ltm-2 with negative liquid CO_2 rich Type 3 secondary FI.

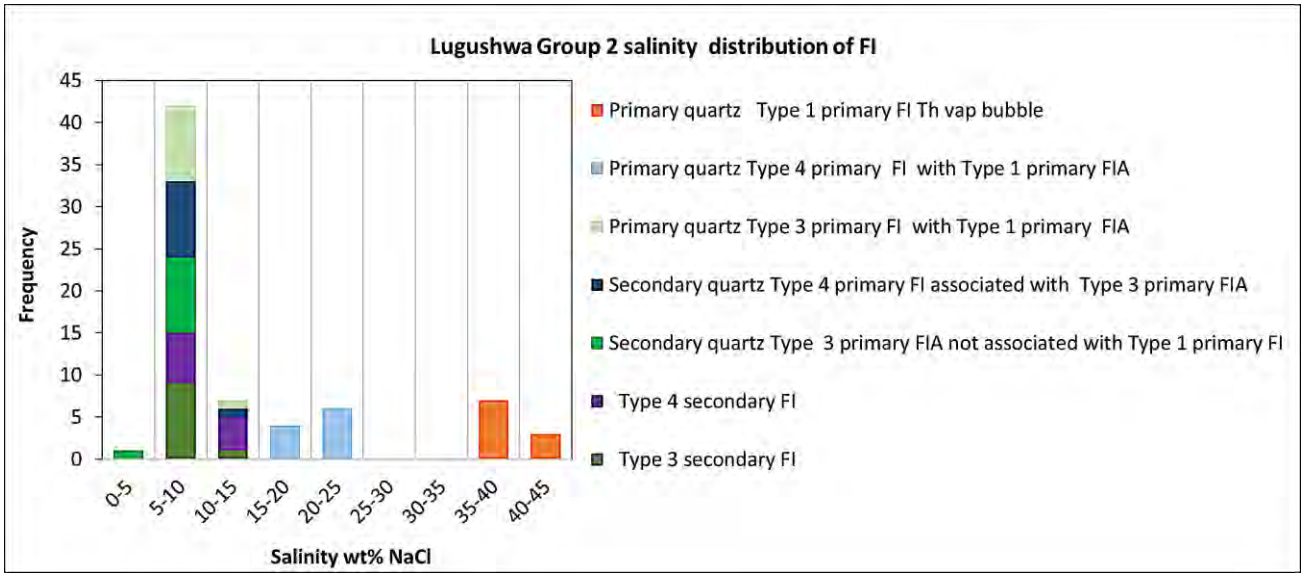

Figure 7.38: Histogram of salinity for Type 1, 3 and 4 primary and secondary FIs within Lugushwa Group 2.

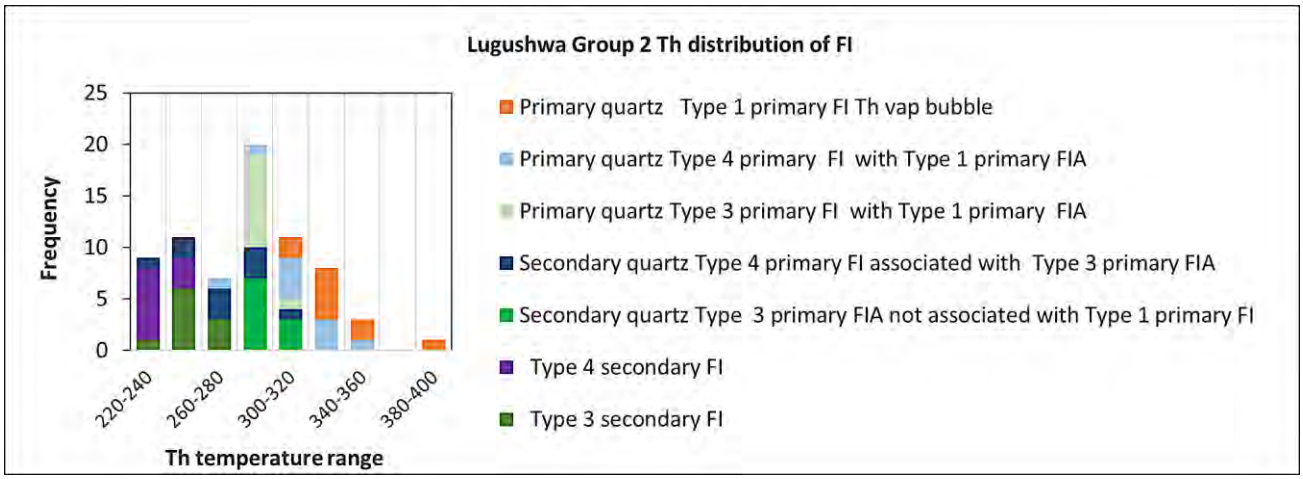

Figure 7.39: Histogram of Th for Type 1, 3, and 4 primary and secondary FIs within Lugushwa Group 2.

In summary, Lugushwa Group 2 veins show the early formation of tourmaline-mica and quartz assemblages together with sulphides by hydrothermal precipitation. During subsequent plastic deformation, quartz recrystallised, sulphur mobilised along grain boundaries, and fluids rich in CO_2 and organic material (C and CH_4) infiltrated and were captured as secondary quartz Type 3 FIs. The overall Th and salinity level of Type 3 primary FIs does not indicate two separate fluid influx events (Figures 7.38 and 38) and therefore, Type 3 FIs, cannot be strictly associated between FIA.

Many of Lugushwa Group 2 veins' mineralogical features, fluid Types and FIAs, microthermometric characteristics are similar to Kamituga Group 2. Overall, however, Lugushwa Group 2 samples contain more organic material in comparison to Kamituga Group 2's; especially in the metapelite hosted sample Ltm-1. In comparison to Kamituga Group 2 there is a lack of homogenisation by halite dissolution in Type 1 FIs and an absence of Type 2 FIs (Figures 7.39). Furthermore, there is an increase in both size and number of liquid CO_2-rich Type 3 FIs, particularly in secondary stage quartz related to subsequent fluid influx events. Sulphides and amorphous organic components are abundant both in hydrothermal primary quartz and in Type 5 primary FIs.

7.3.3 GROUP 3: TOURMALINE-FREE HYDROTHERMAL VEINS

Lugushwa Group 3 samples were taken from dioritic or metapelitic rocks. Primary quartz has interstitial and intergranular sulphides distributed throughout the samples. Secondary quartz, sulphides and calcite were injected into fractures in primary quartz grains. Secondary sulphides formed in secondary quartz and along primary and secondary quartz contact boundaries. Secondary quartz, extensively brecciated and contaminated with amorphous carbon, contains additional sulphides. These are texturally similar to Lugushwa Group 2 samples but not as abundant as in Group 3 samples (Table 7.5). Sulphides, abundant along grain boundaries of recrystallised quartz indicate that sulphur-bearing fluids were injected during or after quartz recrystallisation. As in Group 2, calcite precipitation along fractures post-dates the secondary quartz formation. This indicates a third carbonate-rich fluid influx event.

The complete assemblage of Group 3 samples contains quartz, muscovite, biotite, chlorite and minor apatite and calcite together with sulphides (pyrite, chalcopyrite and arsenopyrite) and Fe-oxides or hydroxides (Table 7.5). The abundance of pyrite and chalcopyrite, compared to arsenopyrite, is dependent on the host rock (Table 7.5). Arsenopyrite is more dominant in diorite-hosted veins, whereas meta-siltstone and metapelites hosted veins contain predominately pyrite and chalcopyrite. As in Kamituga Group 3 samples, these meta-siltstones and metapelites hosted veins contain more organic sedimentary-sourced components. This suggests a metamorphic hydrothermal system with fluids in which organic sedimentary sourced components were transported.

Unmineralised Lugushwa Group 3 quartz vein samples have highly variable sulphide volumes and distribution (Table 7.5). These veins, although deformed, consist of quartz that is usually less recrystallised in comparison to mineralised Lugushwa Group 3 samples (Table 7.5). Sulphide fragments in unrecrystallised quartz display extensive oxidation rims. This suggests that some sulphides belong to primary quartz vein assemblages. There is, however, a second sulphide generation associated with secondary fluid influx events. Secondary quartz-

sulphide associations are, in turn, crosscut by calcite that precipitated along new fractures, indicating a third stage fluid influx event (Figure 4.11). Samples with extensive plastic deformation appear to have undergone a later brittle overprint that led to Fe-hydroxide and oxide formation. This is evident in sample L1 in which several centimetre displacements along brittle fractures are apparent in hand specimens (Figure 4.13).

The few FIs in unrecrystallised primary quartz grains are small (< 7 µm) Type 4 and 6 primary FIs. Type 4 and 6 pseudo-secondary FIs in recrystallised grains occur along intra-crystal fractures and grain boundaries (Figure 7.40A).

In comparison to the unmineralised quartz veins, mineralised veins are structurally deformed with high sulphide levels and consist of a lighter quartz phase that underwent extensive recrystallisation. The extensive fracturing of recrystallised grains is common to all samples. Subgrain boundaries are most prevalent at the host rock-vein boundary - reducing toward the centre of the vein proper. The more mineralised samples display intense ductile strain with distinct undulose extinction, subgrain boundary formation and quartz recrystallisation. Secondary quartz is recrystallised in some areas. The last deformation event that affected these veins was brittle and probably did not correlate with fluid influx (Table 7.5).

There is a distinct secondary quartz phase in samples L4, L6, L7, L19, L20 and L21 due to recrystallisation (Figure 7.40). It is light coloured with foam textures (Table 7.5). This predominantly strain-free recrystallised quartz contains rounded and elongated solid inclusions identified as biotite. These crystals are likely to be xenocrysts sourced from host rock diorites and metapelites (Figure 7.40A). A few primary FIs are located in the larger recrystallised grains and along grain boundaries. These FIs are predominantly equidimensional Type 4 and 6 FIs (<5 µm). Numerous sulphides along the recrystallised grain's margins are partly overgrown by quartz and texturally in a similar position to Type 4 and 6 FIs (Figure 7.40B). Lugushwa Group 3 mineralised samples show intensely recrystallised quartz with typical undulose extinction and subgrain boundaries. They are commonly fractured (Table 7.5).

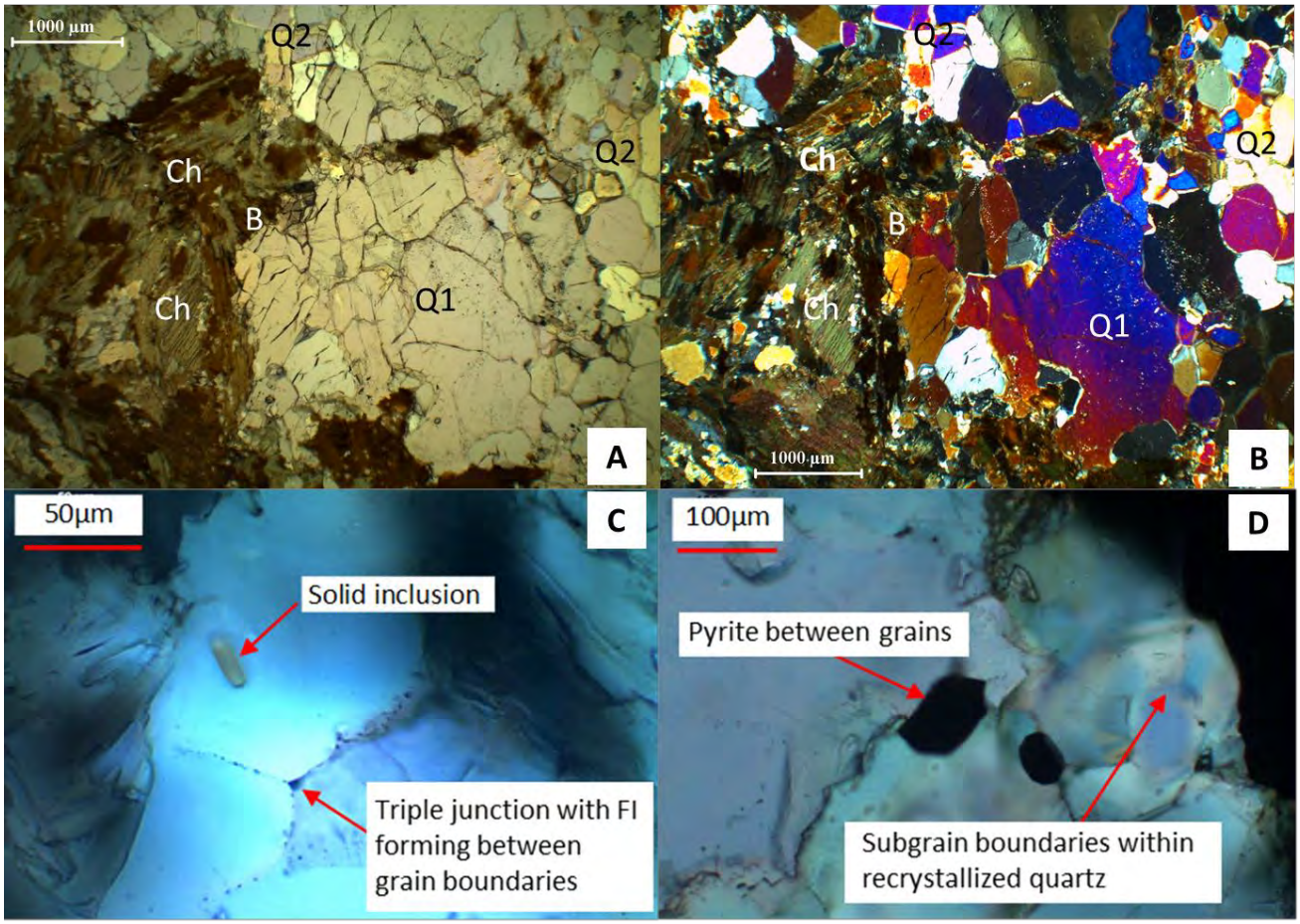

Figure 7.40: Sample L7 (A & B) Indicates different mineral phases present; chloride (Ch), biotite(B), primary quartz (Q1) and the distinct secondary quartz (Q2) phase due to recrystallisation. Sample L4 (C) photograph of recrystallised veins quartz containing solid inclusions and few FIs. Some Type 4 and 6 FI are present along the grain boundary. Recrystallised grains often have elongated biotite solid inclusions. Grain boundaries often form triple point junctions and contain FIs. (D) Sample L4 with recrystallised quartz containing subgrain boundaries. Sulphides (pyrite) are often observed at grain boundaries but not within the grain.

There is a distinct influx of carbon material in samples L7, L19, L20 and L21 near the vein contacts that created a foliated zone (Table 7.5) (Figure 7.41A). Mineralised samples' vein boundaries contain numerous Type 3, 5 and 6 primary FIAs in close proximity to sulphides (Figures 7.42). Type 3 primary FI are also rich in N_2 and CH_4 (Figure 7.43). Macroscopic grey coloured domains are a result of small carbonic inclusions. There is a correlation between the extent of recrystallisation and the degree of gradation at the vein-host rock contact (Figure 7.41B). Metasomatism is indicated where increased amounts of sulphides, biotite and chlorite are common along gradational contacts (Figure 7.41). When present, calcite is disseminated along boundaries of recrystallised quartz grains that are distinctly secondary and post-date the deformation that affected the primary hydrothermal quartz (Figure 7.44). Carbonates also crosscut quartz secondary FI trails, similar to textures seen in Lugushwa Group 2.

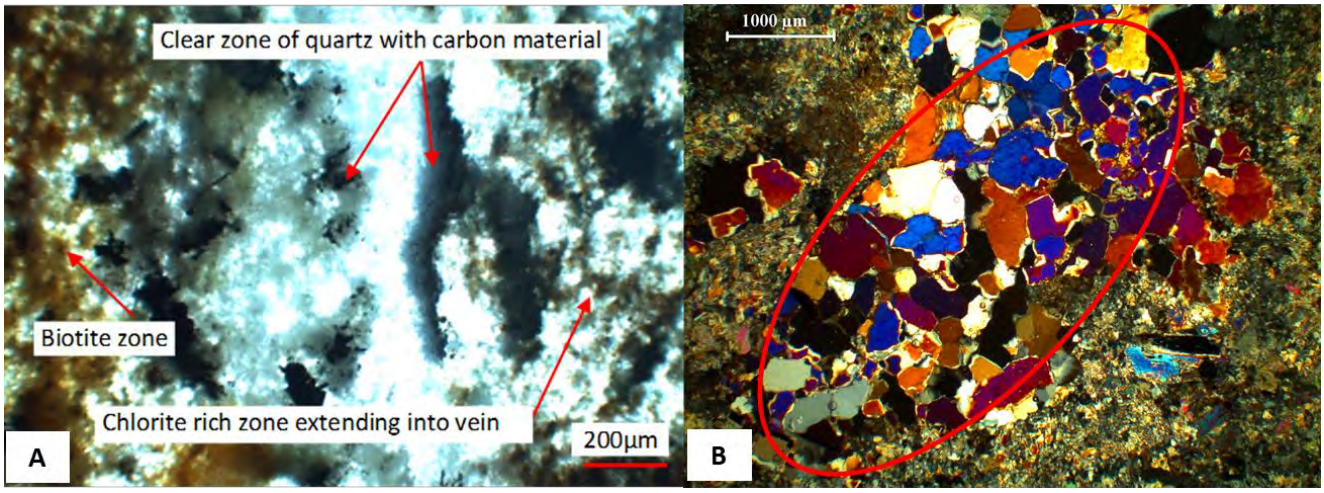

Figure 7.41: Sample L7 (A) indicates clear zonation near the vein boundary, with chlorite and sulphide enrichment; fine-grained recrystallised quartz; sulphides and carbonic ribbons and finally, biotite-rich zone leading into host rock (metasiltstone). The preferred fabric orientation indicates shearing along the vein contact - also evident in hand specimen in sample L7. Sample L7 (B) indicates extensive quartz recrystallisation where the gradational contact is greatest.

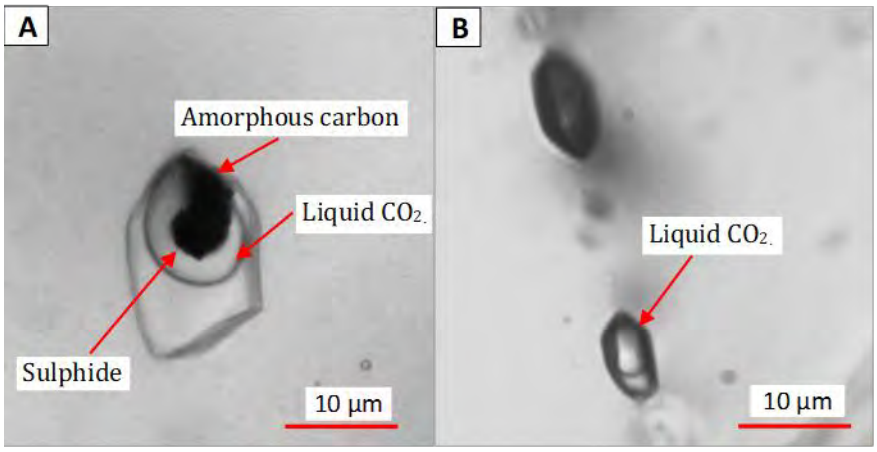

Figure 7.42: Sample L7 (A) indicates a Type 5 primary FI with both uniform sulphides and amorphous carbon within a liquid CO_2 bubble. (B) Type 3 primary FI with liquid CO_2 bubble associated with Type 5 FI in (A).

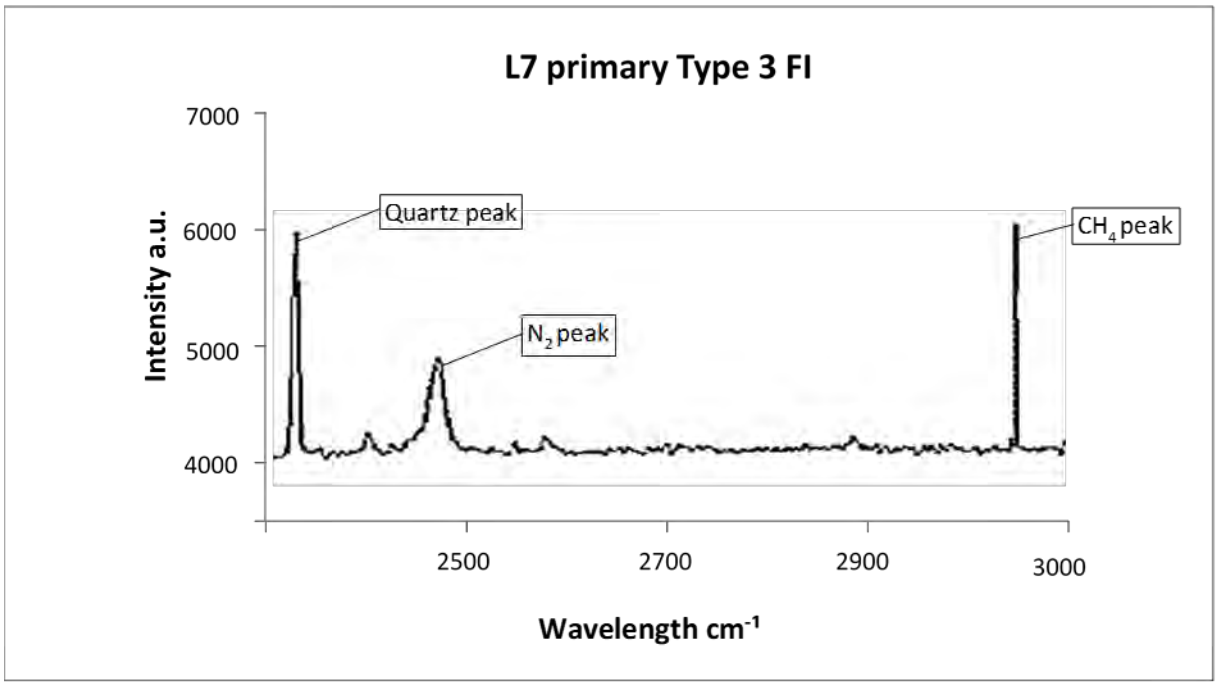

Figure 7.43: Raman spectra of Type 3 primary FI liquid phase in Figure 7.42B of sample L7. The spectra indicate trace amounts of both N_2 and CH_4 within the liquid CO_2 phase.

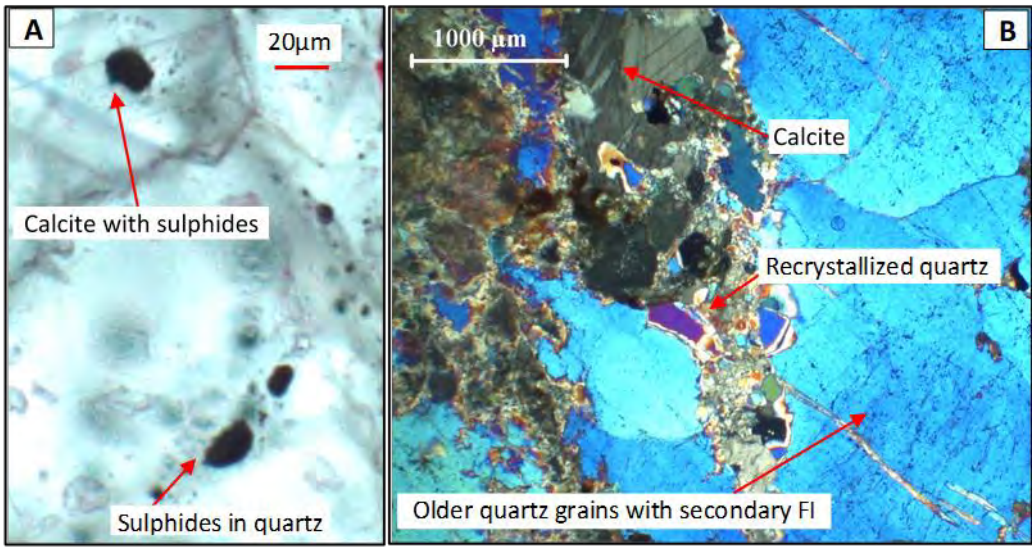

Figure 7.44: Sample L2. (A) Primary vein quartz and calcite with sulphide inclusions along grain boundaries. (B) Cross polarized image indicating recrystallised quartz grains along primary vein quartz boundaries without visible secondary FIs.

7.3.2.1 PRIMARY FIs

Type 4 and 6 (4 - 8 µm) are the dominant primary FIs in all samples. FIs in mineralised samples tend to be smaller than those in unmineralised samples. Type 4 primary FIs contain large vapour bubbles (30 - 50 % volume FI) in mineralised samples. Type 1 primary FIs constitute <10 % of FI across all Group 3 samples (mineralised and unmineralised). Overall, Lugushwa Group 3 samples have lower salinity levels in the primary hydrothermal quartz than primary quartz in Lugushwa Groups 2 samples.

Type 1 and 2 primary FIs (<4 µm) occur only at the centre of primary quartz veins in stockwork samples (Table 7.5). Most Type 1 and 2 primary FIAs also contain vapour CO_2 Type 3 FIs. In comparison to Kamituga Group 3 there is a distinct increase in Type 3 and 5 primary FIAs. The lack of multi-component daughter minerals in FIs (absence of Type 2 primary FIs), and lower salinity levels (reduction and absence of Type 1 and 2 primary FIs), indicates a less likely contribution of a granitoid-associated system (Wilkinson, 2001). These veins, similar to Kamituga Group 3, are interpreted to have formed from a metamorphic hydrothermal system.

Overall, Type 1 and 2 primary FIs total homogenisation occurs between 271 - 378 °C (avg. 314 °C) by vapour bubble dissolution (Figures 7.45). The salinities for Type 1 primary FIs range from 33.8 - 40.6 wt. % NaCl eq. (avg. 35.6 wt. % NaCl eq. (Figure 7.46) as per Sterner et al's. (1988) calculations. The total homogenisation pressures are 4.0 - 15.0 MPa (avg. 7.4 MPa) and the densities range between 1.04 - 1.08 g/cm^3 (avg. 1.05 g/cm^3) as calculated using Steel-MacInnis et al's. (2012) equations (Table 7.7). Type 2 primary FIs average composition is 28 wt. % NaCl eq., 21 % KCl and 51 % H_2O and Th pressures are 5 - 12 MPa according to Samson et al. (2003) ternary diagram. No Type 2 primary FIs contain Fe-chloride daughter minerals. Kamituga Group 3 Type 2 primary FIs contain less halite and sylvite than those in Lugushwa Group 3 samples. Overall Te of -24 °C to -25 °C indicates lower concentrations of Fe-chlorides in solution for all Type 2 primary FIs with only sylvite daughter solids (Roedder, 1984).

Type 3 and 4 FIs associated with Type 1 and 2 primary FIAs have similar Th between 256 - 333 °C (avg. 282 °C). Type 3 and 4 primary FIs, however, have far low salinities, with Type 4 FIs containing 3.4 - 10.5 wt. % NaCl eq. (avg. 7.8 wt. % NaCl eq.) and Type 3 FIs - 4.0, 9.0 wt. % NaCl eq. (avg. 5.8 wt % NaCl) as per Chen (1972 and Bodnar's (1993) equations (Table 7.7). Type 4 FI densities and pressures at total homogenisation are 0.78 - 0.82 g/cm^3 (avg. 0.82 g/cm^3) and 4.3 - 12.5 MPa (avg. 6.3 MPa) (Table 7.7) versus Type 3 FI clathrate melting temperatures and Fermi diad spacing of 103.0 to 104.0 cm^{-1} indicating densities of 0.134 - 0.573 g/cm^3 and pressures of 4.9 - 5.7 MP at clathrate melting as per Fall et al. (2011) and Steel-MacInnis et al's. (2012) calculations.

FIAs contain only Type 3, 4 and 5 primary FIs in secondary stage hydrothermal quartz and have distinctly lower total homogenisation temperatures in comparison to Type 1 hosted primary FIAs (Figure 7.47). This is different from Lugushwa Group 2 in that no Type 5 primary FIs were observed in secondary stage quartz. The Th for Type 3 and 4 primary FIs occurs between 232 - 289 °C (avg. 267 °C) and salinities are 2.0 - 5.8 wt. % NaCl eq. (avg. 4.0 wt. % NaCl eq.), and 5.0 - 7.9 wt. % NaCl eq. (avg. 6.5 wt. % NaCl eq.) respectively as per Chen (1972) and Bodnar's

(1993) calculations (Table 7.7 and Figure 7.46 and 7.47). Type 4 primary FIs show total homogenisation pressures of 2.8 - 7.0 MPa (avg. 5.0 MPa) and densities of 0.81 - 0.86 g/cm^3 (avg. 0.83 g/cm^3) as calculated using Steel-MacInnis et al's. (2012) equations (Table 7.7). Type 3 primary FIs clathrate melting temperatures and Fermi diad spacing of 104.0 to 105.0 cm^{-1} indicate pressures of 5.7 - 24.8 MPa and densities of 0.57 - 0.96 g/cm^3 at clathrate melting as calculated using Fall et al's. (2011) equations. No Type 5 primary FIs homogenise before decrepitating as in all other Groups and deposits. This indicates that solids in Type 5 are xenocrystic particle.

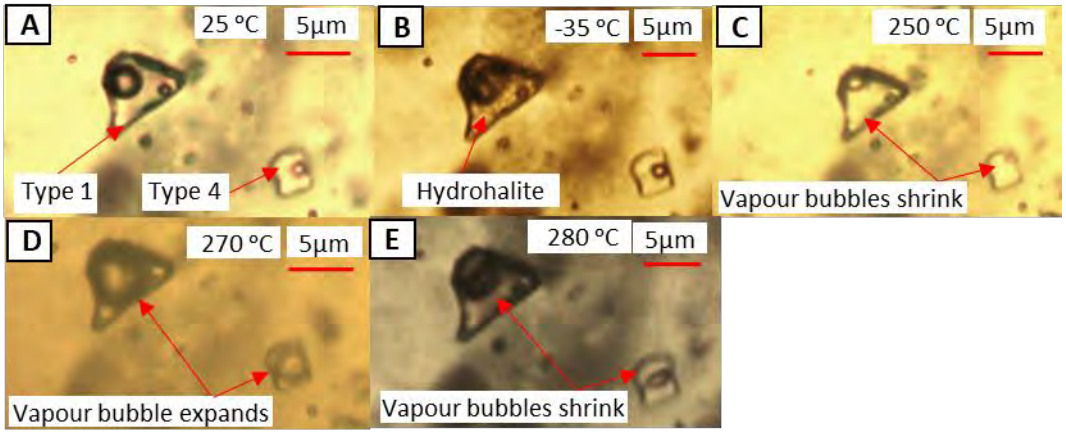

Figure 7.45: Sample L2 heating experiment of Type 1 and 4 FIA in primary vein quartz. (A) Ambient temperatures with halite in Type 1 FI. (B) Hydrohalite formation at -35 °C indicates a high salinity in these FIs. (C – E) Vapour bubble contraction, expansion and final contraction at the same time for both Type 1 and 4 FI indicates simultaneous capturing. The halite dissolves first before the vapour bubble shrinks completely at Th of 320 °C.

7.3.2.2 SECONDARY FIs

All Lugushwa's tourmaline-free Group 3 samples have some form of gradational contact between the host rock and the quartz veins. There are several crosscutting irregularly shaped Type 4 and 6 secondary FI trails (1-2 µm) in these gradational zones. In sample L7a late fluid influx from the host rock is indicated by fractures extending from the host rock into the vein. Fracture trails split up into several branches within primary vein quartz crystal. These fractures contain liquid CO_2-rich Type 3 secondary FIs. These Type 3 secondary FIs are similar to the Type 3 primary FIs in mineralised samples. Recrystallised grains show an increase in number and size of Type 3 secondary FIs that typically become progressively smaller toward the centre of the vein. Overall, secondary FIs in mineralised samples in Group 3 have similar Th and salinity to primary FIs in recrystallised and mineralised samples. This suggests a continuum in fluid characteristics from primary vein formation to vein deformation and recrystallisation.

Few Type 3 secondary FIs are present in unmineralised samples. Unmineralised samples consistently have Th below 300 °C and average salinities of <5 wt. % NaCl as calculated using Chen's (1972) equations. The Th of primary FIs contained in primary quartz or recrystallised quartz is uniform within ±20 °C. Type 4 and 6 secondary FIs (2 - 5 µm) are present near the margins of unmineralised primary and recrystallised quartz. Type 4 secondary FIs have Th of 162 - 340 °C (avg. 212 °C) and low salinities of 0.0 - 9.2 wt. % NaCl eq. (avg. 5 wt. % NaCl eq.) as calculated using Bodnar's (1993) equations. Total homogenisation pressures are 0.7 - 13.8 MPa (avg. 1.9 MPa)

with densities of 0.75 - 0.91 g/cm^3 (avg. 0.89 g/cm^3) calculated using Steel-MacInnis et al's. (2012) equations (Table 7.7).

There is an increased number of Type 3 secondary FIs in mineralised quartz found in close proximity to sulphides as well as in quartz containing amorphous carbon. In mineralised samples Type 3 secondary FIs homogenise between 301 - 348 °C (avg. 334 °C) with average salinities of >5 wt. % NaCl eq. as calculated using Chen's (1972) equations. Type 3 secondary FIs clathrate melting temperatures and Fermi diad spacing of 103.0 to 105.0 cm^{-1} indicate pressures of 4.9 - 24.8 MPa and densities of 0.13 - 0.96 g/cm^3 at clathrate melting as calculated using Fall et al's. (2011) equations (Table 7.7). FIs in mineralised samples show homogenisation pressures and densities in the upper part of the intervals (Table 7.7). Both mineralised and unmineralised samples from Lugushwa display sulphides in veins and stockworks that are located in close proximity to the host rock. In comparison to non-mineralised samples, mineralised samples have the greater abundance of sulphides and chlorite solid inclusions within quartz grains.

Primary quartz and sulphides in Lugushwa Group 3 veins are hydrothermally precipitated. Later plastic deformation recrystallised quartz and possibly mobilised sulphides correlates with infiltration of fluids rich in CO_2 and organic material (C and CH_4). Higher gold grades are seen in veins that show intense quartz recrystallisation, evidence of secondary fluid influx and sulphide precipitation. These features are similar to Kamituga Group 3. More organic materials from Lugushwa's Group 2 and 3 samples were deposited during deformation than in the corresponding veins at Kamituga. A unique and distinct feature of mineralised Group 3 samples in Lugushwa is the strong correlation of sulphides with chlorite. Based on current data and observations it is unclear if this has Au-genetic implications.

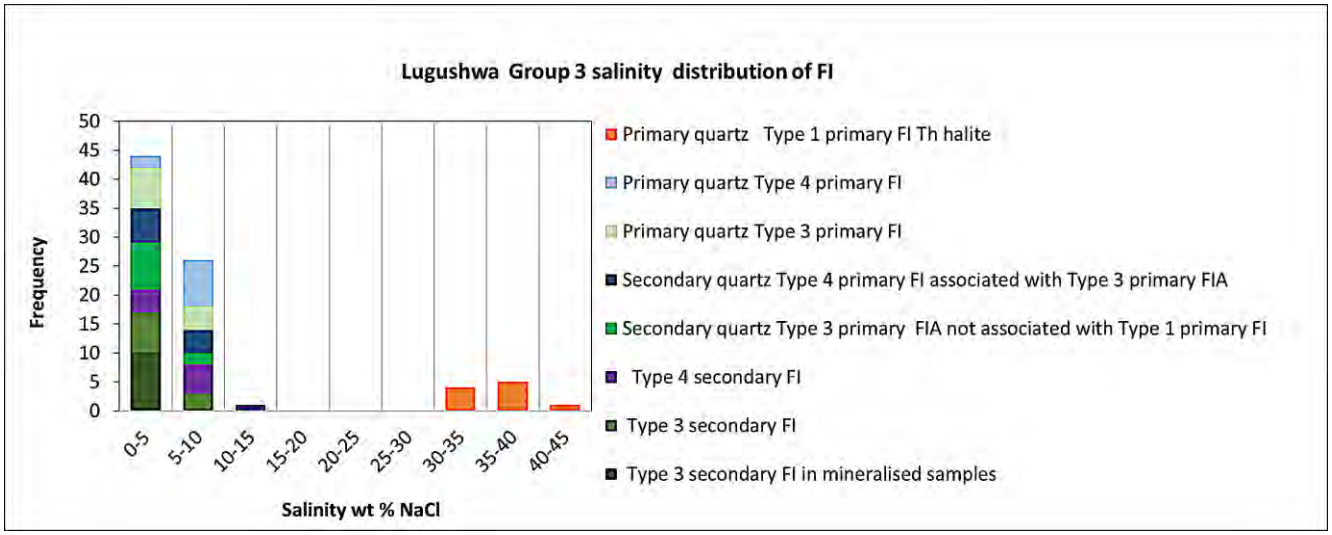

Figure 7.46: Histogram of salinity for Type 1, 3 and 4 primary and secondary FIs within Lugushwa Group 3.

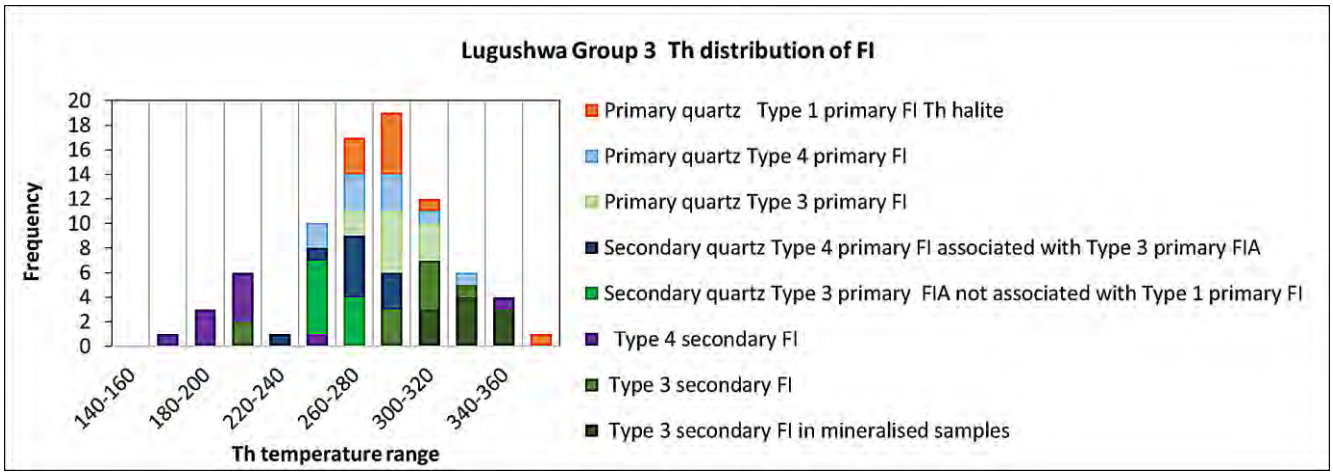

Figure 7.47: Histogram of Th for Type 1, 3 and 4 primary and secondary FIs within Lugushwa Group 3.

Table 7.7 Microthermometric and barometric data for Type 1, 3 and 4 primary and secondary FIs for Lugushwa Group 3.

Phase relationship	FI Type	Tm	Final phase melting	$Th_{(L-V)}$	wt. % NaCl eq.	T @ homog. (°C)	P @ homog. (bar)	r_{BULK} (g/cm$_3$)	Reference
Primary (Hydrothermal) quartz associated primary FIs	Upper Th final by Th (L - V) for Type1	333	Halite	378	40.6	378.0	150	1.04	Sterner et al. (1988) and Steel-MacInnis et al. (2012)
Primary (Hydrothermal) quartz associated primary FIs	Lower Th final by Th (L - V) for Type 1 FI	235	Halite	271	33.8	271.0	40	1.08	Sterner et al. (1988) and Steel-MacInnis et al. (2012)
Primary (Hydrothermal) quartz associated primary FIs	Avg. Th final by Th (L - V) for Type 1 FI	265	Halite	314	35.6	314.0	74	1.05	Sterner et al. (1988) and Steel-MacInnis et al. (2012)
Primary (Hydrothermal) quartz associated primary FIs	Upper Th final by Th (L - V) for Type 4 FI	-7	Ice	333	10.5	333.0	125	0.78	Bodnar (1993) and Steel-MacInnis et al. (2012)
Primary (Hydrothermal) quartz associated primary FIs	Lower Th final by Th (L - V) for Type 4 FI	-2	Ice	256	3.4	256.0	43	0.82	Bodnar (1993) and Steel-MacInnis et al. (2012)
Primary (Hydrothermal) quartz associated primary FIs	Avg. Th final by Th (L - V) for Type 4 FI	-5	Ice	282	7.9	282.0	63	0.82	Bodnar (1993) and Steel-MacInnis et al. (2012)
Primary (Hydrothermal) quartz associated primary FIs	Upper Th Type 3 FI	5	Clathrate	310	9.0	310.0	57	0.57	Chen (1972) and Fall et al. (2010)
Primary (Hydrothermal) quartz associated primary FIs	Lower Th Type 3 FI	8	Clathrate	260	4.0	260.0	49	0.13	Chen (1972) and Fall et al. (2010)
Primary (Hydrothermal) quartz associated primary FIs	Lower Th Type 3 FI	6	Clathrate	289	7.5	289.0	52	0.29	Chen (1972) and Fall et al. (2010)
Secondary (Hydrothermal) quartz Type 4 and 5 primary FIs associated with Type 3 primary FIAs	Upper Th final by Th (L - V) for Type 4 FI	-5	Ice	289	7.9	289.0	70	0.81	Bodnar (1993) and Steel-MacInnis et al. (2012)
Secondary (Hydrothermal) quartz Type 4 and 5 primary FIs associated with Type 3 primary FIAs	Lower Th final by Th (L - V) for Type 4 FI	-3	Ice	232	5.0	232.0	28	0.86	Bodnar (1993) and Steel-MacInnis et al. (2012)
Secondary (Hydrothermal) quartz, Type 4 and 5 primary FIs associated with Type 3 primary FIAs	Avg. Th final by Th (L - V) for Type 4 FI	-4	Ice	267	6.5	267.0	50	0.83	Bodnar (1993) and Steel-MacInnis et al. (2012)
Secondary (Hydrothermal) quartz, Type 3 associated with Type 4 and 5 primary FIAs	Upper Th Type 3 FI	7	Clathrate	276	5.8	276.0	248	0.96	Chen (1972) and Fall et al. (2011)
Secondary (Hydrothermal) quartz. Type 3 associated with Type 4 and 5 primary FIAs	Lower Th Type 3 FI	9	Clathrate	250	2.0	250.0	57	0.57	Chen (1972) and Fall et al. (2011)
Secondary (Hydrothermal) quartz. Type 3 associated with Type 4 and 5 primary FIAs	Lower Th Type 3 FI	8	Clathrate	261	4.0	261.0	169	0.82	Chen (1972) and Fall et al. (2011)
All Type 4 and 6 secondary FIs throughout the samples	Upper Th final by Th (L - V) for Type 4 FI	-6	Ice	340	9.2	340.0	138	0.75	Bodnar (1993) and Steel-MacInnis et al. (2012)
All Type 4 and 6 secondary FIs throughout the samples	Lower Th final by Th (L - V) for Type 4 FI	0	Ice	162	0	162.0	7	0.91	Bodnar (1993) and Steel-MacInnis et al. (2012)
All Type 4 and 6 secondary FIs throughout the samples	Avg. Th final by Th (L - V) for Type 4 FI	-3	Ice	212	5.0	212.0	19	0.89	Bodnar (1993) and Steel-MacInnis et al. (2012)

Table 7.7 cont.: Microthermometric and barometric data for Type 1, 3 and 4 primary and secondary FIs for Lugushwa Group 3.

Phase relationship	FI Type	Tm	Final phase melting	$Th_{(L-V)}$	wt. % NaCl eq.	T @ homog. (°C)	P @ homog. (bar)	r_{BULK} (g/cm$_3$)	Reference
All none mineralised Type 3 secondary FIs throughout the samples	Upper Th Type 3 FI	6	Clathrate	320	7.5	320	248	0.96	Chen (1972) and Fall et al. (2011)
All none mineralised Type 3 secondary FIs throughout the samples	Lower Th Type 3 FI	10	Clathrate	207	0	207.0	49	0.13	Chen (1972) and Fall et al. (2011)
All none mineralised Type 3 secondary FIs throughout the samples	Lower Th Type 3 FI	8	Clathrate	302	4.0	302.0	57	0.57	Chen (1972) and Fall et al. (2011)
All mineralised Type 3 secondary FIs throughout samples	Upper Th Type 3 FI	8	Clathrate	348	4.0	348.0	248	0.96	Chen (1972) and Fall et al. (2011)
All mineralised Type 3 secondary FIs throughout samples	Lower Th Type 3 FI	10	Clathrate	301	0	301.0	57	0.57	Chen (1972) and Fall et al. (2011)
All mineralised Type 3 secondary FIs throughout samples	Lower Th Type 3 FI	9	Clathrate	322	2.0	322.0	131	0.80	Chen (1972) and Fall et al. (2011)

7.4 NAMOYA - GENETIC GROUPS

7.4.1 NAMOYA GROUP 1: PEGMATITE

No pegmatite was sampled in Namoya.

7.4.2 NAMOYA GROUP 2: TOURMALINE-BEARING HYDROTHERMAL VEINS

Namoya Group 2 tourmaline grains are not as abundant as those in other Groups. Prismatic crystals show fragmentation, are typically yellow to brown, small (<50 µm) and optical zonation is absent. Accessory mineral phases included in primary quartz are most numerous closer to the contact with host rock. Where gradational contacts are present, they typically contain tourmaline, muscovite, biotite and sulphides (pyrite > arsenopyrite) that are xenocrysts that originated from the hosting mica schist and graphitic metapelites. Samples have increased secondary FIs, shearing, mobilisation and re-precipitation of sulphide along boundaries of recrystallised quartz (Table 7.8 and Figure 7.48). Overall, the intensity of deformation in Namoya Group 2 samples is higher than in corresponding samples from Lugushwa and Kamituga. Subsequent brittle fractures overprint ductile structures and are typically associated with precipitation of Fe-oxides. Along brittle fractures no previous materials related to vein formation or ductile deformation are remobilised.

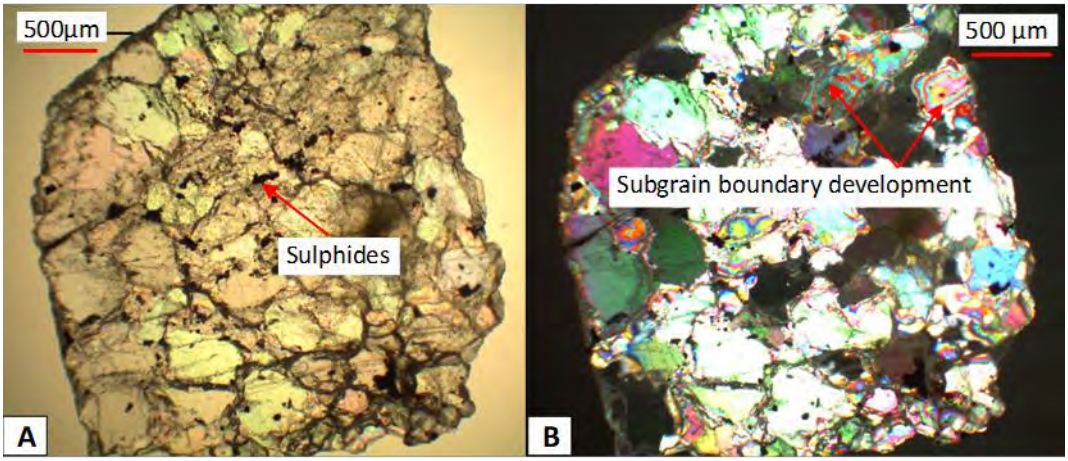

Figure 7.48: Unmineralised sample N9; ~150 µm thick FI wafer. (A) PPL image showing intergranular sulphides. (B) Same image in CPL subgrain boundaries within recrystallised grains. Zones of abundant secondary FIs show microscopically cloudy texture.

Table 7.8: Macro- and microscopic description of Namoya Group 1, 2 and 3 samples and primary, pseudosecondary and secondary FI Types.

Group	Drill core or Sample site	Sample No.	Depth metres and vein thickness (cm) respectively	Deformation features of vein	Au grade g/t	Macroscopically visible sulphides	Macroscopically visible number of quartz species and type	Tourmaline /carbonate present	Host rock and general notes	FI Types present *Listed in decreasing occurrence. Blue represents primary or pseudosecondary FIs and red secondary FIs.
2	Mwendam-Boka pit sample	N23	NA	Minor fragmentation; intense recrystallised quartz;	Not assayed but in mineralised zone	Pyrite	2: Dominant milky (70%) and smoky quartz (30%)	Y/N	Graphitic metapelite	T4, T6, T3, T5, T1 T4, T6, T3, T1
2	Kibishwa quarry unmineralised	N28	NA	None	None	Sulphides concentrated along vein margin	1	Y/N	Interface between dolerite and metapelite	T4, T6, T1, T3, T5 T4, T6, T3, T1
2	NDD 344	N6	69/1.5	Sheared off along semi ductile shear zone	None	Pyrite	1	Y/Y	Sericite schist with intense deformation	T3, T4, T6, T1, T5 T3, T4, T6, T1
2	NDD 180	N9	54/1.5	Pinch-and-swell	None	Medium grained altered pyrite	1	Y/N	Mica schist	T4, T6, T3, T5, T1 T4, T6, T3, T1
3	NDD 344	N3	39.2/ several metres	Slight fragmentation	0.26-15.75	N	1	N/N	Mica schist	T3, T4, T6, T5 T3, T1, T4, T6, T5
3		N5	51.5/>100	Brecciated	1460	Abundant resorption halos	1	N/N	Mica schist	T3, T4, T6, T5 T3, T1, T4, T6, T5
3	NDD 180	N10	58.3/4	Pinch-and-swell	1.99	Medium grained altered pyrite. With alteration halos	1	N/N	Mica schist	T4, T3, T6, T5 T4, T6, T3
3		N11	65.6/50	Brecciated	0.29	Medium grained altered pyrite	1	N/N	Mica schist	T3, T4, T1, T6 T3, T4, T6
3		N15	138/1	Parasitic open to tight folds	2.72	N	1	N/N	Muscovite schist	T4, T3, T6 T4, T6, T3
3		N16	140.8/1	None	1.6	Coarse grained pyrite	1	N/N	Stockwork in very fine grained graphitic metapelite	T4, T3, T6 T4, T6, T3
3	Mwendam-Boka pit sample	N20	NA	Slight fragmentation	Not assayed. How in mineralised zone	Resorption cavities	2: Dominant opaque (70%) and transparent to milky quartz (30 %)	N/N	Graphitic metapelite	T4, T6, T3 T4, T6, T3
3	NDD078	N30	111.6/0.5 – 1	Slight fragmentation	None	N	2: Dominate milky (70%) and smoky quartz (30 %)	N/N	Layered metapelite	T4, T6, T3 T4, T6, T3

7.4.1.1 PRIMARY FIs

The salinity levels in Namoya Group 2 are lower than in Kamituga and Lugushwa Group 2 material. Type 3, 4 and 6 FIs are the dominant primary and secondary FI Types in all Namoya Group 2 samples. The only highly saline FIs in Namoya Group 2 are Type 1 FIs. They are, however, not abundant, nor present in FIAs (Figure 7.49). Type 1 primary FIs are associated with primary hydrothermal quartz. Type 2 FIs are absent.

Type 3 FIs are predominantly liquid CO_2 (Figure 7.50). This is indicative of hydrothermal fluids that have formed from metamorphic devolatilisation reactions. The different sizes of the carbonic liquid phase is an indication of heterogeneous trapping under conditions of fluid-fluid immiscibility (Roedder, 1984; Samson et al., 2003). Type 3 FIs are strongly associated with lower salinity Type 4 and 6 primary FIs (Figure 7.51). This is different from Group 2 Lugushwa and Kamituga samples in which vapour CO_2 Type 3 primary FIs dominate. Namoya Group 2 Type 3 primary FIs are more numerous than in Kamituga and Lugushwa Group 2 samples.

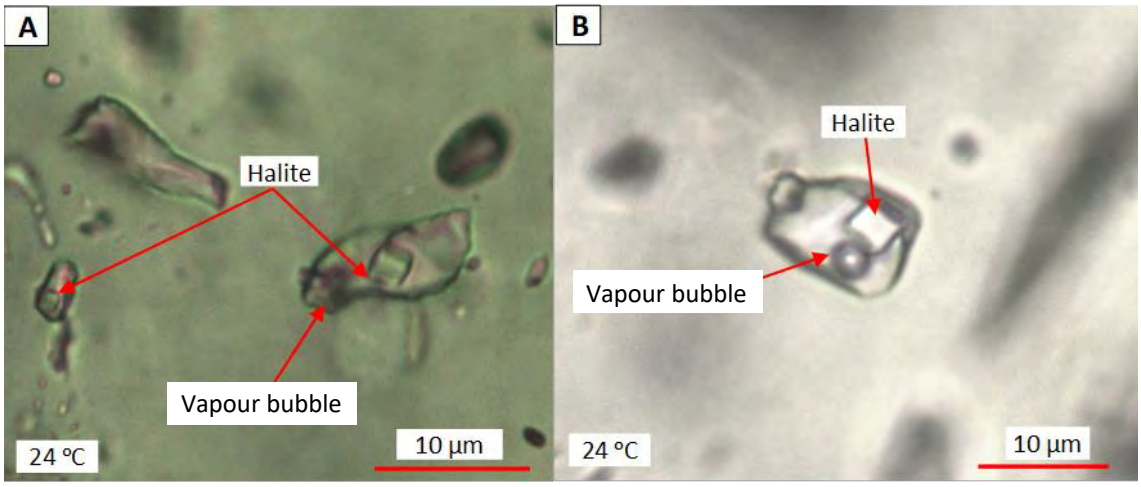

Figure 7.49: Sample N9 Type 1 primary FI distinctly associated with primary and recrystallised hydrothermal quartz.

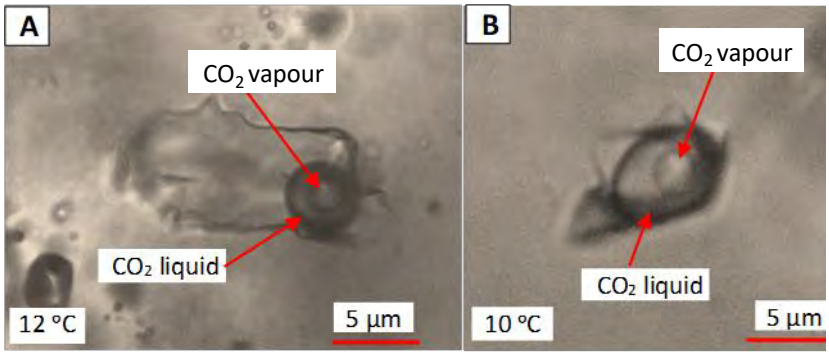

Figure 7.50: Sample N9 (A) Distinct CO_2 bubble develops on cooling but disappears below 12 °C, indicating high density Type 3 FI. (B) Type 3 FI with large volume proportion of liquid bubble CO_2 phases. Those Type 3 FIs with >80 vol % liquid CO_2 show CO_2 homogenisation into liquid CO_2 below 10 °C.

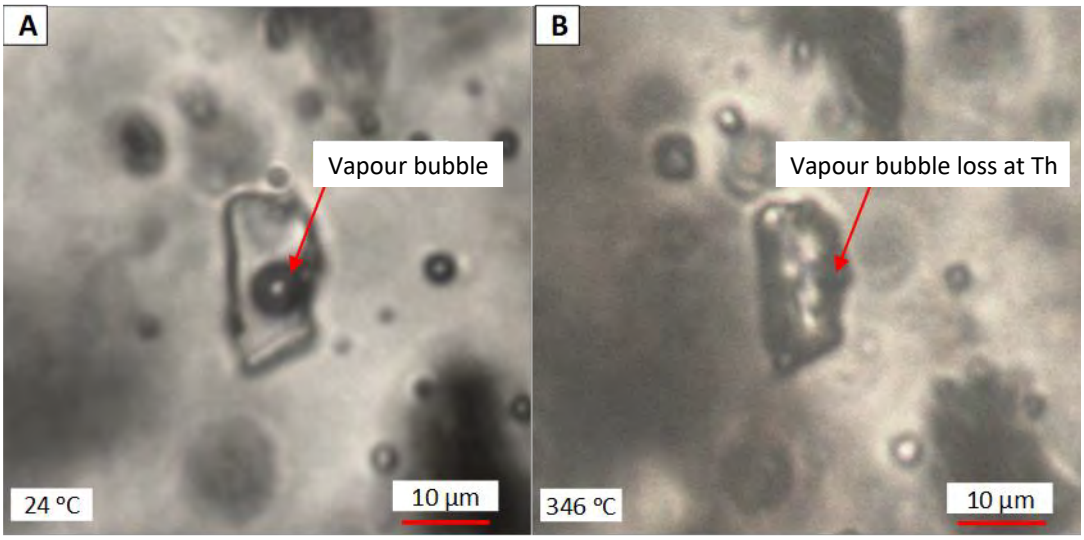

Figure 7.51: Photographs from sample N9. (A) Low salinity Type 4 primary FI at ambient temperatures. (B) High temperature of homogenisation of Type 4 FIs (L - V).

Most quartz grains in Namoya Group 2 samples are small (<200 µm). They show extensive recrystallisation and subgrain boundary development, appear clear in plane polarised light (PPL), and contain few primary FIs. Most recrystallised grains have numerous healed fractures at or near vein margins. Shearing possibly corresponded to fluid influx during quartz recrystallisation. Recrystallised grains have captured secondary fluids that are preserved along healed intergranular fractures. Subsequent brittle fracturing associated with the precipitation of Fe-oxidic material, probably related to the influx of meteoric water, may be later-stage features related to the final exhumation of the TNGB rocks (Figure 7.52 and Table 7.8).

Samples N6 and N28 show intergranular sulphides along the margins of fragmented tourmaline (~200 µm). In other samples, sulphides (<150 µm) are more uniformly distributed but tend to be most numerous along healed fractures in quartz and along vein margins (Figure 7.52A). This suggests that sulphide formation post-dated the precipitation of primary quartz and tourmaline and infiltrated during the deformation of the primary vein.

Namoya Group 2 veins have less organic material than found in Lugushwa Group 2 samples, and despite the extensive recrystallisation, primary vein quartz is preserved in porphyroclasts. Porphyroclasts do not contain sulphide inclusions. Sulphides in Group 2 samples are restricted to the boundaries of recrystallised quartz of which sample N23 is a prime example. N23, extracted from a mineralised zone in the Mwendam Boka pit, not assayed, is the most intensely deformed vein with the highest sulphide contents amongst all Group 2 Namoya samples (Table 7.8). Recrystallised grains in N23 have numerous healed fractures. The recrystallised isometric and smaller grains show a lighter macroscopic colour and have few Type 3 and 4 primary FIs, and no Type 1 primary FIs. This is in stark contrast to the earlier non-recrystallised quartz phase that contains large primary quartz crystals. Primary hydrothermal quartz contains Type 1 primary FIs within the centre of quartz grains - particularly near tourmaline.

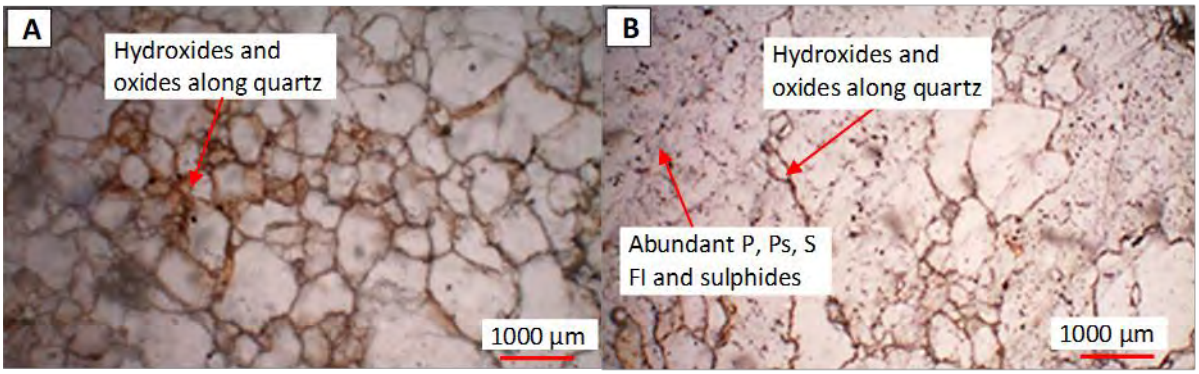

Figure 7.52: Photograph of core sample N9. (A) Recrystallised quartz that was later fractured with sulphides and abundant hydroxides and oxides along fractures. (B) Crystallised quartz with more primary and secondary FIs and sulphides within quartz grains, yet still abundant hydroxides and oxides along fractures.

Group 2 shows an abundance of primary and pseudosecondary FIs within the few remaining unrecrystallised large primary gains (>200 µm) that are greyish or reddish due to oxidation events. The FIs are randomly distributed and more numerous within the centre of the grain. Type 1 pseudosecondary FIs can be mistaken for secondary FIs due to this concentration. There are Type 1 primary and pseudosecondary FIs (4 - 8 µm) closer to larger tourmaline. There are few Type 3, 4 and 6 primary FIs in Type 1 FIAs - a feature typical in Group 2 samples of Kamituga and Lugushwa.

Type 3, 4 and 6 are the dominant FIs throughout Group 2 tourmaline-free vein samples. N23 is the only sample that shows elevated concentrations of N_2 and CH_4 in Type 3 FIs. This spectrum shows that N_2 concentrations must be greater than the CH_4 concentrations in the fluid phase. N_2 is much less sensitive for the Raman effect than CH_4 (Burke, 2001), so the high intensity, compared to CH_4, indicates significant amounts of N_2 (Figure 7.53). Type 3 FIs containing CH_4 are present with Type 5 FIs (containing carbon and or sulphide as solids). Type 5 FIs are not found together with Type 4 and 6 FIs. Namoya Type 3 and 5 FIAs contain few, and relatively small FIs, compared to corresponding samples in Kamituga and Lugushwa Group 2. Type 5 FIs comprise a small CO_2 component that is optically impossible to identify as either CO_2 liquid or vapour given current equipment.

Type 1 primary FIs in primary hydrothermal quartz homogenise between 284 - 365 °C (avg. 303 °C) into the vapour bubble (L - V) or by simultaneous bubble and halite loss (Table 7.9). Salinities range between 36.9 to 39.6 wt. % NaCl eq. (avg. 38.0 wt. % NaCl eq.), total homogenisation pressures are 4.6 - 13.2 MPa (avg. 6.0 MPa) and densities are between 1.04 - 1.09 g/cm^3 (avg. 1.09 g/cm^3) as calculated using Steel-MacInnis et al's. (2012) equations (Table 7.9 and Figures 7.55 and 7.56). Associated Type 3 and 4 primary FIAs have similar Th - 262 - 342 °C (avg. 295 °C) and salinities of 4 - 11.9 wt. % NaCl eq. (avg. 7.5 wt. % NaCl eq.) for Type 3 FI and 5.0 - 12.9 wt. % NaCl eq. (avg. 7.9 wt. % NaCl eq.) for Type 4 FI respectively as per Chen (1972) and Bodnar's (1993) calculations (Table 7.9). Type 3 and 4 FIs have variable densities and pressures with Type 4 showing total homogenisation pressures of 4.7 - 13.7 MPa (avg. 7.6 MPa) and densities of 0.79 - 0.82 g/cm^3 (avg. 0.80 g/cm^3) calculated using Steel-MacInnis et al's. (2012) equations (Table 7.9). Type 3 FIs clathrate melting temperatures and Fermi diad spacing of 104 to 105.5 cm^{-1} indicate pressures of 5.7 - 64.0 MPa (avg. 24.8 MPa) and densities of 0.57 - 1.08 g/cm^3 (avg. 0.96 g/cm^3) at clathrate melting calculated using Fall et al's. (2011) calculations (Table 7.9).

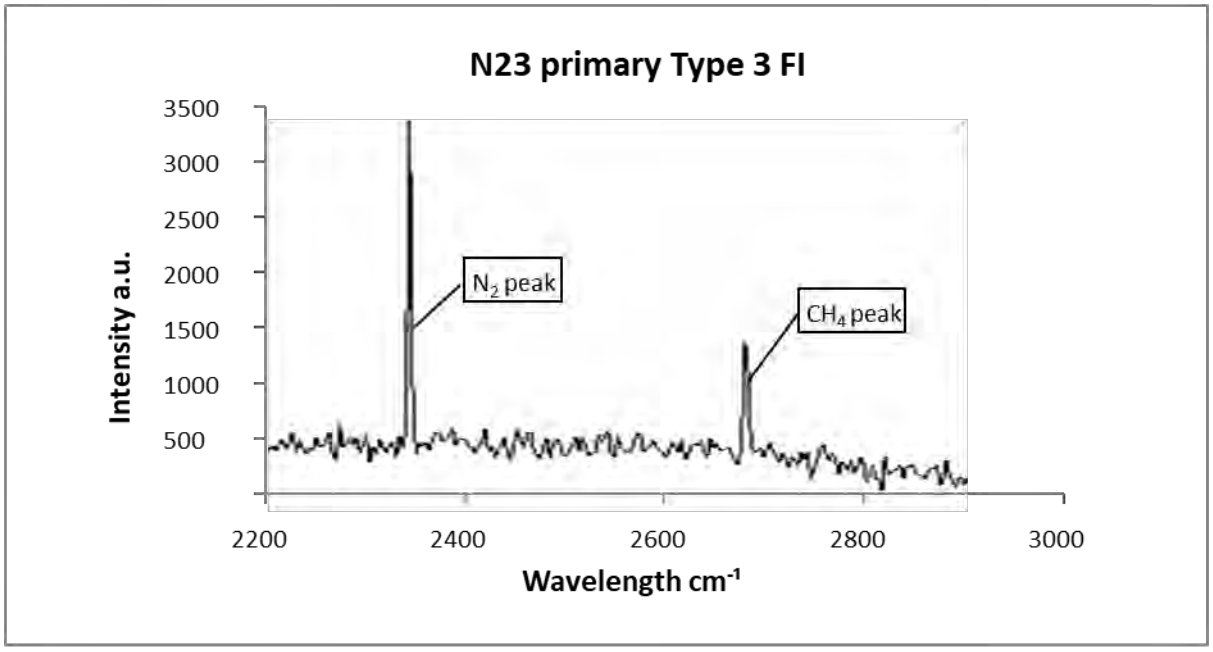

Figure 7.53: Sample N23. (A) Raman spectra for Type 3 primary FI liquid phase. This is a portion of the spectra indicating the presence of significant amounts of N_2 and CH_4.

7.4.1.2 SECONDARY FIs

Unique to Namoya Group 2 is the occurrence of Type 1 secondary FIs together with CO_2 vapour-rich Type 3 secondary FIs (<2 µm) (Figure 7.54). Type 1 secondary FIs are distinguishable from Type 1 primary FIs by their abundant presence along healed fractures. Despite recrystallised grains not hosting Type 1 primary FIs, they do host Type 1 secondary FI (3 - 6 µm) that have FI trails that extend across multiple grain boundaries to vein-host rock contacts. This is most evident in mineralised sample N23 (not assayed but from a mineralised zone). The recrystallised grains contain distinctly larger later stage liquid CO_2-rich Type 3 secondary FIs (3 - 5 µm) that crosscut trails of CO_2 vapour rich Type 3 inclusions in the Type 1 secondary FIAs.

Table 7.9: Microthermometric and barometric data of Type 1, 3 and 4 primary and secondary FIs for Namoya Group 2.

Phase relationship	FI Type	Tm	Final phase melting	Th $_{(L-V)}$	wt. % NaCl eq.	T @ homog. (°C)	P @ homog. (bar)	r_{BULK} (g/cm_3)	Reference
Primary quartz associated Type 1 primary FIs	Upper Th final by Th (L - V) for Type 1 FI	319	Halite	365	39.6	365.0	132	1.04	Sterner et al. (1988), and Steel-MacInnis et al. (2012)
Primary quartz associated Type 1 primary FIs	Lower Th final by Th (L - V) for Type 1 FI	284	Halite	284	36.9	284.0	46	1.09	Sterner et al. (1988) and Steel-MacInnis et al. (2012)
Primary quartz associated Type 1 primary FIs	Avg. Th final by Th (L - V) for Type 1 FI	298	Halite	303	38.0	303.0	60	1.09	Sterner et al. (1988) and Steel-MacInnis et al. (2012)
Primary quartz associated Type 4 primary FIs	Upper Th final by Th (L - V) for Type 4 FI	-9	Ice	342	12.9	342.0	137	0.79	Bodnar (1993) and Steel-MacInnis et al. (2012)
Primary quartz associated Type 4 primary FIs	Lower Th final by Th (L - V) for Type 4 FI	-3	Ice	262	5.0	262.0	47	0.82	Bodnar (1993) and Steel-MacInnis et al. (2012)
Primary quartz associated Type 4 primary FIs	Avg. Th final by Th (L - V) for Type 4 FI	-5	Ice	295	7.9	295.0	76	0.80	Bodnar (1993) and Steel-MacInnis et al. (2012)
Primary quartz associated Type 3 primary FIs	Upper Th Type 3 Fi	3	Clathrate	340	11.9	340.0	640	1.08	Chen (1972) and Fall e al. (2011)
Primary quartz associated Type 3 primary FIs	Lower Th Type 3 FI	8	Clathrate	265	4.0	262.0	57	0.57	Chen (1972) and Fall et al. (2011)
Primary quartz associated Type 3 primary FIs	Avg. Th Type 3 FI	6	Clathrate	289	7.5	289.0	248	0.96	Chen (1972) and Fall et al. (2011)
Type 1 secondary FIs throughout samples	Upper Th final by Th (L - V) for Type 1 FI	309	Halite	373	38.8	373.0	146	1.02	Sterner et al. (1988) and Steel-MacInnis et al. (2012)
Type 1 secondary FIs throughout samples	Lower Th final by Th (L - V) for Type 1 FI	256	Halite	278	35.1	278.0	43	1.08	Sterner et al. (1988) and Steel-MacInnis et al. (2012)
Type 1 secondary FIs throughout samples	Avg. Th final by Th (L - V) for Type 1 FI	267	Halite	301	35.8	301.0	61	1.07	Sterner et al. (1988) Steel-MacInnis et al. (2012 and
Type 4 secondary FIs throughout samples	Upper Th Type 4 FI	-8	Ice	341	11.7	341.0	137	0.78	Bodnar (1993) and Steel-MacInnis et al. (2012)
Type 4 secondary FIs throughout samples	Lower Th Type 4 FI	-5	Ice	280	7.9	280.0	61	0.83	Bodnar (1993) and Steel-MacInnis et al. (2012)
Type 4 secondary FIs throughout samples	Avg. Th Type 4 FI	-6	Ice	293	9.2	293.0	73	0.82	Bodnar (1993) and Steel-MacInnis et al. (2012)
None mineralised Type 3 secondary FIs throughout samples	Upper Th Type 3 FI	7	Clathrate	306	5.8	306.0	248	0.96	Chen (1972) and Fall et al. (2011)
None mineralised Type 3 secondary FIs throughout samples	Lower Th Type 3 FI	10	Clathrate	274	0	274.0	49	0.13	Chen (1972) and Fall et al. (2011)
None mineralised Type 3 secondary FIs throughout samples	Avg. Th Type 3 FI	9	Clathrate	294	2.0	294.0	57	0.57	Chen (1972) and Fall et al. (2011)
Mineralised sample Type 3 secondary FIs	Upper Th Type 3 FI	8	Clathrate	333	4.0	333.0	248	0.96	Chen (1972) and Fall et al. (2011)
Mineralised sample Type 3 secondary FIs	Lower Th Type 3 FI	10	Clathrate	310	0	310.0	57	0.57	Chen (1972) and Fall et al. (2011)
Mineralised sample Type 3 secondary FIs	Avg. Th Type 3 FI	9	Clathrate	321	2.0	321.0	156	0.87	Chen (1972) and Fall et al. (2011)

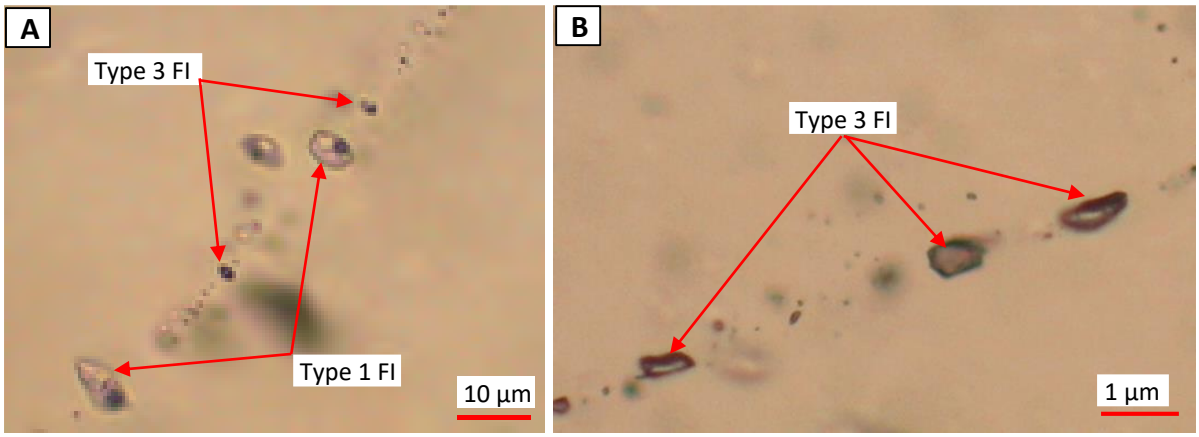

Figure 7.54: Sample N6. (A) Type 1 secondary FIAs with very small CO_2 vapour-rich Type 3 FIs. (B) Liquid CO_2-rich Type 3 secondary FIs.

In all Namoya Group 2 samples, Type 1 secondary FIs homogenise between 278 - 373 °C (avg. 301 °C) for final homogenisation into the vapour bubble (L - V) (Table 7.9). Salinities range between 35.1 to 38.8 wt. % NaCl eq. (avg. 35.8 wt. % NaCl eq.). Total homogenisation pressures are 4.6 - 13.2 MPa (avg. 6.0 MPa) and densities are between 1.04 - 1.09 g/cm^3 (avg. 1.09 g/cm^3). Total homogenisation pressures are 4.5 - 10.9 MPa (avg. 6.3 MPa) and densities of 1.02 - 1.08 g/cm^3 (avg. 1.07 g/cm^3) (Table 7.9) calculated using Steel-MacInnis et al's. (2012) equations. Microthermometric characteristics of the CO_2 vapour-rich Type 3 FIs associated with Type 1 FI could not be determined because of the small size of the FIs. The subsequent liquid CO_2-rich Type 3 secondary FIs are associated with Type 4 and 6 secondary FIs. Type 4 secondary FIs have Th 280 - 341 °C (avg. 293 °C) and show <12 wt. % NaCl eq. at homogenisation pressures of 6.1 - 13.7 MPa (avg. 7.3 MPa) with corresponding densities of 0.78 - 0.83 g/cm^3 (avg. 0.82 g/cm^3) as per and Bodnar (1993) and Steel-MacInnis et al's. (2012) calculations. Type 3 secondary FIs, associated with FIAs in unmineralised samples, homogenise at 274 - 306 °C (avg. 294 °C), and contain lower salinities of 0 - 5.8 wt. % NaCl eq. (avg. 2.0 wt. % NaCl eq.) in both liquid and vapour CO_2-rich FIs as calculated using Chen's (1972) equations (Table 7.9). Clathrate melting temperatures and Fermi diad spacing of 103 to 105 cm^{-1} indicate homogenisation pressures of 4.9 - 24.8 MPa (avg. 5.7 MPa) and densities of 0.13 - 0.96 g/cm^3 (avg. 0.57 g/cm^3) as calculated using Fall et al's. (2011) equations. Th for secondary FIs in the likely mineralised sample of N23 had the highest Th for Group 2 samples in Kamituga, Lugushwa and Namoya with a Th ranges of 310 - 333 °C (avg. 321 °C) with associated pressures of 5.7 - 24.8 MPa and densities of 0.573 - 0.962 g/cm^3 as per Chen (1972) and Fall et al's. (2011) calculations (Figure 7.55 and 7.56).

In summary, Namoya Group 2 quartz veins show the formation of primary quartz-tourmaline assemblages together with sulphides and hydrothermal precipitation. As a result of plastic deformation, Type 3 and 5 FIs, rich in CO_2 and organic material (carbon and CH_4), infiltrated after quartz recrystallisation and sulphide mobilisation. Unlike Groups in Kamituga and Lugushwa, there is evidence of multiple CO_2 fluids - as indicated by several generations of Type 3 secondary FIs. Sample N23 from the mineralised Mwendam Boka pit has the most intensive quartz recrystallisation. Mineralised sample, N23, has Type 3 secondary FIs that have higher Th and

lower salinities than corresponding non-mineralised Type 3 secondary FIs (Figure 7.55 and 7.56). The apparent correlation of gold grade with deformation suggests that gold was probably mobilised and concentrated during deformation and secondary fluid influx episodes as shown in sample N23, where CO_2-rich Type 3 secondary FIs are concentrated - possibly indicating that CO_2-rich secondary fluids are related to gold mineralisation.

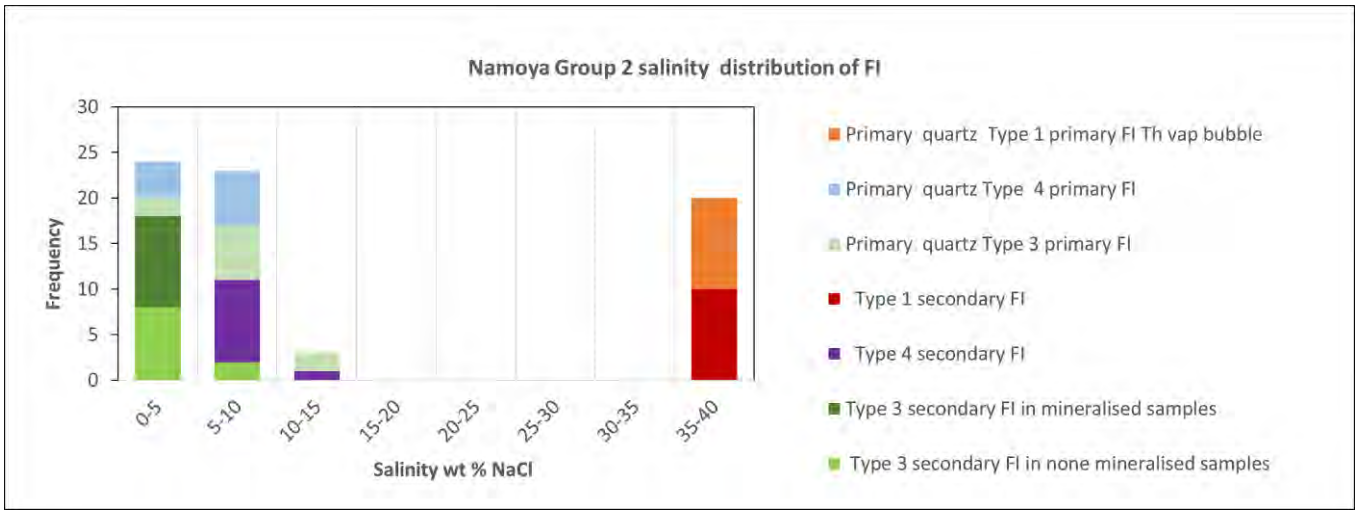

Figure 7.55: Histogram summarising distribution of FI salinity for primary Type 1, 3, and FI within Namoya Group 2 samples. Type 1 FI show somewhat higher salinity than Type 3 and 4.

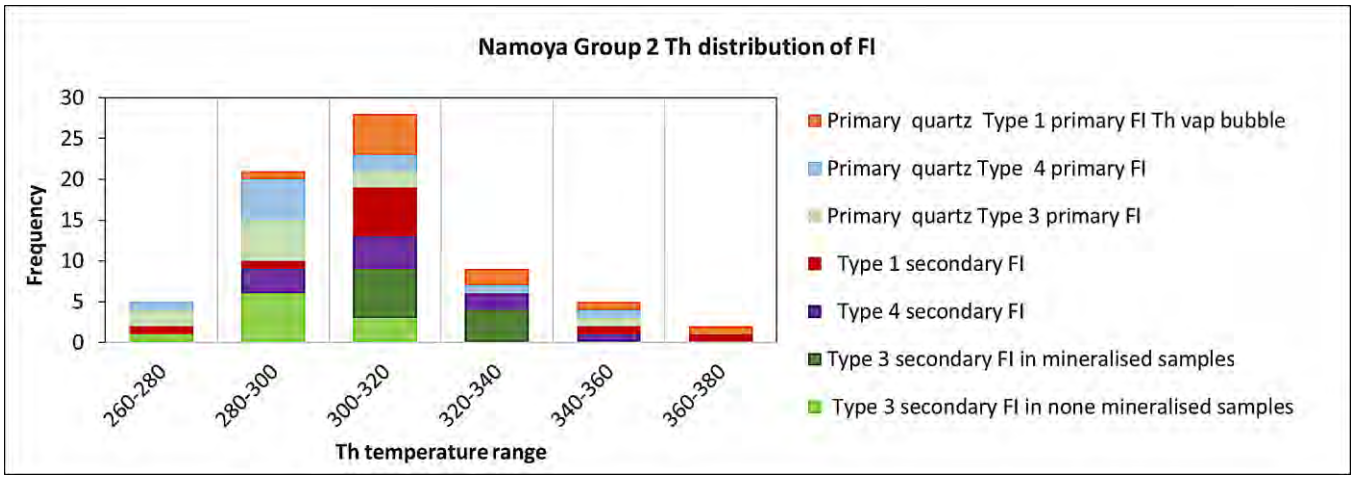

Figure 7.56: Histogram summarising the distribution of primary and secondary FIs' Th for Type 1, 3, and 4 in Namoya Group 2 samples. Type 1 FIs tend to show higher Th of up to 380 °C. Type 3 and 4 FIs commonly homogenise between 280 and 340 °C, overlapping with the "colder" Type 1 FIs.

7.4.3 NAMOYA GROUP 3: TOURMALINE-FREE HYDROTHERMAL VEINS

Namoya Group 3 veins show semi-ductile shear zones, small-scale open to tight folds, pinch-and-swell characteristics and contain entrained crystals or fragments from the host rocks. Fold limbs are displaced along fractures, indicating that brittle shearing followed plastic deformation. All analysed samples, hosted in metapelites or mica schists, are extensively recrystallised. Recrystallised grains show undulose extinction and subgrain formation and fracturing - indicating deformation after recrystallisation (Figure 7.57). Healed fractures contain secondary FIs in recrystallised and primary quartz. Relic primary hydrothermal quartz has variable deformation states - from undeformed to partially recrystallised.

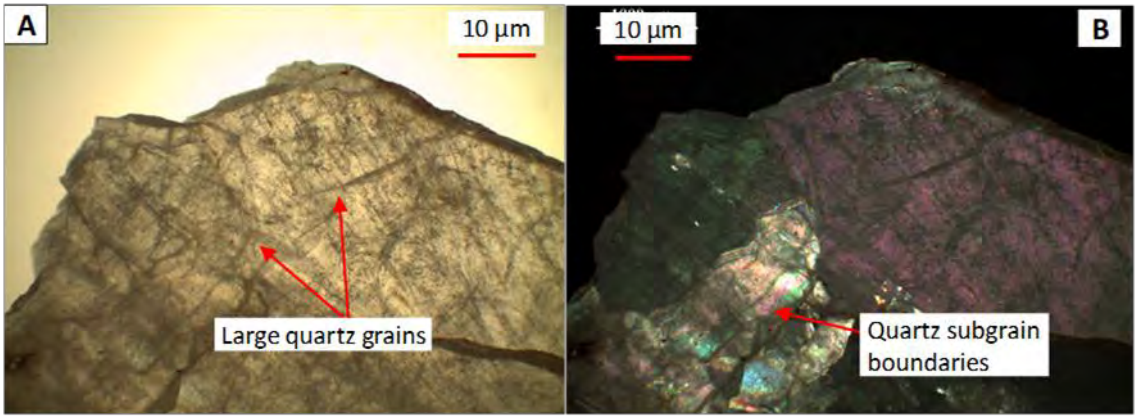

Figure 7.57: (A). Photograph of core sample N3 PPL of extensively recrystallised and fractured quartz and (B) Same image in XPL indicating subgrain boundaries within recrystallised grains.

In comparison to Namoya Group 2, Group 3 fluids have low salinity levels. Few samples contain Type 1 primary FIs. Type 2 primary FIs are absent. FIAs predominately consist of Type 3, 4 and 6 secondary FIs. Type 3, 4 and 6 primary and pseudosecondary FIs are difficult to distinguish due to the abundance of secondary FIs. Type 3 primary FIs are predominantly liquid CO_2-rich, with only a minority showing large CO_2 vapour proportions. A key observation is that mineralised veins contain N_2 and CH_4 liquid CO_2-rich Type 3 primary FIs, with a high correlation between CH_4 levels and mineralisation. This is observed in samples N5, N3 and N15 (Table 7.8).

The crosscutting relationships of secondary FIs trails provide evidence for multistage secondary fluid injections. Namoya Group 3 quartz vein samples show the most intense alteration in the sample collection from the entire TNGB. The samples have highly variable sulphide levels with recrystallised quartz with undulose extinction and subgrain formation (Figure 7.58). Namoya Group 3 quartz vein samples also contain the greatest number of subhedral and amorphous sulphides along grain boundaries and fractures in quartz (Figure 7.58). Highly Au mineralised samples such as N5, N10 and N15, contain sulphides with calcite along fractures (Table 7.8). Secondary oxidation may have occurred during exhumation close to the surface.

In contrast to Lugushwa and Kamituga there is little evidence of organic material (carbon and graphite) entering veins during quartz recrystallisation. The carbon/graphitic material that is emplaced along later fractures extend from vein-host rock contacts proximally into the vein, crosscutting recrystallised quartz grains. Despite the

abundance of sulphides in Namoya Group 3 veins, there is no correlation between sulphide distribution and FIs - as observed in mineralised quartz vein samples from other sites.

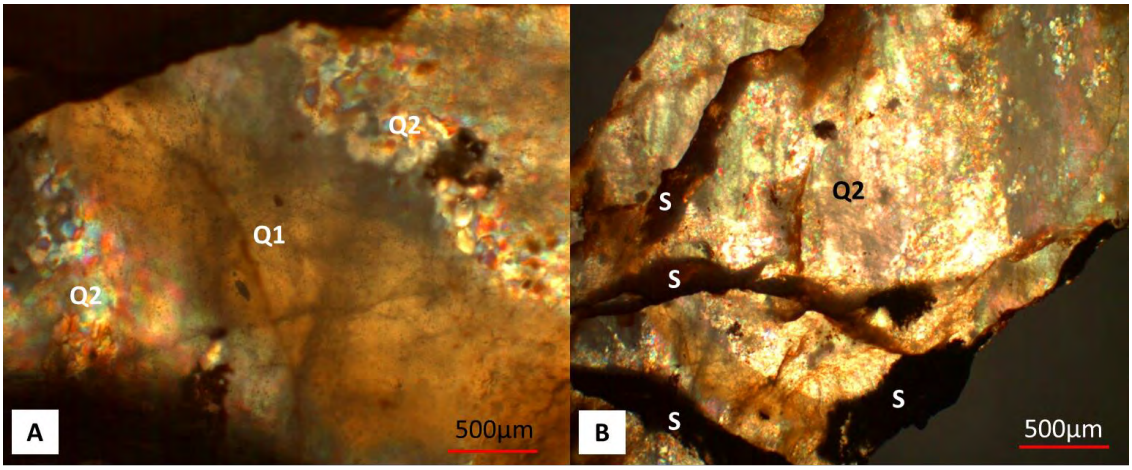

Figure 7.58: (A). Photograph of core sample N5 under PPL contains extensively recrystallised (Q2) and a few larger primary quartz grains (Q1) (B) Sample N5 fractured quartz with late stage sulphides (S).

Recrystallised quartz has few primary and pseudosecondary FIs. Secondary FIs, situated along healed fractures, are highly abundant and obscure primary FIs that may be present. Few Type 3 and 4 primary FIs (3 - 6 µm) were observed in unrecrystallised Group 3 quartz veins.

Secondary inclusion trails cause a milky appearance in quartz. This hampers the detection and assessment of primary FIs. Sulphides, although present in macroscopically visible sizes in sample N20, are not as abundant as the small amorphous grains between and within quartz grains. The milky quartz phase contains Type 4 and 6 secondary FIs (2 - 4 µm) and distinctly negative refractive index liquid CO_2-rich Type 3 secondary FIs. The Type 3 secondary FIs are highly variable in size - ranging between 1 - 11 µm and are equidimensional to elongate. The randomly distributed elongated Type 3 secondary FIs are the largest amongst these Type 3 secondary FIs (>9 µm). All Type 3 secondary FIs contain larger vapour phases than Type 3 primary FIs. Type 3 primary FIs from mineralised veins have elevated proportions of N_2 and CH_4. Many Type 3 secondary FIs are oriented along large crosscutting fractures and are more frequent along subgrain boundaries. Type 5 secondary FIs associated with Type 3 secondary FIs contain both carbon/graphite and sulphide xenocrysts. Type 5 secondary FIs within unrecrystallised grains in samples N5 and N15 typically contain sulphides.

Samples N20 and N30 show two types of quartz; primary hydrothermal quartz porphyroclasts and recrystallised quartz domains. Recrystallised quartz formed from primary quartz during plastic deformation of the veins. Small, isolated biotite grains are present throughout N20 and N30 but are more common in recrystallised quartz domains. In the recrystallised milky quartz abundant secondary FIs are present along healed fractures and grain boundaries - suggesting that these fluids were present during and/or after recrystallisation. The dark quartz porphyroclasts constitute approximately 20 - 30 vol. % in both samples. They are smoky, clouded grey to ochre. These large porphyroclastic grains (200 - 500 µm) contain subgrains and show undulose extinction - indicting that plastic deformation that formed the recrystallised domains also affected the interior of porphyroclasts. Secondary FI trails are oriented at right angles to each other and crosscut porphyroclast boundaries.

7.4.2.1 PRIMARY FIs

Type 1 primary FIAs identified in samples N5 and N11 have Th at 272 - 357 °C (avg. 301 °C) (L – V or L + halite - V) (Table 7.11). Salinities are 33.8 - 36.4 wt. % NaCl eq. (avg. 35.9 wt. % NaCl eq. calculated using Sterner et al's. (1988) equations. Homogenisation pressures are 4.0 - 12.6 MPa (avg. 6.1 MPa) and densities 1.01 - 1.08 g/cm^3 (avg. 1.07 g/cm^3) calculated using Sterner et al's. (1988) equations (Table 7.11). Type 3 and 4 primary FI form at Th between 266 - 338 °C. Type 4 FIs salinities of 3.4 - 11.7 wt. % NaCl eq. (avg. 7.5 wt. % NaCl eq.) are similar to Type 3 FIs 2.0 - 13.2 wt. % NaCl eq. (avg. 5.8 wt. % NaCl eq.) as per Chen (1972) and Bodnar's (1993) calculations (Table 7.10). Type 3 primary FI clathrate melting temperatures and Fermi diad spacing of 104 - 105.5 cm^{-1} indicate homogenisation pressures of 5.7 - 64.0 MPa and densities of 0.57 - 1.081g/cm^3 as calculated using Fall et al's. (2011) equations. These are different from Type 4 FIs total homogenisation pressures of 5.0 - 13.2 MPa (avg. 7.6 MPa) and densities of 0.78 - 0.80 g/cm^3 (avg. 0.79 g/cm^3) calculated using Steel-MacInnis et al's. (2012) equations (Table 7.10).

7.4.2.2 SECONDARY FIs

Recrystallised grains do not host Type 1 primary FIs. Type 1 and 3 secondary FIAs (3 - 6 µm) show FI trails that extend across multiple recrystallised grains to the veins' host rock contacts. This is evident in highly mineralised samples N3, N5 and N15 that contain only liquid CO_2-rich Type 3 secondary FIs (1 - 11 µm) that are distinctly larger than the Type 1 and CO_2 vapour-rich Type 3 secondary FIs (Figure 7.59 and 7.60). Liquid CO_2-rich Type 3 secondary FIs crosscut and overprint Type 3 CO_2 vapour-rich FIs.

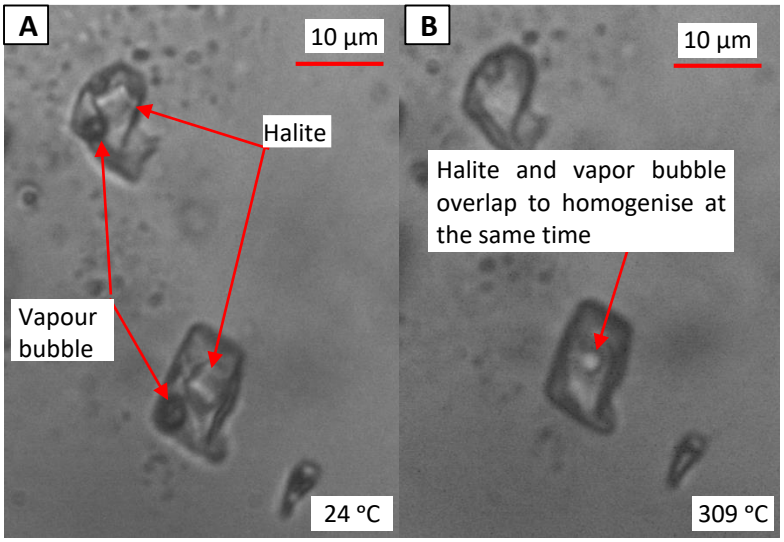

Figure 7.59 Sample N5. (A) Type 1 secondary FIs in mineralised hydrothermal vein. (B) Near simultaneous total halite and vapour bubble homogenisation in Type 1 secondary FIAs.

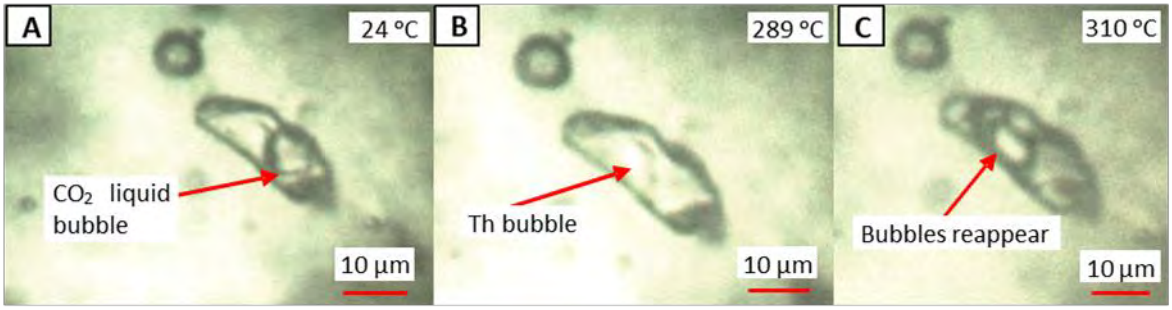

Figure 7.60: Sample N5. (A-B) Transition from ambient of liquid CO_2-rich Type 3 secondary FIs undergoing homogenisation in primary hydrothermal quartz in mineralised sample. (C) Reappearance of a vapour bubble during phase transitions on heating is typical of high-density CO_2, according to Roedder (1984).

Namoya Group 3 liquid CO_2-rich Type 3 secondary FIs have the highest N_2 and CH_4 levels in all TNGB samples, suggesting a significant fluid source in organic-rich metasediments (Figures 7.61 and 7.62). These N_2 and CH_4 rich FI's are most abundant in the highest mineralised samples (e.g. N5 Au 1460 g/t and N3 0.26 – 15.75 Au g/t). Type 1 secondary FIs have Th at 292 - 384 °C (avg. 329 °C) by L - V or L + halite - V (Table 7.10) with salinities of 35.0 - 39.4 wt. % NaCl eq. (avg. 37.0 wt. % NaCl eq.) calculated using Sterner et al's. (1988) equations (Figures 7.62 and 7.63). These are the highest salinities for any secondary FIs across all deposits and are particularly evident in high-ore grades as seen in N3 and N5. This correlates with secondary fluids from Group 2 Namoya. There is a greater abundance of Type 1 secondary FIs in higher-grade samples in comparison to lower grade samples (Table 7.8). Homogenisation pressures are 5.4 - 16.2 MPa (avg. 8.8 MPa) and densities range between 1.02 - 1.07 g/cm^3 (avg. 1.05 g/cm^3) calculated using Steel-MacInnis et al's. (2012) equations (Table 7.8). Type 4 secondary FIs have Th at 256 - 335 °C (avg. 276 °C) and < 12 wt. % NaCl eq. and pressures of 4.3 - 12.8 MPa (avg. 5.8 MPa) with densities of 0.77 - 0.82 g/cm^3 (avg. 0.82 g/cm^3) as per Bodnar (1993) and Steel-MacInnis et al's (2012) calculations. Unmineralised samples contain Type 3 (liquid and vapour CO_2-rich) and Type 4 secondary FIAs that homogenise at 284 - 365 °C (avg. 313 °C) and have low salinities of 0 - 5.8 wt. % NaCl eq. (avg. 2.0 wt. % NaCl eq.) (Table 7.10) as per Chen (1972) and Bodnar's (1993) calculations. Unmineralised Type 3 FIs have clathrate melting temperatures and Fermi diad spacing of 103 to 105 cm^{-1} that indicate homogenisation pressures of 4.9 - 24.8 MPa and densities of 0.13 - 0.96 g/cm^3 at clathrate melting as calculated using Fall et al's. (2011) equations.

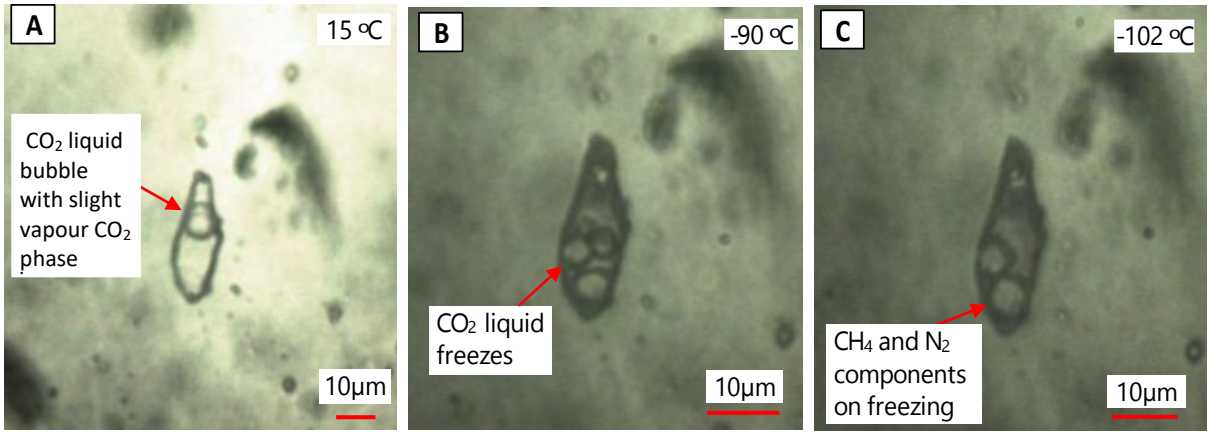

Figure 7.61: Sample N5 photographs of Type 3 secondary FIs undergoing cooling to -102 °C.

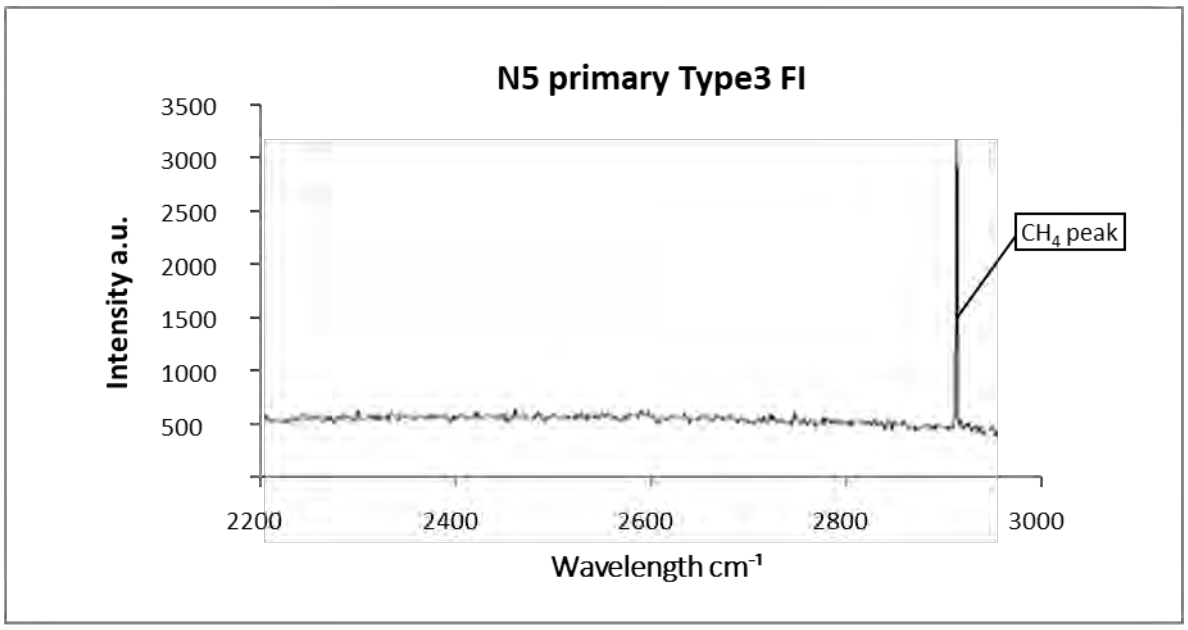

Figure 7.62: Sample N5 Raman spectra of Type 3 FI liquid phase as visible in Figure 7.61.

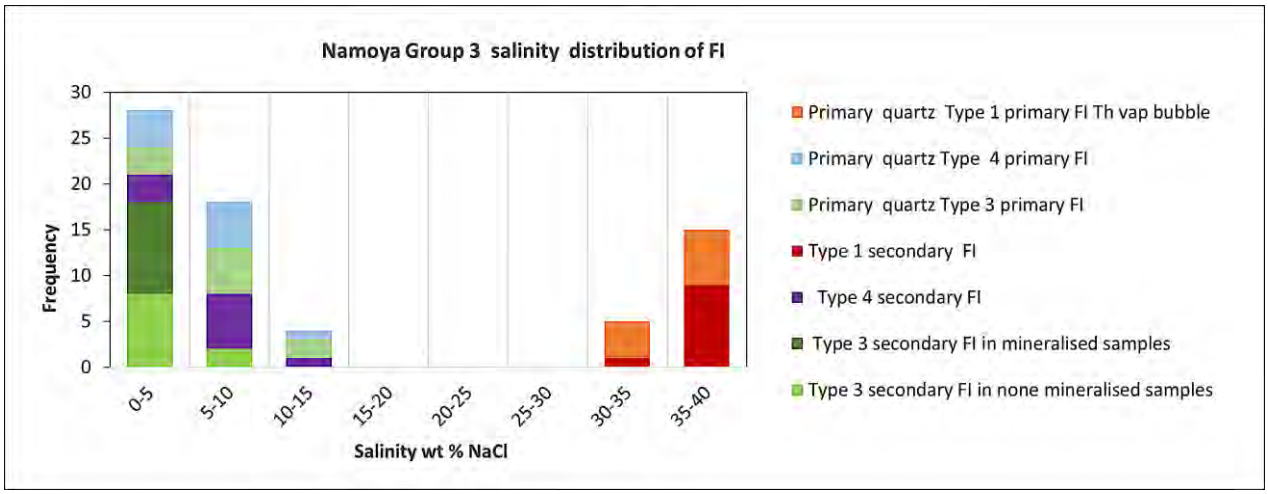

Figure 7.63: Histogram summarising distribution of FI salinity within Namoya Group 3. Note the poor correlation of primary and secondary quartz Th halite Type 1 FIs with other FIs.

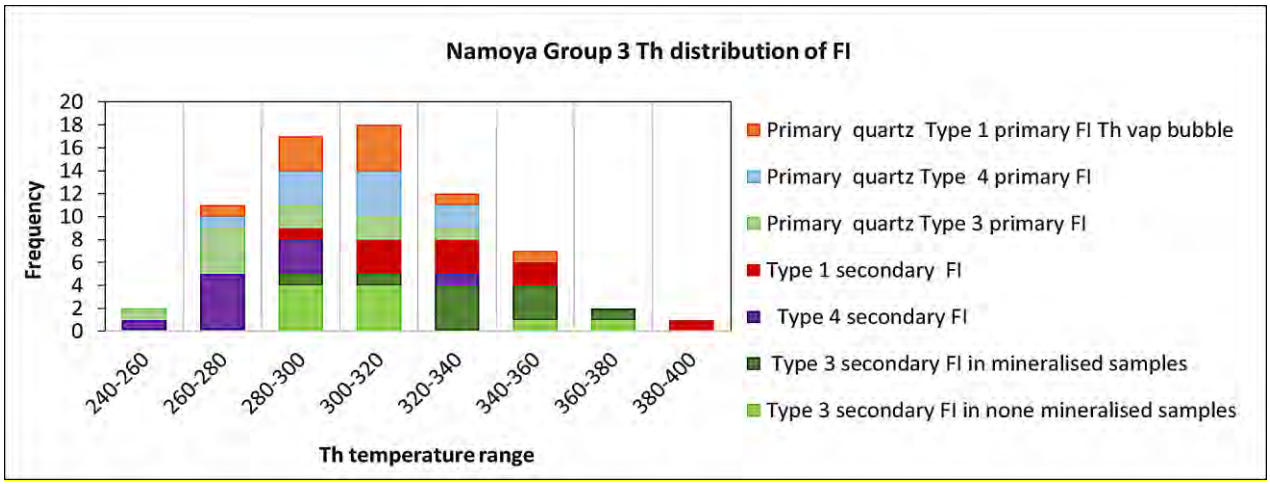

Figure 7.64: Histogram summarising distribution of FI Th within Namoya Group 3.

The temperature of homogenisation for secondary FIs in mineralised samples is the highest for all deposits and Groups. Th ranges from 292 - 380 °C (avg. 355 °C), pressures are 5.7 - 64.0 MPa, corresponding to densities of 0.573 - 1.081 g/cm^3 as calculated using Fall et al's. (2011) equations (Figure 7. 63 and 7.64).

In summary, Group 3 veins suggest that the formation of primary quartz assemblages occurred together with sulphides by hydrothermal precipitation. Subsequent extensive plastic deformation recrystallised quartz and possibly mobilised sulphides. Carbon-saturated CO_2-CH_4 fluid infiltrated during quartz recrystallisation and sulphide mobilisation. The higher gold grade in recrystallised quartz veins suggests that gold was introduced, mobilised and concentrated during deformation and secondary CO_2-rich fluid influx events. There is a high correlation between liquid dominated CO_2-rich FIs and increased mineralisation in Group 3. Group 3 samples have a closer association of increased CH_4 and N_2 levels and gold mineralisation than other samples from across the TNGB. In addition, secondary fluids that correlate with Au mineralisation have very high salinities in the range of ~37 wt. % NaCl eq. This points to a fluid source rich in NaCl and organic materials.

Table 7.10: Microthermometric and barometric data of Type 1. 3 and 4 primary and secondary FIs for Namoya Group 3.

Phase relationship	FI Type	Tm	Final phase melting	Th $_{(L-V)}$	wt. % NaCl eq.	T @ homog. (°C)	P @ homog. (bar)	r_{BULK} (g/cm$_3$)	Reference
Primary quartz associated Type 1 primary FIs	Upper Th final by Th (L - V) for Type 1	277	Halite	357	36.4	357.0	126	1.02	Sterner et al. (1988) and Steel-MacInnis et al. (2012)
Primary quartz associated Type 1 primary FIs	Lower Th final by Th (L - V) for Type 1 FI	235	Halite	272	33.8	272.0	40	1.08	Sterner et al. (1988) and Steel-MacInnis et al. (2012)
Primary quartz associated Type 1 primary FIs	Avg. Th final by Th (L - V) for Type 1 FI	269	Halite	301	35.9	301.0	61	1.07	Sterner et al. (1988) and Steel-MacInnis et al. (2012)
Primary quartz associated Type 1 primary FIs	Upper Th final by Th (L - V) for Type 4 FI	-8	Ice	338	11.7	338.0	132	0.78	Bodnar (1993) and Steel-MacInnis et al. (2012)
Primary quartz associated Type 1 primary FIs	Lower Th final by Th (L - V) for Type 4 FI	-2	Ice	266	3.4	266.0	50	0.80	Bodnar (1993) and Steel-MacInnis et al. (2012)
Primary quartz associated Type 1 primary FIs	Avg. Th final by Th (L - V) for Type 4 FI	-4	Ice	294	6.5	294.0	76	0.79	Bodnar (1993) and Steel-MacInnis et al. (2012)
Primary quartz associated Type 1 primary FIs	Upper Th Type 3 FI	9	Clathrate	331	2.0	331.0	640	1.08	Chen (1972) and Fall et al. (2011)
Primary quartz associated Type 1 primary FIs	Lower Th Type 3 FI	2	Clathrate	276	13.2	276.0	57	0.57	Chen (1972) and Fall et al. (2011)
Primary quartz associated Type 1 primary FIs	Avg. Th Type 3 FI	7	Clathrate	261	5.8	255.0	215	0.92	Chen (1972) and Fall et al. (2011)
All Type 1 secondary FIs	Upper Th final by Th (L - V) for Type 1 FI	316	Halite	384	39.4	384.0	162	1.02	Sterner et al. (1988) and Steel-MacInnis et al. (2012
All Type 1 secondary FIs	Lower Th final by Th (L - V) for Type 1 FI	255	Halite	292	35.0	292.0	54	1.07	Sterner et al. (1988) and Steel-MacInnis et al. (2012)
All Type 1 secondary FIs	Avg. Th final by Th (L - V) for Type 1 FI	284	Halite	329	37.0	329.0	88	1.05	Sterner et al. (1988) and Steel-MacInnis et al. (2012)
All Type 4 and 6 secondary FIs throughout samples	Upper Th final by Th (L - V) for Type 4 FI	-7	Ice	335	10.5	335.0	128	0.77	Bodnar (1993) and Steel-MacInnis et al. (2012)
All Type 4 and 6 secondary FIs throughout samples	Lower Th final by Th (L - V) for Type 4 FI	-2	Ice	256	3.4	256.0	43	0.82	Bodnar (1993) and Steel-MacInnis et al. (2012)
All Type 4 and 6 secondary FIs throughout samples	Avg. Th final by Th (L - V) for Type 4 FI	-4	Ice	276	6.5	276.0	58	0.82	Bodnar (1993) and Steel-MacInnis et al. (2012)
All none mineralised samples with liquid CO_2-rich Type 3 secondary FIs	Upper Th Type 3 FI	7	Clathrate	365	5.8	365.0	248	0.96	Chen (1972) and Fall et al. (2011)
All none mineralised samples with liquid CO_2-rich Type 3 secondary FIs	Lower Th Type 3 FI	10	Clathrate	284	0	284.0	49	0.13	Chen (1972) and Fall et al. (2011)
All none mineralised samples with liquid CO_2-rich Type 3 secondary FIs	Avg. Th Type 3 FI	9	Clathrate	313	2.0	313.0	55	0.80	Chen (1972) and Fall et al. (2011)
Mineralised samples Type 3 secondary FIs throughout samples	Upper Th Type 3 FI	8	Clathrate	380	4.0	380.0	640	1.08	Chen (1972) and Fall et al. (2011)
Mineralised samples Type 3 secondary FIs throughout samples	Lower Th Type 3 FI	10	Clathrate	292	0	292.0	57	0.57	Chen (1972) and Fall et al. (2011)
Mineralised samples Type 3 secondary FIs throughout samples	Avg. Th Type 3 FI	9	Clathrate	355	2.0	355.0	186	0.91	Chen (1972) and Fall et al. (2010)

8. FORMATION CONDITIONS OF FLUID ENTRAPMENT

The purpose of this chapter is to determine the pressures and temperatures at which the fluids of the TNGB were trapped as fluid inclusions. Isochore and salinity vs Th graphs were developed using microthermometric and Raman spectroscopy data presented in Chapter 7. The isochore diagrams were calculated using equations and parameters defined by Bodnar & Vityk (1994) and Lecumberri-Sanchez et al. (2012) for H_2O-NACl systems. The software, HOKIEFLINCS-H_2O-NACl developed by Steel-MacInnis et al. (2012) was applied to determine the H_2O-NACl isochores as described in Chapter 6 section 6.4, 6.5 and 6.6). FI isochore generation for the CO_2 – NaCl – H_2O system was generated from Brown and Lamb (1989) using equations by Kerrick and Jacobs (1981) and Bowers and Helgeson (1983). These values were then compared against the Fortran program for FIs in the H_2O - CO_2 - NaCl system homogenised above 350 as described in Chapter 6 section 6.12.

8.1 KAMITUGA GROUP 1 PEGMATITE

Formation temperatures for Kamituga's Group 1 pegmatite Ktm-3 were determined using the average Th to calculate the isochore readings from Type 1, 3 & 4 primary FIs. The average Th was used as it was most representative of the Th for FI Types – particularly Types 1 and 2 in which the higher Th inclusions indicated decrepitation characteristics. Roedder (1984) and Bodner (2003) both indicated that after decrepitation a high density medium eg. High density saline fluid results from the loss of volatiles (CO2 and CH4). In the case of reequilibrium low and high density Fis usually result from the original unstable larger FI. It is for this reason that the data obtained below is more valid than those based on highest – density fluids. If the highest density fluids of each FI type were used for microthermometry, the results would shift to higher temperatures and pressures by approximately 80 - 100 °C and 1-2 kbar

There are at least two stages of development recorded in Ktm-3 (i) a primary magmatic fluid from which quartz and blue tourmaline formed and (ii) a later secondary hydrothermal fluid influx that formed alteration halos containing brown tourmaline. Type 1 FIs in primary pegmatitic quartz, homogenised by halite loss, are in close relation to surrounding Type 3 and 4 primary FIs that homogenised by vapour bubble loss (V - L). The intersections of isochores for separate Type 1 and 4 fluids are interpreted to represent the capturing conditions for pegmatitic fluids. The two isochores show a similar slope and position in P-T space and intersect at an acute angle at 6 kbar and 763 °C (Figure 8.1). The acute intersection angle of the isochores caused some uncertainty in the P-T estimate. The estimated temperature of 763 °C appears higher than expected for a boron-rich pegmatitic fluid as these usually solidify below the granitic minimum. Büttner et al. (2016) estimated the solidification temperature of pegmatite Ktm-3 as 630 °C. This corresponds to a pressure of about 4 kbar. Figure 8.1 (blue field) indicates likely P-T estimates for the emplacement of the Ktm-3 pegmatite for a temperature range of 530 to 630 °C. The likely conditions of fluid capturing during pegmatite solidification are defined by the position of the isochores at this temperature range. Accordingly, the best P-T estimate for the emplacement of the Ktm-3 pegmatite is 3 - 4 kbar and ~530 and 630 °C.

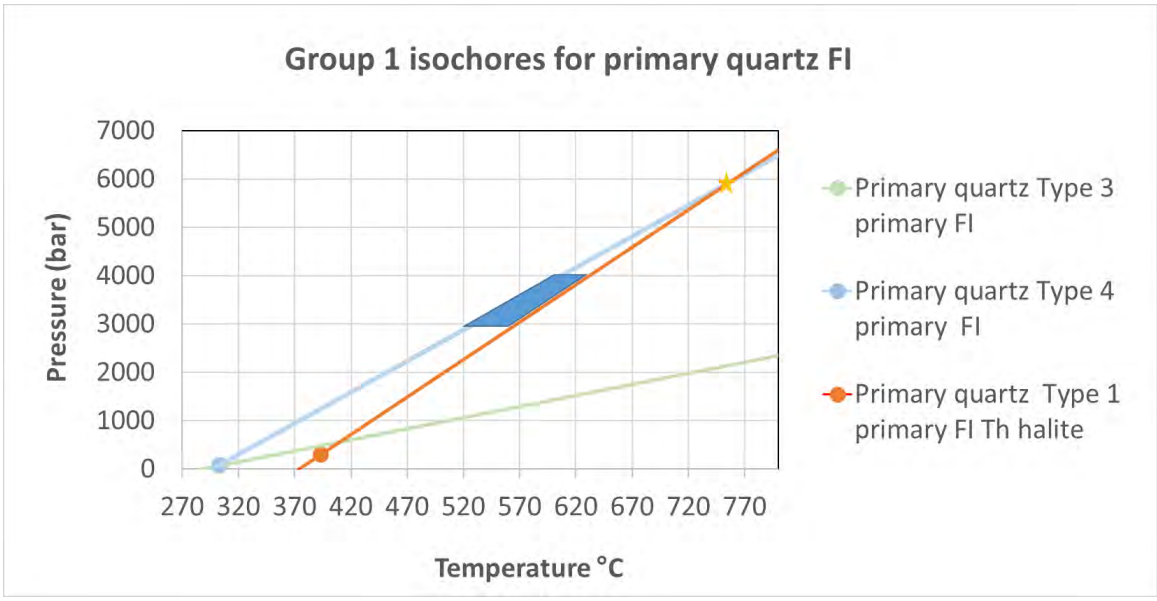

Figure 8.1: Isochore diagram for Ktm-3 primary FIA in primary magmatic quartz. The formation conditions are defined by the intersection of the average Type 1 and 4 primary FI isochores at 763 °C and 6 kbar. The acute intersection angle of the isochores caused some uncertainty in the position of the intersection. A boron-rich pegmatitic fluid is likely to be colder (530 - 630 °C) than this intercept. This implies pressures of ~3 - 4 kbar (blue field) that correspond to a depth-temperature gradient ~45 °C/km. The red and blue points on the isochore lines represent average Th from which isochores are projected.

The secondary quartz in sample Ktm-3 is related to the precipitation from a carbonaceous-hydrous hydrothermal fluid (not strictly Group 1). This secondary quartz contains numerous FIAs with a variety of FIs Types. There is clear distinction between FIAs that contain Type 1 primary FIs and those that do not. The most accurate PT estimation for fluid capture is obtained from Type 1 FI isochores that homogenise into the liquid phase (V – L) with Type 4 FI isochores. The intersection point lies at 1.8 kbar and 445 °C (yellow star in Figure 8.2). These PT conditions have a high uncertainty due to the similar slopes of the relevant isochores. This corresponds to a high temperature/depth gradient of 65 °C/km. Assuming an average density of the overlying crust of 2.7 g/cm^3, 1.8 kbar correspond to a depth of 6800 m.

The intersection between Type 1 primary FI (homogenised by halite loss) isochores and Type 4/Type 3 FIA isochores, suggests capturing conditions of approximately 1.1 kbars and 380 °C (Figure 8.2). This corresponds to 4200 m depth and a high temperature gradient of 90 °C/km. The lowest P-T intersection that defines the field of fluid capturing is the intersection of Type 1 (homogenised by halite loss) and Type 3 isochores at ~0.1 kbar and 330 °C. Hence, the probable P-T conditions of fluid capturing are defined by the isochores for Type 4 FIs associated with Type 3 FIA; Type 1 FIs homogenise by halite loss; Type 1 FIs homogenise by vapour bubble loss and Type 3 FIs associated with Type 1 FIs homogenise by vapour bubble loss with a P-T field that centers at approximately 380 °C and 1 kbar within the blue field (Figure 8.2). This suggests shallow crustal influx of hot

fluids (~4000 m depth ~90-100 °C/km) during the retrograde metasomatic overprint of the pegmatite at P-T conditions that are significantly lower than estimated for pegmatite solidification.

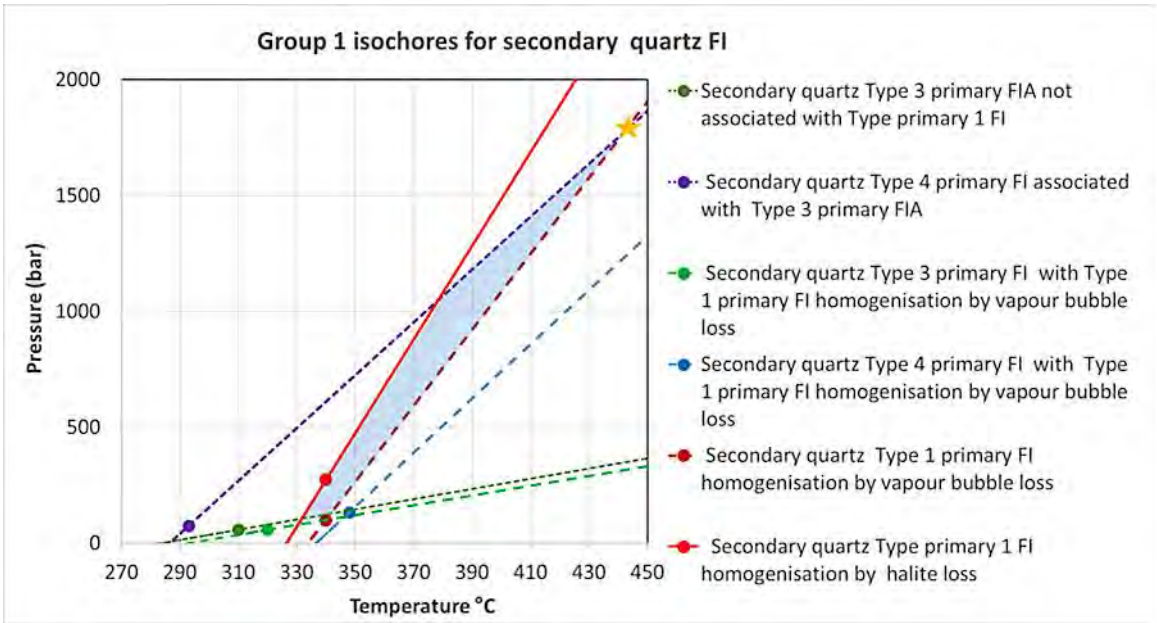

Figure 8.2: Isochore diagram for primary FIs in the secondary (hydrothermal) quartz in pegmatite Ktm-3 (primary FIA). Fluid capturing conditions obtained from the average Type 1 (homogenisation by vapor loss and Type 4 associated with Type 3 FIA). FI isochore intersection at ~445 °C/1.8 kbar (star) corresponding to a depth-temperature gradient of ~65 °C/km. The points on the isochore lines represent average Th from which isochores are projected. The shaded area indicates the possible PT formation condition range.

Primary magmatic Group 1 fluids have higher salinity and Th compared to the secondary fluids that are related to retrograde hydrothermal influx (Figure 8.3). High salinities and Th correspond with a magmatic source of Group 1 pegmatitic fluids (Bodnar, 1993). The lower salinities and Th of the hydrothermal fluids and their higher CO_2 content corresponds to a low-grade metamorphic fluid sourced from pelitic-carbonaceous rocks, which are abundantly present in the host rock sequence of Kamituga.

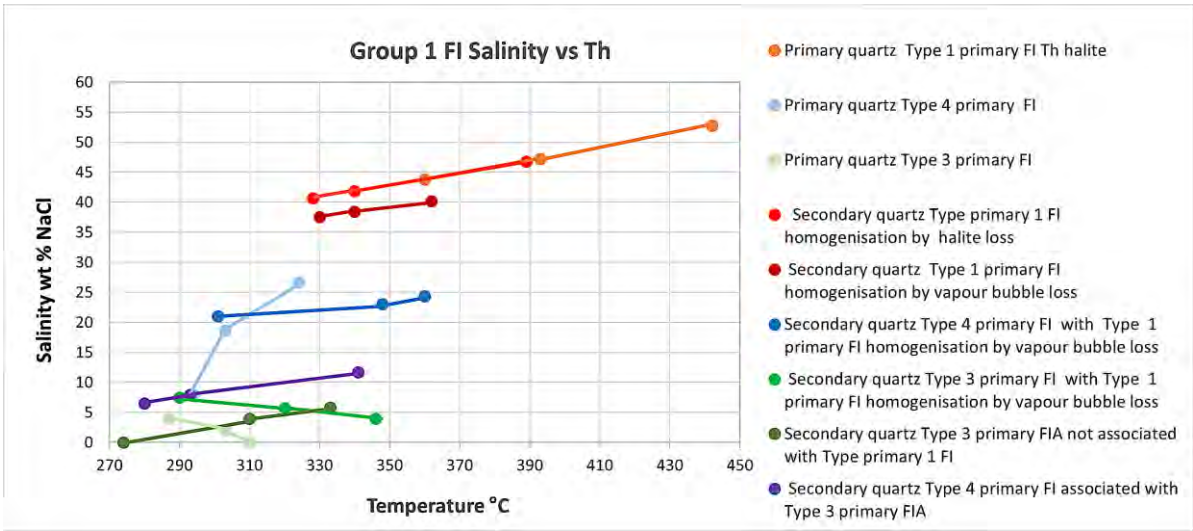

Figure 8.3: Salinity vs Th for Group 1 pegmatite Ktm-3. The graph shows the lower, upper and average Th/salinity values (dots on contour lines) for Types 1, 3 and 4 primary FIs within primary and secondary quartz. There is a decrease in salinity and Th from fluids contained in primary to secondary stage quartz. FIAs not associated with Type 1 primary FIs have the lowest salinity and Th.

8.2 GROUP 2 TOURMALINE-BEARING QUARTZ VEINS

Kamituga's Group 2 primary hydrothermal quartz contains Type 1 primary FIs that homogenise by halite dissolution. The absence of a second coeval fluid species renders P-T determination by isochore intersection impossible (Figure 8.4). Early Kamituga Type 1 FIs homogenise at Th of 356 °C with a corresponding Th pressure of 0.8 kbar, which is higher than Type 1 FI (L - V) from both Lugushwa (0.1 kbars and 336 °C) and Namoya (0.1 kbars and 303 °C). Total homogenisation conditions cannot be used to determine formation conditions unless applied with isochores with conformational fluids that intersect to represent trapping conditions. However, these Th values indicate the minimum conditions of fluid capturing that would have occurred at a much greater depth and therefore greater pressure of entrapment; indicating that fluid capturing took place under greenschist facies conditions.

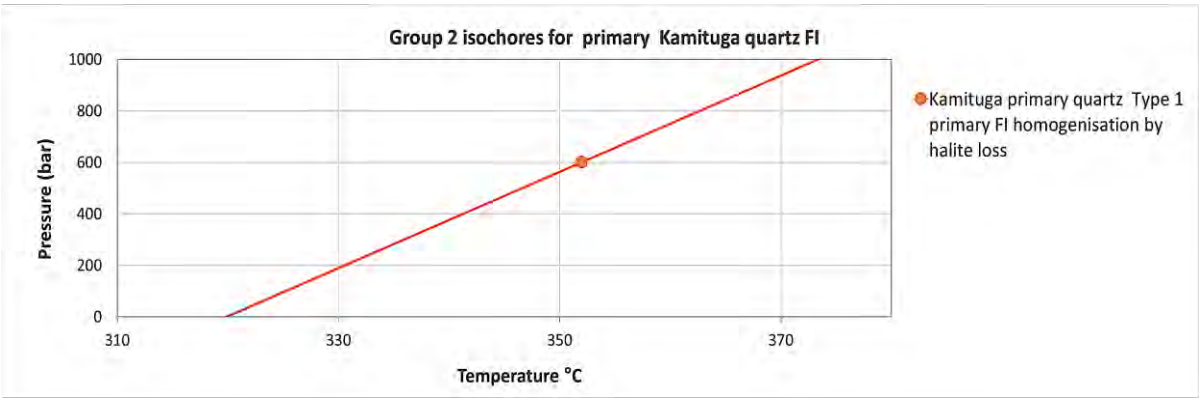

Figure 8.4: Isochore diagram for Kamituga Group 2 primary quartz. Type 1 primary FIs that homogenise by halite dissolution. The absence of a second coeval fluid species renders P-T determination by isochore intersection impossible. Trapping conditions are somewhere along this isochore in the greenschist facies. The orange points on the isochore lines represent average Th from which isochores are projected.

Lugushwa's Type 1, 3 and 4 FIA in primary hydrothermal quartz yield isochore intersections that suggest a fluid capture P-T field between ~0.2 - 1.7 kbar and 316 - 430 °C (Figure 8.5). The intersection point of Type 1 and 4 primary FI isochores at 430 °C and 1.7 kbar (Figure 8.5) likely represents trapping conditions. This is near identical to conditions of secondary hydrothermal fluid influx seen in pegmatitic samples from Kamituga. The acute intersection angle of the isochores, however, adds some uncertainty to this P-T estimate. The P-T field might also lie above the intersection point.

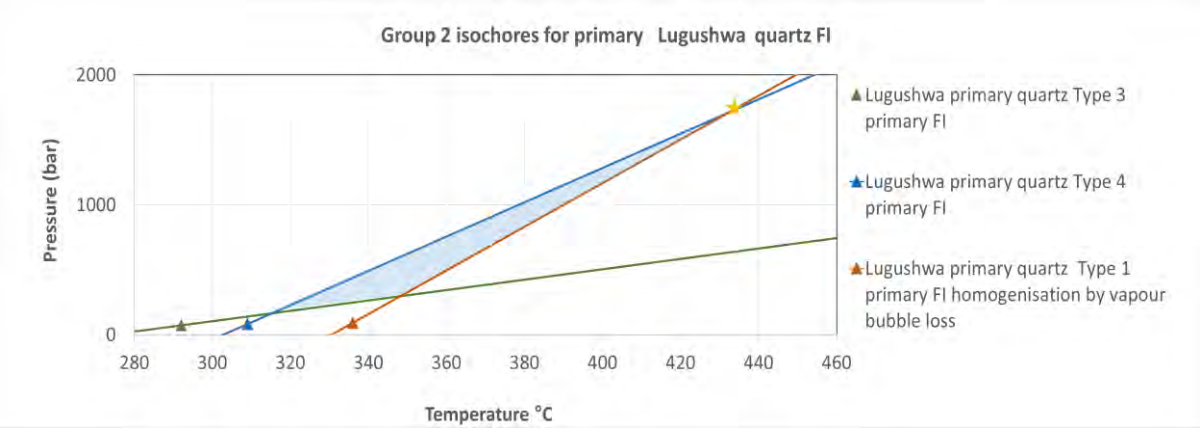

Figure 8.5: Isochore diagram for Lugushwa Group 2 primary quartz. The fluid capturing conditions obtained from the average Type 1 primary (homogenisation by vapor loss) and Type 4 primary (associated with Type 3 FIA) FI isochore intersection at ~430 °C/1.7 kbar (star) corresponding to a depth-temperature gradient of ~65 °C/km. The orange, blue and green triangles on the isochore lines represent average Th from which isochores are projected. The shaded area indicates the possible PT formation condition rang.

Namoya's primary quartz Type 1, 3 and 4 primary FIA isochore intersections yield a low pressure of <1 kbar at lower greenschist facies temperatures - irrespective of the isochore intersection (Figure 8.6). The P-T field outlined by the isochore intersections suggests very high depth-temperature gradients of the fluids during trapping, exceeding 100 °C/km. The highest P-T intersection at ~900 bar and 368 °C (star in Figure 8.6) suggests fluid trapping at a depth of ~3400 m. The fluid temperature is very high for this shallow depth (>100 °C/km), indicating conditions above common geothermal gradients. Such P-T conditions would indicate that hot fluids traveled rapidly upwards, avoiding thermal equilibration with the ambient (typically much lower) geothermal gradient. Further discussion is presented in Chapter 9.

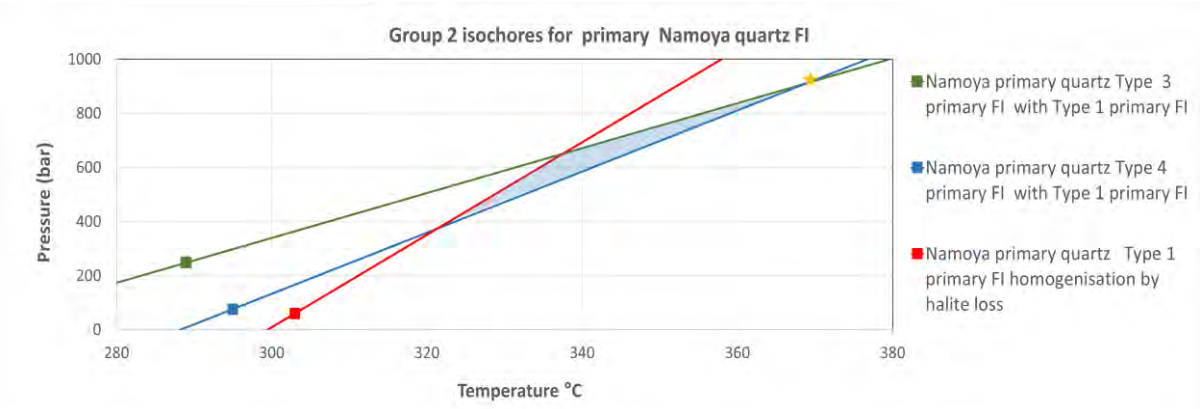

Figure 8.6: Isochore diagram for Namoya Group 2 primary quartz. Isochore intersections yield 0.4 -0.9 kbar and 323 - 368 °C. The highest P-T isochore intersection is at ~368 °C/0.9 kbar (star) for Types 3 and 4 primary FIs (associated with Type 1 primary FIs) and correspond to a depth of ~3400 m and a depth-temperature gradient of > 100 °C/km. The red, blue and green squares on the isochore lines represent average Th from which isochores are projected. The shaded area indicates the possible PT formation condition range.

Kamituga's secondary quartz generation in Group 2 (tourmaline-bearing hydrothermal veins) indicate fluid trapping condition of Type 1 and 4 primary FI isochore intersections at 472 °C and 2.1 kbar (~59 °C/km) (Figure 8.7; ~8000 m depth; 59 °C/km). Intersections with Type 3 FIs fluid isochore (associated with Type 1 FIs) yield unrealistically low pressures for fluid capturing (<0.5 kbar) when compared to the geological environment and associated FIA's entrapment.

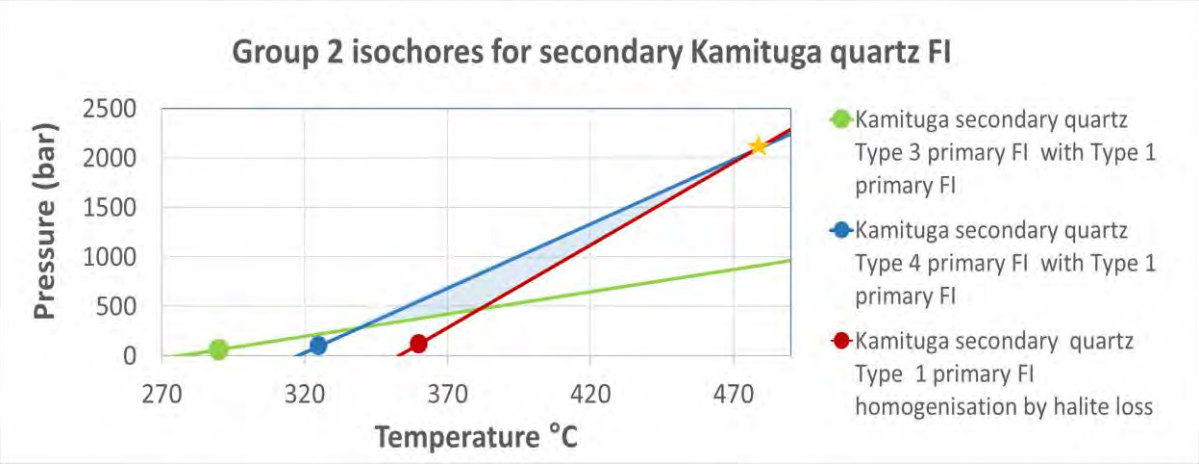

Figure 8.7: Isochore diagram for Kamituga Group 2 secondary quartz. Fluid capturing conditions obtained from the average Type 1 primary (homogenisation by halite loss) and Type 4 primary (associated with Type 1 FI) isochore intersection at ~475 °C/2.1 kbar (star) correspond to a depth of ~8000 m and a depth-temperature gradient of ~59 °C/km. The dots on the isochore lines represent average Th from which isochores are projected. The shaded area indicates the possible PT formation condition range.

Lugushwa's secondary quartz lacks Type 1 primary FIs that provided the best P-T estimates in the other deposits. Type 3 and Type 4 primary FI isochores intersect at ~0.4 kbar and 308 °C (Figure 8.8). This corresponds to a very shallow crustal environment at ~1600 m depth that was exposed to the influx of hot epithermal fluids (~190 °C/km). This possibly epithermal environment is an episode previously not considered in the TNGB. In Namoya's Group 2 vein samples, the hydrothermal recrystallised grains have few FIs. These FIs are decrepitated or indicate alternations.

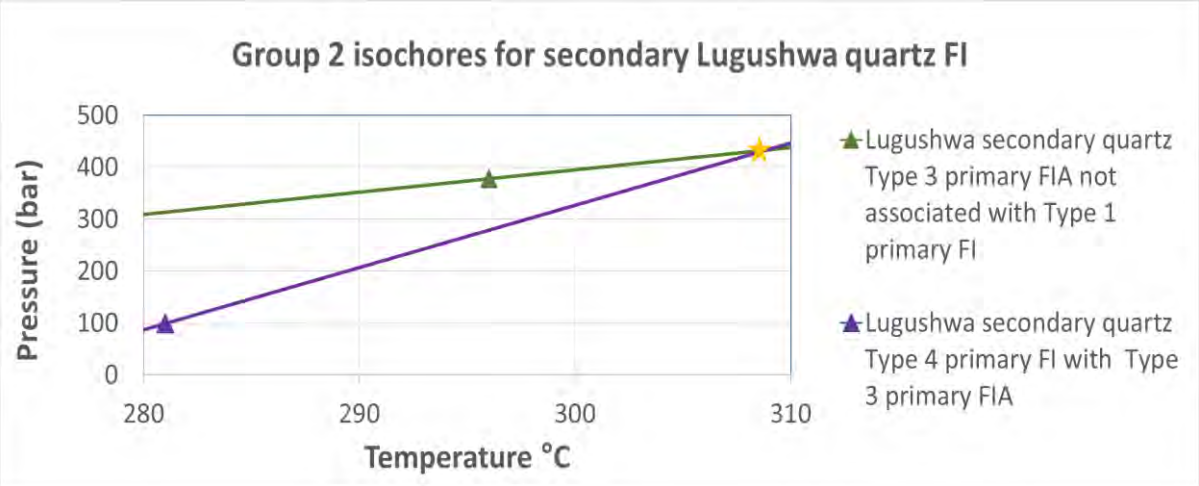

Figure 8.8: Isochore diagram for Lugushwa Group 2 secondary quartz. Fluid capturing conditions obtained from the average Types 3 and 4 primary FI (associated with Type 3 FIA) isochores intersect at ~308 °C/0.4 kbar (star). The triangles on the isochore lines represent average Th from which isochores are projected.

Salinities in Group 2's hydrothermal fluids are lower compared to Kamituga's pegmatitic Group 1 fluids (>55 wt. % NaCl eq. vs. <50 wt. % NaCl eq.) (Figure 8.3, 8.9, 8.10). The Th values cluster between 280 and 370 °C with a high variance in salinity levels between different fluid Types (~3 - 45 wt. % NaCl eq.). Three coherent clusters define Kamituga, Lugushwa and Namoya's Type 1, 3 & 4 primary FIs (Figure 8.9, 8.10). Kamituga's FIs Th values are slightly higher, but the differences in the average values for the three deposits are insignificant.

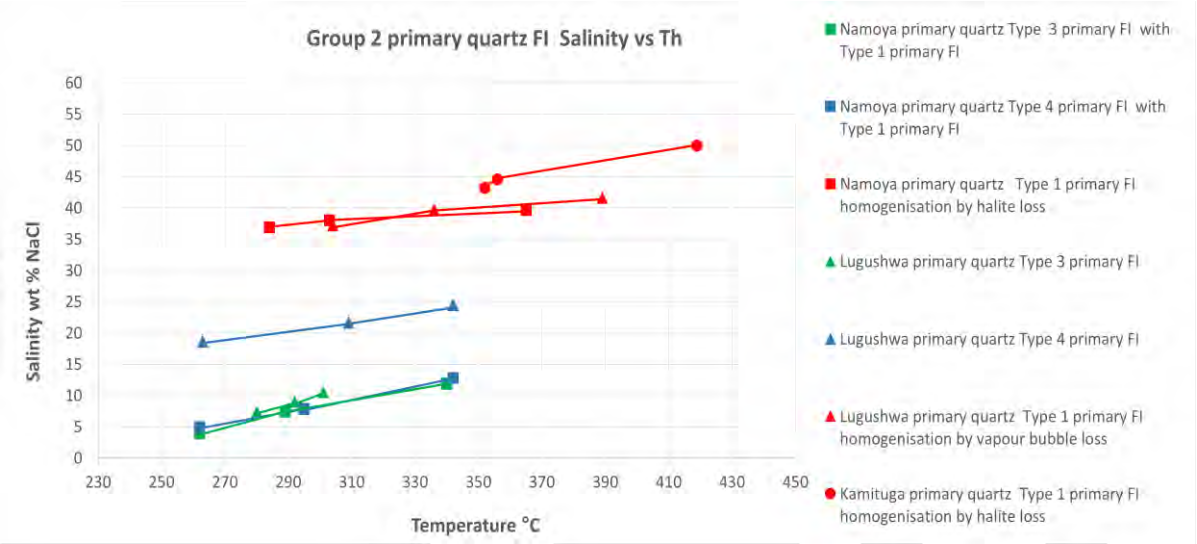

Figure 8.9: In Group 2's primary hydrothermal quartz primary FIs, the salinity vs Th conditions are shown within the lower, upper and average values for Types 1, 3 & 4 primary FIs represented in Kamituga by circles; Lugushwa by triangles and Namoya by squares. Type 1 FIs - red; Type 3 - green and Type 4 - blue. There is a decrease in combined salinity and Th across all FI Types from Kamituga in the northeast to Lugushwa centre, and Namoya in the south of the TNGB.

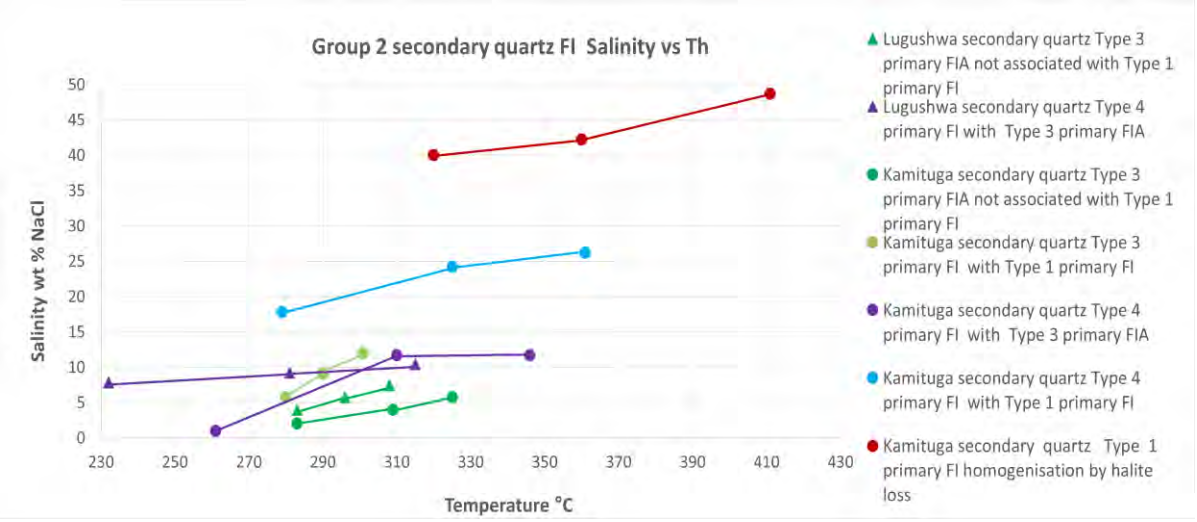

Figure 8.10: Salinity vs Th conditions in secondary quartz FIs in Group 2 are shown as lower, upper and average values for Type 1, 3 & 4 primary FIs. Kamituga is represented by circles and Lugushwa by triangles. Type 1 - red; Type 3 - green and Type 4 - blue/purple. There is a decrease in combined salinity and Th across all primary FI Types in Kamituga and Lugushwa respectively. There is no evidence in Namoya quartz vein samples of FIs that are representative of secondary quartz.

8.3 GROUP 3 TOURMALINE-FREE QUARTZ VEINS IN ALL DEPOSITS

There is coherence in the physical conditions under which fluids formed in primary hydrothermal quartz from the three deposits in Group 3 (i.e. tourmaline-free) samples. Kamituga Group 3 samples consist primary of hydrothermal quartz, but less so when compared to Lugushwa and Namoya's Group 3 samples. Lugushwa and Namoya's Group 3 samples that contain primary FIs have a predominance of Type 1, 3 and 4 primary FIs. Type 1 and 4 primary FI isochore intersections for Lugushwa veins indicate 1.5 kbar and 396 °C (Figure 8.11). this suggests capturing of fluids with a depth-temperature gradient of ~70 °C/km at a depth of approximately 5700m.

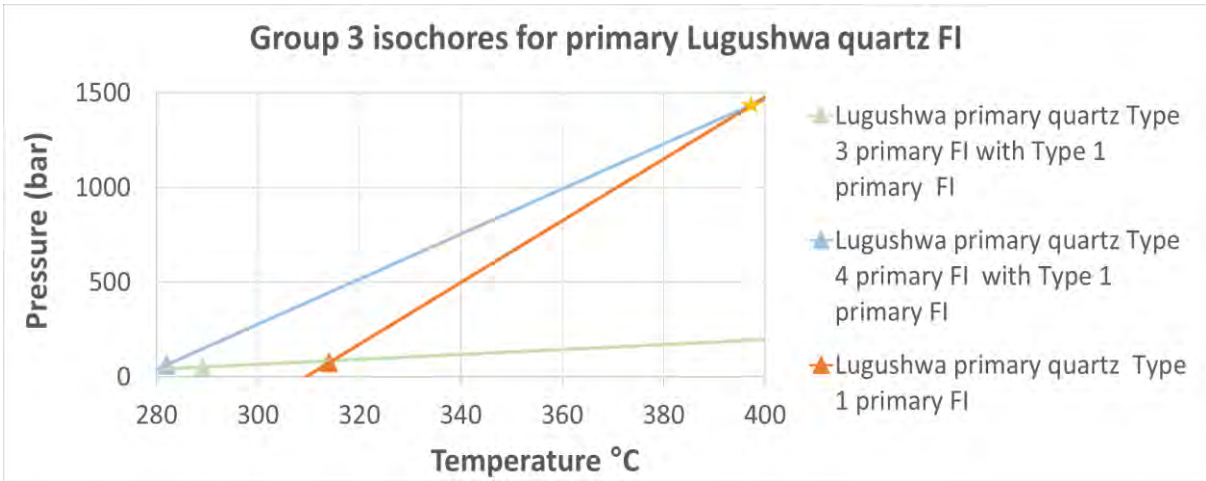

Figure 8.11: Isochore diagram for Lugushwa Group 3 primary quartz. Fluid capturing conditions obtained from the average Type 1 primary FIs (homogenisation by vapor loss) and Type 4 primary isochores (associated with Type 1 primary FI) intersect at ~396°C/1.5 kbar (star). These correspond to a depth-temperature gradient of ~70 °C/km and a capturing depth of ~5700 m. The triangles on the isochore lines represent average Th from which isochores are projected.

Similar formation conditions of fluids contained in primary quartz were obtained for Namoya (1.2 kbar and 388 °C) (Figure 8.12). These P-T conditions represent the intersection of Type 3 and 4 primary FI isochores that yield a depth-temperature gradient of 86 °C/km for primary FIs. Intersections with Type 1 primary FI isochores yield higher gradients that exceed 110 °C/km, with P-T intersections of 800 bar and ~340 °C (Figure 8.12). As Type 1 primary FIs are co-genetic with Type 3 primary FIs (Chapter 7; Section 7.4.3), the intersection at 1.2 kbar is deemed the more reliable P-T estimate for the capture of fluids in primary quartz from Namoya.

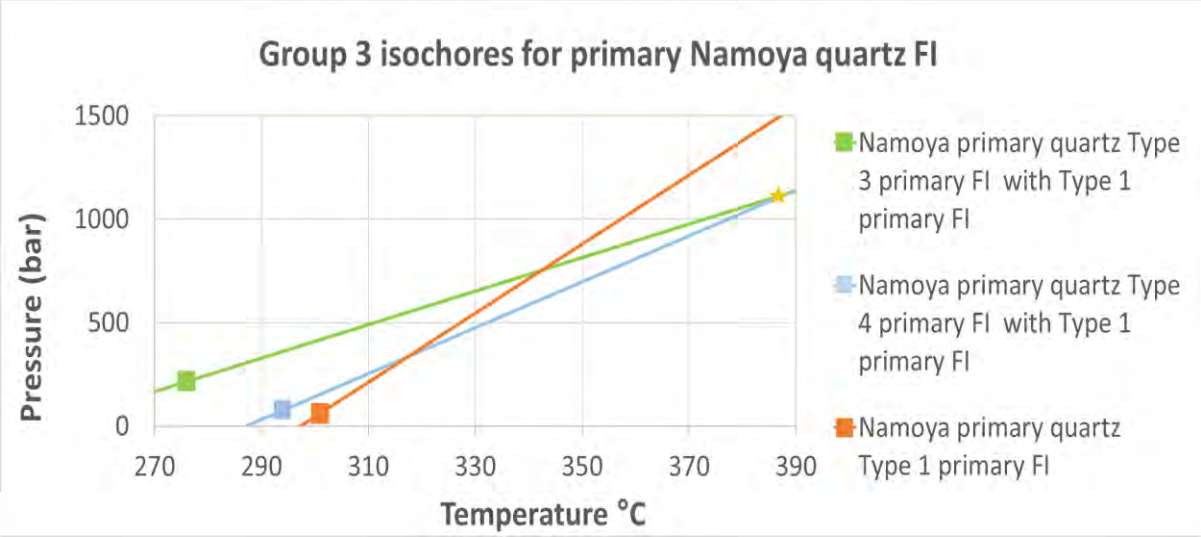

Figure 8.12: Isochore diagram for Namoya Group 3 primary quartz. Fluid capturing conditions obtained from the average Type 3 primary FI (associated with Type 1 primary FI) & Type 4 primary (associated with Type 1 primary FI) isochore intersect at ~388°C/1.2 kbar (star) and correspond to a depth of 4500 m and depth-temperature gradient of ~86 °C/km. The squares on the isochore lines represent average Th from which isochores are projected.

Kamituga's secondary quartz FIs, precipitated during renewed fluid influx, are not suitable for microthermometry. This is because the three isochores do not intersect or intersect below the average Th of the FIAs or intersect above 6 kbar and 650 °C (Figure 8.13).

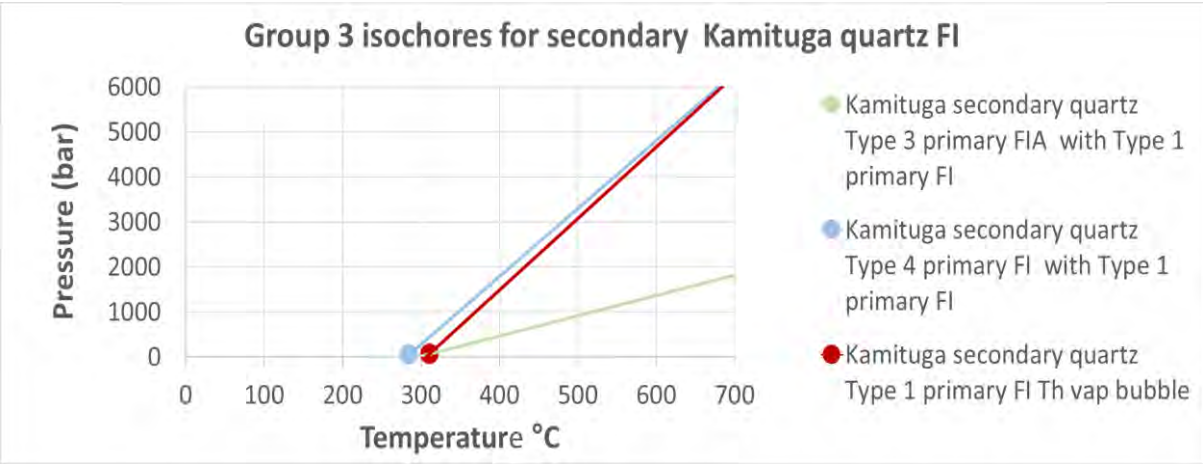

Figure 8.13: Isochore diagram for Kamituga Group 3 secondary quartz. Formation conditions cannot be confirmed as there is no intersection of isochores above the average Th conditions within reasonable limits. (dots).

Isochores for co-genetic Type 3 and Type 4 primary FIs from secondary quartz in Lugushwa show intersections at a low pressure of 0.35 kbar (~1300 m depth) and temperatures of 292 °C (Figure 8.14), implying a depth-temperature gradient exceeding 220 °C/km. If these results are correct, P-T estimate would indicate high heat flux in an epithermal environment. This will be further discussed in Chapter 9.

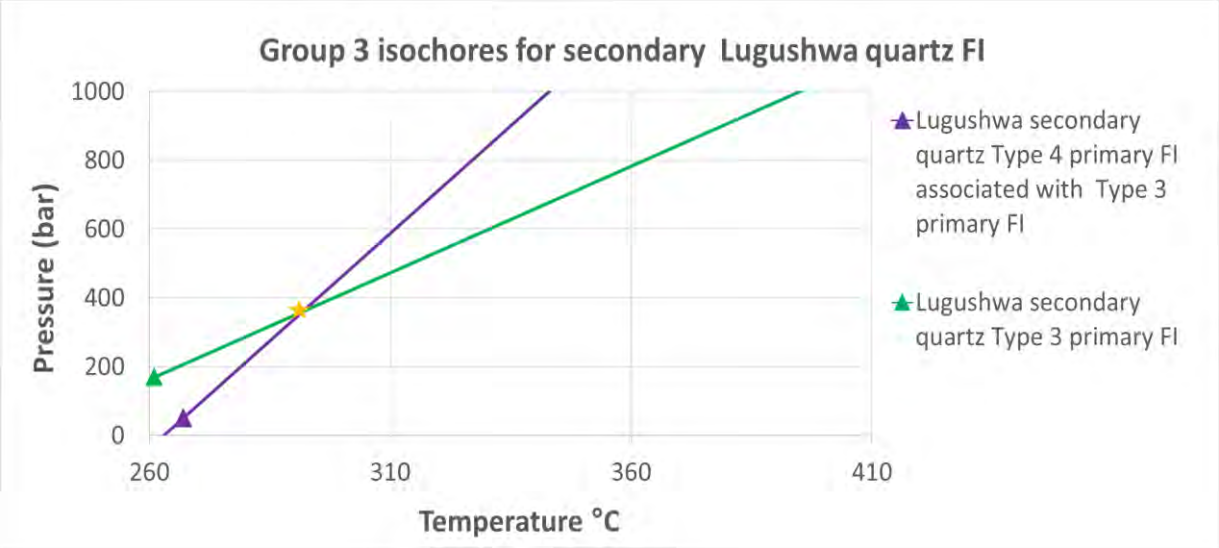

Figure 8.14: Isochore diagram for Lugushwa Group 3 secondary quartz. Fluid capturing conditions from the average cogenetic Type 3 and Type 4 primary FIA's (homogenised by vapor loss) isochore intersect at ~292 °C/0.35 kbar (star) that correspond to a depth of ~1300 m and a depth-temperature gradient of ~220 °C/km. These Type 3 and 4 primary FIAs do not contain Type 1 primary FIs. The triangles on the isochore lines represent average Th from which isochores are projected.

Group 3 fluids in primary quartz show high salinity Type 1 primary (halite-bearing) FIs (32 - 42 wt. % NaCl eq.; Figure 8.15) and lower salinity Type 3 and 4 primary FIs. Type 4 primary FIs in secondary quartz in Kamituga are highly saline (26 wt. % NaCl eq.) (Figure 8.16). Overall, secondary quartz has overlapping salinity ranges with primary quartz. This suggests that primary and secondary quartz may have formed sequentially or in overlapping time periods and from similar fluid sources.

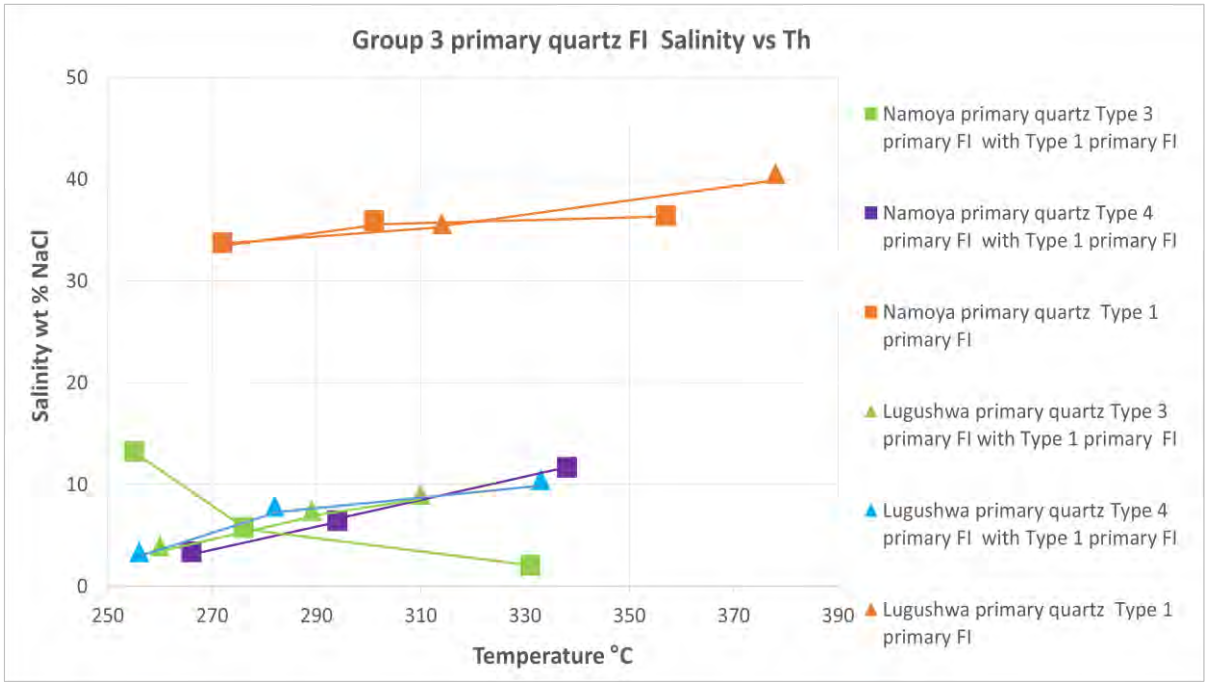

Figure 8.15: Salinity vs. Th conditions in primary quartz primary FIs in Group 3 are shown as lower, upper and average values for Type 1, 3 and 4 primary FIs. Lugushwa - triangles and Namoya - squares. Type 1 - orange; Type 3 – green, and Type 4 - blue/purple. Note two clusters of Type 1 vs Type 3 and 4 primary FIs.

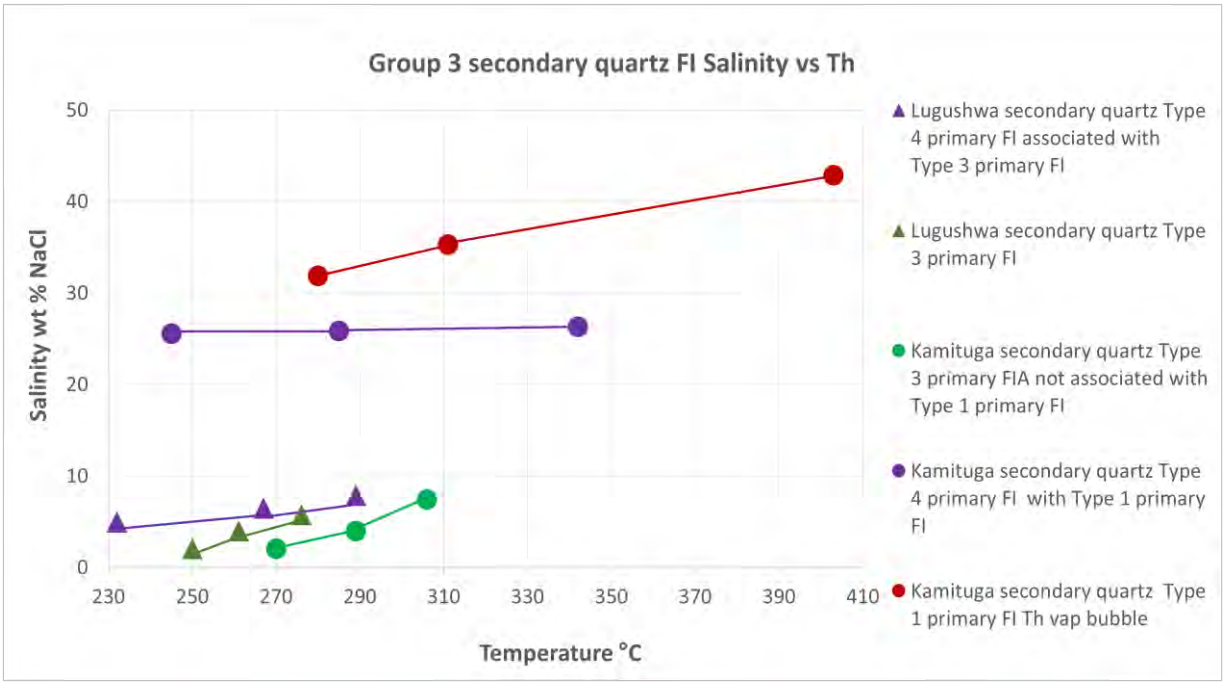

Figure 8.16: Salinity vs Th conditions in secondary quartz primary FIs in Group 3 are shown as lower, upper and average values for Types 1, 3 and 4 primary FIs. Kamituga - circles and Lugushwa - triangles. Type 1 primary FIs - red; Type 3 - green and Type 4 - purple.

As in Group 2, primary and secondary quartz in Group 3 formed from fluids with temperatures in the range of the low-pressure greenschist facies. Fluids precipitating primary hydrothermal quartz in Lugushwa and Namoya's Group 3 samples have similar fluid temperatures of 390 to ~430 °C and ~1.2-1.5 kbar. The precipitation conditions for secondary Group 3 quartz could not be evaluated thermometrically for any deposit due to the rarity of Type 1 primary FIs in the secondary quartz FIAs. However, the position of isochores of other fluid Types suggests that these quartz generations formed under lower greenschist facies conditions. If projected to higher levels (I kbar) and had there been Type 1 primary FIs present with similar characteristics to Group 2 Type 1 FIs, an intersection at this range is probable. This is best illustrated with Kamituga's secondary quartz FIs where the three isochores do not intersect or intersect below the average Th of the FIAs or intersect above 6 kbar and 650 °C (Figure 8.13).

8.4 SECONDARY FIs - ALL GENETIC GROUPS

As described in Chapter 7, the presence of secondary fluids appears to spatially correlate with gold mineralisation in Kamituga, Lugushwa and Namoya. Secondary fluids in Namoya's Group 2 and 3 samples are indistinguishable in their compositional and physical properties. This corresponds to the secondary nature of the fluid influx event that equally affected pre-existing veins, irrespective of the presence or absence of tourmaline. Secondary fluids are present along healed micro-fractures and were captured during a late infiltration event that affected all Groups in Kamituga, Lugushwa and Namoya. As such, secondary fluids from Group 2 and 3 are described together.

Compared to primary fluids that do not show significant regional Th/salinity variations (Figures 8.9, 8.10, 8.15 and 8.16), secondary fluids tend towards higher Th in Namoya compared to Lugushwa and Kamituga (Figure 8.17). In addition, Namoya shows highly saline Type 1 secondary fluids – both of which are absent in Lugushwa and Kamituga. Types 3 and 4 secondary FIs are found in all three deposits. The spread of Th across all measured FIs extends over a wide range (~150 - 380 °C; Figure 8.17). However, the average values for different fluid types at all sites vary considerably less (~280 - 335 °C, a spread of only 55 °C; Figure 8.17).

In Kamituga and Lugushwa, Type 4 secondary FIs show higher Th in mineralised (~290/320 °C) than in non-mineralised samples (~200/220 °C; Figure 8.17). Type 4 secondary FIs in Namoya's mineralised samples were too small to evaluate. The Th of Namoya's unmineralised samples were similar to Kamituga's mineralised samples. Namoya Type 3 secondary FIs show higher Th in mineralised samples than in unmineralised samples. The Th variations in Type 3 secondary FIs is, however, not as great as in Type 4 secondary FIs. These variations imply a succession or evolution of higher temperature mineralised to less- or non-mineralised lower temperature Type 3 and 4 secondary FIs.

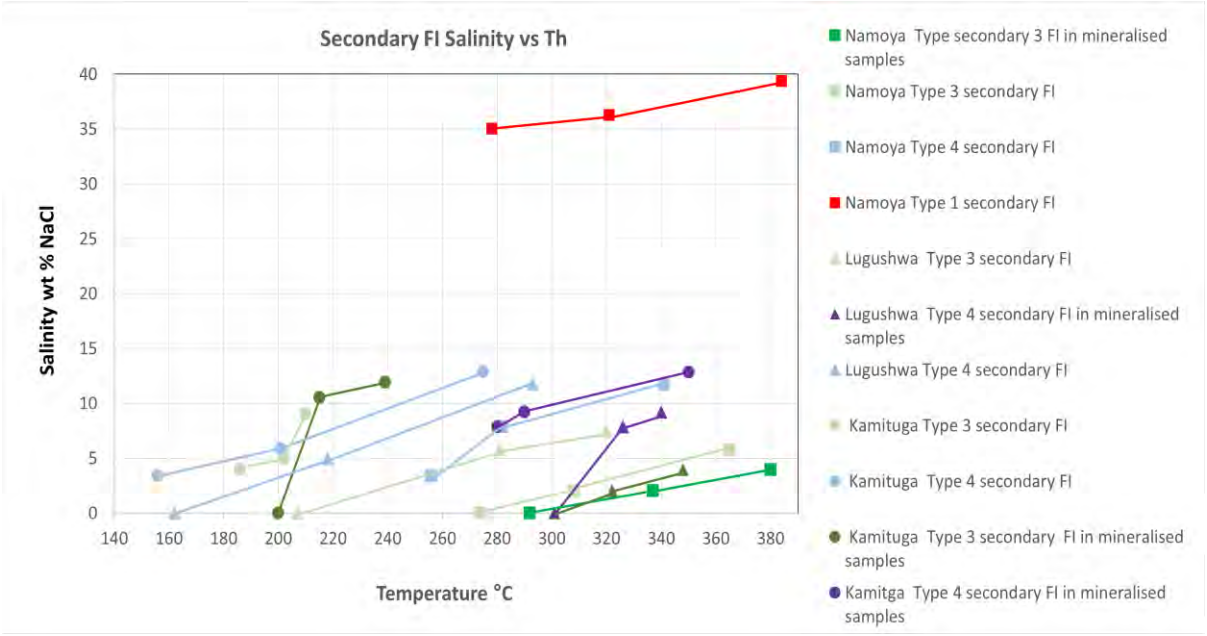

Figure 8.17: Salinity vs Th conditions in secondary FIs (Groups 2 and 3 combined) are shown as lower, upper and average values for Types 1, 3 and 4 secondary FIs. Kamituga - circles; Lugushwa - triangles and Namoya - squares. Type 1 FI – red; Type 3 - green and Type 4 – blue/purple.

Isochores for Namoya's Type 3 secondary FIs have shallow slopes and only intersect below reasonable formational P-T conditions with isochores of Type 1 secondary FIs (Figure 8. 18). Types 1 and 4 secondary FI isochores have steeper slopes and intersect at 1.7 kbar and 415 °C. These data correspond to a depth-temperature gradient of ~64 °C/km and a depth of trapping of ~4600 m; values that are similar to the trapping conditions of most primary fluids in samples obtained in Kamituga, Lugushwa and Namoya. 1.7 kbar and 415 °C are interpreted as the most likely conditions of secondary fluid trapping in Namoya. The most likely reasons for the closer correlation between Type 1 and 4 secondary FIs, as compared against Type 3 secondary FIs, is their

close proximity to each other and their similar salinity values. Type 3 FI have high proportions of volatile components outside of CO_2 which makes evaluating formation conditions harder and less reliable than that of Type 1 and 4 FI.

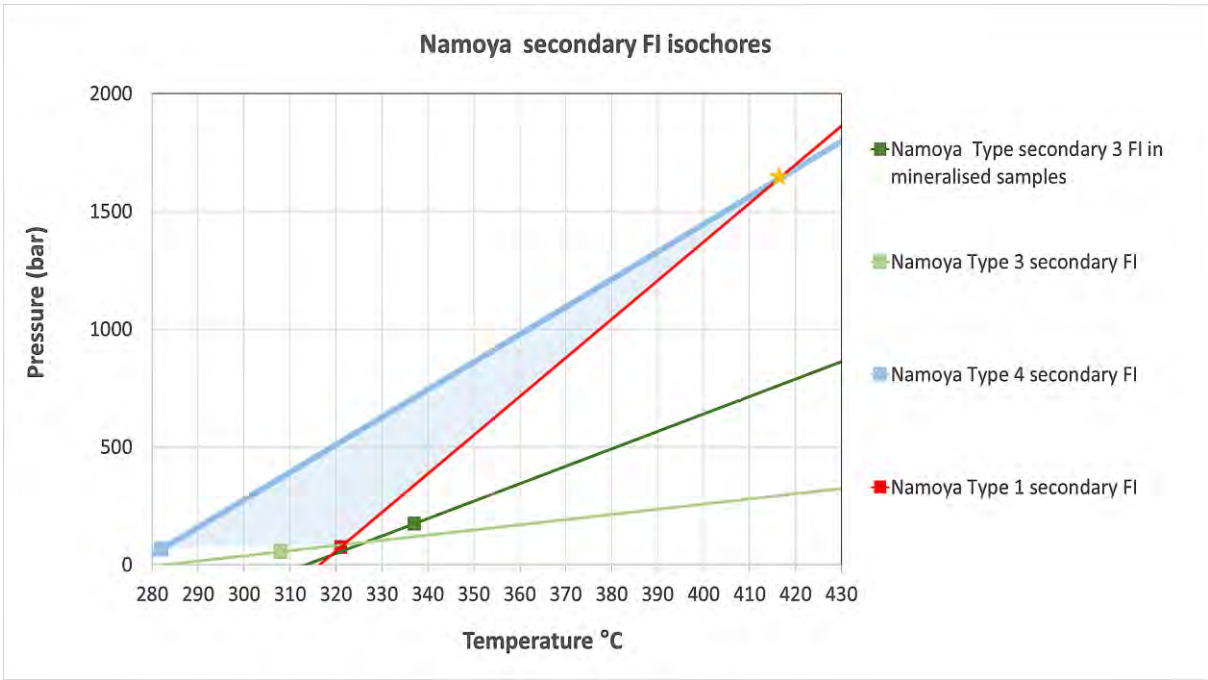

Figure 8.18: Isochore diagram for Namoya's secondary FIs (Group 2 and 3 combined). Formation conditions are defined by the intersection of the average isochores for Types 1 and 4 secondary FIs. Fluid capturing conditions obtained from the average Type 1 secondary (homogenisation by vapor loss) and Type 3 secondary (associated with Type 1 secondary FIs) isochore intersects at ~415 °C/1.7 kbar (star), and correspond to a depth of ~4600 m and a depth-temperature gradient of ~64 °C/km. The squares on the isochore lines represent average Th from which isochores are projected. The shaded area indicates the possible PT formation condition range

Kamituga and Lugushwa's secondary fluids show average homogenisation P-T ranges between 215 and 314 °C at ~0.06 kbar. Isochore graphs for Kamituga and Lugushwa indicate formation conditions of ~300 °C/1.2 kbar and ~337 °C/0.23 kbar, with depth – temperature gradients well over 100 °C/km (Figure 8. 19, 8.20). Rossetti & Colombo (1999) identified that in many deposits' lower temperature secondary FIs probably reflect the involvement of meteoric water or epithermal fluids. This, however, does not reflect the large areas over which epithermal fluids would have affected and evolved. Meteoric fluids, or an overprinted epithermal system, are invoked for these lower Th and salinity FIs and higher depth – temperature gradients in the TNGB.

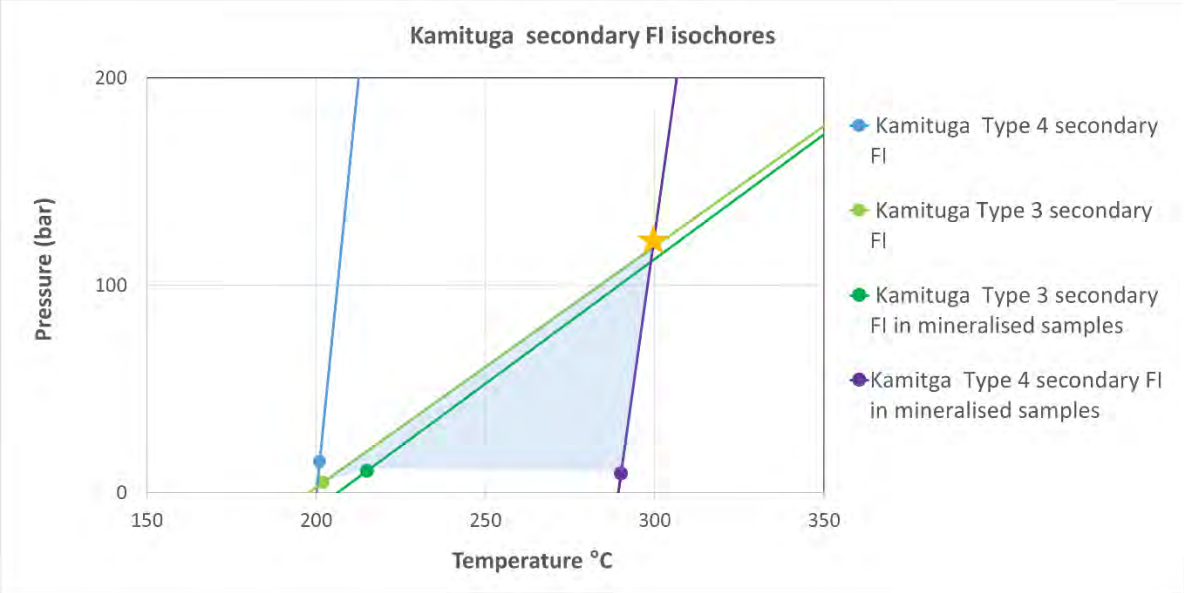

Figure 8.19: Isochore diagram for Kamituga's secondary FIs (Group 2 and 3 combined). Formation conditions are defined by the intersection of the average isochores for Types 3 secondary FIs and Type 4 secondary FIs from mineralised samples. Fluid capturing conditions obtained from this intersection at ~300 °C/1.2 kbar (star). The dots on the isochore lines represent average Th from which isochores are projected. The shaded area indicates the possible PT formation condition range.

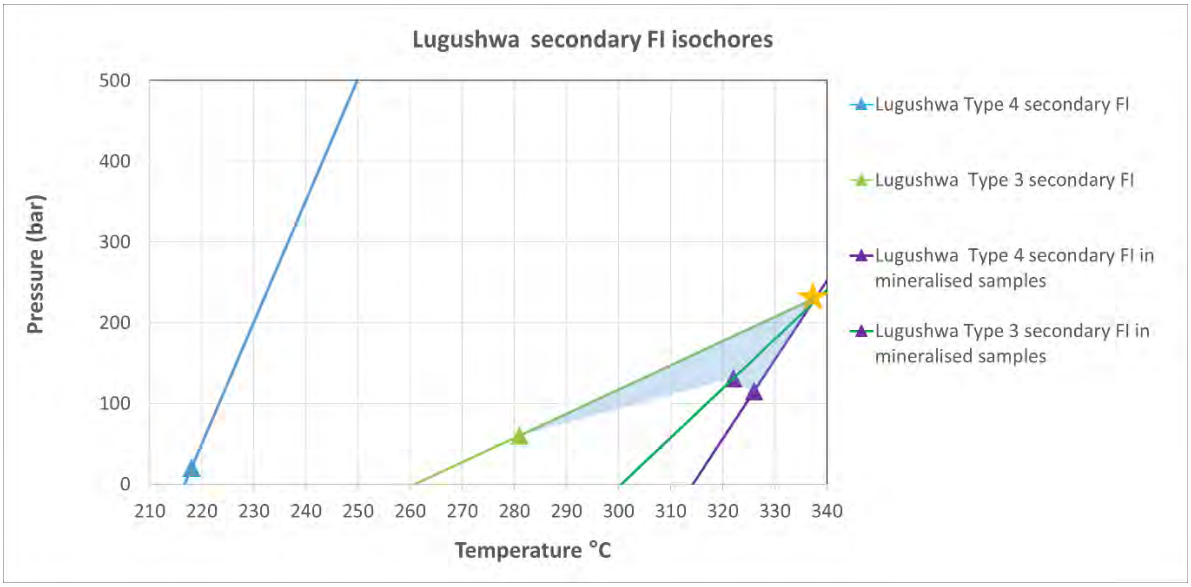

Figure 8.20: Isochore diagram for Lugushwa's secondary FIs (Group 2 and 3 combined). Formation conditions are defined by the intersection of the average isochores for Types 3 secondary FIs and Type 4 secondary FIs from mineralised samples. Fluid capturing conditions obtained from this intersection at ~337 °C/0.23 kbar (star). The dots on the isochore lines represent average Th from which isochores are projected. The shaded area indicates the possible PT formation condition range.

9. DISCUSSION OF FLUID CHARACTERISTICS AND SOURCES IN THE TNGB

9.1 FLUID CHARACTERISTICS AND SOURCES IN THE TNGB

The pressures and temperatures and the origins of the six classified FI Types of the TNGB's (Chapter 6) hydrothermal and magmatic fluids are key to understanding fluid and formation conditions in Kamituga, Lugushwa and Namoya.

Most interpretations have been drawn from the physical and compositional properties of fluid Types 1 to 5. The highly saline Type 1, with only halite as a daughter phase, and Type 2, with halite and an additional non-organic crystal phase (sylvite, Fe-chloride and bischofite) are the prevalent FIs. CO_2 vapour-bearing Type 3, and the aqueous Type 4 FIs are typically co-genetic with Type 1 and/or 2 FIs in FIAs. CO_2 liquid-bearing Type 3 FIs, that typically contain CH_4 and/or N_2, are texturally unrelated to Type 1 and 2 FIs, but may be related to aqueous-saline Type 4 FIs. Type 5 CO_2-liquid FIs contain either sulphide crystals or amorphous or crystalline carbon. Type 6 FIs are single aqueous liquid phase FIs that lack a vapour bubble. Raman and cooling data indicate low salinities (< 18 wt. % NaCl eq.). No visible phase changes occur on heating up to 550 °C and thereby, Type 6 FIs are not considered significant for microthermometric evaluations. CH_4 and carbon-bearing Types 3 and Type 5 FIs suggest fluid sources that are rich in organic material (Shepherd et al., 1991) such as metapelites and distal black shales, common in the TNGB. These rock types, or similar deeper crustal equivalents, are likely source rocks for the fluids that precipitated the primary and secondary quartz in all the Groups 2 and 3 hydrothermal deposits.

Highly saline fluids such as Types 1 & 2 FIs are not indicative of a specific provenance and were formed from either metamorphic-sedimentary or igneous fluid sources Wilkinson (2001). Fe-chlorite is present in primary quartz of Group 1 (pegmatite), a feature that has been described as typical for granitic fluids Wilkinson (2001). The presence of Fe-chlorite in some Group 2 samples (tourmaline bearing-hydrothermal quartz veins, e.g. Ktm-2, K2, K6 and K9 (Chapter 7, Section 7.2.2) from Kamituga may suggest the contribution of granitic fluids to these veins. However, these samples are not gold mineralised. Except for Type 1 and 2 FIAs in Group 1 and Group 2 samples there is no strong indication of magmatic fluids in the analysed samples. This is in contrast to Walemba (2001) and Walemba and Master (2005) findings. They proposed that G4 granitic fluids are an important mineralising fluid source for the gold deposit at Twangiza mine in the north of the TNGB (cf. Chuwa, 2011).

Primary fluids represent the precipitation of hydrothermal quartz that form the bulk phase of all hydrothermal veins. Secondary fluids are associated with fluid influx during deformation and recrystallisation episodes that postdate vein formation. However, primary and secondary fluid associations show the same FI Types, with exception of Type 2 fluids that are absent in secondary inclusions. There is, however, a variance in the abundance of FI Types in primary and secondary fluids. Types 1 and 2 FIs predominate in primary fluids.

Secondary fluids Types are typically Type 3, 4 and 5 FIs (Tables 7.1, 7.5 and 7.8) with CO_2, CH_4 and N_2. This indicates an increase in fluids sourced from organic-rich sedimentary rocks. Salinities tend to decrease in secondary fluids in Lugushwa and Kamituga. In Namoya, however, highly saline secondary Type 1 fluids together with Type 3, 4 and 5 are present in highly mineralised samples, such as sample N5 with ~1460 g Au/t (Table 7.8). Type 5 FIs (CO_2-H_2O) that contain sulphide crystals are typically seen in mineralised veins that are hosted in metapelites and form as secondary FIs. Such fluids are commonly seen in secondary FIAs. Similarly, in brecciated primary quartz or quartz-tourmaline veins, sulphide precipitated between fragmented primary vein material during renewed fluid influx as secondary (Figures 4.3 B & C, Figures 4.4 B & C; Figure 2f, h in Büttner et al., 2016). This indicates the secondary nature of sulphide influx. Secondary calcite may also be present in brecciated quartz or quartz-tourmaline veins that are well mineralised.

As outlined in Chapter 7, Section 7.2 subsequent plastic deformation of quartz was identified as having led to quartz recrystallisation. During recrystallisation, sulphide were mobilised and precipitated in textural association with the deformed parts of veins. Recrystallised quartz (referred to as "sugary quartz" by Banro's staff) is closely associated with visible gold. The deformation and subsequent recrystallisation may have mobilised and precipitated gold. These episodes are associated with the capturing of secondary fluids, which are rich in CO_2 and organic materials (C, N_2 and CH_4). Higher gold grade samples contain more recrystallised quartz, sulphides and CO_2-rich Type 3 FIs - especially the liquid CO_2-rich Type 3 FIs (Tables 9.1, 9.2 and 9.3). Th of Type 3 secondary FIs in mineralised samples is higher than in unmineralised samples, suggesting that mineralising fluids were introduced at somewhat higher temperatures than unmineralised fluids of the same type. In Lugushwa higher gold grades are seen in veins that show intense quartz recrystallisation, evidence of secondary fluid influx and sulphide precipitation. The apparent correlation of higher gold grades with deformation in Namoya Group 2, suggests that gold was probably mobilised and concentrated during deformation and secondary fluid influx episodes as shown in sample N23, in which CO_2-rich Type 3 secondary FIs are concentrated. This suggests that CO_2-rich secondary fluids are related to gold mineralisation. Namoya Group 3 has a closer association of increased CH_4 and N_2 levels and gold mineralisation than other samples across the TNGB. In addition, secondary fluids that correlate with Au mineralisation have very high salinities in the range of ~37 wt. % NaCl eq. This points to a fluid source rich in NaCl and organic materials.

Table 9.1: Representation of distribution and occurrence of FI Types in Group 1.

FI Types and abundance in Group 1 Kamituga									
Deposit	**Type 1**	**Type 2**	**Type 3 (CO_2 liq)**	**Type 3 (CO_2 vap)**	**Type 4**	**Type 5**	**Type 6**	**Legend**	
Kamituga	††	††	†	††	††	†	†	**Present**	†
								Absent	—
								Abundant	††

Table 9.2: Representation of distribution and occurrence of FI Types in Group 2.

FI Types and abundance in Group 2 Kamituga, Lugushwa and Namoya									
Deposit	**Type 1**	**Type 2**	**Type 3 (CO_2 liq)**	**Type 3 (CO_2 vap)**	**Type 4**	**Type 5**	**Type 6**	**Legend**	
Kamituga	††	††	†	†	††	†	†	**Present**	†
Lugushwa	††	—	†	†	††	†	†	**Absent**	—
Namoya	†*	—	††	†	††	††	†	**Abundant**	††
								Only found in secondary FIs	†*

Table 9.3: Distribution and occurrence of FI Types in Group 3.

FI Types and abundance in Group 3 Kamituga, Lugushwa and Namoya									
Deposit	**Type 1**	**Type 2**	**Type 3 (CO_2 liq)**	**Type 3 (CO_2 vap)**	**Type 4**	**Type 5**	**Type 6**	**Legend**	
Kamituga	†	†	††	†	††	††	†	**Present**	†
Lugushwa	†	—	††	†	††	††	†	**Absent**	—
Namoya	†*	—	††	†	††	††	†	**Abundant**	††
								Only found in secondary FIs	†*

There appears to be a connection between the influx of secondary fluids, sulphide precipitation and gold mineralisation. The prevalence of oxidised sulphide in the highly mineralised sample N5 (Figure 4.18) illustrates this relationship. Accordingly, elevated gold grades are connection with the influx of secondary fluids that contain sulphur and CO_2. The abundance of oxidised sulphide in the highly mineralised sample N5 (Figure 4.18) illustrates this relationship. An associated study by Moloto (2018) identified sulphur isotopes in pyrite - suggesting a metasedimentary sulphur sources with sulphur mobilisation under greenschist facies metamorphic conditions. Highly saline secondary Type 1 fluids in Au mineralised and sulphide-bearing samples from Namoya are consistent with evaporitic sedimentary sources for Namoya. Such sources are indicated by high $\delta^{34}S$ isotopic compositions of around +20 in pyrite from highly mineralised veins (Moloto, 2018). Metadiorite hosted veins indicated igneous sulphur sources, suggesting local sulphur mobilisation. These metadiorite-hosted veins are, however, usually barren. Overall, in the TNGB, the highest gold grades coincide with sulphur from

metasedimentary sources (Moloto, 2018). Moloto (2018) also observed native gold in metapelitic sequences in the TNGB. This supports the interpretation that the meta-sedimentary sequence in the TNGB is a potential primary source for the fluids, the sulphur and the gold. In this context, the presence of components that link fluid sources rich in organic materials, such as carbon and CH_4 provide important clues to the provenance of mineralising fluids. The association between gold-mineralisation, hydrothermal quartz veins, sulphides and CO_2–rich fluids has been described in Carlin-type gold deposits and orogenic gold around the world (Groves et al., 2003; Philips & Evans, 2004 and Large et al., 2011). This ostensibly also pertains to the TNGB. The correlation between gold mineralisation and fluid characteristics are best illustrated in fluid influx episodes that postdated the formation of primary Group 1 and Group 2 quartz. These Au mineralising fluids are associated with secondary quartz and secondary inclusions as seen in samples from Kamituga (Ktm-2, K4, K10, K19 and K22) (Table 7.1); Lugushwa (L15) (Table 7.5) and Namoya (N3 and N5) (Table 7.8).

The basement of the TNGB is rich in granites, mostly related to the late Mesoproterozoic to early Neoproterozoic G4 granite emplacement episode (Chuwa, 2011; Tack et al., 2010; Melcher et al., 2015; Büttner, 2016). Granitic fluids are potential sources for primary vein formation in Kamituga Groups 1 and 2. Type 1 and Type 2 fluids may be granitic but are also consistent with low-grade metamorphic fluids (Roedder, 1984; Wilkinson, 2001). Pohl et al. (2013) attributed the late-Kibaran G4 Sn-W granitic episode with gold deposition (~960 - 1000 Ma). Gold mineralisation in the TNGB is present in areas where G4 magmatism is insignificant or absent (Fall, 2008). Fall (2008), a Banro geologist, described gold mineralisation as mesothermal and reduced intrusion-related gold with structural, lithological and hydrothermal controls within deposits. The interpretation that pegmatite fluids are Fe-rich (Büttner et al., 2016) is supported by the presence of Fe-chloride solids in Type 2 primary FIs found in quartz associated with Fe-rich blue tourmaline. According to Roedder (1984) and Wilkinson (2001), highly saline brines; denoted by large halite crystals, sylvite and/or Fe chlorides are typically associated with granitoid bodies. The predominance of CO_2 vapour-rich Type 3 FIs is a characteristic of effervescence in pegmatites; similarly seen in granitoid samples (Wilkinson, 2001). Only 5 – 10 % of Group 2 Type 2 primary FIs contain Fe-chloride daughter crystals. For Group 2 Kamituga, lower salinities and fewer Fe-chloride daughter crystals in FIs suggest a vein system that is not primarily related to granitoid fluid sources as previously postulated by Wilkinson (2001).

9.2 AGE OF MINERALISING EVENTS

No detailed regional geological maps displaying the distribution of Paleo-, Meso- or Neoproterozoic primary rock ages have been produced for the TNGB; and only a few rocks have been dated (Walemba, 2001; Büttner et al., 2016). A regional map of the South Kivu and Maniema Provinces, inferred from remote sensing data, produced by Tack et al. (2010), determined that Namoya is part of the Paleoproterozoic basement, and Lugushwa and Kamituga are situated in the Mesoproterozoic (Figures 1.3 and 3.1). Twangiza in the North of the TNGB (not part of this study), according to Walemba (2001) and Walemba & Master (2005), was formed in the Neoproterozoic Itombwe Supergroup. Boundaries between the large crustal entities are therefore insufficiently defined for interpretation.

Few episodes of the geological evolution of the TNGB have been dated (Walemba, 2001; Büttner et al., 2016). Late-Pan African white mica Ar age of 700 -500 Ma was interpreted by Walemba (2001) to be the same as the mineralisation of Au in Twangiza. Büttner et al. (2016) presented an age of 981±16 Ma for pegmatite KDD033 in Kamituga. This correlates to the age of Kamituga sample Ktm-3 and to late-Kibaran G4 granite emplacement. Büttner et al. (2016) dated an alteration halo of a Lugushwa hydrothermal vein at 677±17 Ma; suggesting an early Pan-African age of fluid activity. No Pan-African granitic or pegmatitic magmatism is known for the area.

According to Moloto's (2018), S-isotope values in the Kamituga, Lugushwa and Namoya, and findings from this study, G4 granitic episodes were unlikely to have been the primary source of gold in the TNGB. The Pan-African orogeny that resulted in long-lasting or repetitive heat influx - sufficient to mobilise hydrothermal fluids, was the more likely source of gold in the TNGB. Walemba (2001) and Walemba & Master (2005) suggest that the Itombwe Supergroup was deposited between ~1020 ± 50 Ma and 575 ± 83 Ma - correlating with Fernandez-Alonso et al's. (2012) theory that sedimentation took place after 710 Ma. The hydrothermal alteration at Lugushwa at 677 Ma may therefore fall into the time of sediment deposition at the surface.

Extensional basin formation related to the Neoproterozoic deposition of Itombwe sediments is a potential mechanism that may have elevated the geothermal gradients in the underlying Meso- and Proterozoic crusts. Hydrothermal fluids may have been mobilised during this time, and the hydrothermal alteration at Lugushwa at ~677 Ma (Büttner et al., 2016) falls into this prolonged period. Furthermore, the subsequent late-Pan-African folding of the Itombwe Supergroup sedimentary rocks, and the underlying basement, may have caused renewed fluid mobilisation during or after the deformation of earlier veins. This is consistent with abundant examples of secondary fluid influx in the course of, or after, deformation and recrystallisation of primary vein quartz. Such fluids have been shown to correlate with elevated gold grades. The secondary influx of mineralised fluids during or after a deformation episode, most likely originating from low-grade metamorphic rocks containing organic material and/or evaporitic sequences, suggests that the main mineralising episodes in the TNGB are related to the Pan-African orogenic cycle.

9.3 FLUID AND VEIN GENERATION

All PT estimations using isochore intersections from the TNGB indicate high fluid temperatures in relation to the pressures at which fluids were captured. The depth-temperature gradient ranges from 60 - 70 °C/km. According to Thompson & Newberry (2000) and Groves et al. (2003) high gradients are associated with shallow-level intrusion-related events and mesothermal orogenic gold deposits that have gradients up to 120 °C/km. In regional metamorphic settings that are unrelated to magmatic activity, such gradients are unlikely to occur. As outlined above, no magmatic activity is known to have occurred in the TNGB during the Pan-African period (De Waele et al., 2008; Tack et al., 2010 and Fernandez-Alonso et al., 2012), the mineralising hydrothermal activity is, however, most likely Pan-African.

There are two ways to explain the high temperatures of the observed fluids in the TNGB. 1) The magmatic heat source is hidden at depth, or granites considered as part of the G4 granite episode are of Pan-African age. The magmatic heat source would have contributed to the emission of heat that would have mobilised the crustal

hydrous fluids in the host rock that contained Au, sulphur and organic components. Granitic fluids may also have contributed to the hydrothermal system, but they cannot be associated with elevated gold grades.

2) Fluids captured in the TNGB's veins were generated at deeper and hotter crustal levels than the levels in which they were captured. Applying orogenic geothermal gradients of 45 °C, not unusual in thinned continental crusts in extensional or rift settings (Gholamrezaie et al., 2018), a fluid of 420 °C possibly could be generated at a depth of approximately 9.4 km and at 2.5 kbar. The TNGB's hydrothermal veins are therefore believed to have formed at 390 - 480 °C between 1.2 and 2.1 kbar, corresponding to a depth of 4.7 - 8.2 km (Table 9.4).

Table 9.4: Conditions of fluid capture across the deposits. Except for Group 1 primary quartz veins (Kamituga pegmatite) all P-T conditions of capture are below 500 °C and 2.1 kbar.

Conditions of fluid capture across the Groups			
Groups	**Primary Quartz (Primary fluids)**	**Secondary Quartz (Primary fluids)**	**Secondary Fluids**
Group 1	600 ° C / 3-4kbar	445 ° C / 1.8kbar	N/A
Group 2	435 ° C /	480 ° C / 2.1kbar	415° C /1.7kbar
Group 3	390 ° C / 1.4kbar	N/A	415° C / 1.7kbar
	390 ° C / 1.2kbar		

This required vertical fluid flow in a range of less than 5 km, and at a rate that prevented significant cooling. On the basis of this study, either of these two options is equally likely. However, when considering other studies such as Walemba and Masters (2005), then orogenic gold mineralisation becomes the deduced conclusion. This deduction is further corroborated by sericites-chlorite and silica alterations with pyrite being typical of orogenic type deposits (Robert et al., 2007).

Host rock temperatures, at the time of fluid influx, cannot be determined. Recrystallised quartz veins, abundant in all deposits, indicate that veins, and hence their host rocks, were at temperatures higher than the minimum temperature for quartz recrystallisation (~290 °C) (Voll, 1976) at the time of deformation. The emplacement depths of most veins for which reliable PT estimates were produced are compatible with host rock temperatures at elevated orogenic geothermal gradients.

Some P-T isochore intersections produced very low pressures (<< 1kbar) that corresponded to depth-temperature gradients well above 100 °C/km (Figure 8.6, 8.8, 8.14, 8. 19, 8.20). Active volcanic and epithermal environments, for which such gradients are typical, are not consistent with the greenschist facies metasedimentary crust in the TNGB. These P-T estimates are deemed unrealistic and probably are the result of the inhibition of halite or sylvite crystallisation in Type 4 FIs >30 wt. % NaCl eq. The crystallisation of daughter phases would have reduced the salinity in the remaining liquid, as described by Bodnar (1993). These Type 4 FIs would have become Type 1 or Type 2 FIs containing halite or halite and an additional daughter phase. Thus, Type

4 FI's hyper-saline brines, shift isochores to positions that do not represent thermometrically meaningful lines in P-T space, and as such, these P-T estimates do not provide geologically meaningful results.

10. CONCLUSIONS

10.1 INTRODUCTION

The aim of the study was to evaluate the succession of hydrothermal events associated with gold mineralisation in similar geological environments within the TNGB, and to investigate the prospect of any association between host rocks and fluid characteristics. The study was conducted, and correlations reached by analysing, in relation to current theoretical theories and local geological reports, the composition and formation of fluid inclusions in quartz veins collected from drill cores and open cast pits from Kamituga, Lugushwa and Namoya. As a result, the following was concluded.

10.2 METHODOLOGY

Six distinct FI Types were identified and characterised. Types 1 to 4 are common in all TNGB fluids, each with genetically specific characteristics. The predominant primary fluids included the highly saline Type 1 - with only halite as a daughter phase, and Type 2 - with halite and an additional non-organic crystal phase. Neither is specifically indicative of any provenance. The presence of Fe-chlorite in Type 2 primary pegmatite and tourmaline-bearing hydrothermal quartz from Kamituga is compatible with a granitic igneous source. Granitic fluids are the obvious source in the pegmatite. CO_2 vapour -bearing Type 3 FIs, and the aqueous-saline CO_2 liquid-bearing Type 3 FIs, typically contain CH_4 and/or N_2. Highly saline Type 4 fluids are typically co-genetic with Type 1 & 2 in FIAs. Type 5 CO_2-rich fluids contain sulphide crystals, or amorphous or crystalline carbon. Carbon, CO_2 and CH_4 bearing Type 3 & 5 FIs indicate fluid sources rich in organic materials. Type 6 FIs are single aqueous liquid phase FIs that lack a vapour bubble, have low salinities and no visible phase changes on heating, and therefore, were not considered significant for microthermometric evaluations.

10.3 RESULTS

In ascertaining what the nature of the primary and secondary fluids are, it was established that primary fluids form primary quartz that have elevated salinities and high Th. Elevated salinities and high Th are seen in Type 1 and 2 FIs and in highly saline Type 4 FIs ($\geq$ 26.3 wt % NaCl eq.). Primary quartz is closely associated with tourmaline. Primary quartz contains Type 1 and 2 FIs that have high Th and homogenise by halite dissolution, particularly when located in close proximity to tourmaline. These features are not associated with secondary fluids forming secondary quartz. Secondary fluids form within recrystallised, resorbed and fractured primary quartz. Secondary quartz host's abundant amounts of remobilised and introduced sulphides, organic material and volatile vapour (CO_2, N_2 and CH_4). Gold mineralisation is typically associated with high abundance of secondary fluid inclusions, suggesting that the gold mineralisation is not related to the primary formation of the veins but to secondary fluid influx. Commonly, and particularly in Namoya and Lugushwa, this process is related to recrystallisation of quartz and to the mobilisation and precipitation of sulphides.

Throughout the three deposits, fluids in Au-mineralised samples contain organic materials (C & CH_4), CO_2 and mobilised sulphides, particularly in association with secondary quartz phases (Chapter 8; Tables 8.1, 8.2 and 8.3). Au grades tend to be high where primary quartz or quartz-tourmaline veins were brecciated during the influx of

secondary sulphur-rich fluids. This indicates that secondary fluid influx events were a major gold source. Namoya's high gold grades correlate to primary quartz phases that are similar to secondary quartz phases in samples from Kamituga and Lugushwa. These fluids are highly saline and contain numerous sulphides as inclusions in quartz, and as a matrix phase. High gold grades also commonly link to a paucity of primary Type 1 & 2 FIs. Namoya's highly saline Type 1 secondary FIs are, however, associated with high gold grades.

Liquid CO_2-rich Type 3 and 5 FIs, in particular secondary FIs in secondary and recrystallised quartz from Kamituga and Lugushwa samples, correlate to high gold grades. Although FIs in Namoya samples are rare in secondary quartz, highly recrystallised samples have higher gold grades when present with both primary and secondary liquid CO_2-rich Type 3 and 5 FIs, suggesting that these fluids may have been mineralised, or were introduced together with the mineralised fluid. Types 4 and 6 are associated with all FI Types and do not reflect a particular fluid episode or source.

Gold mineralisation within the TNGB is associated with alteration and fragmentation of primary quartz phases. These features are not observed in undeformed granitic bodies and pegmatites such as Ktm-3. Granitic fluids do not contain C/CH_4 and CO_2-rich fluids that are characteristic of the fluids associated with gold mineralisation in the TNGB. The late Kibaran is the known as the main episode of granitic magmatism in the TNGB and in other parts of eastern DRC and central East Africa (e.g. Melcher et al., 2015). The younger Neoproterozoic Pan-African cycle however does not have any known association with granitic activity in the TNGB.

10.4 DEDUCTIONS

The introduction and precipitation of Au in quartz veins in the TNGB occurs under shallow-crustal greenschist facies condition, within an approximate P-T range around 415 °C / 1.7 kbar. This corresponds to a depth-temperature gradient of ~64 °C/km and a ~4600 m depth of trapping. Thermo-barometric estimates indicate fluid temperatures that are higher than a likely geothermal gradient would allow, implying an influx of fluids from a somewhat deeper and hotter level. The CH_4, CO_2 and carbon-bearing Types 3 and Type 5 FIs suggest hydrothermal fluids sourced from organic-rich rocks such as black shales and other metapelites. The association of graphite NH_4+ and micas (biotite, muscovite) is characteristic of metamorphic black shales. Fluid inclusions typically exhibit high concentrations of CO_2 and CH_4 in metamorphic black shales. The CO_2 and CH_4 were probably produced through reactions with graphite (Moine et al. 1994). Metamorphic black shales are common in the TNGB (Chuwa, 2011). Shepherd et al. (1991) identified that black shales are an entrapment lithology for gold and that hydrothermal fluids are able to mobilise gold from black shales to precipitate quartz veins. According to Philips and Evans (2004) and Kokh et al. (2017), sulphides, CO_2 and salinity are critical components that control the solubility, mobility and emplacement of gold in quartz veins. Black shales and other metapelites or similar deeper crustal equivalents are likely source rocks for the fluids that precipitated the primary and secondary quartz veins in all hydrothermal samples across the three deposits.

Regional geological variations in the TNGB of the South Kivu and Maniema Provinces required identification in order to contextualise the findings in this study of gold mineralisation. Tack et al. (2010), using remote sensing

data, determined that the Namoya deposit is likely part of the Paleoproterozoic basement, and Lugushwa and Kamituga are situated in the Mesoproterozoic (Figures 1.3 and 3.1). Chuwa (2011) determined that mineralisation settings in the TNGB include fold hinges and limb zones with well-developed stockworks in the hinge zones in Lugushwa; and shear zones and associated stockwork zones in Namoya and Kamituga. Büttner et al. (2016) proposed that early Pan-African hydrothermal activity occurred at Lugushwa (677 ± 17 Ma; Rb-Sr mineral data). This suggests that the TNGB underwent at least two episodes of heat influx that caused hydrothermal vein formation. According to Tack et al. (2010) the region underwent greenschist facies metamorphism and deformation in the Neoproterozoic, during the Pan-African orogeny (~530 - 720 Ma). This is also evident from the metamorphism and deformation in the Itombwe Supergroup, which is of Neoproterozoic depositional age, but reached greenschist facies conditions (Walemba and Masters, 2005). The Twangiza gold deposit at the northern end of the TNGB is located in the Itombwe Supergroup (Walemba and Masters, 2005; Chuwa, 2011). All this suggests that the gold mineralisation in the TNGB is related to secondary fluid mobilisation during Pan-African greenschist facies metamorphism and deformation, reactivating and overprinting an earlier hydrothermal vein system.

The association of gold-mineralising fluids in the TNGB with C, CH_4 and CO_2, and with sulphur, suggests a primary source of gold that was rich in organic materials. Black shales may be a likely candidate as they are common in the TNGB and also contain abundant pyrite (Chuwa, 2011); a possible source of the commonly observed secondary sulphide in hydrothermal veins. A sedimentary source of sulphur is also indicated by S-isotopic signatures (Moloto, 2018). The gold mineralisation in the TNGB, formed from greenschist facies metamorphic fluids rich in organic components and sulphur is consistent with Large et al.'s (2011) mineralisation models. Gold in such hydrothermal environments would rely on a AuHS species for deposion. Where cooling, H_2S loss, pH change and oxidation are seen to be effective mechanisims for gold precipitation, dependent on local ore formation conditions (Seward, 1973 & 1984; Rytuba & Dickson, 1977; Seward, 1984; Gibert et al., 1998; Suleimenov & Krupp,1994). Large's models indicate that black shales have high primary gold concentrations. According to Large et al. (2011), primary gold in black shale-rich sedimentary sequences are mobilised and enriched in hydrothermal systems during low-grade metamorphic orogenic overprint.

The number and multiplicity of varying characteristics of the FI Types analysed from Kamituga, Lugushwa and Namoya samples is evidence of the diversity in the formation and evolution of gold deposits in the TNGB. These facets and factors are, in turn, as a result of a the development of variable and multiple fluid influx events and interactions with host rock and imported materials that resulted in complex polyphase quartz veins; the product of which created viable gold deposits throughout the aptly named, Twangiza-Namoya Gold Belt, in the South Kivu and Maniema Provinces of the DRC.

REFERENCES

Bakker, R. J., 1997. Clathrates: Computer programs to calculate fluid inclusion V-X properties using clathrate melting temperatures. Computers & Geosciences, 23, 1-18.

Bakker, R. J. & Diamond, L. W. 2000. Determination of the composition and molar volume of H_2O-CO_2 fluid inclusion by microthermometry. Geochimica et Cosmochimica, Acta, 64, 1753-1764.

Bakker, R. J., Dubessy, J., & Catherlineau, M. 1996. Improvements in clathrate modelling: 1. NaCl-C H_2O– CO_2 system with various salts. Geochimica et Cosmochimica, Acta, 60, 1657-1681.

Banro, 2017. Banro Corporation: http://www.banro.com/: Quick Report. Accessed 31/03/2017.

Barton, P. B. & Chou, I. M. 1993. Calculation of the vapor-saturated liquidus for the NaCl-CO_2-H_2O system. Geochimica et Cosmochimica, Acta, 57, 2715-2723.

Bodnar, R.J. 1983. A Method of Calculating Fluid Inclusion Volumes based on Vapor Bubble Diameters and P-V-T-x Properties of Fluid Inclusions. Economic Geology, 78, 535-542.

Bodnar, R. J., Burnham, C. W., & Sterner, S. M. 1985. Synthetic fluid inclusions in natural quartz. III. Determination of phase equilibrium properties in the system H2O-NaCl to 1000 °C and 1500 bar. Geochimica et Cosmochimica, Acta, 49, 1861-1873.

Bodnar, R. J., Binns, P. R., & Hall, D. L. 1989. Synthetic Fluid Inclusions. VI. Quantitative Evaluation of the Decrepitation Behaviour of Fluid Inclusions in Quartz at one Atmosphere confining Pressure. Journal Metamorphic Geology, 7, 229-242.

Bodnar, R. J., 1993. Revised equation and table for determining the freezing point depression of H_2O-NaCl solutions. Geochimica et Cosmochimica Acta, 57, 683-684.

Bodnar, R. J., & Vityk, M.O. 1994. Interpretation of microthermometric data for H_2O-NaCl fluid inclusions. In Fluid Inclusions in Minerals, Methods and Applications. (eds. B. De Vivo, B. and M. L. Frezzotti). Virginia Tech, Blacksburg, 117-130.

Bodnar, R. J. 2003. Reequilibration of Fluid Inclusions. Fluid Inclusions: Analysis and Interpretation. Mineralogical Association Canada. Short Course Series, 3, 213-230.

Boiron, M. C., & Dubessy J. 1994. Determination of fluid inclusion compositions: Microanalytical techniques. In De Vivo, B. and Frezzotti, M.L. (Eds.) Short Course of the Working Group (IMA) 'Fluid inclusions in minerals': Methods and Applications. Pontignano, Sienna, 1-4 September, 45-72.

Bowers, T. S., & Helgeson, H. C. 1983. Calculation of the thermodynamic and geochemical consequences of nonideal mixing in the system H2O-CO2-NaCl on phase relations in geologic systems; Equation of state for H2O-CO2-NaCl fluids at high pressures and temperatures. Geochimica et Cosmochimica Acta, 47, 1247-1275.

Bowers, T. S., & Helgeson, H. C. 1985. FORTAN programs for generating fluid inclusion isochores and fugacity coefficients for the system H_2O-CO_2-NaCl at high pressures and temperatures. Computers & Geosciences, 11, 203-213.

Brinckmann, J., Lehmann, B., & Timm, F. 1994. Proterozoic gold mineralization in NW Burundi. OreGeology Reviews 9, 85–103.

Brinckmann, J., Lehmann, B., Hein, U., Höhndorf, A., Mussallam, K., Weiser, T., & Timm, F. 2001. La géologie et la minéralisation primaire de l'or de la chaîne Kibarienne, Nord- Ouest du Burundi, Afrique orientale. Geologisches Jahrbuch Reihe D. 101, 195.

Brown, P. E., & Lamb, W. M. 1989. P-V-T properties of fluids in the system H2O±CO2±NaCl: New graphical presentations and implications for fluid inclusion studies. Geochimica et Cosmochimica Acta, 53, 1209-1221.

Burke, E. A. J. 2001. Raman microspectrometry of fluid inclusions. Lithos, 55, (2001)139-158.

Büttner, S. H., Reid, W. K., & Erasmus, R. 2016. Late Permian tectonics and fluid influx during the Cape Orogeny: evidence from fault-bound quartz veins in the Cape Supergroup, South Africa. South African Journal of Geology, 119 (2), 379-398.

Büttner, S. H., Reid, W., Glodny, J., Wiedenbeck, M., Chuwa, G., Moloto, T., & Gucsik, A. 2016. Fluid sources in the Twangiza-Namoya Gold Belt (Democratic Republic of Congo): evidence from tourmaline and fluid compositions, and from Rb-Sr isotope systematics. Precambria Research 280, 161-178.

Cahen, L., Snelling, N. J., Delhal, J., Vail, J.R., Bonhomme, M., & Ledent, D. 1984. The Geochronology and Evolution of Africa. Oxford University Press, Oxford, pp512.

Chen, H.-S. 1972. The thermodynamics and composition of carbon dioxide hydrate. MS thesis, Syracuse University, Syracuse, New York.

Chuwa, M. G. 2011. A review of gold deposits in the Twangiza-Namoya Gold Belt, Eastern Democratic Republic of Congo, with emphasis on grass-root exploration models. MSc, Rhodes University, Grahamstown, South Africa, pp184.

Davis, D. W., Lowenstein T. K., & Spencer R. J. 1994. Melting behaviour of fluid inclusions in laboratory grown halite crystals in the systems NaCl-H_2O, NaCl-KCl-H_2O, NaCl-$MgCl_2$-H_2O, and NaCl-$CaCl_2$-H_2O. Geochimica et Cosmochimica, Acta, 54, 591-601.

De Waele, B., Johnson, S. P., & Pisarevsky, S. A. 2008. Palaeproteroic to Neoproteoic growth and evolution of the eastern Congo Craton: Its role in the Rodinia puzzle. Precambria Research. Science Direct. 160, 127-141.

De Waele, B., Thomas, R. J., Macey, P. H., Horstwood, M. S. A., Tucker, R. D., Pitfield, P. E. J., Schofield D. I., Goodenough, K. M., Bauer, W., Key, R. M., Potter, C. J., Armstrong, R. A., Miller, J. A., Randriamananjara, T., Ralison, V., Rafahatelo, J. M. Rabarimanana, M., & Bejoma, M. 2011. Provenance and tectonic significance of the Paleoproterozoic metasedimentary succession of central and northern Madagascar. Precambria Research. Science Direct. 189, 18 - 42.

De Waele, B., Lacorde, M. Vergara, F., & Chan, G. 2015. New insights on Proterozoic tectonics and sedimentation along the peri-Gondwanan West African margin based on zircon U-Pb Shrimp geochronology. Precambria Research. Science Direct. 259, 156 - 175.

Diamond, L. W. 1992. Stability of CO_2 – clathrate hydrate + CO_2 H_2O fluid inclusions. In De Vivo, B. & Frezzotti, M.L. (Eds.)

Diamond, L. W. 1994. Introduction to phase relations of CO_2-H_2O fluid inclusions. In De Vivo, B. and Frezzotti, M.L. (Eds.) Short Course of the (IMA) Working Group “Inclusions in Minerals”. Methods and Applications. Pontignano: Sienna,1-4 September,131-158.

Diamond, L. W. 1994b. Salinity of multivolatile fluid inclusions determined from clathrate hydrate stability. Geochimica et Cosmochimica, Acta, 58, 19-41.

Diamond, L. W. 2001. Review of the systematics of CO_2-H_2O fluid inclusions. Lithos, 55, 69-99.

Dubessy, J., Boiron M.-C., Moissette, A., Monnion, C., & Sretenskaya, N. 1992. Determination of water, hydrates and pH in fluid inclusions by micro-Raman spectrometry. European Journal of Mineralogy, 4, 885-894.

Erokhin, A. M. 1993. New method of determining Co_2 density and solution concentration in H_2O-CO_2-NaCl inclusions from the gas-hydrate melting point. Geochem. Int. 30, 107-129.

Fall, H. G. 2007a. Petrographic study of gold mineralisation. Lugushwa project. Company report. Banro Corporation.

Fall, H. G. 2007b. Petrographic study of gold mineralisation. Namoya project. Company report. Banro Corporation.

Fall, H. G. 2008. Overview of the geology, gold mineralisation and resource potential of the Twangiza-Namoya Gold Belt, eastern Democratic Republic of the Congo. Technical report. Banro Congo Mining SARL.

Fall, H. G., & Chuwa, G. 2007. Lugushwa concession: Summary of prospects geology, mineralisation and resource potential. Company report. Banro Congo Mining SARL. 38p.

Fall, A. Tattitch, B., & Bodnar, R. J. 2011. Combined microthermometric and Raman spectroscopy technique to determine the salinity of H_2O-CO_2-NaCl fluid inclusions based on clathrate melting. Geochimica et Cosmochimica, Acta, 75, 951-964.

Fernandez-Alonso, M., Cutten, H., De Waele, B., Tack, L., Tahon, A., Baudet, D., & Barritt, S. D. 2012. The Mesoproterozoic Karagwe-Ankole Belt (formerly the NE Kibara Belt): The results of prolonged extensional intracratonic basin development punctuated by two short-lived far-field compressional events. Precambrian Research, 216-219, 63-86.

Frezzotti, M.C., Tecce, F., & Casagli, A. 2012. Raman spectroscopy for fluid inclusion analysis. Journal of Geological Exploration, 112, 1-120.

Garrabos, Y., Turfev, R., Le Neindre, B., Zalczer, G., & Beysens, D. 1980. Rayleigh and Raman scattering near the critical point of carbon dioxide. Journal of Chemical Physics, 72, 4637-4651.

Garrabos, Y., Chandrasekharan, V., Echstgui, M. A., & Marsault-Herail, F. 1989. Density effect on the raman Fermi resonance in the fluid phase of CO_2. Chemical Physics Letters, 160, 250-256.

Gholamrezaie, E., Scheck-Wenderoth, M., Sipple, J., and Strecker, M. R. 2018. Variability of the geothermal gradients across two differently aged magma-rich continental rift margins of the Atlantic Ocean: The Southwest African and the Norwegian margins. Solid Earth, 9, 139-158.

Gibert F., Pascal M-L, and Pichavant M. (1998) Gold solubility and speciation in of in KCl (0.5m) solution under hydrothermal conditions (350–450°C, 500 bars). Geochimica et Cosmochimica, Acta, 62, (17): 2931-2947.

Goldstein, R. H., & Reynolds, T. J. 1994. Systematics of Fluid Inclusions in Diagenetic Minerals. Society for Economic Palaeontologists and Mineralogists, Tulsa, 199.

Groves, D. I., Goldfarb, R. J., Robert, F., & Hart, C. J. R. 2003. Gold Deposits in metamorphic Belts: Overview of Current Understanding, Outstanding Problems, Future Research and Exploration Significance. Economic Geology, 98, 1-29.

Henley, R. H. 1984. Aquifer boiling and excess enthalpy wells. In Fluid-Mineral Equilibria in Hydrothermal Systems, R. W. Henley, A. H. Truesdell, & P. B. Barton Jr. (Eds.), Vol. 1, Reviews in Economic Geology Publishing Company. El Paso TX, pp. 143-175.

Hall, D. L., Sterner, S. M., & Bodnar, R. J. 1988. Freezing point depression of NaCl-KCl-H_2O solutions. Economic Geology, 83, 197-202.

Huizenga, J. M., & Touret, J. L. R. 1999. Fluid inclusions in shear zones: The case of the Umwindsi shear zone in the Harare-Shamva-Bindura greenstone belt, NE Zimbabwe. European Journal of Mineralogy, 11, 1079-1090.

Jackson, J. A., & White, N. J. 1989. Normal faulting in the upper continental crust: observations from regions of active extension. Journal of Structural Geology, 11, 15-36.

Kelly, W. C., & Turneaure, F. S. 1970. Mineralogy, paragenesis and geothermometry of the tin and tungsten deposits of the eastern Andes, Bolivia. Economic Geology, GeoScience World, 65 (6): 609-680.

Kerkhof, A. M., Van den. 2012. Isochoric phase diagrams. Short course. Universität Göttingen.

Kerkhof, A. M., Van den., & Hein U.F. 2001. Fluid inclusion petrography. Lithos, 55, 27-47. Kerkhof, A. M., Van den., & Thiéry R. 2001. Carbonic inclusions. Lithos, 55 49-68.

Kerrick, D. M., and Jacobs, G. K. 1981. A modified Redlich-Kwong equation for H_2O, CO_2, and H_2O-CO_2 mixtures at elevated pressures and temperatures. American Journal of Science, 281 735-767.

Knight, C. L., & Bodnar, R. J. 1989. Synthetic fluid inclusions: IX. Critical PVTX properties of NaCl- H_2O solutions. Geochimica et Cosmochimica, Acta, 53, 3-8.

Kokh, M. A., Akinfiev, N.N., Pokrovski, G. S., and Savi, S. 2017. The role of carbon dioxide in the transport and fractionation of metals by geological fluids. Geochimica et Cosmochimica, Acta, 197, 433-466.

Large, R. R., Bull, S. W., and Maslennikov, V. V. 2011. A carbonaceous sedimentary source-rock model for carli-type and orogenic gold deposits. Economic Geology and The Bulletin of The Society of Economic Geologists, 106 (3), 331-358.

Lecumberri-Sanchez, P., Steel-MacInnis, M., & Bodnar, R. J. 2012. A numerical model to estimate trapping conditions of fluid inclusions that homogenize by halite disappearance. Geochimica et Cosmochimica, Acta, 92, 14-22

Mbuya, P. W., Machano, R., & Murhula, P. 2008. Geological overview of the Namoya Project, Maniema Province, Democratic Republic of the Congo. Company report, Banro Corporation.

Melcher, F., Graupner, T., Gäbler, H.-E., Sitnikova, M., Henjes-Kunst, F., Oberthür, T., Gerdes, A., & Dewaele, S. 2015. Tantalum–(niobium–tin) mineralisation in African pegmatites and rare metal granites: constraints from Ta–Nb oxide mineralogy, geochemistry and U Pb geochronology. Ore Geology Reviews, 64, 667–719.

Mernagh, T. P., & Wilde A. R. 1989. The use of the later Raman microbe for the determination of salinity in fluid inclusions. Geochimica et Cosmochimica, Acta, 53, 765-771.

Moine, B., Guillot, C., & Gilbert, F. 1994. Controls of the composition of nitrogen rich fluids originating from reaction with graphite and ammonium-bearing biotite. Geochimica et Cosmochimica, Acta, 58, 5503-5523.

Moloto, T. R. P. 2018. Sulphur isotope study of pyrite from the Twangiza-Namoya Gold Belt, (South Kivu, DRC): a proxy of Gold provenance. MSc, Rhodes University, Grahamstown, South Africa.

Nockolds, S. R., Knox, R. W. & Chinner, G. A. 1978. Petrology for Students. Cambridge: Cambridge University Press, pp 435.

O'Donovan, G., Kentwell, D., Brodie-Good, B., McRobbie, S., & Pittuck, M. 2005. Resource estimation and exploration potential at the Kamituga, Lugushwa, and Namoya concessions, Democratic Republic of Congo. NI 43-101 Technical Report. SRK, pp111.

Pohl, W. 1994. Metallogeny of the Northeastern Kibara Belt, Central Africa- Recent perspectives. Ore Geology Reviews, 9, 105-130.

Philips, G. N., & Evans, K. A. 2004. Role of CO_2 in the formation of gold deposits. Nature. 24 June.

Pohl, W. L., Biryabarema, M., & Lehmann, B. 2013. Early Neoproterozoic rare metal (Sn, Ta, W) and gold metallogeny of the Central Africa Region: a review. Applied Earth Science, 122, 66-82.

Pohl, W., & Günther, M. A. 1990. The origin of Kibaran (late Mid-Proterozoic) tin, tungsten and gold quartz vein deposits in Central Africa: a fluid inclusions study. Mineral. Deposita, 26, 51-59.

Ramboz, C., Pichavant, M., & Weisbrod, A. 1982. Fluid immiscibility in natural processes: Use and misuse of fluid inclusion data: II. Interpretation of fluid inclusion data in terms of immiscibility. Chemical Geology, 37, 29-48.

Roberts, S., & Beattie, I. 1995. Micro-Raman spectroscopy in the earth sciences. In Potts, P. J., Bowles, J. F. W., Reed, S. J. B., & Cave, M. R. (Eds., Microprobe Techniques in the Earth Sciences, Chapman & Hall, London, pp. 387-408.

Robert, F., Brommecker, R., Bourne, B. T., Dobak, P.J., Mc Ewan, C.J., Rowe, R. R. & Zhou, X. 2007. Models and Exploration methods for major gold deposit types. In Proceedings of Exploration 07: Fifth Decennial International conference on Mineral Exploration, B. Milkereit (ed). 691-711.

Roedder, E. 1984. Fluid Inclusions. Mineralogical Society of America Reviews in Mineralogy, 12, 85-101, 644 and 646.

Roedder, E., & Bodnar, R. J. 1980. Geological Pressure Determinations from Fluid Inclusion Studies. Annual Reviews of Earth and Planetary Sciences, 8, 263-301.

Rossetti, P. & Colombo, F. 1999. Andularia-sericite gold deposits of marmato (Caldas, Colmbia): field and petrographical data. Geological Society Publications, Special Publication. 155, 167-182.

Rosso, K. M., & Bodnar, R. J. 1995. Microthermometric and Raman spectroscopic detection limits of CO_2 in fluid inclusions and the Raman spectroscopic characterization of CO_2. Geochimica et Cosmochimica, Acta, 59, 3961-3975.

Rusill, J., Williams, B., & Holwell, D. A. 2009. Geophysical interpretation and target generation for the Twangiza-Namoya Gold Belt, DRC. Report prepared for Banro Corporation. SRK Exploration services. pp. 34.

Rytuba J. J. and Dickson F. W. (1977) Reaction of pyrite 1 pyrrhotite 1 quartz 1 gold with NaCl-H2O solutions, 300–500°C, 500 to 1500 bars and genetic implications. 4th IAGOD Symp. Varnia, Bulgarian Acad. Sciences Sofia, II, 1974.

Samson, I., Anderson, A., & Marshall, D. (Eds.). 2003. Fluid Inclusions: Analysis and interpretation. Mineralogical Association of Canada, 1, 7-58.

Schmidt-Mumm, A. 2008. Introduction to Fluid Inclusion Research, Short course handbook, Adelaide University, pp 57.

Seward T. M. (1973) Thio complexes of gold and the transport of gold in hydrothermal ore solutions. Geochim. Cosmochim. Acta 37, 370– 399.

Seward T. M. (1984) The transport and deposition of gold in hydrothermal system. In Gold '82: The Geology, Geochemistry, and Genesis of Gold Deposits (ed R. P. Foster), pp. 165–181. A. A. Blakeman.

Shepherd, T. J., Rankin A. H., & Alderton D. H. M. 1985. A Practical Guide to Fluid Inclusion Studies. Blackie, Glasgow, pp 235.

Shepherd, T. J., Bottrell, S. H., & Miller, M.F. 1991. Fluid inclusion volatiles as an exploration guide to black shale-hosted god deposits, Dolgellau gold belt, North Wales, UK. Journal of Geochemical Exploration, 42 5-24.

Skead, M. B. 2007. Third NI 43-101 Technical report, Lugushwa project, South Kivu Province, Democratic Republic of Congo. Company report. Banro Corporation.

Steel-MacInnis, M., Lecumberri-Sanchez, P., & Bodnar, R. J. 2012. HOKIEFLINCS-H_2O-NACl: A Microsoft Excel spreadsheet for interpreting microthermometric analysis of synthetic fluid inclusions in the hydrothermal diamond-anvil cell. Am. Mineral. 83, 995-1007.

Sterner, S. M., Hall D. L., & Bodnar, R. J., 1988. Synthetic fluid inclusions. V: Solubility relations in the system NaCl-KCl-H_2O under vapour-saturated conditions. Geochimica et Cosmochimica, Acta, 52, 989-1006.

Suleimenov O. M. and Krupp R. E. (1994) Solubility of hydrogen sulphide in pure water and in NaCl solutions, from 20 to 320°C and at saturation pressures. Geochim. Cosmochim. Acta 58, 2433–2444.

Tack, L., Wingate, M. T. D., De Waele, B., Meert, J., Belousova, E., Griffin, B., Tahon, A., & Fernandez-Alonso, M. 2010. The 1375 Ma "Kibaran event" in Central Africa: Prominent emplacement of bimodial magmatism under extensional regime. Precambrian Research, 180, 63-84.

Thiéry, R., Vidal, J., &, Dubessy, J. 1994. Phase equilibria modelling applied to fluid inclusions: liquid-vapor equilibria and calculation of the molar volume in the CO_2-CH_4-N_2 system. Geochimica et Cosmochimica, Acta, 58, 1073-1082.

Thompson, J. F. H., & Newberry, R. J. 2001 Gold deposits related to reduced granitic intrusions. Economic Geology, v, 13, 377-400.

Voll, G. 1976. Recrystallization of quartz, biotite, feldspars from Erstfeld to the Leventina Nappe, Swiss Alps, and its geological significance. Schweiz. Mineral. Petrogr. Mitt, 56, 641–647.

Walemba, K. M. A. 2001. Geology, Geochemistry, and Tectono-metallogenic Evolution of Neuproterozoic Gold Deposits in the Kadubu Area, Kivu, Democratic Republic of Congo. PhD. University of Witwatersrand, Johannesburg, South Africa. pp 491.

Walemba, K. M. A., & Master, S. 2005. Neoproterozoic diamictites from the Itombwe Synclinorium, Kivu Province, Democratic Republic of Congo: Palaeoclimatic significance and regional correlations. Journal of African Earth Sciences, 42, 200-210.

Wilkinson, J.J. 2001. Fluid inclusions in hydrothermal ore deposits. Lithos, 55, 229-272.

Wopenka, B., & Pasteris, J. D. 1987. Raman intensities and detection limits of geochemically relevant gas mixtures for a laser Raman microprobe. Anal. Chem. 59, 2165-2170.

Zhang, Y. F., & Frantz, J .D. 1992. Hydrothermal reactions involve equilibrium between minerals and mixed volatiles: 2. Investigations of fluid properties in the Co_2 –CH_4 – H_2O system using synthetic fluid inclusions. Chemical Geology, 100, 51-72.